Report on combined web crippling and bending moment failure of first-generation trapezoidal steel sheeting

Report TUE-BCO-00-09

Report on Combined Web Crippling and Bending Moment Failure of First-Generation Trapezoidal Steel Sheeting

Appendices to the thesis

H. Hofmeyer

ISBN 90-6814-115-5

This research was supported by the Technology Foundation STW, applied science division of NWO and the technology programme of the Ministry of Economic Affairs.

Contents

Notation

General variables

F	Actual concentrated load, can be in combination with bending moment [N].
k	Stiffness between concentrated load and web crippling deformation [N/mm].
M	Actual bending moment, can be in combination with concentrated load [Nmm].
M_u	Ultimate bending moment if there is no concentrated load [Nmm].
Δh_w	Web crippling deformation. The reduction of height h_w [mm].
Δ ...	Difference of ...
δ ...	Incremental ...

Sheeting variables (see also thesis [Hofm00a], chapter 2, figure 2-3)

b_{bf}	Bottom flange width [mm].
b_{bffl}	Flat bottom flange width [mm].
b_m	Total width between top flange middles [mm].
b_{tf}	Top flange width [mm].
b_{tffl}	Flat top flange width [mm].
b_w	Web width [mm].
b_{wfl}	Flat web width [mm].
E	Modulus of elasticity [N/mm^2].
f_y	Steel yield strength [N/mm^2].
h_m	Sheeting height as shown in figure 2-3, chapter 2, thesis [Hofm00a] [mm].
h_w	Sheeting height as shown in figure 2-3, chapter 2, thesis [Hofm00a] [mm].
L_{lb}	Load-bearing plate width [mm].
L_{span}	Span length [mm].
r_{bf}	Radius of bottom corner [mm].
r_{ibf}	Interior radius of bottom corner [mm].
r_{itf}	Interior radius of top corner [mm].
r_{tf}	Radius of top corner [mm].
t	Steel plate thickness [mm].
θ_w	Angle between web and flange [deg.].

Yield line distances

$L_{bf;left;edge}$ $L_{bf;right;edge}$	Distance between left / right two yield lines in bottom flange at the bottom corner [mm].
$L_{bf;left;in}$ $L_{bf;right;in}$	Distance between load-bearing plate and inner left / right yield line in bottom flange [mm].
$L_{bf;left;out}$ $L_{bf;right;out}$	Distance between load-bearing plate and outer left / right yield line in bottom flange [mm].
L_{tf}	Distance between support and yield line in top flange [mm].
L_w	Distance between bottom corner and yield line in web [mm].
L_{yb}	Distance between yield lines in bottom flange (Bakker's model) [mm].
L_{yt}	Distance between yield lines in top flange (Bakker's model) [mm].

Appendix 1 (ultimate failure mechanical model)

b	Substitute variable for beam on elastic foundation model.
b, L	Width and length of plate for Marguerre's equations [mm].
d_Q, d_P	Distances of point Q and P to line of intersection top flange and web [mm].
dx	Infinite small piece of sheeting in length direction.
E	Modulus of elasticity [N/mm^2].
F	Actual concentrated load [N].
f_1	Function.
$Fmin$, $Fmax$	Minimum and maximum values for the estimation of load F [N].
F_{test}	Ultimate load F_u measured during an experiment.
I	Moment of inertia for sheeting longitudinal section for sheeting part above the load-bearing plate [mm^4].
I_s	Moment of inertia for total sheeting cross-section [mm^4].
k	Stiffness between concentrated load and web crippling deformation [N/mm].
K_1, K_2	Factors in Marguerre's equations.
M	Actual bending moment, can be in combination with concentrated load [Nmm].
M_a	Bending moment in sheeting part above the load-bearing plate [Nmm].
P, Q, R, S, T	Points on the bottom flange.
q	Equally distributed load [N/mm^2].
R_h	Reaction force for sheeting part above the load-bearing plate [N].
u, w, v	Displacements along the x, y, and z-axis (should not be u, v, w, which seems to be more logical, see figure 1-3).
w_0	Out-of-plane displacement of modelled part bottom flange [mm].
w_a	Deflection of point a [mm], used in the beam on elastic foundation model.
$wmin$, $wmax$	Minimum and maximum values for the estimation of displacement w_0 [mm].
w_P, w_R, w_S	Out-of-plane displacements of point P, R, and S [mm].
x, y, z	Variables defining coordinate system.
y_0	Initial imperfection of midpoint in modelled part of bottom flange [mm].
z_p	Distance between centre of gravity and bottom flange [mm].
Δh_w	Web crippling deformation. The reduction of height h_w [mm].
α	Part of the web, used in the beam on elastic foundation model.
α, β	Substitution variables for Marguerre's equations [mm].
λ, C_1, C_2, C_3, D, p	Substitution variables.
ν	Poisson constant (0.3).
σ_{VM}	Von Mises stress [N/mm^2].
$\sigma_{x\,max\,,z\,max}$	Normal stresses in the outer fibres caused by bending moment in direction of x/z-axis [N/mm^2].
$\sigma_{x,z}$	Normal stress in direction of x / z axis [N/mm^2].
σ_z	Compressive stress in bottom flange [N/mm^2].
τ_{xz}	Shear stress in plane perpendicular to the x-axis, in z-direction [N/mm^2].

Appendix 2 and 3 (post-failure mechanical models)

$\bar{e}$	Main value for experimental values for the ultimate load.
$\bar{m}$	Main value for model predictions of the ultimate load.

$\{A, B, C, D, E, F, G, H, I, J, K\}$	Set of factors to simplify formulae.
a	Length of yield eye / flip disc [mm].
A, B, C	Constants.
A, B, C, D, E	Parameters to illustrate mathematical techniques.
a, b, c, d, e, f	Constants to illustrate mathematical techniques.
A_w, A_f, A_t	Web / flange / total area for U-section [mm^2].
b	Substitute variable for calculation F_e.
b	Width of yield eye / flip disc [mm].
b_1, b_2, b_3	Distances in figure 3-5 to determine relationship Δh_w and φ_c.
c_1	Substitution variable.
d_1, d_2, d_3	Differences between predicted loads [N].
e_i	Experiment i.
f, g, h, i	Functions to illustrate mathematical techniques.
F_{2p}	Load to deform two parts adjacent to the load-bearing plate [N].
F_{bf}	Normal force in the bottom flange [N].
F_{cs}	Load to deform cross-section [N].
F_{csu}	Ultimate load of cross-section [N].
F_e	Load to deform cross-section elastically [N].
F_l	Extra force due to the indentation of the cross-section [N].
$f_{l1,2}$	Length factor 1, 2.
F_p	Load to deform cross-section plastically [N].
F_{ylbf}	Load to form yield lines in the bottom flange [N].
h	U-section height [mm].
h	Sheeting height to illustrate web crippling stiffness in figure 2-13 [mm].
I_s	Moment of inertia for complete sheeting cross-section [mm^4].
L_{bf}	Abbreviation for $L_{bf;left;out}$.
L_i	Length yield line i.
L_{yw}	Specific yield line length in figure 3-2.
$M_{i,e}$	Internal / external bending moment [Nmm].
n	Number of experiments.
P_i	Point i.
s	Distance of bottom flange to centre of gravity sheet section [mm].
$s_{e,m}$	Standard deviation for experiments / model predictions.
u	Deformation of U-section [mm].
u_1, F_1	A specific deformation / force value of the U-section [mm].
$u_{4;fl,w}$	Horizontal / vertical displacement of point P4 [mm].
u_a, u_b	Movements of yield lines in the cross-section [mm].
w_{tf}	Distance between yield lines as shown in figure 3-2 [mm].
x, y, z	Variables to illustrate mathematical techniques.
x, α, β	Substituting variables.
Δ	Out-of-plane deflection yield eye / flip disc [mm].
Δb_{wfl}	Reduction of distance b_{wfl} [mm].
δE_e	Incremental external energy.
δE_{e1}	Incremental external energy cross-section only.
δE_{e2}	Incremental external energy cross-section and sheet section deflection.
δE_i	Incremental internal dissipated energy.

ϕ	Substitution variable
φ	Support rotation [rad.].
φ_i	Rotation of yield line i [rad.]
φ_{it}, φ_Δ	Specific yield line angles (no rotations) used in figure 3-1.
φ_w	Rotation around point P1 for line P1-P4 [rad.].
ρ	Standard deviation for experiments.

Appendix 4 (cross-section behaviour)

d, w, h	Distances [mm] in cross-section figure 4-10.
d_1, d_2	Distances as defined in figure 4-11 [mm].
dx	Infinite small piece of sheeting in length direction.
d_y	Movement of yield line in web [mm].
h_1, h_2	Variables to illustrate the web crippling deformation Δh_w [mm].
H_s	Horizontal load [N].
L_y	Distance from top web to yield line in web [mm].
$M_{i,s}$	Bending moment *i, s* [N].
M_{pl}	Plastic bending moment [Nmm].
P	Axial load in the web [N].
P_{cr}	The buckling load of the web [N].
rotx, roty, rotz	Rotations around the *x*-, *y*-, and *z*-axes.
u_1, u_2	Movement of upper and lower part cross-section as shown in figure 4-11 [mm].
ux, uy, uz	Displacements along the *x*-, *y*-, and *z*-axes.
V_s	Vertical load [N].
α, β	Variables for local coordinate system in cross-section (figure 4-10).
ϕ, ψ	Functions by Timoshenko.
η	Substitution variable.
φ_I	Rotation at location *I*.

Introduction

In this report, six appendices are presented. These appendices are meant to be used with the thesis [Hofm00a].

The first appendix presents the model of thesis chapter 5 a little more extendedly. Appendix 2 shows a detailed description of the post-failure models, as presented in chapter 6 of the thesis. The third appendix is used to present all derivations too tedious to present in appendix 2. Finally, appendix 4 shows pure cross-section behaviour for sheeting, using finite element simulations and mechanical models.

Appendix 5 and 6 present several listings of Turbo Pascal programs and input files for the finite element program Ansys 5.4.

1 Appendix ultimate failure mechanical model

1.1 Beam on elastic foundation model

In 1995, Vaessen developed a model for the prediction of the web crippling stiffness, based on the beam on elastic foundation theory [Vaes95a], [Bakk99a]. The web crippling stiffness equals the force F (figure 1-1) divided by the web crippling deformation (figure 1-1) Δh_w. During the development of the model, it was thought that all sections behave like situation II in figure 5-4 of the thesis [Hofm00a]. For the model, global beam deflection is not taken into account.

The model uses cross-section slices (width dx) as springs in the beam on elastic foundation theory. The bottom flange and a part of the web are used as the beam. This is shown in figure 1-1.

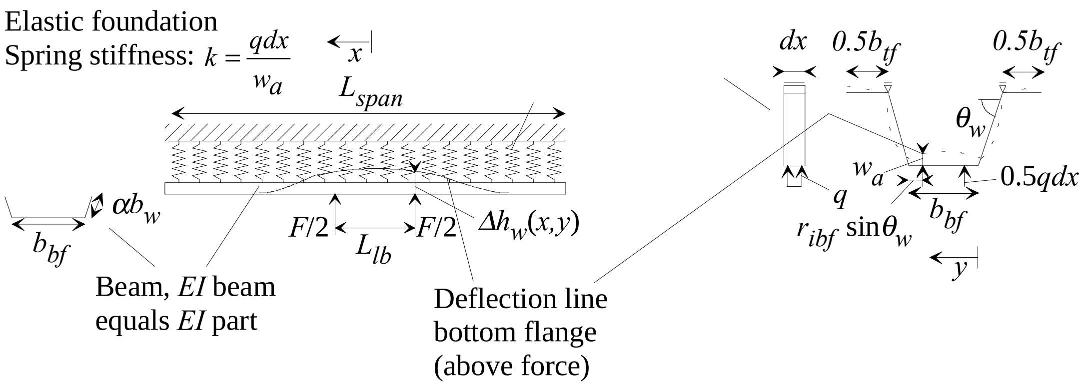

Figure 1-1. Principles of beam on elastic foundation model.

The elastic foundation spring stiffness k is derived for a certain load qdx. Here, q is an equally distributed load along the length dx:

$$k = \frac{1}{\dfrac{b_w \sin^2\theta_w}{Et} + \dfrac{\cos\theta_w}{Et}\left(\dfrac{b_w \cos\theta_w\left(b_{bf} + \frac{2}{3}b_w\right) + r_{ibf} * b_{bf} * \sin\theta_w - r_{ibf}{}^2 \sin^2\theta_w}{b_{bf} + \frac{2}{3}b_w}\right) + b} \tag{1.1}$$

$$b = r_{ibf}{}^2 \sin^2\theta_w \left(\frac{b_w\left(b_{bf} - \frac{4}{3}r_{ibf}\sin\theta_w\right) + r_{ibf}\sin\theta_w\left(b_{bf} - \frac{3}{2}r_{ibf}\sin\theta_w\right)}{Et\left(3b_{bf} + 2b_w\right)}\right) \tag{1.2}$$

The beam's bending stiffness EI equals that for the small part at the left corner in figure 1-1. The part contains a part αb_w of the web.

$$EI = E\frac{b_{bf}t^3}{12} + Et\alpha b_w\left(\frac{\alpha^2 b_w^2 + t^2}{12} - \frac{\cos 2\theta_w\left(\alpha^2 b_w^2 - t^2\right)}{12} + \frac{t\alpha b_w \sin 2\theta_w}{2}\right)$$
$$+ Eb_{bf}t\left(\frac{\alpha^2 b_w^2 \sin\theta_w + t\alpha b_w}{b_{bf} + 2\alpha b_w}\right)^2 + E\frac{t\alpha b_w}{2}\left(\frac{b_{bf}\alpha b_w \sin\theta_w + tb_{bf}}{b_{bf} + 2\alpha b_w}\right)^2 \tag{1.3}$$

If the elastic foundation stiffness k and the beam bending stiffness EI are known, the beam on elastic foundation theory can be used to determine Δh_w. Note that Δh_w is the decrease in section height above the load F. Although Δh_w depends on x and y (in figure 1-1), Vaessen only derived Δh_w for $x = L_{lb}/2$ and $y = r_{ibf}{*}\sin\theta_w$, being the point of load application, which equals:

$$\Delta h_w\left(\frac{L_{lb}}{2}, r_{ibf}\sin\theta_w\right) = F\frac{1 + f_1(\beta L_{lb}) - \frac{1}{2}f_1\left(\beta\left(L_{span} - L_{lb}\right)\right) + \frac{1}{2}e^{-\beta\left(L_{span} - L_{lb}\right)}}{\sqrt[4]{1024EIk^3}} \tag{1.4}$$

$$\beta = \sqrt[4]{\frac{k}{4EI}} \qquad \alpha = 0.118 r_{ibf}^{0.89} \tag{1.5}$$

$$f_1(\beta x) = e^{-\beta x}(\cos\beta x + \sin\beta x) \tag{1.6}$$

For the ultimate failure mechanical model in section 5.1 of the thesis [Hofm00a], it is necessary to predict the local flange deformation at $y=b_{bf}/2$. To obtain this, the cross-section behaviour is shown again in figure 1-2.

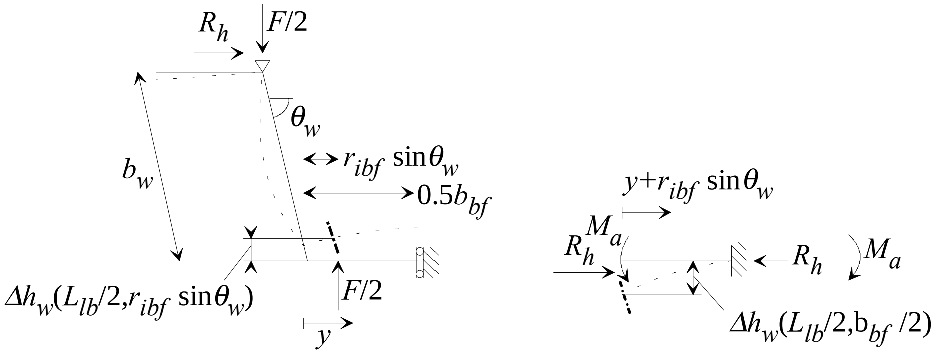

Figure 1-2. Simplification of cross-section behaviour.

In figure 1-2, the bottom flange of the cross-section is modelled as a beam as shown on the right in the figure. It is assumed that R_h does not influence the deflection of the beam (second order effects ignored). Then, the following can be derived:

$$M_a = \frac{k\Delta h_w}{2}\left(b_w\cos\theta_w + r_{ibf}\sin\theta_w\right) - R_h\left(b_w\sin\theta_w - \Delta h_w\right) \tag{1.7}$$

$$\Delta h_w\left(\frac{L_{lb}}{2},\frac{b_{bf}}{2}\right)=\Delta h_w\left(\frac{L_{lb}}{2},r_{ibf}\sin\theta_w\right)+\frac{M_a\left(\frac{b_{bf}}{2}-r_{ibf}\sin\theta_w\right)^2}{2EI} \tag{1.8}$$

$$R_h=\frac{k\Delta h_w}{4b_w\sin\theta_w}\left(\frac{\frac{2}{3}b_w{}^2\cos\theta_w+r_{ibf}b_{bf}\sin\theta_w+b_{bf}b_w\cos\theta_w-r_{ibf}{}^2\sin^2\theta_w}{\frac{1}{2}b_{bf}+\frac{1}{3}b_w}\right) \tag{1.9}$$

The latter formula was derived by Vaessen. This appendix can be summarised as follows. For a sheet section, loaded by a load-bearing plate, the displacement of the bottom corner relative to the upper corner can be calculated (web crippling deformation $\Delta h_w(L_{lb}/2,r_{ibf}*\sin\theta_w)$ and d_Q in section 5.1.2 of the thesis [Hofm00a]). If this deformation is known, the displacement of the bottom flange middle relative to the bottom corner can be predicted ($\Delta h_w(L_{lb}/2,\mathrm{b}_{bf}/2)$ and d_P in section 5.1.2 of the thesis [Hofm00a]).

1.2 Marguerre's equations

Marguerre's equations are partial differential equations that describe the relationship between stresses and deformations at arbitrary locations in a plate with arbitrary geometry [Marg38a]. For a specific geometry and specific boundary conditions, approximate analytical solutions for the differential equations are included in a book by Murray [Murr85a].

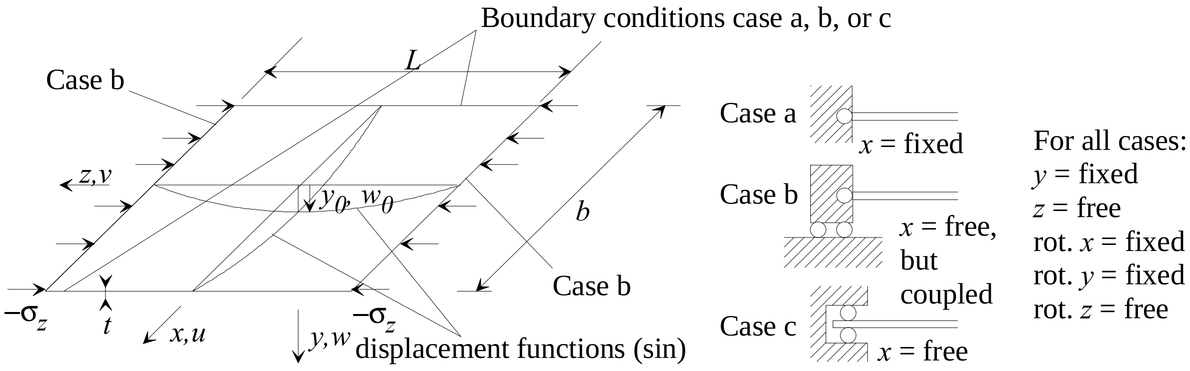

Figure 1-3. Plate under compression. Three cases for boundary conditions.

Figure 1-3 presents a rectangular plate with an initial deflection y_0. Plate edges that are loaded by stress are supported as case b. The two other edges are supported as case a, b, or c. For case a, each individual point along the edge is fully fixed in x-direction, thus the edge cannot move and cannot deform. For case b, all points on the edge are coupled in x-direction, thus the edge can move but cannot deform. For case c, each point is free in x-direction, thus the edge can move and deform. For the model in chapter 5 of the thesis [Hofm00a], only case c will be used, because case c yielded the best results.

An initial displacement field is variable for x and z and is described by:

$$y = y_0 \cos \beta x \cos \lambda z \qquad (1.10)$$

The displacement field itself is also variable for x and z and is described by:

$$w = w_0 \cos \beta x \cos \lambda z \qquad (1.11)$$

$$\beta = \frac{\pi}{b} \qquad (1.12)$$

$$\lambda = \frac{\pi}{L} \qquad (1.13)$$

Variables in the formulae above are defined in figure 1-3. For this plate it was derived:

$$
\begin{aligned}
&-\frac{bL}{32}\frac{2Dw_0\left(\beta^2+\lambda^2\right)^2}{Et}-2p\left(w_0+y_0\right)\left(\lambda^2+\nu\beta^2K_1\right)\\
&-\frac{bL}{32}\frac{w_0\left(w_0+y_0\right)\left(w_0+2y_0\right)}{8}\left\{\beta^4\left(2K_1+1\right)+\lambda^4\right\}\\
&+\frac{1}{8}L\beta^2\lambda C_1K_2\left(w_0+y_0\right)\sin\lambda b\\
&+\frac{1}{8}L\lambda^2C_2K_2\left(w_0+y_0\right)\left(\beta^2-\lambda^2\right)\frac{\lambda b}{2}\left(\frac{1}{\lambda^2}-\frac{1}{\beta^2+\lambda^2}\right)\cosh\lambda b+\\
&+\frac{1}{8}L\lambda^2C_2K_2\left(w_0+y_0\right)\left(\beta^2-\lambda^2\right)\frac{\lambda b}{2}\left(\frac{\lambda^2-\beta^2}{2\left(\beta^2+\lambda^2\right)}-\frac{1}{\lambda^2}\right)\sinh\lambda b\\
&+\frac{LC_2K_2\lambda^3\beta\left(w_0+y_0\right)}{4\left(\beta^2+\lambda^2\right)}\left[\frac{\beta b}{2}\cosh\lambda b-\frac{\lambda b\sinh\lambda b}{\beta^2+\lambda^2}\right]=0
\end{aligned}
\tag{1.14}
$$

and:

$$
C_1=\frac{\beta^2w_0\left(w_0+2y_0\right)\left(b\coth\lambda b+1/\lambda\right)}{32\lambda^2\left(b\sinh\lambda b-b\cosh\lambda b\coth\lambda b-\frac{\cosh\lambda b}{\lambda}\right)}
\tag{1.15}
$$

$$
C_2=\frac{\beta^2w_0\left(w_0+2y_0\right)}{16\lambda^2\left(b\sinh\lambda b-b\cosh\lambda b\coth\lambda b-\frac{\cosh\lambda b}{\lambda}\right)}
\tag{1.16}
$$

$$
D=\frac{Et^3}{12\left(1-\nu^2\right)}
\tag{1.17}
$$

$$
\begin{aligned}
&\text{Case a}\rightarrow K_1=1\wedge K_2=0\\
&\text{Case b}\rightarrow K_1=0\wedge K_2=0\\
&\text{Case c}\rightarrow K_1=0\wedge K_2=1
\end{aligned}
\tag{1.18}
$$

$$
p=\frac{\sigma_z b}{E}
\tag{1.19}
$$

Using the formulae presented above, the central deflection w_0 can be determined for a given value of σ_z (figure 1-3) by means of an iterative procedure.

If the central deflection w_0 is known, stresses at each location can be calculated using the following formulae:

$$\frac{\sigma_z(x,z)}{E} = \frac{w_0(w_0+2y_0)\lambda^2\cos 2\beta x}{8} + p + K_2\left(4C_1\lambda^2\cosh 2\lambda x + C_2\left(4\lambda^2 x\sinh 2\lambda x + 4\lambda\cosh 2\lambda x\right)\right)\cos 2\lambda z \tag{1.20}$$

$$\frac{\sigma_x(x,z)}{E} = \frac{\beta^2 w_0(w_0+2y_0)(K_1+\cos 2\lambda z)}{8} - 4\lambda^2 K_2(C_1\cosh 2\lambda z + C_2 x\cosh 2\lambda x)\cos 2\lambda z + K_1\nu p \tag{1.21}$$

$$\frac{\tau_{xz}(x,z)}{E} = 2\lambda K_2\left[2\lambda C_1\sinh 2\lambda x + C_2(2\lambda x\cosh 2\lambda x + \sinh 2\lambda x)\right]\sin 2\lambda z \tag{1.22}$$

$$\sigma_{z\,\max}(x,z) = \pm\frac{Ew_0 t\left(\lambda^2+\nu\beta^2\right)}{2\left(1-\nu^2\right)}\cos\lambda z\cos\beta x \tag{1.23}$$

$$\sigma_{x\,\max}(x,z) = \pm\frac{Ew_0 t\left(\beta^2+\nu\lambda^2\right)}{2\left(1-\nu^2\right)}\cos\lambda z\cos\beta x \tag{1.24}$$

The stresses σ_x and σ_z are the membrane stresses at a location in x and z direction respectively. τ_{xz} is the shear stress in the x-z plane. The stresses $\sigma_{x\max}$ and $\sigma_{z\max}$ are bending stresses at the outer fibres caused by a bending moment in the plate around z and x axes respectively. It can be concluded that, for an applied average stress σ_z, if all plate variables are known, the end-deformation w_0 and stresses at each location on the plate can be calculated.

1.3 Model equations

The ultimate failure model as presented in section 5.1.2 of the thesis [Hofm00a] can be described in 6 steps as follows. A flow diagram of the solving processes in the model is shown in figure 1-4. Equations are also presented by their corresponding number.

Step 1
Use figure 5-2 of the thesis [Hofm00a]. A certain load F is assumed to work on the load-bearing plate. The beam on elastic foundation method presented in appendix 1, section 1.1, can be used to predict the reduction of distance d_Q. This by using equations 1.1 to 1.6 to solve $\Delta h_w(L_{lb}/2, r_{ibf}*\sin\theta_w)$. Although the beam on elastic foundation method is developed by assuming bottom flange deflection according type II (figure 5-4 of the thesis [Hofm00a]), here it is assumed that the reduction of distance d_Q can be predicted for type I and III using the same method as well. Note that the displacement predicted here is caused by the local indentation of the section due to the load action.

Step 2
The reduction of distance d_P is calculated by equation 1.7 to 1.9 as $\Delta h_w(L_{lb}/2, b_{bf}/2)$. If d_P is known, out-of-plane displacement w_P of point P can be calculated as d_P-d_Q. The out-of-plane displacement w_R of point R can be predicted because P and R are on the (sine) displacement line of the modelled part for Marguerre's equations. Thus (using equation 1.10):

$$w_P = w_R \cos\left(\frac{\pi}{b_{bf}}\left(\frac{1}{4}b_{bf}\right)\right) \Leftrightarrow w_R = \sqrt{2}w_P \qquad (1.25)$$

Step 3
The out-of-plane displacement w_R of point R due to the local indentation of the section is regarded as an initial imperfection of the modelled part of the bottom flange in figure 5-2 of the thesis [Hofm00a]. More precisely, out-of-plane displacement w_R is set equal to initial imperfection y_0 in Marguerre's equations 1.10 to 1.24.

Step 4
Because load F is acting on the section, a bending moment is working in the section, which results in compressive stress acting on the modelled part of the bottom flange in figure 5-2 of the thesis [Hofm00a]. This compressive stress is set equal to the stress σ_z in Marguerre's equations. This stress is calculated by considering the full cross-section for the determination of the moment of inertia. The bending moment in the section equals:

$$M = \frac{F\left(L_{span} - L_{lb}\right)}{4} \qquad (1.26)$$

The stress σ_z in the bottom flange can now be calculated by using the moment of inertia I_s of the sheet section and the distance z_p between the centre of gravity and the bottom flange:

$$\sigma_z = \frac{Mz\,p}{I_s} \tag{1.27}$$

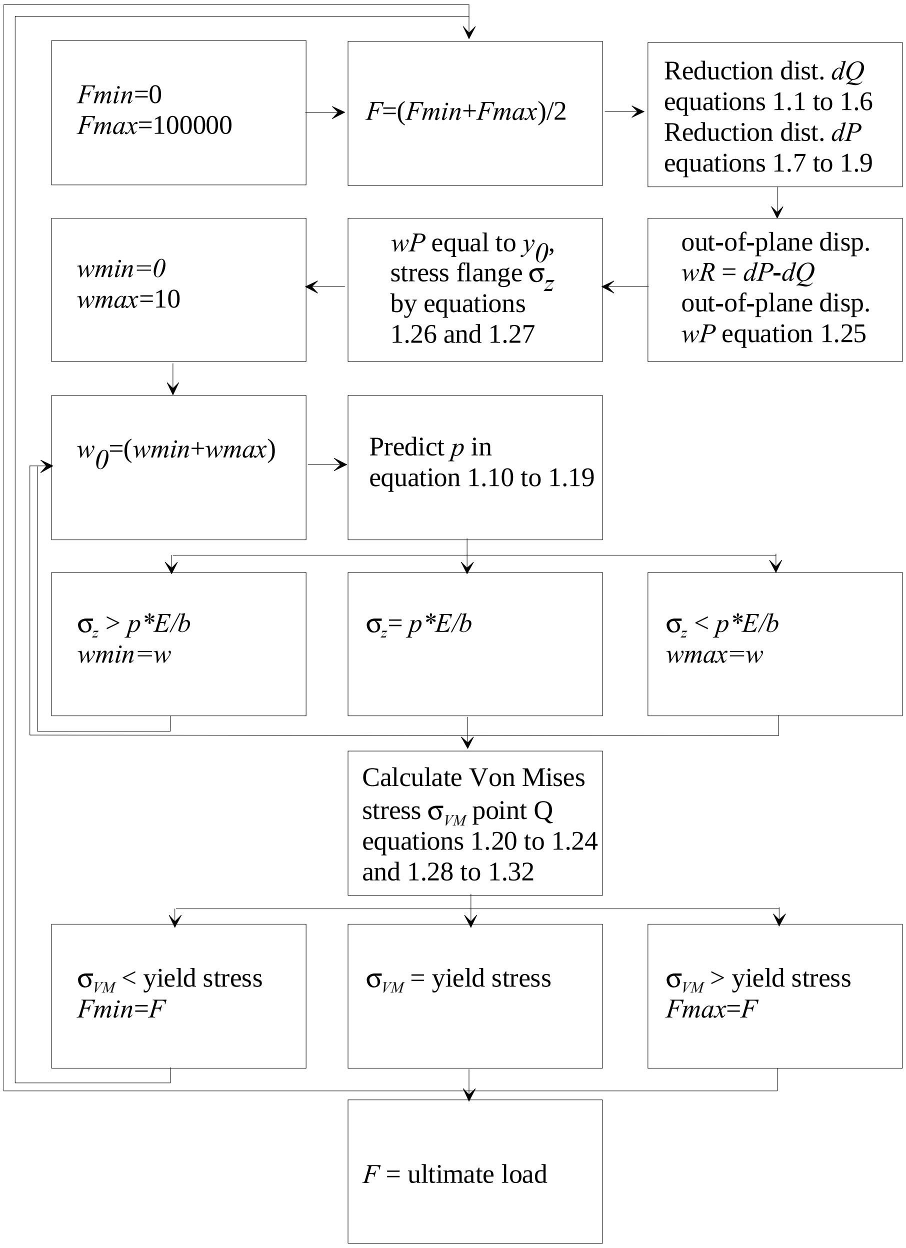

Figure 1-4. Flow diagram of solving process.

Step 5

Marguerre's equations can be used to calculate the stress at point Q (or T) in figure 5-5 of the thesis [Hofm00a]. First equations 1.10 to 1.19 are used to estimate w_0 iterative using a bisection method. Then, equations 1.20 to 1.24 can be used to calculate the various stresses. The Von Misses stress is calculated as:

$$\sigma_{VM1}{}^2 = (\sigma_z + \sigma_{z\,\max})^2 + (\sigma_y + \sigma_{y\,\max})^2 - 2(\sigma_z + \sigma_{z\,\max})(\sigma_y + \sigma_{y\,\max}) + 3\tau_{xz} \tag{1.28}$$

$$\sigma_{VM2}{}^2 = (\sigma_z - \sigma_{z\,\max})^2 + (\sigma_y - \sigma_{y\,\max})^2 - 2(\sigma_z - \sigma_{z\,\max})(\sigma_y - \sigma_{y\,\max}) + 3\tau_{xz} \tag{1.29}$$

$$\sigma_{VM} = \max(|\sigma_{VM1}|, |\sigma_{VM2}|) \tag{1.30}$$

$$x = \frac{1}{2} b_{bbfl} \tag{1.31}$$

$$z = \frac{1}{4} b_{bffl} \text{ for point Q and } z = 0 \text{ for point T} \tag{1.32}$$

Step 6
If this stress σ_{VM} is lower than the yield stress, a higher load F should be tried and vice versa. This iterative process is carried out using a bisection method. If the stress at Q (or T) equals the yield stress, the load F is regarded as the ultimate load.

1.4 Tomà and Stark experiments

Exper-iment	b_{tf}	b_w	b_{bf}	r_{tf} (= r_{bf})	θ_w	L_{span}	L_{lb}	t	f_y	F_{test}	Model F_u	Euro-code3 F_u
A20	119.0	42.1	40.0	4.6	72.0	1080	100	0.71	372.0	2101	1530	2143
A21	77.0	70.9	70.0	6.6	81.0	1080	100	0.82	372.0	4074	2943	4256
A22	77.0	70.9	70.0	6.6	81.0	1080	100	0.82	363.0	4116	2899	4177
A23	77.0	70.9	70.0	6.6	81.0	1080	100	0.71	312.0	2852	2020	3039
A24	77.0	70.9	70.0	6.6	81.0	1080	100	0.71	333.0	2830	2107	3194
A56	90.0	67.2	76.0	4.6	79.0	1080	100	0.69	341.0	3082	2010	3044
C1	119.0	42.1	40.0	4.6	72.0	1080	55	0.72	317.0	1688	1342	1773
C2	119.0	42.1	40.0	4.6	72.0	1080	100	0.72	328.0	1983	1471	1993
C3	119.0	42.1	40.0	4.6	72.0	1080	150	0.72	325.0	2171	1585	2139
C4	40.0	42.1	119.0	4.6	72.0	1080	110	0.72	332.0	2160	1027	1144
C5	40.0	42.1	119.0	4.6	72.0	1080	160	0.71	354.0	2310	1504	1763
C6	40.0	42.1	119.0	4.6	72.0	1080	110	0.71	358.0	2125	1428	1690

1.5 Wing experiments

Experiment	b_{tf}	r_{tf} (= r_{bf})	b_{bf}	b_w	θ_w	L_{span}	L_{lb}	t	f_y	F_{test}	Model F_u	Euro-code3 F_u
1W-CBC	94.0	3.15	47.7	94.7	89.0	457	25.4	1.52	231.0	8852	9669	7701
2W-CBC	95.0	2.87	49.3	94.2	89.5	465	25.4	0.97	274.4	4226	4610	4676
4W-CBC	93.5	3.15	98.8	95.0	88.5	467	25.4	1.52	231.0	11957	18624	11014
10W-CBC	94.5	3.15	48.9	95.0	70.0	508	25.4	1.52	231.0	8452	8601	6862
11W-CBC	96.5	2.87	48.5	96.5	70.0	508	25.4	0.97	274.4	4066	3985	4113
12W-CBC	96.5	2.69	50.0	100.8	70.0	508	25.4	0.61	265.4	1726	2012	1993
13W-CBC	94.5	3.15	98.9	94.7	70.0	508	25.4	1.52	231.0	11903	16541	9794
19W-CBC	96.5	3.15	48.8	95.3	50.5	508	25.4	1.52	231.0	7233	7290	5891
20W-CBC	97.0	2.87	48.5	99.6	50.5	508	25.4	0.97	274.4	3559	3352	3541
21W-CBC	97.5	2.69	50.1	96.5	50.5	508	25.4	0.61	265.4	1557	1628	1719
22W-CBC	94.0	3.15	100.7	95.0	50.0	508	25.4	1.52	231.0	9786	14139	8492
28W-CBC	95.5	2.71	99.8	95.5	90.0	775	25.4	0.64	265.4	2117	3188	2719
29W-CBC	95.5	2.71	99.8	95.5	90.0	775	76.2	0.64	265.4	2616	3423	3504
30W-CBC	95.5	2.69	100.1	95.8	90.0	782	50.8	0.61	265.4	2562	3085	2905
31W-CBC	95.5	2.69	100.4	95.8	90.0	940	50.8	0.61	265.4	2447	2596	2666
32W-CBC	95.5	2.71	100.3	95.8	90.0	940	25.4	0.64	265.4	2002	2690	2519
33W-CBC	95.5	2.69	100.4	97.0	90.0	940	76.2	0.61	265.4	3007	2690	2920
37W-CBC	96.5	2.69	99.8	96.8	70.0	940	25.4	0.61	265.4	1673	2367	2084
38W-CBC	96.0	2.69	99.5	97.0	70.0	940	50.8	0.61	265.4	2117	2428	2406
39W-CBC	96.5	2.69	99.5	97.0	70.0	940	76.2	0.61	265.4	2562	2507	2639
40W-CBC	95.5	2.87	50.7	96.0	70.0	508	25.4	0.97	274.4	3452	4152	4189
41W-CBC	96.5	2.71	54.0	91.2	70.0	508	25.4	0.64	265.4	2002	2217	2262
42W-CBC	94.5	3.15	50.7	94.2	70.0	508	25.4	1.52	231.0	10347	8897	7005
43W-CBC	95.5	3.15	64.0	96.8	50.0	508	25.4	1.52	231.0	10231	9232	6814
44W-CBC	96.5	2.87	63.8	98.6	50.0	508	25.4	0.97	274.4	3229	4328	4014
45W-CBC	96.0	2.87	63.1	123.7	50.0	508	25.4	0.97	274.4	3452	4527	3996
46W-CBC	96.0	2.87	63.8	72.1	50.0	508	25.4	0.97	274.4	3336	4328	3994
47W-CBC	95.0	2.71	100.0	96.0	70.0	508	25.4	0.64	265.4	2847	4462	2810
48W-CBC	95.5	2.71	100.0	96.3	70.0	508	50.8	0.64	265.4	3825	4710	3373
49W-CBC	95.5	2.71	100.0	96.3	70.0	508	76.2	0.64	265.4	4119	4984	3802
50W-CBC	94.0	3.15	104.4	94.5	70.0	508	25.4	1.52	231.0	13647	17439	10008
53W-CBC	93.0	3.15	129.7	98.0	50.0	508	25.4	1.52	231.0	12535	17970	9432
58W-CBC	94.0	3.15	99.1	94.5	90.0	318	50.8	1.52	231.0	16574	26836	6192
59W-CBC	94.0	3.15	99.4	97.5	90.0	318	76.2	1.52	231.0	18238	29352	6192
63W-CBC	94.5	3.15	99.4	97.0	90.0	775	25.4	1.52	231.0	9902	12755	9125
64W-CBC	94.5	2.87	99.7	97.3	90.0	775	25.4	0.97	274.4	4733	6124	5326
65W-CBC	94.0	3.15	99.1	97.8	90.0	927	25.4	1.52	231.0	9341	11056	8351
66W-CBC	94.5	2.87	100.2	97.3	90.0	927	25.4	0.97	274.4	4341	5299	4976
67W-CBC	94.5	3.15	99.1	97.3	90.0	1689	25.4	1.52	231.0	6228	6882	6149
68W-CBC	94.5	2.87	100.5	97.3	90.0	1684	25.4	0.97	274.4	2891	3200	3844
71W-CBC	95.5	2.69	54.1	96.8	70.0	1008	25.4	0.61	265.4	1112	1134	1477
72W-CBC	95.0	2.87	52.8	98.0	70.0	1008	25.4	0.97	274.4	2891	2391	3110
73W-CBC	95.5	3.15	52.4	98.0	70.0	1001	25.4	1.52	231.0	5676	5260	4993
74W-CBC	95.0	2.87	106.1	97.5	70.0	1003	25.4	0.97	274.4	4448	4969	4521
75W-CBC	95.0	3.15	106.5	98.8	70.0	1003	25.4	1.52	231.0	9012	10552	7712

Experiment	b_{tf}	r_{tf} (= r_{bf})	b_{bf}	b_w	θ_w	L_{span}	L_{lb}	t	f_y	F_{test}	Model F_u	Euro-code3 F_u
76W-CBC	96.5	2.69	66.7	99.8	50.0	991	25.4	0.61	265.4	1228	1189	1422
77W-CBC	95.5	2.87	64.8	99.6	50.0	988	25.4	0.97	274.4	3007	2468	3006
78W-CBC	95.5	3.15	66.6	101.1	50.0	998	25.4	1.52	231.0	6121	5493	4939
80W-CBC	96.0	2.87	131.1	99.6	50.0	978	25.4	0.97	274.4	4341	5231	4411
81W-CBC	96.0	3.15	131.7	99.6	50.0	975	25.4	1.52	231.0	9564	11142	7476
82W-CBC	95.5	2.69	53.6	97.0	70.0	1753	25.4	0.61	265.4	890	671	1014
83W-CBC	95.5	2.69	53.6	97.0	70.0	508	25.4	0.61	265.4	2117	2119	2091
84W-CBC	95.0	2.87	53.7	97.5	70.0	1753	25.4	0.97	274.4	1895	1476	2150
85W-CBC	95.0	2.87	53.7	97.5	70.0	508	25.4	0.97	274.4	4119	4397	4299
86W-CBC	94.5	3.15	54.3	98.8	70.0	1753	25.4	1.52	231.0	3781	3364	3613
87W-CBC	94.5	3.15	54.3	98.8	70.0	516	25.4	1.52	231.0	8790	9279	7238
88W-CBC	96.5	2.69	106.8	96.5	70.0	1753	25.4	0.61	265.4	1334	1449	1595
90W-CBC	94.5	2.87	107.7	97.0	70.0	1753	25.4	0.97	274.4	3336	3141	3592
92W-CBC	95.0	3.15	107.3	97.8	70.0	1753	25.4	1.52	231.0	6672	6841	5856
93W-CBC	95.0	3.15	107.3	97.8	70.0	533	25.4	1.52	231.0	11121	17176	9993
94W-CBC	96.0	2.69	64.7	98.8	50.0	1753	25.4	0.61	265.4	890	672	969
95W-CBC	96.0	2.69	64.7	98.8	50.0	521	25.4	0.61	265.4	1895	2078	1920
96W-CBC	96.5	2.87	66.8	99.3	50.0	1740	25.4	0.97	274.4	2002	1525	2280
97W-CBC	96.5	2.87	66.8	99.3	50.0	521	25.4	0.97	274.4	4226	4434	4060
98W-CBC	95.0	3.15	66.6	100.3	50.0	1727	25.4	1.52	231.0	4119	3430	3556
99W-CBC	95.0	3.15	66.6	100.3	50.0	521	25.4	1.52	231.0	8452	9327	6880
102W-CBC	97.0	2.87	132.1	99.3	50.0	1753	25.4	0.97	274.4	3114	3202	3587
104W-CBC	97.0	3.15	134.9	100.1	50.0	1715	25.4	1.52	231.0	7117	7270	5844
105W-CBC	97.0	3.15	134.9	100.1	50.0	533	25.4	1.52	231.0	11121	18017	9525
106W-CBC	96.5	2.69	102.2	96.8	90.0	1758	25.4	0.61	265.4	1557	1461	1703
107W-CBC	96.5	2.69	102.2	96.8	90.0	566	25.4	0.61	265.4	2669	4176	2802
108W-CBC	96.5	2.69	102.2	96.8	90.0	566	50.8	0.61	265.4	3114	4376	3342
109W-CBC	97.5	3.15	51.5	97.8	90.0	1735	25.4	1.52	231.0	4003	3432	3818
110W-CBC	97.5	3.15	51.5	97.8	90.0	559	25.4	1.52	231.0	8896	8818	7441
111W-CBC	97.5	3.15	51.5	97.8	90.0	572	50.8	1.52	231.0	9786	9265	8155
115W-CBC	97.0	2.69	50.6	97.0	90.0	1727	25.4	0.61	265.4	890	678	1067
118W-CBC	98.0	3.15	51.1	98.3	90.0	1024	25.4	1.52	231.0	6005	5339	5297
119W-CBC	96.0	2.87	50.7	97.0	90.0	1011	25.4	0.97	274.4	2669	2427	3306
120W-CBC	96.0	2.69	50.4	97.5	90.0	1003	25.4	0.61	265.4	1334	1123	1530
121W-CBC	96.0	2.87	67.1	95.0	50.0	533	50.8	0.97	274.4	3559	4616	4624
122W-CBC	97.0	3.15	101.7	97.5	90.0	566	101.6	1.52	231.0	19572	19582	14201
123W-CBC	97.0	3.15	102.1	97.8	90.0	559	127.0	1.52	231.0	22241	21198	15326
126W-CBC	95.0	2.69	108.7	92.5	70.0	495	101.6	0.61	265.4	3559	5564	3987
127W-CBC	95.5	2.69	108.4	92.2	70.0	495	127.0	0.61	265.4	4003	5918	4323
130W-CBC	97.0	3.15	100.6	98.0	90.0	318	101.6	1.52	231.0	19261	32898	6192
131W-CBC	97.5	3.15	100.3	97.8	90.0	318	127.0	1.52	231.0	23753	36789	6192
132W-CBC	95.0	2.69	107.4	95.5	70.0	508	101.6	0.61	265.4	4146	5409	3933
133W-CBC	96.5	2.69	108.4	94.7	70.0	508	127.0	0.61	265.4	4083	5813	4278
138W-CBC	94.5	2.87	63.5	95.5	50.0	533	50.8	0.97	274.4	4502	4377	4477
141W-CBC	94.0	3.15	99.1	94.0	90.0	521	25.4	1.52	231.0	14483	17269	10685
142W-CBC	96.0	2.69	100.1	95.8	90.0	775	25.4	0.61	265.4	1833	3009	2496
143W-CBC	95.5	2.87	99.4	95.3	90.0	775	25.4	0.97	274.4	4030	6104	5334

Experiment	b_{tf}	r_{tf} (= r_{bf})	b_{bf}	b_w	θ_w	L_{span}	L_{lb}	t	f_y	F_{test}	Model F_u	Euro-code3 F_u
144W-CBC	94.0	3.15	98.8	94.0	90.0	775	25.4	1.52	231.0	11414	12768	9072
145W-CBC	94.5	2.69	101.5	96.0	90.0	2337	76.2	0.62	269.6	1397	1183	1695
146W-CBC	95.5	2.69	100.4	95.8	90.0	2337	76.2	0.61	269.6	1370	1142	1633
147W-CBC	95.0	2.69	100.3	95.5	90.0	2337	76.2	0.62	269.6	1388	1166	1680
148W-CBC	95.0	2.69	100.6	95.8	90.0	2337	127.0	0.61	269.6	1548	1179	1751
149W-CBC	95.5	2.69	102.4	95.8	90.0	2337	127.0	0.62	269.6	1512	1234	1829
150W-CBC	95.0	2.68	100.7	96.0	90.0	2337	127.0	0.60	269.6	1450	1153	1700
151W-CBC	95.5	2.69	74.7	96.3	90.0	2337	76.2	0.61	269.6	1130	814	1297
152W-CBC	95.0	2.69	75.2	96.0	90.0	2337	76.2	0.61	269.6	1157	819	1304
153W-CBC	95.5	2.68	75.0	95.8	90.0	2337	50.8	0.61	269.6	996	805	1246
154W-CBC	95.5	2.68	75.2	95.8	90.0	2337	50.8	0.61	269.6	979	807	1249
155W-CBC	95.5	2.69	75.1	95.8	90.0	2337	101.6	0.61	269.6	1165	831	1345
156W-CBC	95.5	2.68	75.0	96.3	90.0	2337	101.6	0.61	269.6	1076	831	1344
157W-CBC	94.5	2.69	101.5	96.0	90.0	1016	50.8	0.62	269.6	2242	2531	2677
158W-CBC	95.5	2.69	100.4	95.8	90.0	1016	50.8	0.61	269.6	2144	2446	2586
159W-CBC	95.5	2.69	100.4	95.8	90.0	1016	76.2	0.61	269.6	2651	2516	2821
160W-CBC	95.0	2.69	100.6	95.8	90.0	1016	76.2	0.61	269.6	2642	2521	2824
161W-CBC	95.0	2.69	100.3	95.5	90.0	1016	101.6	0.62	269.6	3123	2644	3101
162W-CBC	95.0	2.69	100.6	95.8	90.0	1016	101.6	0.61	269.6	2785	2597	3017
163W-CBC	95.5	2.69	102.4	95.8	90.0	1016	101.6	0.62	269.6	2740	2712	3138
164W-CBC	95.5	2.69	102.4	95.8	90.0	1016	127.0	0.62	269.6	3060	2800	3316
165W-CBC	95.0	2.68	100.7	96.0	90.0	1016	127.0	0.60	269.6	2882	2627	3097
166W-CBC	95.0	2.68	100.7	96.0	90.0	1016	127.0	0.60	269.6	2971	2627	3097
167W-CBC	95.5	2.69	74.7	96.3	90.0	1016	50.8	0.61	269.6	2019	1757	2207
168W-CBC	95.5	2.69	74.7	96.3	90.0	1016	50.8	0.61	269.6	2019	1757	2207
169W-CBC	95.0	2.69	75.2	96.0	90.0	1016	76.2	0.61	269.6	2215	1822	2395
170W-CBC	95.0	2.69	75.2	96.0	90.0	1016	76.2	0.61	269.6	2126	1823	2395
171W-CBC	95.5	2.68	75.0	95.8	90.0	1016	101.6	0.61	269.6	2402	1878	2539
172W-CBC	95.5	2.68	75.0	95.8	90.0	1016	101.6	0.61	269.6	2251	1878	2539
173W-CBC	95.5	2.68	75.2	95.8	90.0	1016	101.6	0.61	269.6	2384	1883	2544
174W-CBC	95.5	2.69	75.1	95.8	90.0	711	50.8	0.61	269.6	2393	2477	2694
175W-CBC	95.5	2.69	75.1	95.8	90.0	711	50.8	0.61	269.6	2331	2478	2694
176W-CBC	95.5	2.68	75.2	95.8	90.0	711	76.2	0.61	269.6	2260	2589	2967
177W-CBC	95.5	2.68	75.0	96.3	90.0	711	76.2	0.61	269.6	2402	2587	2964
178W-CBC	95.5	2.68	75.0	96.3	90.0	711	101.6	0.61	269.6	3078	2705	3195
179W-CBC	95.5	2.68	75.2	95.8	90.0	406	50.8	0.61	269.6	2740	4362	3411
180W-CBC	95.5	2.69	75.1	95.8	90.0	406	50.8	0.61	269.6	2847	4354	3408
181W-CBC	95.5	2.69	75.1	95.8	90.0	406	76.2	0.61	269.6	3559	4685	3858
182W-CBC	95.5	2.68	75.0	96.3	90.0	406	76.2	0.61	269.6	3185	4694	3856
183W-CBC	95.5	2.68	75.0	96.3	90.0	406	76.2	0.61	269.6	3354	4694	3856
184W-CBC	96.0	2.69	74.4	196.6	90.0	457	76.2	0.62	337.8	3514	8617	4295
185W-CBC	95.5	2.83	73.2	196.6	90.0	457	76.2	0.89	288.9	6628	10583	6684
186W-CBC	96.0	2.69	74.4	196.9	90.0	457	76.2	0.61	337.8	3648	8486	4170
187W-CBC	95.0	2.83	73.6	196.1	90.0	457	76.2	0.89	288.9	6663	10619	6691
188W-CBC	96.0	2.68	74.4	196.6	90.0	584	152.4	0.60	337.8	3825	7374	4509
189W-CBC	95.5	2.83	73.4	196.3	90.0	584	152.4	0.89	288.9	8274	9518	7444
190W-CBC	96.0	2.69	74.3	196.6	90.0	584	152.4	0.61	337.8	3986	7489	4641

Experiment	b_{tf}	r_{tf} (= r_{bf})	b_{bf}	b_w	θ_w	L_{span}	L_{lb}	t	f_y	F_{test}	Model F_u	Euro-code3 F_u
191W-CBC	95.0	2.83	73.4	196.3	90.0	584	152.4	0.89	288.9	8274	9510	7432
192W-CBC	95.0	2.84	74.6	196.1	90.0	584	152.4	0.92	273.7	7918	9550	7553
193W-CBC	95.0	2.84	74.3	195.6	90.0	584	152.4	0.92	273.7	7473	9495	7537
194W-CBC	96.0	2.71	75.5	197.1	90.0	584	152.4	0.66	317.8	4537	7794	5222
195W-CBC	95.5	2.89	73.9	196.6	90.0	584	152.4	1.03	299.2	9786	11783	9422
196W-CBC	96.0	2.71	75.2	197.4	90.0	584	152.4	0.66	317.8	5026	7770	5212
197W-CBC	95.0	2.89	74.3	196.3	90.0	584	152.4	1.03	299.2	10453	11831	9433
198W-CBC	96.0	2.71	74.9	197.1	90.0	432	76.2	0.66	317.8	4048	9329	4765
199W-CBC	95.0	2.89	74.2	196.3	90.0	432	76.2	1.03	299.2	8896	13926	8737
200W-CBC	96.0	2.71	75.3	196.9	90.0	457	76.2	0.66	317.8	4003	8764	4704
201W-CBC	95.5	2.89	74.2	196.6	90.0	457	76.2	1.03	299.2	8452	13074	8547
1WR-CBC	95.5	5.09	85.1	90.4	90.0	2951	50.8	0.63	317.8	1023	843	1327
2WR-CBC	95.5	5.09	85.1	90.4	90.0	1321	50.8	0.63	317.8	1637	1776	2294
4WR-CBC	93.0	5.28	82.4	91.9	90.0	2946	50.8	1.00	299.2	2277	1733	2755
5WR-CBC	93.0	5.28	82.4	91.9	90.0	1321	50.8	1.00	299.2	3932	3525	4630
6WR-CBC	93.0	5.28	82.4	91.9	90.0	508	50.8	1.00	299.2	6219	7950	7052
7WR-CBC	88.4	6.33	83.7	89.4	90.0	2946	50.8	1.54	302.0	4591	4293	4590
8WR-CBC	88.4	6.33	83.7	89.4	90.0	1321	50.8	1.54	302.0	8229	8450	8280
9WR-CBC	88.4	6.33	83.7	89.4	90.0	508	50.8	1.54	302.0	13781	18027	13385
13WR-CBC	93.0	6.78	84.2	87.1	90.0	2946	50.8	0.85	284.1	1646	1267	2161
14WR-CBC	93.0	6.78	84.2	87.1	90.0	1321	50.8	0.85	284.1	2776	2566	3535
16WR-CBC	88.4	6.71	83.0	88.9	90.0	2946	50.8	1.54	302.0	4786	4253	4558
17WR-CBC	88.4	6.71	83.0	88.9	90.0	1321	50.8	1.54	302.0	8469	8372	8221
18WR-CBC	88.4	6.71	83.0	88.9	90.0	508	50.8	1.54	302.0	13505	17824	13288
25WR-CBC	81.3	9.88	84.5	80.0	90.0	2946	50.8	1.54	302.0	4350	4148	4356
26WR-CBC	81.3	9.88	84.5	80.0	90.0	1321	50.8	1.54	302.0	7687	8411	7896
27WR-CBC	81.3	9.88	84.5	80.0	90.0	508	50.8	1.54	302.0	12206	18023	12741
28WR-CBC	98.6	5.09	104.9	94.7	70.0	2946	50.8	0.63	317.8	1219	1040	1422
29WR-CBC	98.6	5.09	104.9	94.7	70.0	1321	50.8	0.63	317.8	2037	2189	2331
31WR-CBC	100.1	5.20	102.8	94.2	70.0	2946	50.8	0.85	284.1	2002	1516	2302
32WR-CBC	100.1	5.20	102.8	94.2	70.0	1321	50.8	0.85	284.1	3265	3098	3779
34WR-CBC	97.5	5.55	105.0	90.2	70.0	2946	50.8	1.55	288.2	5898	5190	5373
35WR-CBC	97.5	5.55	105.0	90.2	70.0	1321	50.8	1.55	288.2	10542	10115	8948
36WR-CBC	97.5	5.55	105.0	90.2	70.0	508	50.8	1.55	288.2	14679	21201	13570
40WR-CBC	97.5	6.85	104.1	96.5	70.0	2946	50.8	1.00	299.2	2642	2105	3102
41WR-CBC	97.5	6.85	104.1	96.5	70.0	1321	50.8	1.00	299.2	4502	4251	4864
43WR-CBC	94.5	7.13	105.4	91.4	70.0	2946	50.8	1.54	302.0	5729	5207	5454
44WR-CBC	94.5	7.13	105.4	91.4	70.0	1321	50.8	1.54	302.0	9795	10144	9050
45WR-CBC	94.5	7.13	105.4	91.4	70.0	508	50.8	1.54	302.0	14875	21158	13598
49WR-CBC	91.4	9.24	105.9	90.4	70.0	2946	50.8	1.00	299.2	2509	2153	3002
50WR-CBC	91.4	9.24	105.9	90.4	70.0	1321	50.8	1.00	299.2	3959	4297	4706
52WR-CBC	92.5	11.90	103.3	87.9	70.0	2946	50.8	1.54	302.0	5213	5129	5289
53WR-CBC	92.5	11.90	103.3	87.9	70.0	1321	50.8	1.54	302.0	8532	10036	8699
54WR-CBC	92.5	11.90	103.3	87.9	70.0	508	50.8	1.54	302.0	13078	21226	12891
58WR-CBC	100.6	7.56	124.8	99.3	50.0	2946	50.8	0.85	284.1	1993	1501	2161
59WR-CBC	100.6	7.56	124.8	99.3	50.0	1321	50.8	0.85	284.1	3381	3082	3429
61WR-CBC	97.5	7.92	125.2	98.0	50.0	2946	50.8	1.55	288.2	6112	4885	5104

Experiment	b_{tf}	r_{tf} (= r_{bf})	b_{bf}	b_w	θ_w	L_{span}	L_{lb}	t	f_y	F_{test}	Model F_u	Euro-code3 F_u
62WR-CBC	97.5	7.92	125.2	98.0	50.0	1321	50.8	1.55	288.2	10987	9592	8325
63WR-CBC	97.5	7.92	125.2	98.0	50.0	508	50.8	1.55	288.2	13478	20085	12299
67WR-CBC	101.1	6.85	126.0	99.1	50.0	2946	50.8	1.00	299.2	2696	2098	3032
68WR-CBC	101.1	6.85	126.0	99.1	50.0	1321	50.8	1.00	299.2	4653	4271	4777
70WR-CBC	99.1	8.73	130.2	96.5	50.0	2946	50.8	1.54	302.0	5925	5189	5459
71WR-CBC	99.1	8.73	130.2	96.5	50.0	1321	50.8	1.54	302.0	10578	10160	8745
72WR-CBC	99.1	8.73	130.2	96.5	50.0	508	50.8	1.54	302.0	14377	21236	12676
76WR-CBC	95.5	10.02	133.3	90.2	50.0	2946	50.8	1.00	299.2	2491	2249	3083
77WR-CBC	95.5	10.02	133.3	90.2	50.0	1321	50.8	1.00	299.2	4226	4494	4659
79WR-CBC	96.5	10.30	130.2	91.9	50.0	2946	50.8	1.54	302.0	5925	5274	5360
80WR-CBC	96.5	10.30	130.2	91.9	50.0	1321	50.8	1.54	302.0	9724	10277	8594
82WR-CBC	82.3	6.85	101.4	98.6	65.0	2946	101.6	1.00	299.2	2535	1961	2874
83WR-CBC	82.3	6.85	101.4	98.6	65.0	1321	152.4	1.00	299.2	5738	4270	5417
88WR-CBC	96.0	7.13	104.5	90.4	65.0	2946	101.6	1.54	302.0	6628	5110	5638
89WR-CBC	96.0	7.13	104.5	90.4	65.0	1321	152.4	1.54	302.0	13718	10724	10598
94WR-CBC	95.5	8.45	129.7	98.8	50.0	2946	101.6	1.00	299.2	3114	2186	3354
95WR-CBC	95.5	8.45	129.7	98.8	50.0	1321	152.4	1.00	299.2	6405	4713	5911
99WR-CBC	90.4	10.30	131.9	97.8	50.0	1321	152.4	1.54	302.0	14902	10995	10392
100WR-CB	90.4	10.30	131.9	97.8	50.0	2946	101.6	1.54	302.0	7322	5282	5608
101WR-CB	95.5	5.09	85.1	90.4	90.0	1321	101.6	0.63	317.8	1842	1852	2612
102WR-CB	93.0	5.28	82.4	91.9	90.0	1321	101.6	1.00	299.2	4777	3694	5195
103WR-CB	88.4	6.33	83.7	89.4	90.0	1321	101.6	1.54	302.0	10249	8878	9130
105WR-CB	93.0	6.78	84.2	87.1	90.0	1321	101.6	0.85	284.1	3514	2674	4007
106WR-CB	88.4	6.71	83.0	88.9	90.0	1321	101.6	1.54	302.0	10587	8785	9065
109WR-CB	81.3	9.88	84.5	80.0	90.0	1321	101.6	1.54	302.0	9519	8766	8717
110WR-CB	98.6	5.09	104.9	94.7	70.0	1321	101.6	0.63	317.8	2331	2281	2692
111WR-CB	100.1	5.20	102.8	94.2	70.0	1321	101.6	0.85	284.1	4288	3235	4342
112WR-CB	97.5	5.55	105.0	90.2	70.0	1321	101.6	1.55	288.2	10871	10624	9991
114WR-CB	97.5	6.85	104.1	96.5	70.0	1321	101.6	1.00	299.2	5542	4427	5561
115WR-CB	94.5	7.13	105.4	91.4	70.0	1321	101.6	1.54	302.0	11859	10597	10131
117WR-CB	91.4	9.24	105.9	90.4	70.0	1321	101.6	1.00	299.2	5320	4461	5395
118WR-CB	92.5	11.90	103.3	87.9	70.0	1321	101.6	1.54	302.0	10871	10415	9773
120WR-CB	100.6	7.56	124.8	99.3	50.0	1321	101.6	0.85	284.1	4920	3205	3973
121WR-CB	97.5	7.92	125.2	98.0	50.0	1321	101.6	1.55	288.2	12482	10008	9352
123WR-CB	101.1	6.85	126.0	99.1	50.0	1321	101.6	1.00	299.2	5534	4449	5509
124WR-CB	99.1	8.73	130.2	96.5	50.0	1321	101.6	1.54	302.0	12651	10579	9868
126WR-CB	95.5	10.02	133.3	90.2	50.0	1321	101.6	1.00	299.2	5489	4664	5406
127WR-CB	96.5	10.30	130.2	91.9	50.0	1321	101.6	1.54	302.0	12882	10680	9706
128WR-CB	95.5	5.09	85.1	90.4	90.0	508	101.6	0.63	317.8	3381	4920	4444
129WR-CB	93.0	5.28	82.4	91.9	90.0	508	101.6	1.00	299.2	7784	8856	8534
130WR-CB	88.4	6.33	83.7	89.4	90.0	508	101.6	1.54	302.0	16681	20029	15929
132WR-CB	93.0	6.78	84.2	87.1	90.0	508	101.6	0.85	284.1	5560	6412	6357
133WR-CB	88.4	6.71	83.0	88.9	90.0	508	101.6	1.54	302.0	17126	19777	15814
136WR-CB	81.3	9.88	84.5	80.0	90.0	508	101.6	1.54	302.0	14902	19828	15180
138WR-CB	100.1	5.20	102.8	94.2	70.0	508	101.6	0.85	284.1	6005	7981	6465
139WR-CB	97.5	5.55	105.0	90.2	70.0	508	101.6	1.55	288.2	19350	23526	16280
141WR-CB	97.5	6.85	104.1	96.5	70.0	508	101.6	1.00	299.2	8896	10577	8397

Experiment	b_{tf}	r_{tf} (= r_{bf})	b_{bf}	b_w	θ_w	L_{span}	L_{lb}	t	f_y	F_{test}	Model F_u	Euro-code3 F_u
142WR-CB	94.5	7.13	105.4	91.4	70.0	508	101.6	1.54	302.0	19795	23333	16342
145WR-CB	92.5	11.90	103.3	87.9	70.0	508	101.6	1.54	302.0	16681	23221	15527
1E-CBC	43.7	4.76	75.9	76.5	85.0	1321	50.8	1.57	293.0	7945	7567	5244
2E-CBC	43.7	4.76	75.9	76.5	85.0	2921	50.8	1.57	293.0	4048	3755	2322
3E-CBC	43.7	4.76	75.9	76.5	85.0	1334	76.2	1.57	293.0	8505	7720	5298
4E-CBC	43.7	4.76	75.9	76.5	85.0	1321	101.6	1.57	293.0	9519	8027	5465
5E-CBC	43.7	4.76	75.9	76.5	85.0	541	50.8	1.57	293.0	13282	15759	9705
6E-CBC	43.7	4.76	75.9	76.5	85.0	521	76.2	1.57	293.0	15515	17220	10770
7E-CBC	43.7	4.76	75.9	76.5	85.0	516	101.6	1.57	293.0	16974	18516	11657
1C-CBC	35.1	3.63	77.3	128.3	81.5	3493	50.8	0.91	286.1	1557	1027	888
2C-CBC	35.1	3.63	77.3	128.3	81.5	3454	76.2	0.91	286.1	1601	1048	905
3C-CBC	35.1	3.63	77.3	128.3	81.5	3462	101.6	0.91	286.1	1699	1056	910
4C-CBC	35.1	3.63	77.3	128.3	81.5	3556	38.1	0.91	286.1	1406	1004	869
5C-CBC	35.1	3.56	77.6	128.5	81.5	3556	38.1	0.76	282.0	1210	763	699
6C-CBC	35.1	3.56	77.6	128.5	81.5	3556	50.8	0.76	282.0	1139	767	702
7C-CBC	35.1	3.56	77.6	128.5	81.5	3556	76.2	0.76	282.0	1281	774	707
8C-CBC	35.1	3.56	77.6	128.5	81.5	3556	101.6	0.76	282.0	1254	781	712
9C-CBC	35.1	3.63	77.3	128.3	81.5	1600	38.1	0.91	286.1	2722	2144	1920
10C-CBC	35.1	3.63	77.3	128.3	81.5	1613	50.8	0.91	286.1	2874	2148	1957
11C-CBC	35.1	3.63	77.3	128.3	81.5	1613	76.2	0.91	286.1	3051	2191	1989
12C-CBC	35.1	3.63	77.3	128.3	81.5	1613	101.6	0.91	286.1	3336	2237	2023
13C-CBC	35.1	3.56	77.6	128.5	81.5	1638	38.1	0.76	282.0	2028	1603	1478
14C-CBC	35.1	3.56	77.6	128.5	81.5	1588	50.8	0.76	282.0	2224	1666	1559
15C-CBC	35.1	3.56	77.6	128.5	81.5	1588	76.2	0.76	282.0	2358	1698	1627
16C-CBC	35.1	3.56	77.6	128.5	81.5	1588	101.6	0.76	282.0	2616	1733	1654
17C-CBC	35.1	3.63	77.3	128.3	81.5	648	38.1	0.91	286.1	5053	4952	3613
18C-CBC	35.1	3.63	77.3	128.3	81.5	635	50.8	0.91	286.1	5365	5158	3846
19C-CBC	35.1	3.63	77.3	128.3	81.5	648	76.2	0.91	286.1	6183	5292	4119
20C-CBC	35.1	3.63	77.3	128.3	81.5	635	101.6	0.91	286.1	6939	5672	4466
21C-CBC	35.1	3.56	77.6	128.5	81.5	635	38.1	0.76	282.0	3737	3938	2803
22C-CBC	35.1	3.56	77.6	128.5	81.5	635	50.8	0.76	282.0	4092	4024	2959
23C-CBC	35.1	3.56	77.6	128.5	81.5	648	76.2	0.76	282.0	4849	4120	3183
24C-CBC	35.1	3.56	77.6	128.5	81.5	648	101.6	0.76	282.0	5320	4317	3412
1U-CBC	32.0	4.35	38.9	75.4	70.0	1651	50.8	0.79	291.6	952	722	724
2U-CBC	32.0	4.35	38.9	75.4	70.0	1702	38.1	0.79	291.6	1032	694	696
3U-CBC	32.0	4.35	38.9	75.4	70.0	1638	50.8	0.79	291.6	1085	727	729
4U-CBC	32.0	4.35	38.9	75.4	70.0	1651	38.1	0.79	291.6	1014	714	718
5U-CBC	32.0	4.35	38.9	75.4	70.0	699	50.8	0.79	291.6	1886	1602	1675
6U-CBC	32.0	4.35	38.9	75.4	70.0	762	38.1	0.79	291.6	1886	1449	1514
7U-CBC	32.0	4.35	38.9	75.4	70.0	737	50.8	0.79	291.6	2171	1526	1610
8U-CBC	32.0	4.35	38.9	75.4	70.0	775	38.1	0.79	291.6	1957	1427	1496
9U-CBC	32.0	4.35	38.9	75.4	70.0	1638	50.8	0.79	291.6	1041	727	729
10U-CBC	32.0	4.35	38.9	75.4	70.0	1664	38.1	0.79	291.6	1165	708	712
11U-CBC	32.0	4.35	38.9	75.4	70.0	1651	50.8	0.79	291.6	996	722	724
12U-CBC	32.0	4.35	38.9	75.4	70.0	1651	38.1	0.79	291.6	1165	714	718
13U-CBC	32.0	4.35	38.9	75.4	70.0	1626	50.8	0.79	291.6	1094	732	735
14U-CBC	32.0	4.35	38.9	75.4	70.0	1638	38.1	0.79	291.6	1050	719	724

Experiment	b_{tf}	r_{tf} (= r_{bf})	b_{bf}	b_w	θ_w	L_{span}	L_{lb}	t	f_y	F_{test}	Model F_u	Euro-code3 F_u
15U-CBC	32.0	4.35	38.9	75.4	70.0	1626	50.8	0.79	291.6	1130	732	735
16U-CBC	32.0	4.35	38.9	75.4	70.0	1638	38.1	0.79	291.6	979	719	724
17U-CBC	32.0	4.35	38.9	75.4	70.0	381	50.8	0.79	291.6	3737	2779	2522
18U-CBC	32.0	4.35	38.9	75.4	70.0	394	38.1	0.79	291.6	3398	2592	2331
19U-CBC	32.0	4.35	38.9	75.4	70.0	406	50.8	0.79	291.6	3594	2622	2426
20U-CBC	32.0	4.35	38.9	75.4	70.0	394	38.1	0.79	291.6	3701	2592	2331
21U-CBC	32.0	4.35	38.9	75.4	70.0	470	50.8	0.79	291.6	3016	2296	2210
22U-CBC	32.0	4.35	38.9	75.4	70.0	368	38.1	0.79	291.6	3318	2754	2422
23U-CBC	32.0	4.35	38.9	75.4	70.0	432	50.8	0.79	291.6	2838	2478	2333
24U-CBC	32.0	4.35	38.9	75.4	70.0	381	38.1	0.79	291.6	3167	2671	2375
25U-CBC	32.0	4.35	38.9	75.4	70.0	686	76.2	0.79	291.6	2393	1717	1813
26U-CBC	32.0	4.35	38.9	75.4	70.0	724	76.2	0.79	291.6	2384	1631	1737
55R-CBC	21.8	2.20	59.5	24.1	45.0	1626	38.1	1.20	284.8	2091	1259	818
56R-CBC	21.8	2.20	59.5	24.1	45.0	1626	50.8	1.20	284.8	2144	1270	824
57R-CBC	21.8	2.20	59.5	24.1	45.0	1626	76.2	1.20	284.8	2197	1291	838
58R-CBC	21.8	2.20	59.5	24.1	45.0	660	38.1	1.20	284.8	4644	3211	2088
59R-CBC	21.8	2.20	59.5	24.1	45.0	660	50.8	1.20	284.8	4946	3280	2132
60R-CBC	21.8	2.20	59.5	24.1	45.0	660	76.2	1.20	284.8	5338	3422	2225
64R-CBC	21.8	1.92	61.0	24.1	45.0	1626	38.1	0.65	336.5	916	822	528
65R-CBC	21.8	1.92	61.0	24.1	45.0	1626	50.8	0.65	336.5	988	831	532
66R-CBC	21.8	1.92	61.0	24.1	45.0	1626	76.2	0.65	336.5	996	850	541
67R-CBC	21.8	1.92	61.0	24.1	45.0	660	38.1	0.65	336.5	1717	1922	1242
68R-CBC	21.8	1.92	61.0	24.1	45.0	660	50.8	0.65	336.5	1939	1984	1294
69R-CBC	21.8	1.92	61.0	24.1	45.0	660	76.2	0.65	336.5	2197	2112	1385

1.6 Tsai experiments

Exper-iment	b_{tf}	r_{tf} (= r_{bf})	b_{bf}	b_w	θ_w	L_{span}	L_{lb}	t	f_y	F_{test}	Model F_u	Euro-code3 F_u
191	35.2	6.4	56.4	100.6	78.7	560	100	0.83	294.0	4363	3496	3681
192	35.2	6.4	56.4	100.6	78.7	720	100	0.83	294.0	3948	2917	2860
193	35.2	6.4	56.4	100.6	78.7	1040	100	0.83	294.0	2915	2170	1996
194	35.2	6.4	56.4	100.6	78.7	1200	100	0.83	294.0	2480	1898	1736
195	35.2	6.4	56.4	100.6	78.7	1520	100	0.83	294.0	2053	1471	1381
196	35.2	6.4	56.4	100.6	78.7	2000	100	0.83	294.0	1615	1099	1057
291	62.5	8.4	55.4	61.6	75.4	560	100	0.85	306.0	4608	4340	3848
292	62.5	8.4	55.4	61.6	75.4	720	100	0.85	306.0	3930	3750	3080
293	62.5	8.4	55.4	61.6	75.4	1040	100	0.85	306.0	2920	2977	2224
294	62.5	8.4	55.4	61.6	75.4	1200	100	0.85	306.0	2690	2698	1960
295	62.5	8.4	55.4	61.6	75.4	1520	100	0.85	306.0	2255	2272	1587
296	62.5	8.4	55.4	61.6	75.4	2000	100	0.85	306.0	1660	1766	1239

2 Appendix post-failure mechanical models

2.1 Methodology

Introduction
This section 2.1 presents a methodology to develop post-failure mechanical models. In this report, it is tried to treat the development systematically. For instance, there are different methods to find the ultimate load using a load deformation curve, this is presented in sections 2.1.1 and 2.1.2. Sheet section behaviour can be split up in several "components", which will be explained in section 2.1.3 and 2.1.4. In the final section (2.1.5), some mathematical techniques will be presented to simplify the post-failure mechanical models developed.

2.1.1 Prediction ultimate load

Definition of the ultimate load
Figure 2-1 presents the three possible load deformation curves for sheet sections in a three-point bending test: one for each post-failure mode. The y-axis indicates the load. The x-axis indicates the web crippling deformation. See appendix 1, figure 1-1, for an explanation of web crippling deformation.

For all three post-failure modes, the ultimate load is defined by the highest load that can be found in the curve.

Three types of behaviour
If a sheet section is loaded in a three point bending test (like the experiments in chapter 3 of the thesis [Hofm00a]), the entire sheet section will first behave elastically. This means that when the sheet section is unloaded, it will return to its original shape. If the sheet section is deformed further, a local part of the sheet section will behave plastically. This means that if the section is unloaded, this local part will remain deformed. The behaviour from the start of loading until first local plastic behaviour is defined as elastic behaviour. During further increase of deformation, increasingly local parts will become plastic until no other parts will become plastic. The behaviour from first local plastic behaviour until no other parts will become plastic is defined as elasto-plastic behaviour. Further increase of the deformation leads to more plastic deformation in all local plastic parts. However, no new local plastic parts will occur. At that moment, further sheet section behaviour is defined as plastic behaviour. For elasto-plastic and plastic behaviour, elastic deformations still can increase in elastic areas of the section. For plastic behaviour however, these elastic deformations are negligible compared to plastic deformations.

Determination of the ultimate load
Figure 2-2 shows the load deformation curve for a sheet section again. In these diagrams elastic, elasto-plastic, and plastic behaviour are shown. The curve for the yield eye post-failure mode is left out, because the curve is the same as the yield arc post-failure mode, only the plastic part of the curve moves back after the ultimate load.

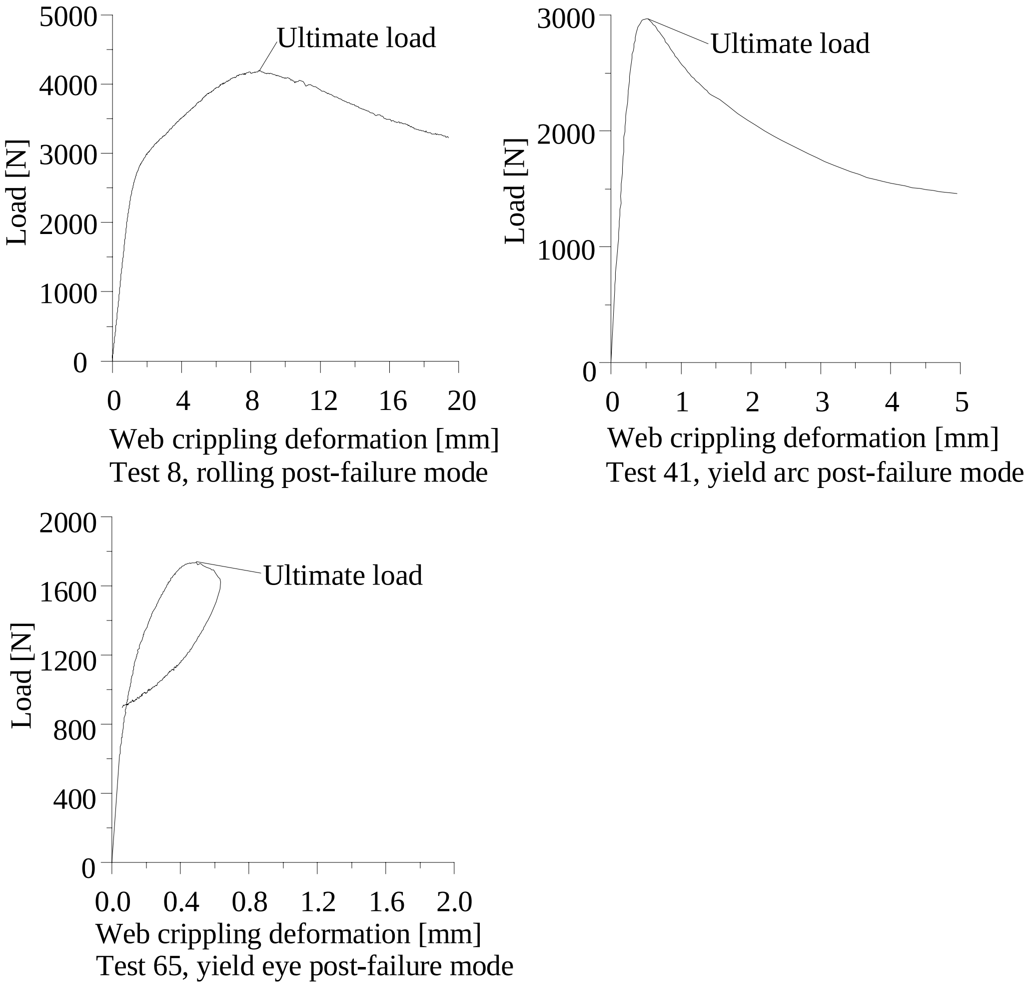

Figure 2-1. Rolling (test 8), yield arc (test 41), and yield eye (test 65) post-failure modes.

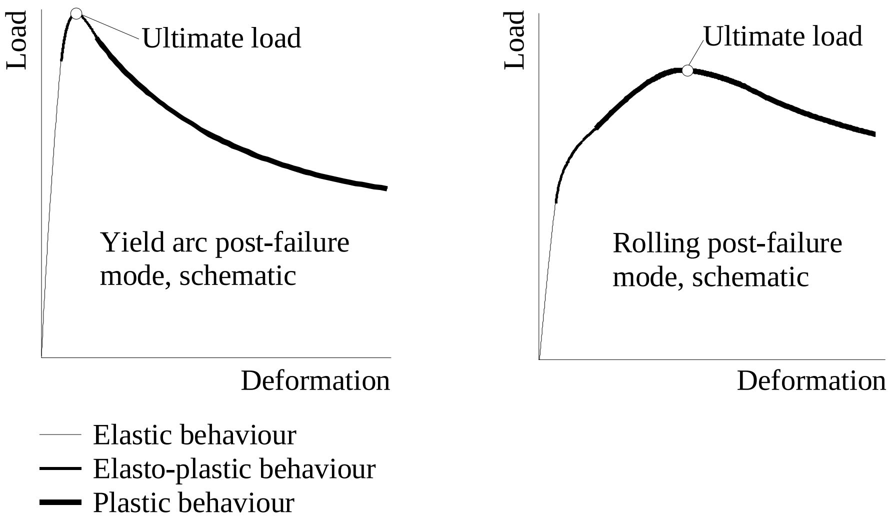

Figure 2-2. Elastic, elasto-plastic, and plastic behaviour of a sheet section.

It is possible to predict the ultimate load by describing the elastic, elasto-plastic, and plastic behaviour of the sheet section, in other words, to describe the entire curve figure 2-2 shows. Then the maximum value of the curve is regarded as the ultimate load. However, to describe all three types of behaviour, and specially the elasto-plastic behaviour, is a complex task. Some simplifications have been developed to overcome this problem. In section 2.1.2, two methods will be presented that neglect elasto-plastic or neglect both elasto-plastic and plastic behaviour to predict the ultimate load. Section 2.1.3 will present a method to simplify the description of elastic and plastic behaviour using the principle of components.

In the next sections, elastic behaviour can be linear or non-linear, regardless the example curves that show often linear behaviour. Plastic behaviour is always non-linear.

2.1.2 Neglecting types of behaviour

Method A: neglecting elasto-plastic behaviour

It is possible to intersect theoretical curves representing elastic and plastic behaviour to predict the ultimate load. Figure 2-3 shows the ultimate load prediction for three possibilities: a negative slope of the plastic curve, a zero slope, and a positive slope of the plastic curve.

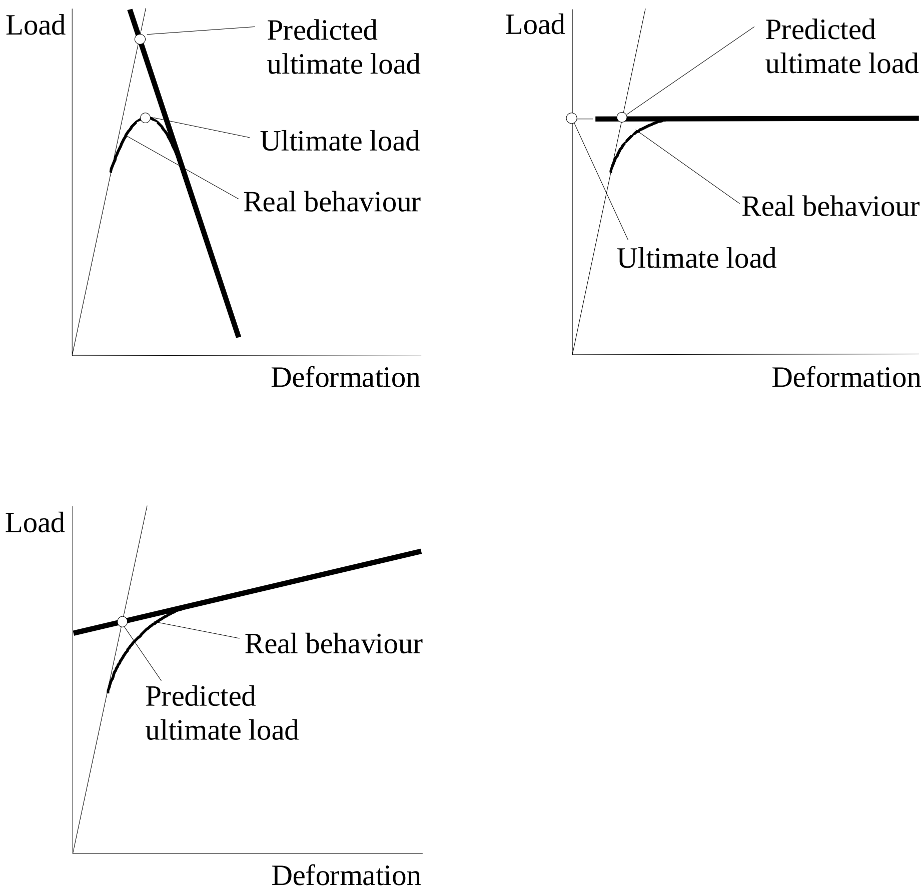

Figure 2-3. Prediction of the ultimate load for three different plastic curves. Line definitions are listed in figure 2-2.

If the plastic curve has a negative slope, the prediction of the ultimate load is an overestimation of the (real) ultimate load. If the plastic curve has a positive slope, the ultimate load is not known, but at least the predicted ultimate load is an underestimation of the ultimate load. If the plastic curve has a zero slope, the predicted ultimate load equals the ultimate load. This method A has similarities with the method of Merchant-Rankine [Merc56a].

Method A for sheet sections
In the case of a sheet section, only plastic curves as shown in figure 2-4 occur. This figure 2-4 presents the consequences for sheet sections for predicting the ultimate load by intersecting a theoretical elastic and plastic curve.

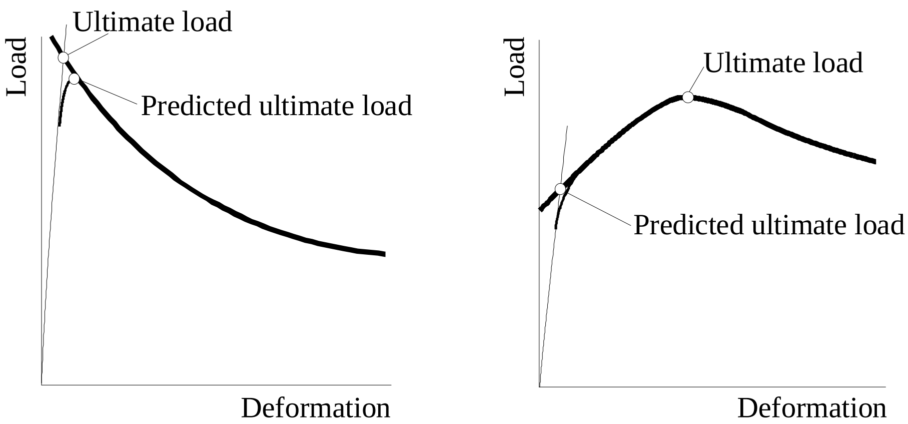

Figure 2-4. Prediction of the ultimate load for a sheet section. Line definitions in figure 2-2.

If the plastic curve has a negative slope, the prediction of the ultimate load is an overestimation of the (real) ultimate load. If the plastic curve increases first but decreases thereafter, the predicted ultimate load is an underestimation of the (real) ultimate load.

Method B: neglect both elasto-plastic and plastic behaviour
To predict the ultimate load, it is also possible to assume that the ultimate load is reached at the moment elasto-plastic behaviour starts. This means a very small local part of the sheet section yields but in fact the sheet section acts still largely elastic. This method was used for the development of the ultimate failure mechanical model in chapter 5 of the thesis [Hofm00a]. Figure 2-5 presents this assumption for the ultimate load for a sheet section.

For method B, the predicted ultimate load is always an underestimation of the ultimate load. This method B has similarities with the method of Perry-Robertson [Robe28a].

2.1.3 The principle of elastic and plastic components

This section explains the principle of components. The components will be introduced using the example of a U-section under axial load. Method A of section 2.1.2 is used. However, the principle of splitting up the behaviour into components is (of course) also applicable to method B of section 2.1.2. Then, only elastic components are used.

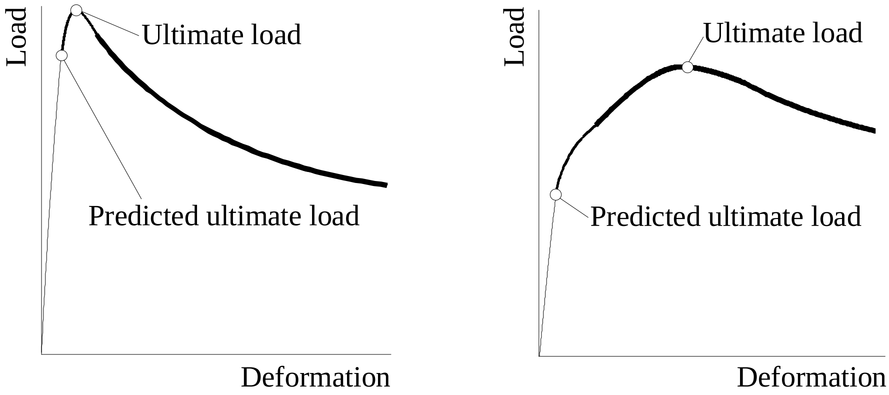

Figure 2-5. Assumption that ultimate load is reached if elasto-plastic behaviour starts. Line definitions are listed in figure 2-2.

As mentioned in section 2.1.1, sheet section behaviour can be split up into elastic, elasto-plastic, and plastic behaviour. In this section, only elastic and plastic behaviour will be studied. This because elasto-plastic behaviour will not be used in either method A or B (in section 2.1.2).

Figure 2-6 shows a U-section under compression. Only elastic and plastic behaviour is presented. Elastic buckling is not taken into account to keep the example as simple as possible, thus the elastic behaviour is linear. The intersection of the elastic and plastic curve predicts the ultimate load.

Figure 2-6 shows the elastic curve of the U-section. This curve can be derived by using Hooke's law. The total area A_t equals the area of the web A_w and the two flanges $2A_f$. Formula 2.1 describes the elastic curve.

$$F = u\frac{E * A_t}{h} \tag{2.1}$$

Figure 2-7 presents this curve again, now labelled with A_t. It can be assumed that only the web of the U-section has certain stiffness and the flanges have no stiffness. This means the elastic curve should be derived making only use of the web area A_w (see also formula 2.1). Figure 2-7 shows this curve on the left labelled with 'A_w'. Alternatively, it can be assumed that only the two flanges have certain stiffness. This elastic curve, based on the area of the two flanges $2A_f$ is also shown in figure 2-7 on the left indicated with '$2A_f$'.

If the elastic curves '$2A_f$' or 'A_w' are used to predict the ultimate load instead of curve 'A_t', the prediction will differ from the originally derived prediction of the ultimate load. These differences d_1 and d_2 are shown in figure 2-7 on the right. It is possible that difference d_1 is small enough to justify the simplification of only bringing the stiffness of the two flanges into account. If difference d_2 is large, this indicates the stiffness of the two flanges can not be neglected to predict the ultimate load.

The elastic behaviour of the web (and thus the curve A_w) is defined as a component. In the same way, the elastic behaviour of the two webs (curve $2A_f$) is defined as a component.

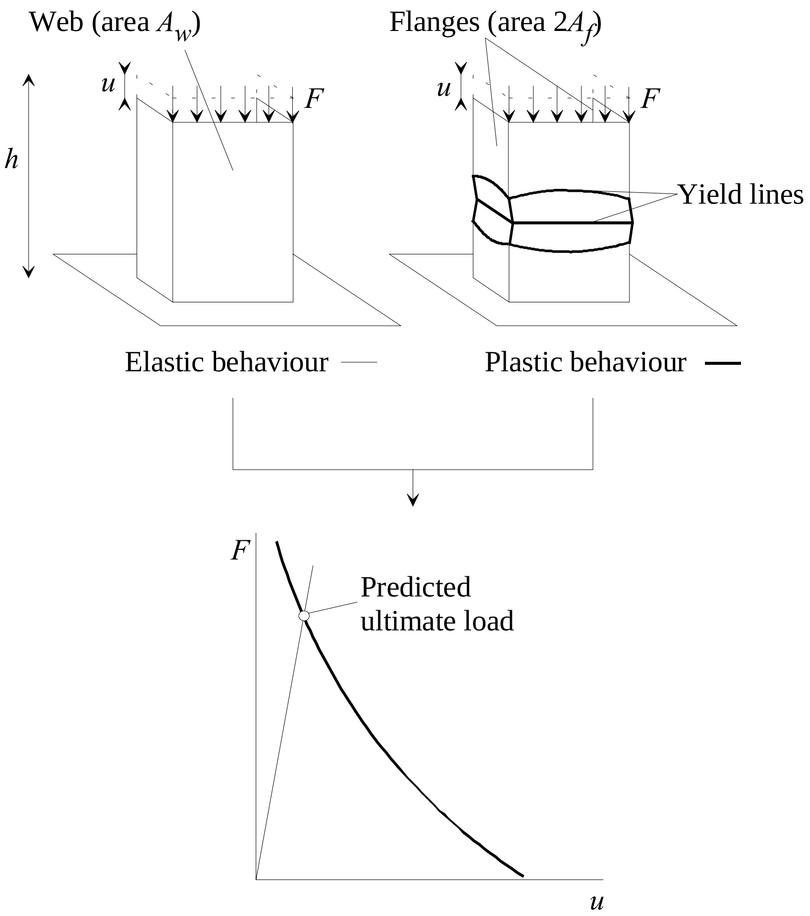

Figure 2-6. U-section under compression. Intersection of elastic and plastic curves predicts the ultimate load.

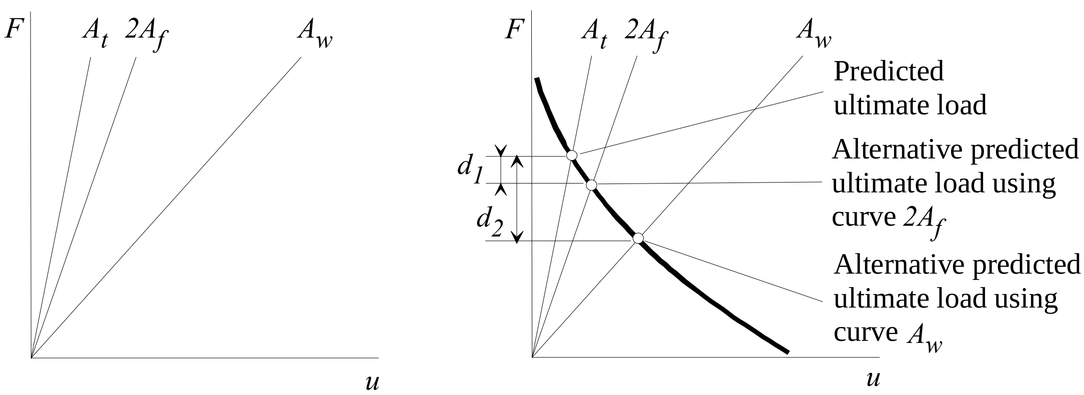

Figure 2-7. On the left different elastic curves for the U-section. On the right predictions of the ultimate load are made for different elastic curves.

Plastic components U-section

Plastic behaviour can be split up into components using the same method as for elastic components. Figure 2-6 on the right shows the U-section plastically deformed. Yield lines are located in the web and in the two flanges. Now, it is assumed that only in the web yield lines occur and that the flanges have no stiffness. The plastic behaviour for the web is described by the curve shown in figure 2-8 on the left.

If it is assumed that yield lines only occur in the two flanges and the web has no stiffness, than another curve presents the plastic behaviour, also shown in figure 2-8 on the left. If the plastic curve for the web only is used to predict the ultimate load, there is a difference d_1 between the predicted ultimate load and the alternatively predicted one. If this difference is small, it is acceptable to use the plastic curve for the web only, in other words to neglect the plastic behaviour of the flanges. Difference d_2 occurs if the alternative predicted load is determined using the plastic curve of the flanges only. This difference is large, with means that taking only into account the plastic behaviour of the flanges is not sufficient: the plastic web behaviour should also be taken into account.

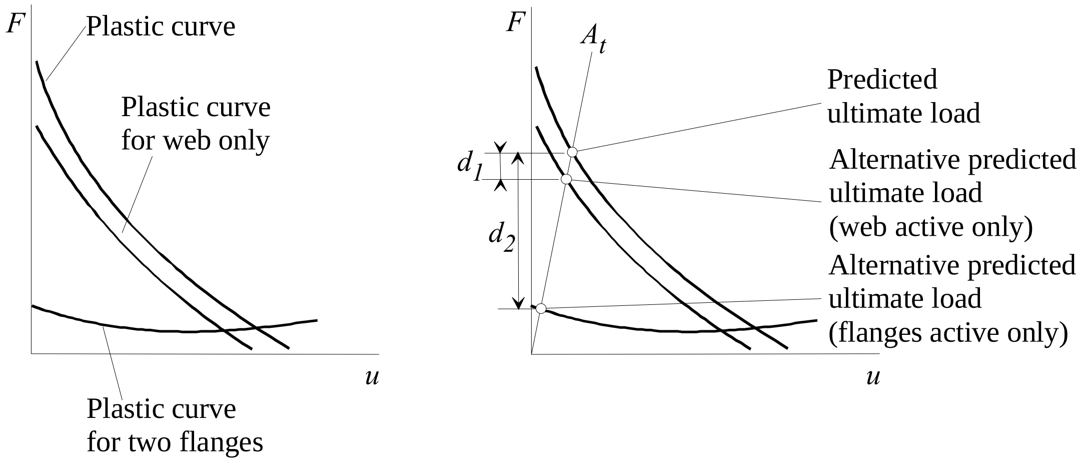

Figure 2-8. Different descriptions of the plastic curve lead to different predictions of the ultimate load.

General framework for components

The idea of splitting elastic or plastic behaviour into components can now be presented in a more general framework. Figure 2-9 presents this framework. The elastic and plastic behaviour can be presented as an elastic and plastic curve. The elastic and plastic curve can only be described by many complex formulae. If the behaviour (elastic or plastic) is split up into components, as explained, each component is described by a much more simple formula. For each component, the influence on the prediction of the ultimate load can be investigated as described in figure 2-7 and figure 2-8. If this influence on the prediction is not large, the component can be left out. Thus, the prediction of the ultimate load will be simplified.

Summary

The ultimate load of a sheet section was defined. It is very difficult to predict this load by describing elastic, elasto-plastic, and plastic behaviour. Two methods are introduced to predict the ultimate load: the intersection of the elastic and plastic curves (A) or to predict the ultimate load by the start of elasto-plastic behaviour (B). Components make it possible to simplify the description of elastic and plastic curves.

2.1.4 Corrections for method A

The previous section introduced components and their ability to reduce the complexity of describing the elastic and plastic curve. If components are used, another possibility shows up to simplify the prediction of the ultimate load. It can be seen as an correction of method A.

In section 2.1.2, the ultimate load was predicted by calculating the intersection of the elastic and the plastic curve. In the case of the U-section of section 2.1.3, figure 2-6 shows this prediction. At the moment of presenting figure 2-6 for the first time, components were not defined. Thus, elastic and plastic curves describe all components of the U-section's behaviour. In other words: both flange and web behaviour (elastic and plastic) are taken into account.

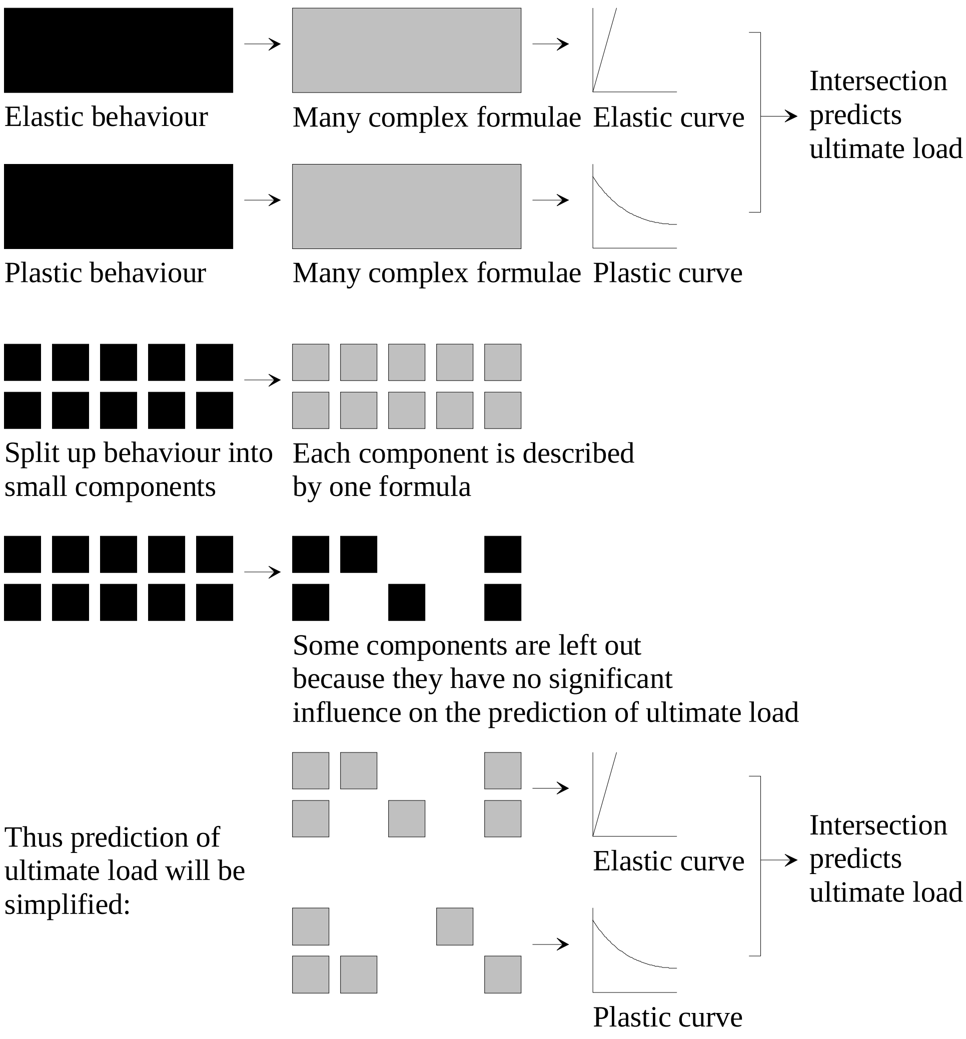

Figure 2-9. Elastic and plastic behaviour are split up into components. Some components can be neglected, thus making the prediction of the ultimate load less complex.

The calculation of the intersection in figure 2-6 is complex because the elastic curve is described by the flanges and web elasticity and the plastic curve is described by the plastic behaviour of both flanges and web. If the elastic and plastic loads are set equal, the displacement should be solved out of the large formulae describing elastic and plastic behaviour. If the elastic and plastic formulae would be simple, the displacement could be solved more easily.

In section 2.1.3, it was clear (qualitative) that for elastic behaviour of the U-section, the flanges' elasticity was an important factor, whereas the web elasticity was less important (see also figure 2-7). For plastic behaviour, web behaviour was far more important than flange behaviour. So, the intersection of elastic and plastic behaviour could be determined by the intersection of the elastic curve for only flange behaviour and the plastic curve for only web behaviour. Figure 2-10 shows this on the right (on the left a normal prediction taking all components into account). It seems that this is exactly the same as presented as method A. However, for method A it was important that the difference between the predicted ultimate load and the real ultimate load was small. For this method, the difference between the ultimate and the predicted ultimate load needs not to be small, because it can be corrected afterwards as shown in the next paragraph.

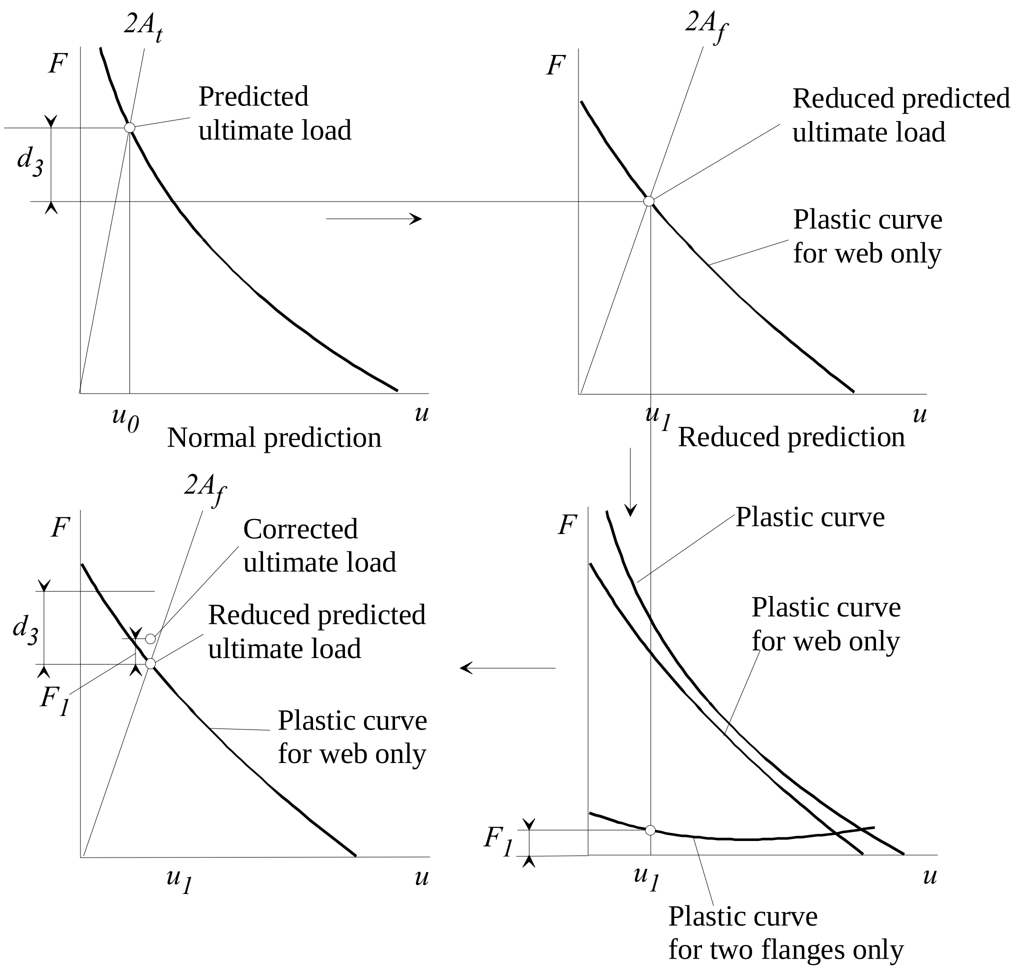

Figure 2-10. Ultimate load is predicted by using only a few components for elastic and plastic behaviour. Thereafter the reduced predicted ultimate load is corrected for plastic components that were left out.

The ultimate load was predicted by the intersection of an elastic and plastic curve using only the most contributing components. This predicted load will be defined as "Reduced predicted ultimate load". Figure 2-10 shows that the plastic curves for the web or the two flanges are known (figure 2-8 present these). It is possible to find out for u_1 (the deformation at reduced predicted ultimate load) which plastic load is needed to deform the two flanges F_1**.** The plastic behaviour of the flanges was not taken into account during the prediction of the ultimate load. Load F_1 can be added to the reduced predicted ultimate load to correct for the plastic behaviour of the flanges.

Note that the correction does not restore accuracy completely. If the intersection between the elastic curve and the plastic curve was calculated for the complete plastic curve (all components), u_1 would equal u_0, and thus load F_1.would equal d_3.

2.1.5 Mathematical techniques

In section 2.1.3, components were presented. Each component was described by a formula. These formulae can be simplified by mathematical techniques like sensitivity analysis, rewriting of formulae, etc. In the next few paragraphs, these mathematical techniques will be introduced. The mathematical techniques are coded by the character 'M' and a sequential number.

M1: removing small terms in defined variable space

This technique makes it possible to remove certain terms in a formula because for all possible values of variables, these terms do not have significant influence on the formula output. A possible formula for a component is:

$$f(x,y,z) = g(x,y) + h(y,z) + i(x,z) \tag{2.2}$$

Because the variables *x*, *y*, and *z* have a practical meaning, (for instance *x* could be the plate thickness), their values will be restricted to practical values as follows:

$$a < x < b \tag{2.3}$$

$$c < y < d \tag{2.4}$$

$$e < z < f \tag{2.5}$$

This set of constrains (formula 2.3 to 2.5) is defined as a defined variable space. Changing *x*, *y*, and *z* between their minimal and maximal values, the value for the functions *g*, *h*, and *i* can be calculated. Figure 2-11 presents these values.

Function *f* should be simplified within the defined variable space and function *g*, *h*, or *i* should be removed. Figure 2-11 shows clearly that function *i* can be removed more easily than functions *g* or *h*. Thus the simplified function will be:

$$f(x,y,z) = g(x,y) + h(y,z) \tag{2.6}$$

M2: Assuming small angles
A function describing a component can contain variables that describe angles. It is possible that these angles are so small, that it is allowed to simplify sine- and cosine-functions as follows:

$$\sin(\alpha) = \alpha \tag{2.7}$$

$$\cos(\alpha) = 1 \tag{2.8}$$

M3: Making complex functions linear
This technique makes complex functions linear. Functions can be made linear to make them more simple. It can also be necessary to make functions linear to write a variable in this function explicitly. An example will explain this.

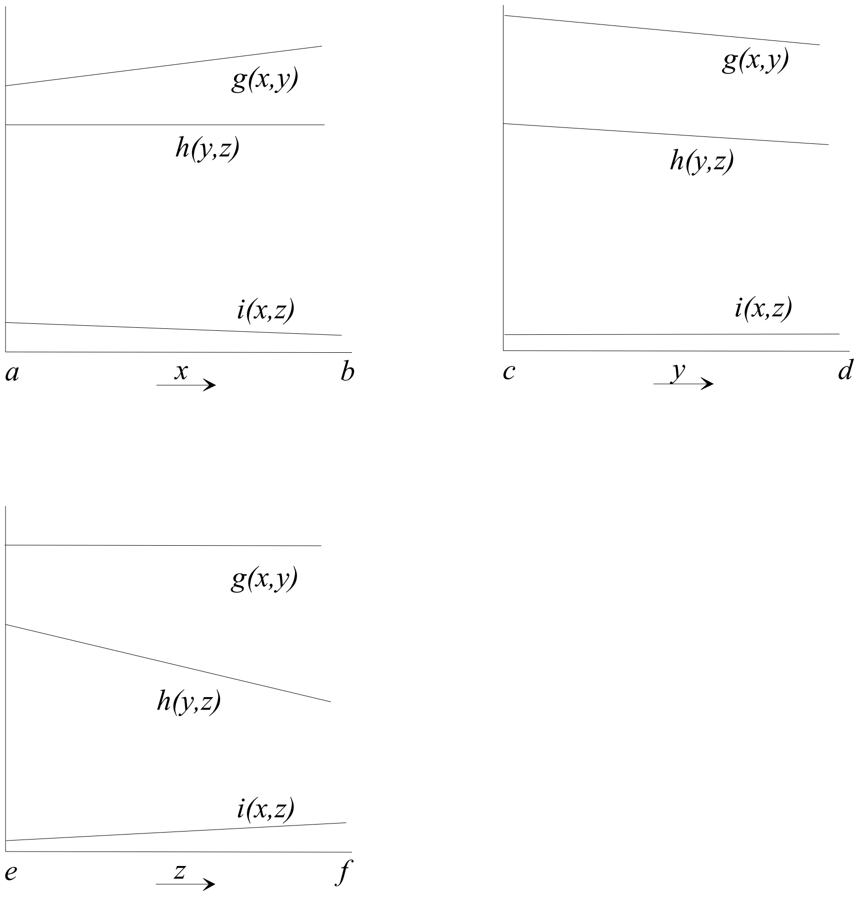

Figure 2-11. For x, y, and z, function i values can be neglected.

A component is described by the following function:

$$f(x, y, z) \tag{2.9}$$

Assume it is necessary to rewrite this formula in such a way that the variable *x* is explicitly written:

$$f(x, y, z) \Leftrightarrow x = g(y, z) \tag{2.10}$$

Assume it is very difficult to rewrite formula 2.10 in this way. Therefore, formula 2.9 will be made linear as follows. First, the behaviour of formula 2.9 will be observed in a defined variable space. This space is:

$$a < x < b \tag{2.11}$$

$$c < y < d \tag{2.12}$$

$$e < z < f \tag{2.13}$$

In figure 2-12 on the left, *x* is varied whereas *y* and *z* remain constant. There is a linear relation between function *f* and *x*. On the right and bottom in figure 2-12, the relations between *f* and variable *y* and *z* are shown.

Regarding figure 2-12, a possible linear form of formula 2.9 could be:

$$f(x, y, z) = Ax + By + Cy^2 + Dz + E \tag{2.14}$$

Parameters A, B, C, D, and E can be found by the well-known technique of regression analysis. It is not difficult to see that rewriting formula 2.14 leads to:

$$x = -\frac{By + Cy^2 + Dz + E}{A} \tag{2.15}$$

M4: Selecting terms to minimise a variable

It is possible that a value for a variable should be found by minimising the function of a component. As an example, it is possible that the ultimate load of a sheet section is minimal for a certain distance between two yield lines. This technique M4 makes it more easy to find a reasonable approximation for this distance. An example: the load of a component equals:

$$F_u = (x, y, z) \tag{2.16}$$

To find for which value of *x* function 2.16 is minimal, the function should be differentiated with respect to *x* and the root of this function equal to zero should be found. Consequently, a very complex formula occurs.

It is worth trying to differentiate only a part of the function with respect to *x* and find the root, because a less complex formula occurs.

Thus:

$$\frac{\partial F_u}{\partial x} = \frac{\partial(x, y)}{\partial x} = 0 \Leftrightarrow x = g(x, y) \tag{2.17}$$

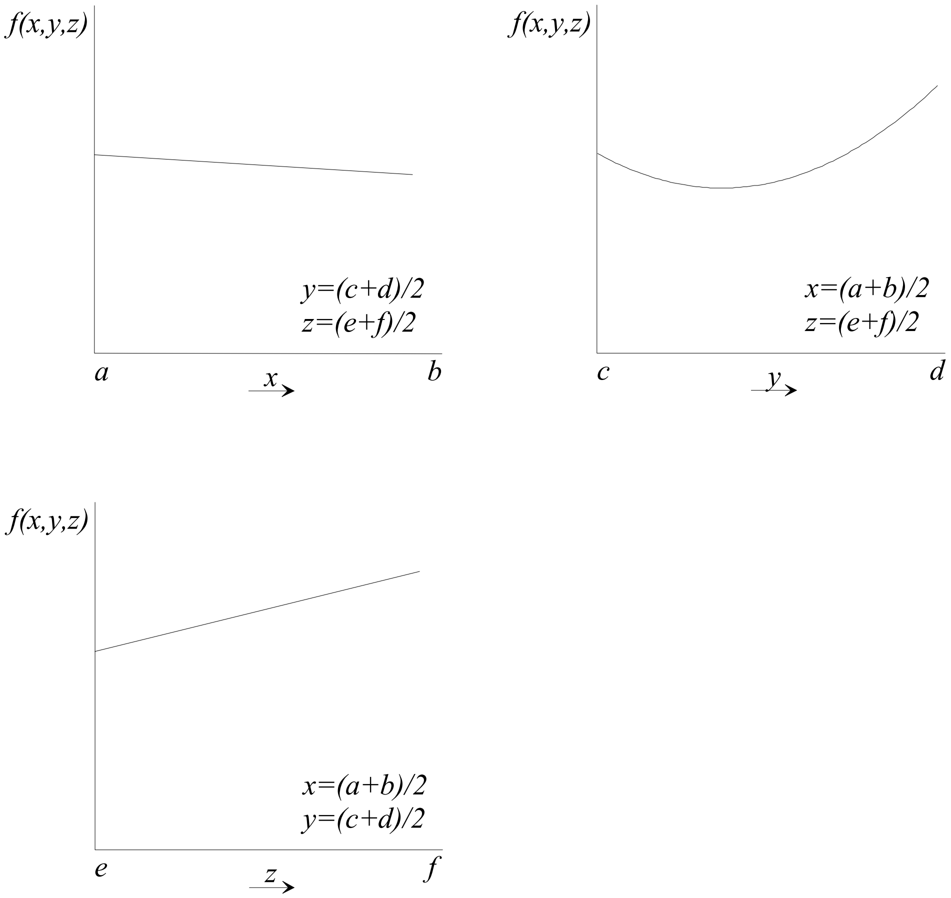

Figure 2-12. Behaviour of function f for variable x, y, and z.

Function 2.16 uses variables x, y, and z. The simplification of formula 2.16 should be tested in the defined variable-space (formula 2.11 to 2.13). If for all combinations of possible values for x, y, and z, $x = g(x,y)$ is a reasonable approximation, the simplification of 2.17 is allowed.

Introduction to the development of the post-failure mechanical models

The information provided in section 2.1.1 to 2.1.5 gives a framework for the development of post-failure mechanical models to predict the ultimate load of sheet sections. In the next sections, the development of the post-failure mechanical models will be described. Where useful, reference will be made to section 2.1.1 to 2.1.5. It should be noted that in the following sections the framework will not be followed rigidly. The framework in sections 2.1.1 to 2.1.5 merely makes it easier to understand the next sections.

2.2 Models for the yield arc post-failure mode

This section 2.2 presents models for the yield arc post-failure mode. First, some general information about sheet section behaviour is presented. Thereafter, sections present the components for the yield arc post-failure mode. Finally, the components are combined and the post-failure mechanical models are presented in the last section.

Plastically, a sheet section can fail (as is presented in thesis [Hofm00a], chapter 3) by three different post-failure modes: the rolling, the yield arc, and the yield eye post-failure modes. Elastically, a sheet section behaves equal for all post-failure modes. Therefore, elastic components will be only presented in this section 2.2 for the yield arc post-failure mode. Plastic components will be presented in all sections for all post-failure modes.

2.2.1 Components: elastic behaviour

A sheet section, in a three point bending test, behaves elastically as shown in figure 2-13. The load-bearing plate indents the sheet section. For the middle line of the bottom flange, at the edges of the load-bearing plate indentation is stronger than in the middle of the load-bearing plate. Where the sheet section is indented, webs and bottom flange bend to make the cross-section indentation possible. The top flanges only rotate, due to the bending of the webs. Flange or web buckling is not taken into account.

Component E1
For component E1, only the sheet section part above the load-bearing plate is observed, as figure 2-14 shows. It is assumed that this sheet section part deforms uniformly along the length, although this is not true (see figure 2-13).

Model Vaessen
In 1995, Vaessen developed mechanical models for predicting the elastic relationship between load and web crippling deformation for sheet sections [Vaes95a]. A part of one of his models can be used to predict the elastic load F_e on the load-bearing plate for a certain web crippling deformation Δh_w as follows:

$$F_e = \frac{\Delta h_w}{\dfrac{b_w \sin^2(\theta_w)}{EA} + \dfrac{\cos(\theta_w)}{EA} \dfrac{b_w \cos(\theta_w)\left(\frac{2}{3} b_w + b_{bf}\right) + r_{ibf} b_{bf} \sin(\theta_w) - r_{ibf}{}^2 \sin^2(\theta_w)}{b_{bf} + \frac{2}{3} b_w} + b} \tag{2.18}$$

$$\text{where } b = r_{ibf}{}^2 \sin^2(\theta_w) \frac{b_w\left(b_{bf} - \frac{4}{3} r_{ibf} \sin(\theta_w)\right) + r_{ibf} \sin(\theta_w)\left(b_{bf} - \frac{3}{2} r_{ibf} \sin(\theta_w)\right)}{EI\left(3 b_{bf} + 2 b_w\right)} \tag{2.19}$$

$$I = \frac{L_{lb}}{12} t^3 \tag{2.20}$$

$$A = L_{lb} t \tag{2.21}$$

F_e = load for elastic behaviour [N].
Δh_w = web crippling deformation [mm].
b_w = web width [mm].
θ_w = angle between web and flange [rad.].
b_{bf} = bottom flange width [mm].
r_{ibf} = interior corner radius between web and bottom flange [mm].
E = modulus of elasticity [N/mm^2].
L_{lb} = load-bearing plate / support width [mm].
t = steel plate thickness [mm].

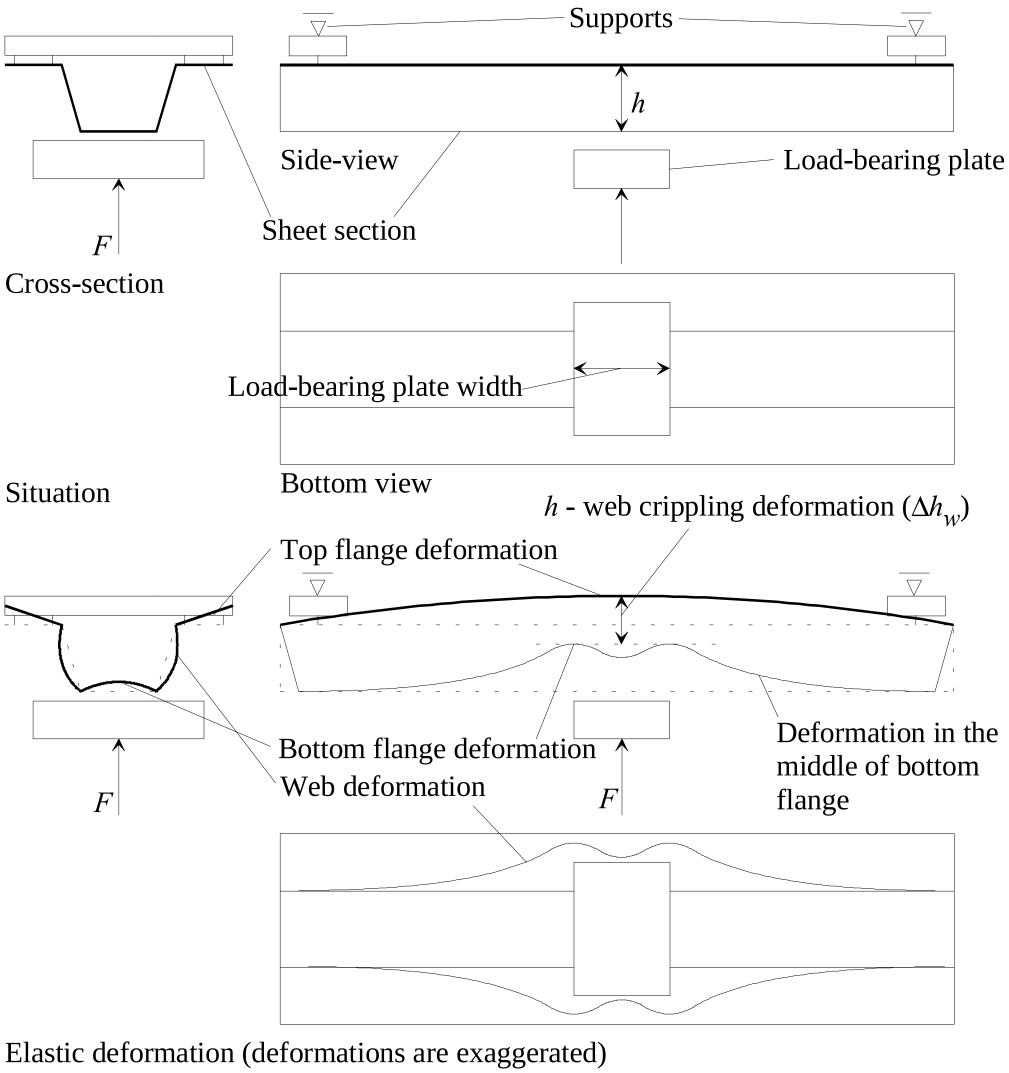

Figure 2-13. Elastic deformation of a sheet section.

This is valid for first-order elastic behaviour. Figure 3-2 in the thesis [Hofm00a] can be used as reference for all variables used in formulae 2.18 to 2.21. A more detailed discussion of the origin of formulae of component E1 can be found in appendix 3, section 3.1.

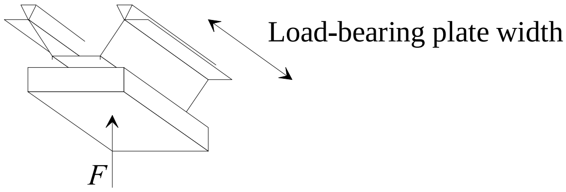

Figure 2-14. Sheet section above the load-bearing plate.

2.2.2 Components: plastic behaviour for the yield arc post-failure mode

In this section, components that describe plastic behaviour of the yield arc post-failure mode will be described. Each component is coded by "A" followed by a (sequential) number. Component A1 describes the plastic behaviour of the sheet section above the load-bearing plate. Component A2 does the same for parts adjacent to the part above the load-bearing plate. Component A3 describes plastic behaviour for the bottom flange near the load-bearing plate. Component A4 and A5 finally, describe the influence of the span length to the ultimate load.

A1: Cross-section behaviour
For the yield arc post-failure mode, the plastic behaviour of the cross-section is modelled as shown in figure 2-15. Making use of the principle of virtual displacements, the plastic load F_p related to the web crippling deformation Δh_w equals:

$$F_p = 2\frac{2}{\sqrt{3}}\frac{f_y t^2}{4} L_{lb}\left(\frac{\delta\varphi_a}{\delta\Delta h_w}+\frac{\delta\varphi_b}{\delta\Delta h_w}+\frac{\delta\varphi_c}{\delta\Delta h_w}\right) \qquad (2.22)$$

$$\text{where}\ \frac{\delta\varphi_a}{\delta\Delta h_w} = \frac{\dfrac{\left(\dfrac{\delta x}{\delta\Delta h_w}\right)}{b_w - L_w} + \dfrac{\left(L_w^2-(b_w-L_w)^2-x^2\right)\left(\dfrac{\delta x}{\delta\Delta h_w}\right)}{2(b_w-L_w)x^2}}{\sqrt{1-\dfrac{\left(L_w^2-(b_w-L_w)^2-x^2\right)^2}{4(b_w-L_w)^2x^2}}} + \frac{\sec\theta_w}{1+\dfrac{(h_w-\Delta h_w)^2\sec^2\theta_w}{b_w^2}} \qquad (2.23)$$

$$\text{and}\ x = \sqrt{(h_w-\Delta h_w)^2 + b_w^2\cos^2\theta_w} \qquad (2.24)$$

F_p = load for plastic behaviour [N].
f_y = steel yield strength [N/mm^2].
L_w = distance between yield lines [mm].
φ_i = rotation yield line *i* [rad.].
x = substitute variable.

The factors $\delta\varphi_b/\delta\Delta h_w$ and $\delta\varphi_c/\delta\Delta h_w$ are likewise complex as factor $\delta\varphi_a/\delta\Delta h_w$ and can be found in appendix 3.2, formula 3.15 and 3.16. Distance L_w is predicted by a model presented in appendix 4, section 4.3.

A2: Load to deform webs parts adjacent to load-bearing plate

Figure 2-16 shows that not only the modelled cross-section indents during loading, but also two parts adjacent to the modelled cross-section, over a length L_{bf}. The load to indent the cross-section per mm equals $F_p\,/L_{lb}$. Therefore, the load to indent a piece with width L_{bf} equals F_p*L_{bf} / L_{lb}. Because the indentation equals Δh_w at one end and zero at the other, it is estimated that only half the load is needed. Because there are two parts, the load to deform the two parts adjacent to the load-bearing plate, load F_{2p}, simply equals:

$$F_{2p} = F_p \frac{L_{bf}}{L_{lb}} \tag{2.25}$$

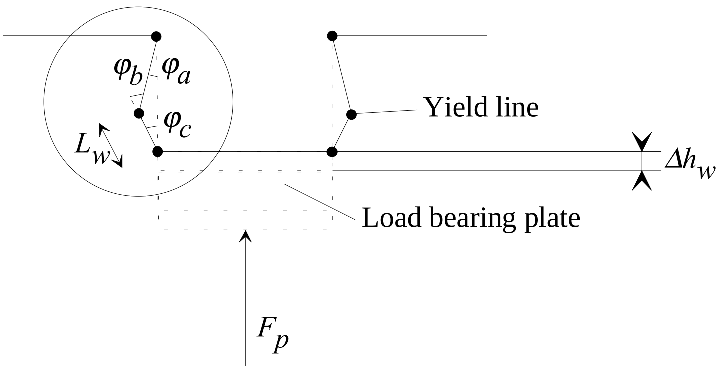

Figure 2-15. Plastic behaviour for modelled cross-section.

A3: Load to deform flanges adjacent to load-bearing plate

Figure 2-16 shows that in the bottom flange of the sheet section yield lines occur. These yield lines dissipate energy, like the yield lines in the modelled cross-section. The extra load F_{ylbf} needed to generate the extra energy dissipated by these yield lines equals:

$$F_{ylbf} = 2\frac{2}{\sqrt{3}}\frac{f_y t^2}{4} b_{bf}\left(\frac{\delta\varphi_d}{\delta\Delta h_w} + \frac{\delta\varphi_e}{\delta\Delta h_w}\right) \tag{2.26}$$

$$\frac{\delta\varphi_e}{\delta\Delta h_w} = \frac{\left(h_w + w_{tf} - \Delta h_w\right)}{\left(h_w - \Delta h_w\right)\sqrt{L_{bf}^2 - w_{tf}^2}} \tag{2.27}$$

$$w_{tf} = \sqrt{L_{bf}^2 - \left(L_{bf}\cos\varphi - h_w \sin\varphi\right)^2} \Leftrightarrow \left(L_{bf}\cos\varphi - h_w\sin\varphi\right) = \sqrt{L_{bf}^2 - w_{tf}^2} \tag{2.28}$$

$$\varphi_d = \varphi_e - \varphi \Leftrightarrow \frac{\delta\varphi_d}{\delta\Delta h_w} = \frac{\delta\varphi_e}{\delta\Delta h_w} - \frac{\delta\varphi}{\delta\Delta h_w} \tag{2.29}$$

The factor $\delta\varphi/\delta\Delta h_w$ in formula 2.29 is complex and can be predicted only with complicated formulae. The factor is presented in appendix 3.3, formula 3.33. A more detailed derivation of the formulae of component A3 and the meaning of variables like φ, φ_d, and φ_e can also be found in appendix 3.3.

Length-effect

The ultimate load of the modelled cross-section F_{csu} can be predicted by intersection of F_e and F_p (formula 2.18 and 2.22). In practice, the load acting on the load-bearing plate F (figure 2-16) does not equal the load at the modelled cross-section F_{cs}. This means that the ultimate sheet section load F_u does not equal the ultimate cross-section load F_{csu}. Instead, the load at the modelled cross-section F_{cs} equals the load acting on the load-bearing plate F plus an extra force $(f_{lx}\text{-}1)F$ due to indentation of the cross-section. Figure 2-16 illustrates this. Then, in total a force F^*f_{lx} is working on the sheet section.

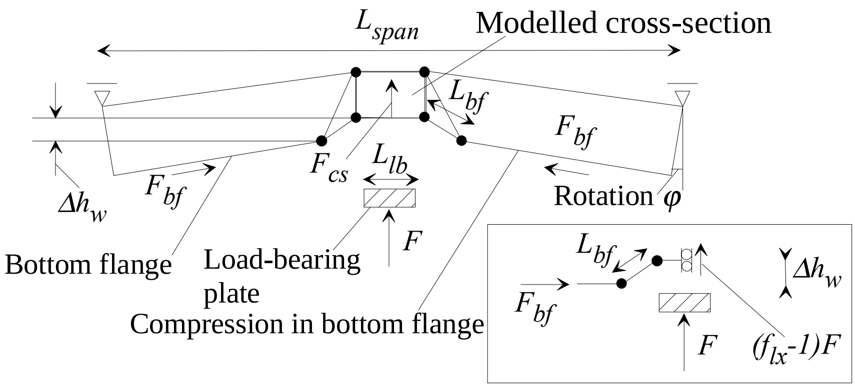

Figure 2-16. Load at modelled cross-section F_{cs} equals load acting on load-bearing plate F plus an extra force F_l due to indentation of the cross-section.

If the modelled cross-section deforms, yield lines develop in the bottom flange, which behave like hinges. Besides these yield lines, compressive forces develop in the bottom flange, due to the bending moment in the sheet section. These compressive forces, through the hinges, will increase the force on the modelled cross-section. This increase of force depends strongly on the section length. Therefore, this effect will be defined as ‘length-effect’.

Two components to describe this 'length-effect' have been developed. The first component is correct in a mechanical way, but produces complex formulae. The second component equals the first component but uses some simplifications.

A4: Length factor 1

The first component uses virtual displacements to predict the internal and external incremental energy. During an incremental change of the modelled cross-section indentation Δh_w, the load F acting on the sheet section moves. Not only the distance Δh_w (which is the case for only the indented cross-section) but also for an extra displacement caused by the deflection of the sheet section. The incremental energy can be written as follows (use figure 2-16):

$$\delta E_{e1} = F_{cs}\delta\Delta h_w \tag{2.30}$$

$$\delta E_{e2} = F\left(\delta\Delta h_w + \delta\varphi\left(\frac{L_{span} - L_{lb}}{2}\right)\right) \tag{2.31}$$

δE_{e1} = incremental external energy cross-section only.
δE_{e2} = incremental external energy cross-section and sheet section deflection.
$\delta\Delta h_w$ = incremental modelled cross-section indentation.
$\delta\varphi$ = incremental sheet section rotation.

Influences of stress on yield line energy dissipation are neglected and it is assumed that the yield line pattern does not change geometrically during deformation. Then, because both mentioned external energy terms should equal the incremental internal energy and internal energy is equal for both cases, it can be derived that:

$$\delta E_{e1} = \delta E_{e2} \Leftrightarrow$$

$$F_{cs}\delta\Delta h_w = F\left(\delta\Delta h_w + \delta\varphi\left(\frac{L_{span} - L_{lb}}{2}\right)\right) \Leftrightarrow F = \frac{F_{cs}\delta\Delta h_w}{\left(\delta\Delta h_w + \delta\varphi\left(\frac{L_{span} - L_{lb}}{2}\right)\right)} \Leftrightarrow$$

$$F = F_{cs}\frac{1}{\left(1 + \frac{\delta\varphi}{\delta\Delta h_w}\left(\frac{L_{span} - L_{lb}}{2}\right)\right)} = F_{cs} * f_{l1} \tag{2.32}$$

f_{l1} = length factor 1

The factor $\delta\varphi/\delta\Delta h_w$ is complex and can be predicted only with complicated formulae. This is shown in appendix 3.3, formula 3.33.

A5: Length factor 2
A part of length factor 1 can be simplified, avoiding the complex calculating of factor $\delta\varphi/\delta\Delta h_w$. Formula 3.33 is here presented:

$$\frac{\delta\varphi}{\delta\Delta h_w} = \frac{w_{tf}}{\sqrt{L_{bf}{}^2 - w_{tf}{}^2}\,(h_w - \Delta h_w)} \tag{3.33}$$

If it is assumed that w_{tf} equals approximately Δh_w (see figure 3-2), this formula 3.33 can be simplified into:

$$\frac{\delta\varphi}{\delta\Delta h_w} = \frac{\Delta h_w}{\sqrt{L_{bf}{}^2 - \Delta h_w{}^2}\,(h_w - \Delta h_w)} \tag{2.33}$$

Then, length factor 2 is described by the formula:

$$F = F_{cs} \frac{1}{\left(1+\frac{\Delta h_w}{\sqrt{Lbf^2 - \Delta h_w^2}\,(h_w - \Delta h_w)}\left(\frac{L_{span} - L_{lb}}{2}\right)\right)} = F_{cs} * f_{l2} \tag{2.34}$$

Summary of loads
The modelled cross-section is loaded during elastic behaviour by F_e (formulae 2.18 to 2.21) and during plastic behaviour by F_p (formulae 2.22 to 2.24). The two curves of F_e and F_p form an envelope for the behaviour of the modelled cross-section for load F_{cs}. The ultimate load of the cross-section equals F_{csu}.

Besides the load F_{csu} to indent the modelled cross-section, other loads are needed for the whole sheet section. The load F_{2p} (formula 2.25) to deform the two web parts adjacent to the modelled cross-section and the load F_{ylbf} (formulae 2.26 to 2.29) to deform the bottom flange.

Due to the interaction between bending moment and concentrated load, F_{cs} will become smaller, resulting in a force $F_{cs} * f_{l1}$ or $F_{cs} * f_{l2}$ (formulae 2.32 and 2.34).

Determination of yield line distances
All the forces of the previous paragraph result in the load at which the section fails F_u. The only problem is the unknown values of L_{bf} and L_w (figure 2-16 and 2-15). Distance L_{bf} can be found by minimisation of the load F_u. Regarding formulae 2.18 to 2.32, which are all needed to predict F_u, it will be clear that this minimisation leads to many complex formulae. Therefore, simplified formulae will be derived of formulae 2.18 to 2.32 in the next section, where after it is possible to determine L_{bf}. Distance L_w can be found by a mechanical model in appendix 4, section 4.3.

2.2.3 Prediction of the ultimate load using components

Introduction
Section 2.1 presented the methodology used in this appendix to develop post-failure mechanical models to predict the ultimate load for sheet sections. For the yield arc post-failure mode, section 2.2.1 and 2.2.2 presented components that can be used to describe elastic and plastic curves. Now, these components and mathematical techniques (presented in paragraph 2.1.5) will be used to develop the post-failure mechanical models that predict the ultimate load for the yield arc post-failure mode. The mechanical models will have a code that makes them easily recognisable. The character "M" stands for model, "A" for the yield arc post-failure mode and, later, "R" for the rolling post-failure mode and "E" for the yield eye post-failure mode.

In this appendix 2, many derivations made for developing the post-failure models will only be briefly discussed. Appendix 3 will present derivations with full details.

Model MA1: Used components and mathematical techniques
For this mechanical model, the following components are used. For elastic behaviour component E1. For plastic behaviour component A1, A2, A3, and A4. All mathematical techniques M1, M2, M3, M4, and M5 are used.

Development
As already discussed in section 2.1.2 the ultimate load of a sheet section can be predicted by an intersection of the elastic and plastic curve. Although there are other methods available (for example method B in section 2.1.2) method A will be used. Furthermore, the reduction method presented in section 2.1.4 is used. For model MA1, the reduction method is used in such a way that, for calculating the intersection, elastic and plastic curves only pay attention to the behaviour above the load-bearing plate. Thus, all other components will be neglected. For the part above the load-bearing plate the ultimate load is calculated. Thereafter corrections can be made by including other components. This is all conform section 2.1.4 and thus needs no further explanation here.

Definition modelled cross-section
Figure 2-17 shows again the modelled cross-section. Although the behaviour of the sheet section part above the load-bearing plate is not constant along the length (which is clearly shown in figure 2-17), the modelled cross-section is assumed to do so.

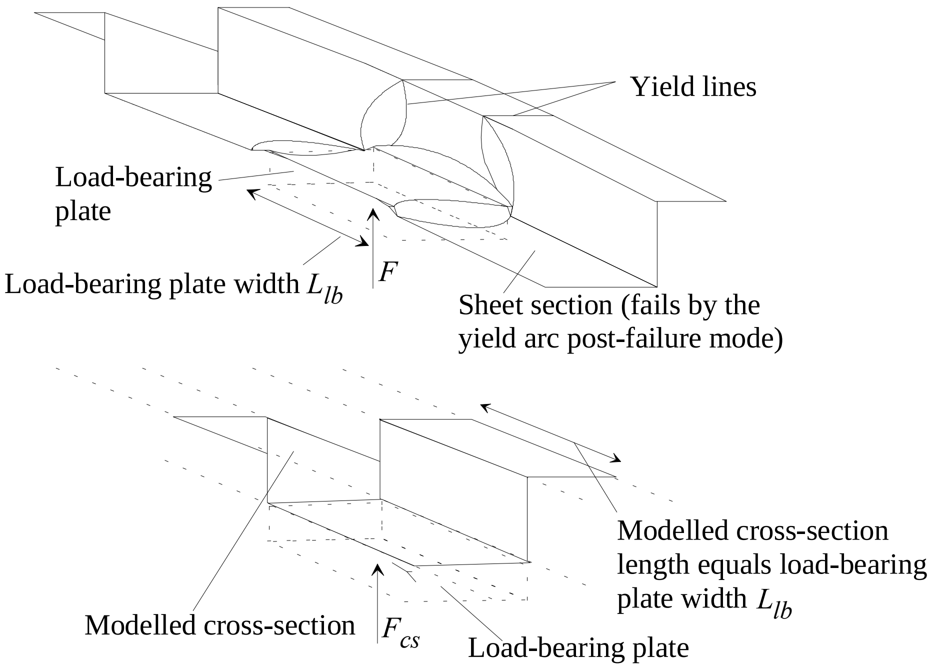

Figure 2-17. Modelled cross-section.

The length of the modelled cross-section equals the load-bearing plate width that is defined by L_{lb}.

Intersection of E1 and A1

If the modelled cross-section as shown in figure 2-17 behaves elastically, formulae 2.18 to 2.21 yield. Using mathematical technique M1, (paragraph 2.1.5) formulae 2.18 to 2.21 are reduced to:

$$F_e = \frac{EI\left(3b_{bf} + 2b_w\right)\Delta h_w}{r_{ibf}{}^2 \sin^2(\theta_w) b_w \left(b_{bf} - \frac{4}{3} r_{ibf} \sin(\theta_w)\right)} \tag{2.35}$$

Details are presented in appendix 3, section 3.5, formulae 3.69 to 3.77. Mathematical technique M1 uses a defined variable space. In this case, the variable space is defined as variable space A as follows:

$$50 < b_w < 150 \text{ [mm].} \tag{2.36}$$

$$50 < \theta_w < 90 \text{ [degrees].} \tag{2.37}$$

$$50 < L_{lb} < 150 \text{ [mm].} \tag{2.38}$$

$$0.5 < t < 1.5 \text{ [mm].} \tag{2.39}$$

$$40 < b_{bf} < 150 \text{ [mm].} \tag{2.40}$$

$$1 < r_{bf} < 12 \text{ [mm].} \tag{2.41}$$

$$0.1 < \Delta h_w < 10 \text{ [mm].} \tag{2.42}$$

Using techniques M3 and M1 for variable space A, formula 2.22, 2.23, and 2.24 can be reduced. Setting equal the reduced formulae to formula 2.35 yields to the predicted ultimate load of the modelled cross-section. This load is defined as F_{csu}. Details are presented in appendix 3.6, formulae 3.78 to 3.93.

$$F_{csu} = \frac{-\alpha - \beta + \sqrt{4A\alpha h_w (b_w - L_w) L_w k + (\beta + \alpha)^2}}{2A(b_w - L_w) L_w} \tag{2.43}$$

$$k = \frac{EI\left(3b_{bf} + 2b_w\right)}{r_{ibf}{}^2 \sin^2(\theta_w) b_w \left(b_{bf} - \frac{4}{3} r_{bf} \sin(\theta_w)\right)} \tag{2.44}$$

$$\alpha = f_y L_{lb} t^2 \tag{2.45}$$

$$\beta = kL_w (C + BL_w)(b_w - L_w) \tag{2.46}$$

$$A = 0.0624 \tag{2.47}$$

$$B = -0.0101 \tag{2.48}$$

$$C = 0.5633 \tag{2.49}$$

Summarised, formulae 2.43 to 2.49 predict the ultimate load by intersection of an elastic curve using component E1 and a plastic curve using component A1.

Correction of intersection E1 and A1 with A2

The prediction in the previous paragraph can be improved by adding component A2 to formulae 2.43 to 2.49. As already described in paragraph 2.2.2 component A2 can be described using formula 2.25. For the ultimate load F_{csu}, the elastic load F_e and the plastic load F_p are equal to F_{csu}.

Therefore, formula 2.25 changes into:

$$F_{2p} = F_{csu} \frac{L_{bf}}{L_{lb}} \tag{2.50}$$

The ultimate load of the modelled cross-section F_{csu} can be corrected by adding the load F_{2p}.

Correction of intersection E1 and A1 with A3

In section 2.2.2, component A3 was presented. Formulae 2.26 to 2.29, describing this component, are quite complex. Therefore, technique M5 is used: component A3 is simplified.

The yield lines in the bottom flange are as shown in figure 2-18. For this moment, it is assumed that the bottom flange part 1 and 3 do not rotate relatively to each other.

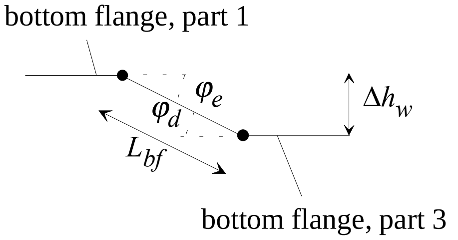

Figure 2-18. New simple model to predict the force F_{ylbf} to deform the bottom flange.

Using formula 2.26 and figure 2-18, the force F_{ylbf} can be predicted as follows:

$$\varphi_d = \varphi_e = \arcsin \frac{\Delta h_w}{L_{bf}} \tag{2.51}$$

$$\frac{\delta\varphi_d}{\delta\Delta h_w} = \frac{\delta\varphi_e}{\delta\Delta h_w} = \frac{1}{L_{bf}\sqrt{1-\left(\frac{\Delta h_w}{L_{bf}}\right)^2}} = \frac{1}{\sqrt{L_{bf}^2 - \Delta h_w^2}} \tag{2.52}$$

$$F_{ylbf} = 2\frac{2}{\sqrt{3}}\frac{f_y t^2}{4} b_{bf}\left(\frac{\delta\varphi_d}{\delta\Delta h_w} + \frac{\delta\varphi_e}{\delta\Delta h_w}\right) \tag{2.26}$$

The ultimate load of the modelled cross-section F_{csu} can be corrected by adding the load F_{ylbf}.

Correction intersection E1 and A1 with A4
In section 2.2.2 component A4 was presented. If mathematical technique M2 (section 2.1.5) is used with variable angle φ in formula 2.28 component A4 can be rewritten as:

$$f_{l1} = \frac{1}{1+\left(\frac{L_{span} - L_{lb}}{2}\right)\frac{\sqrt{L_{bf}^2 - (L_{bf} - h_w\varphi)^2}}{(L_{bf} - h_w\varphi)(h_w - \Delta h_w)}} \tag{2.53}$$

Web crippling deformation Δh_w was calculated by formulae 3.88 and 3.89 for finding F_{csu} in formula 2.34. Rotation φ can be calculated by formula 3.97, appendix 3.7.

Further details are presented in appendix 3.7, formulae 3.94 to 3.99. Using this length factor f_{l1} (component A4), the ultimate load of the sheet section can be calculated as follows:

$$F_u = (F_{csu} + F_{2p} + F_{ylbf})f_{l1} \tag{2.54}$$

Finding yield line distance L_{bf}
The distance between yield lines L_{bf} is shown in figure 2-16. The distance L_{bf} can be determined by varying L_{bf} and finding the minimum value for the ultimate load F_u (formula 2.54). To differentiate formula 2.54 to L_{bf} and find the root is difficult. Therefore, mathematical technique M4 is used. If only F_{csu}, F_{2p} and F_{ylbf} of formula 2.54 are used, the following equation should be solved. Details are presented in appendix 3.8, formulae 3.100 to 3.110.

$$\frac{\partial F_u}{\partial L_{bf}} = \left(\frac{\partial F_{csu}}{\partial L_{bf}} + \frac{\partial F_{2p}}{\partial L_{bf}} + \frac{\partial F_{ylbf}}{\partial L_{bf}}\right) = 0 \tag{2.55}$$

Note that the correct equation should be:

$$\frac{\partial F_u}{\partial L_{bf}} = \left(\frac{\partial F_{csu}}{\partial L_{bf}} + \frac{\partial F_{2p}}{\partial L_{bf}} + \frac{\partial F_{ylbf}}{\partial L_{bf}}\right)f_{l1} + (F_{csu} + F_{2p} + F_{ylbf})\frac{\partial f_{l1}}{\partial L_{bf}} = 0 \tag{2.56}$$

Equation 2.55 can be solved easily. The result equals:

$$L_{bf} = \sqrt{\frac{2 f_y t^2 L_{lb} b_{bf} \, 2.601}{4 F_{csu}}} \tag{2.57}$$

2.2.4 Overview of formulae

In this section, an overview of formulae needed to use model MA1 is given. If all formulae are used in sequence, a prediction of the ultimate load of a sheet section results.

First, calculate the ultimate load of the modelled cross-section:

$$F_{csu} \frac{-\alpha - \beta + \sqrt{4 A \alpha h_w (b_w - L_w) L_w k + (\beta + \alpha)^2}}{2 A (b_w - L_w) L_w} \tag{2.43}$$

$$k = \frac{EI(3 b_{bf} + 2 b_w)}{r_{bf}^{\,2} \sin^2 \theta_w b_w \left(b_{bf} - \frac{4}{3} r_{bf} \sin \theta_w \right)} \tag{2.44}$$

$$\alpha = f_y L_{lb} t^2 \tag{2.45}$$

$$\beta = k L_w (C + B L_w)(b_w - L_w) \tag{2.46}$$

$$A = 0.0624 \tag{2.47}$$

$$B = -0.0101 \tag{2.48}$$

$$C = 0.5633 \tag{2.49}$$

Distance L_w is predicted by a method presented in appendix 4, section 4.3. Now, yield line distance L_{bf} can be calculated.

$$L_{bf} = \sqrt{\frac{2 f_y t^2 L_{lb} b_{bf} \, 2.601}{4 F_{csu}}} \tag{2.57}$$

Then F_{2p}, F_{ylbf}, and f_{l1} can be calculated:

$$F_{2p} = F_{csu} \frac{L_{bf}}{L_{lb}} \tag{2.50}$$

$$F_{ylbf} = 2\frac{f_y t^2}{4} b_{bf}\left(\frac{\delta\varphi_d}{\delta\Delta h_w} + \frac{\delta\varphi_e}{\delta\Delta h_w}\right) \qquad (2.26)$$

$$\frac{\delta\varphi_d}{\delta\Delta h_w} = \frac{\delta\varphi_e}{\delta\Delta h_w} = \frac{1}{L_{bf}\sqrt{1-\left(\frac{\Delta h_w}{L_{bf}}\right)^2}} = \frac{1}{\sqrt{L_{bf}^2 - \Delta h_w^2}} \qquad (2.52)$$

The prediction of the ultimate load equals:

$$F_u = \left(F_{csu} + F_{2p} + F_{ylbf}\right) f_{l1} \qquad (2.54)$$

With:

$$f_{l1} = \frac{1}{1+\left(\frac{L_{span} - L_{lb}}{2}\right)\frac{\sqrt{L_{bf}^2 - \left(L_{bf} - h_w\varphi\right)^2}}{\left(L_{bf} - h_w\varphi\right)\left(h_w - \Delta h_w\right)}} \qquad (2.53)$$

Web crippling deformation Δh_w was calculated by formulae 3.88 and 3.89 for finding F_{csu} in formula 2.34. Rotation φ can be calculated by formula 3.97, appendix 3.7.

2.2.5 Other models

Model MA2
Model MA2 equals model MA1 with exception of component A2. This component is not taken into account. This means that force F_{2p} is removed from formula 2.54:

$$F_u = \left(F_{csu} + F_{ylbf}\right) f_{l1} \qquad (2.58)$$

Model MA3
Model MA3 equals model MA1 with exception of component A3. This component is not taken into account. This means that force F_{ylbf} is removed from formula 2.54:

$$F_u = \left(F_{csu} + F_{2p}\right) f_{l1} \qquad (2.59)$$

Model MA4
Model MA4 equals model MA1 with exception of the components A2 and A3. These components are not taken into account. This means that forces F_{2p} and F_{ylbf} are removed from formula 2.54:

$$F_u = F_{csu} * f_{l1} \qquad (2.60)$$

Model MA5
Model MA5 equals model MA1 with exception of component A4. Instead of this component, component A5 is used. Component A5 is described by formula 2.34. Formula 2.54 changes into:

$$F_u = \left(F_{csu} + F_{2p} + F_{ylbf}\right) f_{l2} \tag{2.61}$$

Model MA6
Model MA6 equals model MA5 with exception of component A2. This component is not taken into account. This means that force F_{2p} is removed from formula 2.61:

$$F_u = \left(F_{csu} + F_{ylbf}\right) f_{l2} \tag{2.62}$$

Model MA7
Model MA7 equals model MA5 with exception of component A3. This component is not taken into account. This means that force F_{ylbf} is removed from formula 2.61:

$$F_u = \left(F_{csu} + F_{2p}\right) f_{l2} \tag{2.63}$$

Model MA8
Model MA8 equals model MA5 with exception of the components A2 and A4. These components are not taken into account. This means that forces F_{2p} and F_{ylbf} are removed from formula 2.61:

$$F_u = F_{csu} * f_{l2} \tag{2.64}$$

Model MA9
Model MA9 equals model MA1 with exception of component A5. This component is removed and is not replaced by an other component. This means that the length factor f_{l1} is removed from formula 2.54:

$$F_u = F_{csu} + F_{2p} + F_{ylbf} \tag{2.65}$$

Model MA10
Model MA10 equals model MA9 with exception of component A2. This component is not taken into account. This means that force F_{2p} is removed from formula 2.65:

$$F_u = F_{csu} + F_{ylbf} \tag{2.66}$$

Model MA11
Model MA11 equals model MA9 with exception of component A3. This component is not taken into account. This means that force F_{ylbf} is removed from formula 2.65:

$$F_u = F_{csu} + F_{2p} \tag{2.67}$$

Model MA12

Model MA12 equals model MA9 with exception of the components A2 and A3. These components are not taken into account. This means that forces F_{2p} and F_{ylbf} are removed from formula 2.65:

$$F_u = F_{csu} \tag{2.68}$$

2.3 Models for the rolling post-failure mode

This section 2.3 will have the same structure as the previous section 2.2. First, a component will be presented, this time for the rolling post-failure mode. However, this component is a plastic component. The elastic component for the rolling post-failure mode is equal to the elastic component of the yield arc post-failure mode.

In the second part of this section, the components are used to predict the mode initiation load for the rolling post-failure mode. Note that the mode initiation load does not equal the ultimate load. The differences between mode initiation load and ultimate load are covered in the thesis [Hofm00a], chapter 3, section 3.3.2. The mode initiation load is not suitable for predicting the ultimate load, but it is especially suitable for predicting when the rolling post-failure mode occurs. The post-failure mechanical models as presented in this appendix are used in the thesis [Hofm00a] to predict when a post-failure mode occurs.

2.3.1 Components: plastic behaviour for the rolling post-failure mode

The only difference between the rolling post-failure mode and the yield arc post-failure mode is the plastic behaviour of the cross-section. Therefore, only one component is described in this section. The component for the rolling post-failure mode is coded by "R" followed by a (sequential) number.

Component R1: Cross-section behaviour

This model is based on the model of Bakker [Bakk92a], however, only cross-section behaviour is modelled. To make a simple model for the rolling post-failure mode, the sheet section behaviour is modelled like for the yield arc post-failure mode. It is assumed that the modelled cross-section above the load-bearing plate fails if the sheet section fails. The modelled cross-section width is equal to the load-bearing plate width. This is shown in figure 2-17.

The plastic behaviour of the cross-section is modelled as shown in figure 2-19. Making use of principle of virtual displacements [Bakk92a], the plastic load F_p related to the cross-section indentation Δh_w equals:

$$F_p = 2\frac{\delta u_a}{\delta\Delta h_w}\frac{1}{r_{bf}}\frac{2}{\sqrt{3}}\frac{f_y t^2}{4}L_{lb} + 2\frac{\delta u_b}{\delta\Delta h_w}\frac{1}{r_{bf}}\frac{2}{\sqrt{3}}\frac{f_y t^2}{4}L_{lb} + 2\frac{\delta\varphi_c}{\delta\Delta h_w}\frac{2}{\sqrt{3}}\frac{f_y t^2}{4}L_{lb} \tag{2.69}$$

$$\frac{\delta u_a}{\delta\Delta h_w} = \frac{\sin(\theta_w + \varphi_c)}{1-\cos(\theta_w + \varphi_c)} \tag{2.70}$$

$$\frac{\delta u_b}{\delta\Delta h_w} = \frac{\sin(\theta_w + \varphi_c)}{1-\cos(\theta_w + \varphi_c)} + \frac{r_{bf}}{b_{wfl}\text{-}\Delta b_{wfl}} \tag{2.71}$$

$$\Delta b_{wfl} = \frac{b_{wfl}\left(\cos\theta_w - \cos(\theta_w + \varphi_c)\right) + r_{bf}\left(\sin\theta_w + \varphi_c - \sin(\theta_w + \varphi_c)\right)}{1 - \cos(\theta_w + \varphi_c)} \tag{2.72}$$

Calculating φ_c as:

$$\varphi_c = -\frac{\Delta h_w \sin\left(\frac{\theta_w}{2}\right)}{\Delta h_w \cos\left(\frac{\theta_w}{2}\right) - b_w \sin\left(\frac{\theta_w}{2}\right)} \tag{2.73}$$

u_i = movement of yield line *i.*
δu_i = incremental movement of yield line *i.*
r_{bf} = corner radius bottom flange.
Δb_w = change of web width b_w..

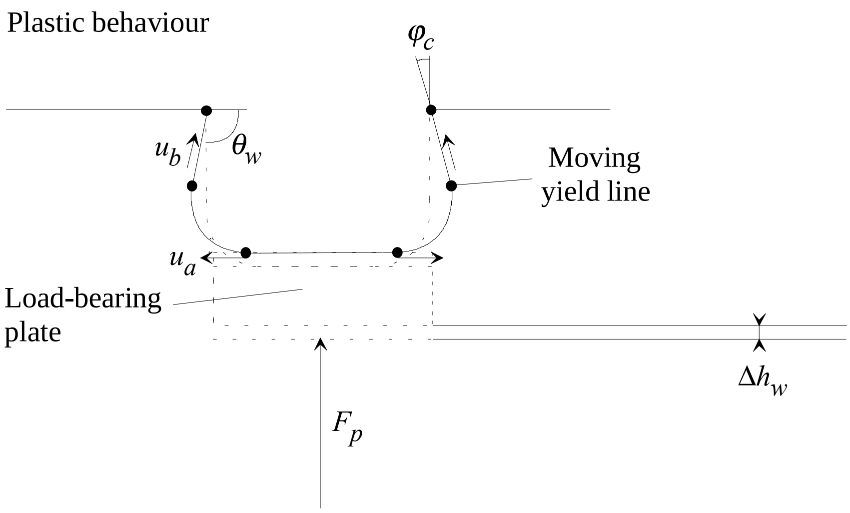

Figure 2-19. Rolling post-failure mode, plastic behaviour.

The derivation of formulae 2.69 to 2.73 is presented in appendix 3.4, formulae 3.41 to 3.68.

Other components
For both length effect 1 and length effect 2, the parts adjacent to the support, the yield lines in the bottom flange, and the determination of yield line distances, the same considerations and formulae are valid as for the yield arc post-failure mode. However, as figure 2-19 shows, distance L_w needs not to be determined (compare with figure 2-15).

2.3.2 Prediction of the ultimate load using components

Model MR1
For this post-failure mechanical model, the following components are used. For elastic behaviour component E1. For plastic behaviour component R1, A2, A3, and A4. Method A

mentioned in section 2.1.2 is used to predict the ultimate load. All mathematical techniques M1, M2, M3, M4, and M5 will be used.

Equal to model MA1, this model MR1, predicting the ultimate load for the rolling post-failure mode, will be based on the reduction method presented in section 2.1.4. The ultimate load is predicted by intersection of an elastic and plastic curve. These curves pay only attention to the modelled cross-section section (the part above the load-bearing plate, defined in section 2.2.3, figure 2-17).

For the elastic curve, component E1 describes the behaviour of the modelled cross-section. The plastic curve for the modelled cross-section is described by component R1.

After the prediction of the ultimate load of the modelled cross-section, the predicted ultimate load is corrected. This correction is carried out using components that describe the behaviour of parts adjacent to the load-bearing plate or components describing a length effect. For the yield arc and rolling post-failure modes, these components are equal. This means the ultimate load prediction for the rolling post-failure mode is corrected with the same components as for the model MA1: the components A2, A3, and A4.

Intersection of E1 and R1
If the modelled cross-section as shown in figure 2-17 behaves elastically formulae 2.18 to 2.21 yield. Using mathematical technique M1, (paragraph 2.1.5) formulae 2.18 to 2.21 are reduced to:

$$F_e = \frac{EI\left(3b_{bf} + 2b_w\right)\Delta h_w}{r_{bf}^{\,2}\sin^2(\theta_w)b_w\left(b_{bf} - \frac{4}{3}r_{bf}\sin(\theta_w)\right)} \tag{2.35}$$

Details are presented in appendix 3.5, formulae 3.69 to 3.77. Mathematical technique M1 uses a defined variable space. In this case, the variable space is defined as variable space A (see formulae 2.36 to 2.42).

Using mathematical technique M1 for defined variable space A (formulae 2.36 to 2.42), the formulae describing the plastic behaviour for the rolling mechanism (2.69 to 2.73) can be simplified into:

$$F_p = 2*2\frac{\sin(\theta_w)+\varphi_c\cos(\theta_w)}{1-\cos(\theta_w)+\varphi_c\sin(\theta_w)}\frac{1}{r_{bf}}\frac{2}{\sqrt{3}}\frac{f_y t^2}{4}L_{lb} \tag{2.74}$$

Details are presented in appendix 3.9, formulae 3.111 to 3.121. Now, the elastic (formula 2.35) and plastic load (formula 2.74) of the modelled cross-section can be set equal. Consequently, the predicted ultimate load F_{csu} of the modelled cross-section can be solved (appendix 3.9, formulae 3.111 to 3.121):

$$F_{csu} = -k \frac{2b_w \left(\frac{L_{lb} 2 f_y t^2}{\sqrt{3} r_{bf}} \right) \cos\left(\frac{\theta_w}{2} \right) \sin\left(\frac{\theta_w}{2} \right)}{-b_w k - \left(\frac{L_{lb} 2 f_y t^2}{\sqrt{3} r_{bf}} \right) + b_w k \cos(\theta_w)} \tag{2.75}$$

Correction of intersection E1 and R1 with A2
This correction equals the correction with component A2 for the yield arc post-failure mode. To the ultimate load F_{csu} (formula 2.75), load F_{2p} should be added (formula 2.50).

Correction of intersection E1 and R1 with A3
This correction equals the correction with component A3 for the yield arc post-failure mode. The ultimate load F_{csu} (formula 2.75) should be added with load F_{ylbf} (formula 2.52 and 2.26).

Correction intersection E1 and R1 with A4
This correction equals the correction with component A4 for the yield arc post-failure mode. The ultimate load of the cross-section should be multiplied with the length factor f_{l1} (formula 2.53).

Finding yield line distance L_{bf}
Finding yield line distance L_{bf} is equal for the rolling post-failure mode and the yield arc post-failure mode. Thus, formula 2.57 can be used.

2.3.3 Overview of formulae

In this section, an overview of formulae needed to use model MR1 is given. If all formulae are used in sequence, a prediction of the mode initiation load of a sheet section results. First, calculate the mode initiation load of the modelled cross-section:

$$F_{csu} = -k \frac{2b_w \left(\frac{L_{lb} 2 f_y t^2}{\sqrt{3} r_{bf}} \right) \cos\left(\frac{\theta_w}{2} \right) \sin\left(\frac{\theta_w}{2} \right)}{-b_w k - \left(\frac{L_{lb} 2 f_y t^2}{\sqrt{3} r_{bf}} \right) + b_w k \cos(\theta_w)} \tag{2.75}$$

With:

$$k = \frac{EI(3b_{bf} + 2b_w)}{r_{bf}^2 \sin^2 \theta_w b_w \left(b_{bf} - \frac{4}{3} r_{bf} \sin\theta_w \right)} \tag{2.44}$$

Now, yield line distance L_{bf} can be calculated:

$$L_{bf} = \sqrt{\frac{2 f_y t^2 L_{lb} b_{bf} \, 2.601}{4 F_{csu}}} \tag{2.57}$$

Then F_{2p}, F_{ylbf}, and f_{l1} can be calculated:

$$F_{2p} = F_{csu} \frac{L_{bf}}{L_{lb}} \tag{2.50}$$

$$F_{ylbf} = 2 \frac{f_y t^2}{4} b_{bf} \left(\frac{\delta\varphi_d}{\delta\Delta h_w} + \frac{\delta\varphi_e}{\delta\Delta h_w} \right) \tag{2.26}$$

$$f_{l1} = \frac{1}{1 + \left(\frac{L_{span} - L_{lb}}{2} \right) \frac{\sqrt{L_{bf}^2 - (L_{bf} - h_w\varphi)^2}}{(L_{bf} - h_w\varphi)(h_w - \Delta h_w)}} \tag{2.53}$$

$$\frac{\delta\varphi_d}{\delta\Delta h_w} = \frac{\delta\varphi_e}{\delta\Delta h_w} = \frac{1}{L_{bf}\sqrt{1 - \left(\frac{\Delta h_w}{L_{bf}} \right)^2}} = \frac{1}{\sqrt{L_{bf}^2 - \Delta h_w^2}} \tag{2.52}$$

The prediction of the mode initiation load equals:

$$F_u = (F_{csu} + F_{2p} + F_{ylbf}) f_{l1} \tag{2.54}$$

2.3.4 Other models

Model MR2
Model MR2 equals model MR1 with exception of component A2. This component is not taken into account. This means that force F_{2p} is removed from formula 2.54:

$$F_u = (F_{csu} + F_{ylbf}) f_{l1} \tag{2.76}$$

Model MR3
Model MR3 equals model MR1 with exception of component A3. This component is not taken into account. This means that force F_{ylbf} is removed from formula 2.54:

$$F_u = (F_{csu} + F_{2p}) f_{l1} \tag{2.77}$$

Model MR4
Model MR4 equals model MR1 with exception of the components A2 and A3. These components are not taken into account. This means that forces F_{2p} and F_{ylbf} are removed from formula 2.54.

$$F_u = F_{csu} * f_{l1} \tag{2.78}$$

Model MR5
Model MR5 equals model MR1 with exception of component A4. Instead of this component, component A5 is used. Component A5 is described by formula 2.34. Thus, formula 2.54 changes into:

$$F_u = \left(F_{csu} + F_{2p} + F_{ylbf}\right) f_{l2} \tag{2.79}$$

Model MR6
Model MR6 equals model MR5 with exception of component A2. This component is not taken into account. This means that force F_{2p} is removed from formula 2.79:

$$F_u = \left(F_{csu} + F_{ylbf}\right) f_{l2} \tag{2.80}$$

Model MR7
Model MR7 equals model MR5 with exception of component A3. This component is not taken into account. This means that force F_{ylbf} is removed from formula 2.79:

$$F_u = \left(F_{csu} + F_{2p}\right) f_{l2} \tag{2.81}$$

Model MR8
Model MR8 equals model MR5 with exception of the components A2 and A3. These components are not taken into account. This means that forces F_{2p} and F_{ylbf} are removed from formula 2.79:

$$F_u = F_{csu} * f_{l2} \tag{2.82}$$

Model MR9
Model MR9 equals model MR1 with exception of component A4. This component is removed and is not replaced by an other component. This means that the length factor f_{l1} is removed from formula 2.54:

$$F_u = F_{csu} + F_{2p} + F_{ylbf} \tag{2.83}$$

Model MR10
Model MR10 equals model MR9 with exception of component A2. This component is not taken into account. This means that force F_{2p} is removed from formula 2.83:

$$F_u = F_{csu} + F_{ylbf} \tag{2.84}$$

Model MR11

Model MR11 equals model MR9 with exception of component A3. This component is not taken into account. This means that force F_{ylbf} is removed from formula 2.83:

$$F_u = F_{csu} + F_{2p} \tag{2.85}$$

Model MR12

Model MR12 equals model MR9 with exception of the components A2 and A3. These components are not taken into account. This means that forces F_{2p} and F_{ylbf} are removed from formula 2.83:

$$F_u = F_{csu} \tag{2.86}$$

2.4 Model for the yield eye post-failure mode

Introduction

In this section, a model for the yield eye post-failure mode will be presented. The post-failure model is based on method A (paragraph 2.1.2) and uses elastic component E1 (section 2.2.1) and a new plastic component introduced in this section.

2.4.1 Plastic component

Component Y1: flip-disc action

The yield eye post-failure mode has an eye like yield line pattern located on the bottom flange (see also chapter 3, thesis [Hofm00a]). In 1981, Murray and Khoo presented a paper that discussed some models to describe the behaviour of simple yield line patterns [Murr81a]. One of these patterns was called a flip-disc pattern and has a strong geometrical similarity to the eye like yield line pattern of the yield eye post-failure mode. Figure 2-20 shows a thin-walled plate compressed by a force F_{bf}.

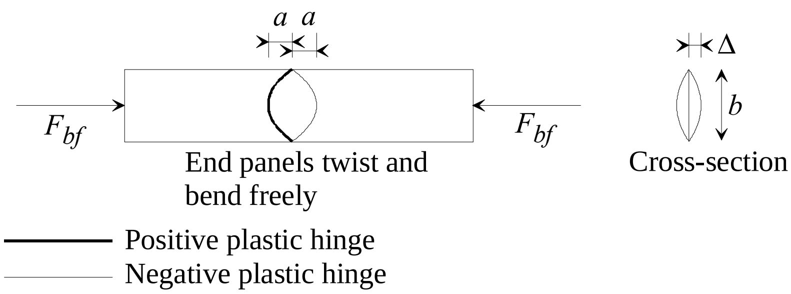

Figure 2-20. Thin-walled plate. Flip-disc pattern.

According to Murray and Khoo, the force F_{bf} can be predicted using the following formula:

$$F_{bf} = \frac{f_y t b}{6}\left[1 - \frac{2\Delta}{t} + \sqrt{\left(\frac{2\Delta}{t}\right)^2 + 1} - \frac{6\Delta}{t\left(1 + 4a^2/b^2\right)} + 4\sqrt{\left(\frac{3\Delta}{2t\left(1 + 4a^2/b^2\right)}\right)^2 + 1}\right] \tag{2.87}$$

With:

a	$=0.2b$
P	= compressive force [N].
Δ	= flip-disc out-of-plane deflection [mm].
b	= plate width [mm].
a	= flip-disc half width [mm].
t	= steel plate thickness [mm].
f_y	= steel yield strength [N/mm^2].

2.4.2 Prediction of the ultimate load using components

Elastic component E1 describes the relationship between the concentrated load F acting on the sheet section and the sheet section web crippling deformation Δh_w. Plastic component Y1 defines the load F_{bf} acting on the bottom flange needed to form a plastic mechanism for a certain flip-disc out-of-plane deflection Δ (previous section).

For model ME1, elastic and plastic curves have different load and deformation variables. Figure 2-21 illustrates this problem.

A relationship between the load at the sheet section F and the load at the bottom flange F_{bf} should be developed. Furthermore a relationship between the elastic cross-section deformation variable Δh_w and the plastic flip-disc deformation variable Δ should be developed.

Cross-section deformation versus flip-disc deformation
Figure 2-22 shows a possible relationship for this. It shows that for elastic behaviour, it is assumed that a certain width adjacent to the modelled cross-section will deform like the modelled cross-section. This certain width is set equal to the distance $2a$ between yield lines in the bottom flange during plastic deformation. Thus, it can be derived:

$$\frac{2\Delta}{2a} = \frac{\Delta h_w}{2a} \Leftrightarrow \Delta = 0.5\Delta h_w \tag{2.88}$$

Δ = flip-disc out-of-plane deflection [mm].

Δh_w = web crippling deformation [mm].

Load at section versus load at bottom flange
Looking at figure 2-22 shows that the external bending moment in the section equals:

$$M_e = \frac{F L_{span}}{4} \tag{2.89}$$

M_e = external bending moment [Nmm].
F = concentrated load of support on section [N].
L_{span} = span length [mm].

Making the following assumptions:

- One concentrated load F models the load of the load-bearing plate.
- The flip-disc occurs at the position of this concentrated load, the location of highest bending moment.

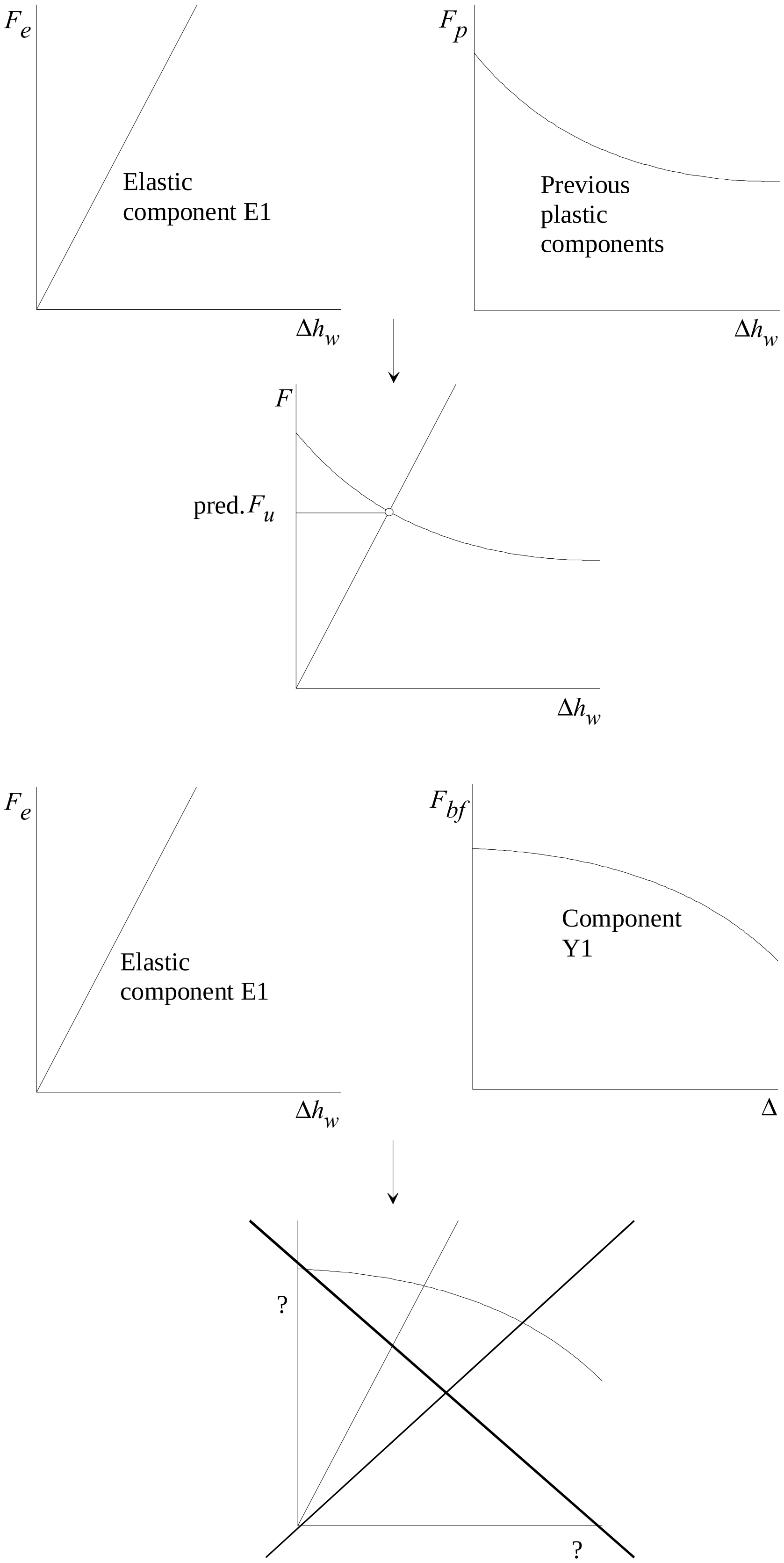

Figure 2-21. Intersection of different defined elastic and plastic curves is not possible.

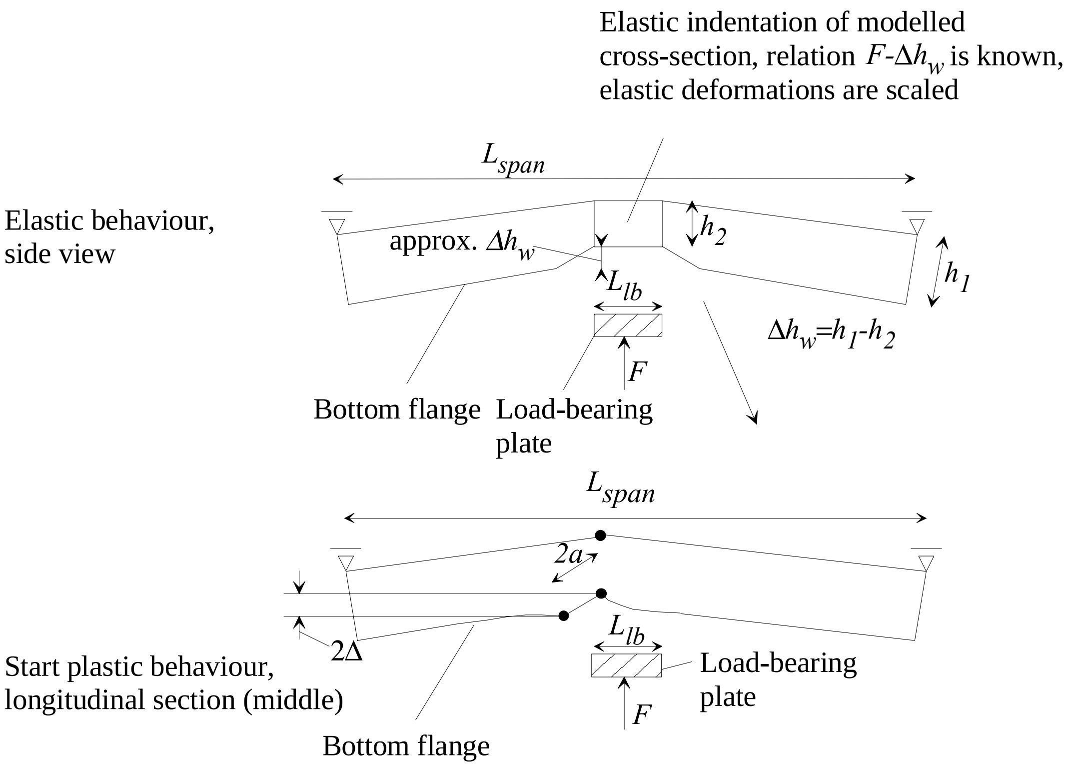

Figure 2-22. Relationship between elastic cross-section deformation and plastic flip-disc deflection.

The internal bending moment in the section equals:

$$\frac{F_{bf}}{b_{bf}t} = \frac{M_i}{I_s}s \Leftrightarrow M_i = \frac{F_{bf}I_s}{b_{bf}s*t} \tag{2.90}$$

M_i = internal bending moment [Nmm].
b_{bf} = bottom flange width [mm].
I_s = moment of inertia [mm^4].
s = distance of bottom flange to centre of gravity sheet section [mm].

Because the internal and external bending moment should be equal, it can be derived that:

$$\frac{FL_{span}}{4} = \frac{F_{bf}I_s}{b_{bf}s*t} \Leftrightarrow F = \frac{4F_{bf}I_s}{L_{span}b_{bf}s*t} \tag{2.91}$$

Calculation of intersection of E1 and Y1
Formula 2.88 can be substituted into the simplified formula describing component E1 (formula 2.35).

This results in:

$$F_e = \frac{EI(3b_{bf} + 2b_w)2\Delta}{r_{ibf}{}^2 \sin^2(\theta) b_w \left(b_{bf} - \frac{4}{3} r_{ibf} \sin(\theta_w) \right)} \tag{2.92}$$

Formula 2.87 describing component Y1 can be substituted into formula 2.91. This results in:

$$F_p = \frac{4I_s}{L_{span} b_{bf} s * t} *$$
$$\frac{f_y tb}{6} \left[1 - \frac{2\Delta}{t} + \sqrt{\left(\frac{2\Delta}{t}\right)^2 + 1} - \frac{6\Delta}{t\left(1 + 4a^2/b^2\right)} + 4\sqrt{\left(\frac{3\Delta}{2t\left(1+4a^2/b^2\right)}\right)^2 + 1} \right] \tag{2.93}$$

If the elastic load F_e and the plastic load F_p are set equal, the flip-disc out-of-plane displacement can be solved. Then the ultimate sheet section load F_u can be calculated by using the value for Δ into formulae 2.92 or 2.93.

2.5 Post-failure model results

2.5.1 Verification methods

Correlation coefficient
One method to find out how well a model like MA1 predicts the ultimate load for experiments is a measurement of correlation between model predictions and experiments. The correlation checks whether there is a linear relationship between two variables, in this case the experimental values of the ultimate load and the model predictions. If there is a linear relationship, the correlation coefficient equals 1. If there is no relationship, the coefficient equals 0. The correlation coefficient can be calculated as follows:

Determine the mean values and standard deviations of *e* and *m*:

$$\bar{e} = \frac{1}{n}\sum_{i=1}^{n} e_i \tag{2.94}$$

$\bar{e}$ = main value for experimental values for the ultimate load.
n = number of experiments.
e_i = experiment *i*.

$$\bar{m} = \frac{1}{n}\sum_{i=1}^{n} m_i \tag{2.95}$$

$\bar{m}$ = main value for model predictions of the ultimate load.
m_i = model prediction *i*.

$$s_e = \sqrt{\frac{1}{n-1} * \sum_{i=1}^{n}\left(e_i{}^2 - \bar{e}^2\right)} \tag{2.96}$$

s_e = standard deviation for experiments.

$$s_m = \sqrt{\frac{1}{n-1} * \sum_{i=1}^{n}\left(m_i{}^2 - \bar{m}^2\right)} \tag{2.97}$$

s_m = standard deviation for model predictions.

Now the correlation coefficient ρ can be calculated as:

$$\rho = \frac{\sum_{i=1}^{n}\left(e_i m_i - n\bar{e}\bar{m}\right)}{(n-1)s_e s_m} \tag{2.98}$$

Average and coefficient of variation

The correlation coefficient indicates whether there is a qualitative relationship between the experimental values and the model predictions. Nevertheless, it is not known whether the model predicts the experimental values well quantitatively. Therefore, for every experiment the ratio between model value and experimental value is calculated. Then the average, standard deviation, and coefficient of variation are calculated for the ratios of all experiments. The coefficient of variation equals the standard deviation divided by the average. An average close to 1 indicates that the model predicts the experimental values well (on average). A low (close to zero) coefficient of variation indicates this is not only the case on average, but for the most individual experiments also.

Experiments

For checking post-failure mechanical models, only experiments can be used for which the post-failure mode is specified for each experiment. For instance, it would not be useful to check whether the yield arc post-failure model predicts experiments well, if rolling post-failure mode experiments are used. For this reason, only the experiments in chapter 3 of the thesis [Hofm00a] are used. Other experiments (see chapter 2 of the thesis) do not specify the post-failure modes. An exception has been made for experiments failing by the rolling post-failure mode. Only 7 experiments in chapter 3 of the thesis fail by this post-failure mode and these experiments all have the same nominal variable values. Therefore, for checking the rolling post-failure models, experiments of Bakker [Bakk92a] are used.

2.5.2 Verification of yield arc post-failure models

Experiments of chapter 3 of the thesis [Hofm00a] are used failing by the yield arc post-failure mode. These experiments are listed in thesis [Hofm00a] table A-4, appendix A, and coded by post-failure mode A. Table 2-1 shows the correlation, average, etc. for the experiments and Eurocode3 predictions. Table 2-2 shows the experiments and several (not all) yield arc post-failure models as presented in section 2.2.

Table 2-1. Eurocode3 predictions for experiments failing by the yield arc post-failure mode.

Experiments A (33)		Correlation	Average	Standard deviation	Coefficient of variation
Eurocode3		0.95	0.93	0.09	0.09

Table 2-2. Post-failure model predictions for experiments failing by the yield arc post-failure mode.

Experiments A (33)	Components E1,A1 + ...	Correlation	Average	Standard deviation	Coefficient of variation
Model MA1	A2+A3+A4	0.70	1.32	0.36	0.27
Model MA3	A2+A4	0.68	1.16	0.33	0.28
Model MA2	A3+A4	0.63	0.90	0.29	0.32
Model MA4	A4	0.59	0.74	0.27	0.36
Model MA12	-	0.43	0.90	0.32	0.36

Eurocode3 predictions are much better than the post-failure models' predictions. However, table 2-2 shows clearly that the more (or better) components, the better the results of the mechanical models. Chapter 6 of the thesis [Hofm00a] will suggest some differences between Eurocode3 and the models as a possible cause for the differences in performance.

2.5.3 Verification of rolling post-failure models

Experiments of Bakker's thesis [Bakk92a] are used that are failing by the rolling post-failure mode, see thesis [Hofm00a] table A-5, appendix A. Furthermore, the 7 experiments of thesis chapter 3 (failing by the rolling post-failure mode) are used.

Table 2-3 shows the correlation, average, etc. for the experiments and Eurocode3 predictions. The ultimate load of the experiments F_{test} is used for the comparison, not the mode initiation load F_{imec}, because the Eurocode3 predicts the ultimate load for sheet sections. In fact, almost no Bakker experiments satisfy the conditions for using the Eurocode3 (see thesis [Hofm00a] chapter 2 for more details). However, to have some possibilities to compare the Eurocode3 and the post-failure models, the experiments are still used.

Table 2-4 shows the experiments and several (not all) rolling post-failure models as presented in section 2.3. Now, the mode initiation load F_{imec} is used for the comparison, because the post-failure models predict the mode initiation load.

Table 2-3. Eurocode3 predictions for experiments failing by the rolling post-failure mode.

Bakker experiments (28) and experiments chapter 3 (7)		Correlation	Average	Standard deviation	Coefficient of variation
Eurocode3		0.67	0.95	0.19	0.20

Table 2-4. Post-failure model predictions for experiments failing by the rolling post-failure mode.

Bakker experiments (28) and experiments chapter 3 (7)	Components E1,R1 + ...	Correlation	Average	Standard deviation	Coefficient of variation
Model MR1	A2+A3+A4	0.85	0.83	0.18	0.21
Model MR3	A2+A4	0.85	0.69	0.15	0.22
Model MR2	A3+A4	0.81	0.46	0.12	0.26
Model MR4	A4	0.73	0.31	0.12	0.37
Model MR12	-	0.70	0.43	0.15	0.34

Model predictions are much better than the Eurocode3 predictions. However, Eurocode3 predicts the ultimate load, the post-failure models predict the mode initiation load. Table 2-4 shows clearly that the more (or better) components, the better the results.

2.5.4 Verification of yield eye post-failure model

Experiments of chapter 3 of the thesis [Hofm00a] are used that failed by the yield eye post-failure mode, see thesis table A-4, appendix A, and coded by post-failure mode E.

Table 2-5 shows the correlation, average, etc. for the experiments and Eurocode3 predictions.

Table 2-6 shows the experiments and the yield eye post-failure model predictions as presented in section 2.4.

Table 2-5. Eurocode3 predictions for experiments failing by the yield eye post-failure mode.

Experiments E (7)		Correlation	Average	Standard deviation	Coefficient of variation
Eurocode3		0.87	0.91	0.10	0.11

Table 2-6. Post-failure model predictions for experiments failing by the yield eye post-failure mode.

Experiments E (7)		Correlation	Average	Standard deviation	Coefficient of variation
Model ME1		0.91	1.03	0.37	0.36

Both the Eurocode3 and the yield eye post-failure model predict the experimental values well. The standard deviation of the post-failure model is significantly higher than for Eurocode3. These conclusions are based on 7 experiments only.

2.6 Conclusions

A methodology to develop post-failure mechanical models has been presented. This methodology separates sheet section behaviour into components.

For the yield arc and rolling post-failure modes, mechanical models have been developed which first predict the ultimate load for a piece of the sheet section above the load-bearing plate. Hereafter, this prediction is corrected for pieces of the sheet section adjacent to the load-bearing plate and the length effect. Mathematical techniques have been used to simplify the model equations.

For the yield eye post-failure model the model transforms elastic cross-section behaviour in an elastic flip-disc out-of-plane displacement. For plastic flip-disc behaviour, an existing model is used. By setting equal elastic and plastic loads of the section, the ultimate load can be predicted.

The developed models are compared with experiments. For the yield arc and yield eye post-failure modes the experiments presented in chapter 3 of thesis [Hofm00a] are used. For the rolling post-failure mode, experiments carried out by Bakker are used. The more detailed the models are, the higher is the correlation with the experiments. This indicates that the methodology works well. The components used in this report are exemplary. Better components may result in a better correlation.

3 Appendix detailed derivations post-failure models

3.1 Derivation of formulae 2.18 to 2.21

These formulae were derived by Maarten Vaessen in 1995 [Vaes95a]. Some remarks should be made to fully understand his master thesis in the context of this thesis.

Page 125 [Vaes95a]: '… of the establishment of the portal frame model both…'
The 'portal frame model' as mentioned by Vaessen was intended to describe the elastic web crippling stiffness of hat sections, sheet sections, and trapezoidal sheeting. The first step in order to create this 'portal frame model' was to predict the relation between the applied forces and the indentation of a small prismatic cross-section part of a sheet section. This small prismatic part can be seen as the same as the 'modelled cross-section' in this thesis. However, Vaessen assumes a cross-section dx small. In this thesis, the modelled cross-section has a width equal to L_{lb}.

Page 125: '… the assumptions as stated in section 3.2, the cross section…'
Two of the assumptions as stated in section 3.2 are related to the 'portal frame model' and are not important for the modelled cross-section in this thesis. Important assumptions are: The rounding of the corners of the modelled cross-section is ignored (1). However, the eccentricity of the two concentrated loads due to the rounding is taken into account. Although the support creates an equally distributed load at the top flange first, curling of the top flange makes it acceptable to replace the distributed load by two concentrated loads (2). Shear deformations in the modelled cross-section are ignored (3). Only axial forces and bending moments are taken into account.

Page 125: Figure A.1
Vaessen rotates the modelled cross-section 180 degrees in all his figures. Vaessen defines the bottom flange in this report as top flange and vice versa.

Page 130: '… the reciprocal two-dimensional web crippling…'
This reciprocal two-dimensional web crippling stiffness equals the web crippling deformation divided by the support load. Therefore, the support load equals the web crippling stiffness divided by this reciprocal web crippling stiffness. Rewriting the formulae in the master thesis and defining variables as used in this report, formula 2.18 to 2.21 can be derived.

Page 125-130: defining variables
The following variables are used in Vaessen's thesis:

b_{tf}	= top flange width.
$r_{i;tf}$	= interior corner radius between web and top flange.
θ_w	= angle between web and flange.
F	= distributed load of support, modelled as concentrated load.
R_h	= horizontal reaction.
A,B,C,D	= points.
u_i	= horizontal displacement point i.
w_i	= vertical displacement point i.

φ_i	= rotation point *i.*
x	= direction of cross-section width (perpend. to plane cross-section).
E_i	= accumulated elastic energy.
$\Delta h_{w;2D}$	= web crippling deformation (vertical displacement point A).
$k_{\Delta hw;2D}$	= web crippling stiffness (load divided by web crippling deformation).

3.2 Derivation of formulae 2.22, 2.23, and 2.24

A yield line, a line like concentrated zone in thin-walled steel where yielding occurs, dissipates energy when the two accompanying plate parts rotate in relation to each other. Bakker [Bakk92a] stated that, for a yield line only subject to bending stresses along the length, and no strains in length direction, the energy dissipated by the yield line could be calculated as follows:

$$E_i = \frac{2}{\sqrt{3}} \frac{f_y t^2}{4} * L_i * \varphi_i \tag{3.1}$$

E_i	= dissipated energy yield line *i.*
f_y	= steel plate yield stress.
t	= steel plate thickness.
L_i	= length yield line *i.*
φ_i	= rotation yield line *i.*

Figure 3-1 shows the plastic behaviour for the modelled cross-section for the yield arc post-failure mode. The figure shows a cross-section having the same width as the support (width is perpendicular to the paper plane). Yield lines are indicated by black dots. The variable L_w defines the distance between two yield lines.

By setting equal external energy and internal dissipated energy, the load needed to deform the cross-section for a certain cross-section indentation Δh_w can be predicted. However, yield line rotation is not correlated linearly to the indentation. By setting equal incremental external energy and incremental internal dissipated energy, this problem is solved. The incremental external energy equals the load multiplied by a virtual, very small deviation $\delta\Delta h_w$ of the indentation Δh_w, thus:

$$\delta E_e = F_p * \delta\Delta h_w \tag{3.2}$$

δE_e	= incremental external energy.
F_p	= load at cross-section for plastic cross-section behaviour.
$\delta\Delta h_w$	= virtual, very small deviation of cross-section indentation.

The incremental internal dissipated energy equals the sum of the incremental energy dissipated for each yield line, thus:

$$\delta E_i = \sum_{i=1}^{n} \frac{2}{\sqrt{3}} \frac{f_y t^2}{4} L_i \delta\varphi_i \tag{3.3}$$

δE_i = incremental internal dissipated energy.

Setting equal incremental internal and external energy, the load F_p can be predicted:

$$F_p * \delta\Delta h_w = \sum_{i=1}^{n} \frac{2}{\sqrt{3}} \frac{f_y t^2}{4} L_i \delta\varphi_i \Leftrightarrow$$

$$F_p = \frac{2}{\sqrt{3}} \frac{f_y t^2}{4} \sum_{i=1}^{n} L_i \frac{\delta\varphi_i}{\delta\Delta h_w} \tag{3.4}$$

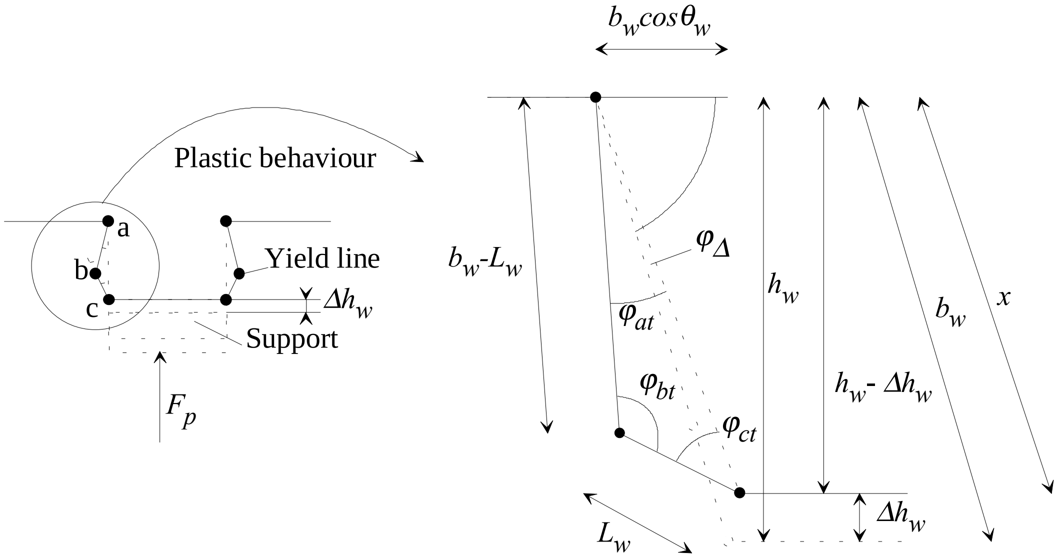

Figure 3-1. Definition of variables for determination yield line rotations.

In case of the modelled cross-section, three yield lines occur: yield lines a, b, and c (see figure 3-1 on the left). Because these yield lines occur at both sides of the cross-section, their derivatives to $\delta\Delta h_w$ need only be calculated once. Thereafter, F_p can be doubled to give a correct prediction. The length of the yield lines equals the width of the modelled cross-section L_{lb} (figure 2-14). Thus:

$$F_p = 2\frac{2}{\sqrt{3}} \frac{f_y t^2}{4} L_{lb}\left(\frac{\delta\varphi_a}{\delta\Delta h_w} + \frac{\delta\varphi_b}{\delta\Delta h_w} + \frac{\delta\varphi_c}{\delta\Delta h_w}\right) \tag{3.5}$$

Now, the incremental change of the yield line rotations related to an incremental change of the web crippling deformation Δh_w should be determined. Figure 3-1 shows this:

$$\tan(\theta_W - \varphi_\Delta) = \frac{h_W - \Delta h_W}{b_W \cos\theta_W} \Leftrightarrow \varphi_\Delta = \theta_W - \arctan\left(\frac{h_W - \Delta h_W}{b_W \cos\theta_W}\right) \tag{3.6}$$

$$x = \sqrt{(h_W - \Delta h_W)^2 + {b_W}^2 \cos^2\theta_W} \tag{3.7}$$

Using the cosines rule, a relation between the angles φ_{at}, φ_{bt}, and φ_{ct} and the sides of the triangle *abc* can be derived.

$$ {L_W}^2 = (b_W - L_W)^2 + x^2 - 2x(b_W - L_W)\cos\varphi_{at} \Leftrightarrow$$

$$\varphi_{at} = \arccos\left(\frac{{L_W}^2 - (b_W - L_W)^2 - x^2}{-2x(b_W - L_W)}\right) \tag{3.8}$$

$$\mathrm{x}^2 = (b_W - L_W)^2 + {L_W}^2 - 2(b_W - L_W)L_W\cos\varphi_{bt} \Leftrightarrow$$

$$\varphi_{bt} = \arccos\left(\frac{\mathrm{x}^2 - (b_W - L_W)^2 - {L_W}^2}{-2(b_W - L_W)L_W}\right) \tag{3.9}$$

$$(b_W - L_W)^2 = x^2 + {L_W}^2 - 2xL_W\cos\varphi_{ct} \Leftrightarrow$$

$$\varphi_{ct} = \arccos\left(\frac{(b_W - L_W)^2 - x^2 - {L_W}^2}{-2xL_W}\right) \tag{3.10}$$

Figure 3-1 shows that the real rotations of the yield lines *a*, *b*, and *c* can be derived making use of formula 3.6.

$$\varphi_a = \varphi_{at} - \varphi_\Delta = \arccos\left(\frac{{L_W}^2 - (b_W - L_W)^2 - x^2}{-2x(b_W - L_W)}\right) - \theta_W + \arctan\left(\frac{h_W - \Delta h_W}{b_W \cos\theta_W}\right) \tag{3.11}$$

$$\varphi_b = \varphi_{bt} = \arccos\left(\frac{\mathrm{x}^2 - (b_W - L_W)^2 - {L_W}^2}{-2(b_W - L_W)L_W}\right) \tag{3.12}$$

$$\varphi_c = \varphi_{ct} + \varphi_\Delta = \arccos\left(\frac{(b_W - L_W)^2 - x^2 - {L_W}^2}{-2xL_W}\right) + \theta_W - \arctan\left(\frac{h_W - \Delta h_W}{b_W \cos\theta_W}\right) \tag{3.13}$$

Formulae 3.7, 3.11, 3.12, and 3.13 can be derived to the web crippling deformation. This results in the following derivatives:

$$\frac{\delta\varphi_a}{\delta\Delta h_w}=-\frac{\dfrac{\left(\dfrac{\delta x}{\delta\Delta h_w}\right)}{b_w-L_w}+\dfrac{\left(L_w{}^2-(b_w-L_w)^2-x^2\right)\left(\dfrac{\delta x}{\delta\Delta h_w}\right)}{2(b_w-L_w)x^2}}{\sqrt{1-\dfrac{\left(L_w{}^2-(b_w-L_w)^2-x^2\right)^2}{4(b_w-L_w)^2x^2}}}-\frac{\sec\theta_w}{b_w\left(1+\dfrac{(h_w-\Delta h_w)^2\sec^2\theta_w}{b_w{}^2}\right)} \tag{3.14}$$

$$\frac{\delta\varphi_b}{\delta\Delta h_w}=\frac{x\left(\dfrac{\delta x}{\delta\Delta h_w}\right)}{(b_w-L_w)L_w\sqrt{1-\dfrac{\left(-L_w{}^2-(b_w-L_w)^2+x^2\right)^2}{4(b_w-L_w)^2L_w{}^2}}} \tag{3.15}$$

$$\frac{\delta\varphi_c}{\delta\Delta h_w}=-\frac{\dfrac{\left(\dfrac{\delta x}{\delta\Delta h_w}\right)}{L_w}+\dfrac{\left(-L_w{}^2+(b_w-L_w)^2-x^2\right)\left(\dfrac{\delta x}{\delta\Delta h_w}\right)}{2L_wx^2}}{\sqrt{1-\dfrac{\left(-L_w{}^2+(b_w-L_w)^2-x^2\right)^2}{4L_w{}^2x^2}}}+\frac{\sec\theta_w}{b_w\left(1+\dfrac{(h_w-\Delta h_w)^2\sec^2\theta_w}{b_w{}^2}\right)} \tag{3.16}$$

$$\frac{\delta x}{\delta\Delta h_w}=-\frac{(h_w-\Delta h_w)}{\sqrt{(h_w-\Delta h_w)^2+b_w{}^2\cos^2\theta_w}} \tag{3.17}$$

Formulae 3.5, 3.14, and 3.7 equal formulae 2.22, 2.23, and 2.24 in chapter 2.

3.3 Derivation of formulae 2.26, 2.27, 2.28, and 2.29

Figure 3-2 shows the yield lines in the bottom flange. These yield lines behave the same as the yield lines in the modelled cross-section. Therefore, formula 3.5 can be rewritten for the load F_{ylbf} as follows.

$$F_{ylbf}=2\frac{2}{\sqrt{3}}\frac{f_yt^2}{4}b_{bf}\left(\frac{\delta\varphi_d}{\delta\Delta h_w}+\frac{\delta\varphi_e}{\delta\Delta h_w}\right) \tag{3.18}$$

The length of the yield lines d and e equals the bottom flange width b_{bf}. Now, the derivatives of yield line rotations φ_d and φ_e should be derived. This derivation is based on the work of Bakker [Bakk92a]. However, some simplifications have been carried out, making it worth to rewrite her derivations in this appendix. The simplifications will be mentioned in the text.

Using figure 3-2, it can be derived that:

$$L_{yw} = |P_1, P_4| = \sqrt{h_w{}^2 + L_{bf}{}^2} \tag{3.19}$$

$$\sin\varphi_w = \frac{h_w}{L_{yw}} \tag{3.20}$$

$$\cos\varphi_w = \frac{L_{bf}}{L_{yw}} \tag{3.21}$$

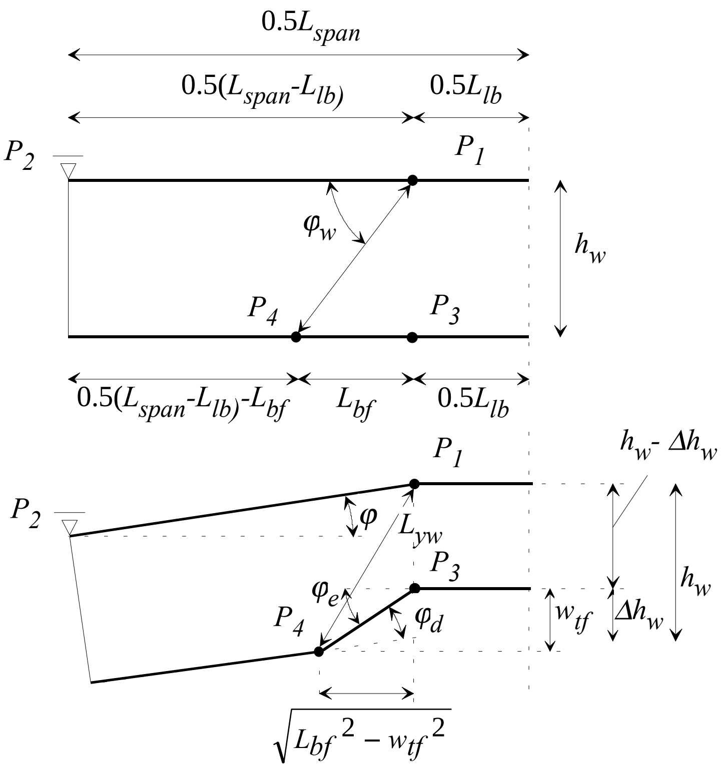

Figure 3-2. Not deformed and deformed longitudinal section of sheet section.

Furthermore, figure 3-2 shows:

$$w_{tf} + (h_w - \Delta h_w) = L_{yw}\sin(\varphi_w + \varphi) = L_{yw}(\sin\varphi_w\cos\varphi + \cos\varphi_w\sin\varphi) \tag{3.22}$$

Inserting 3.20 and 3.21 in 3.22 makes it possible to predict the cross-section indentation as a function of w_{tf} and φ:

$$\Delta h_w = -(h_w\cos\varphi + L_{bf}\sin\varphi) + w_{tf} + h_w \tag{3.23}$$

Now, w_{tf} should be determined. Therefore, the horizontal movement of point P4 will be considered in figure 3-3.

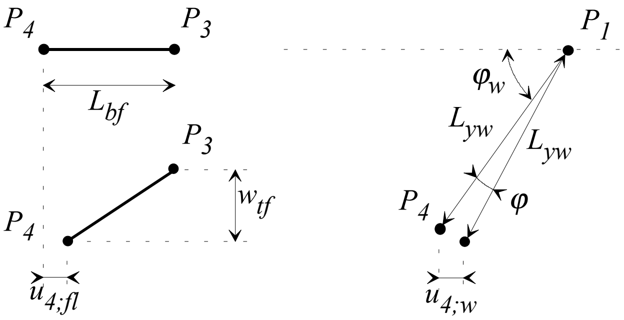

Figure 3-3. Two different ways to observe the horizontal displacement of point P4.

The horizontal displacement $u_{4;fl}$ of point P4 due to w_{tf} equals:

$$u_{4;fl} = L_{bf} - \sqrt{L_{bf}^2 - w_{tf}^2} \tag{3.24}$$

The horizontal displacement $u_{4;w}$ of point P4 due to the rotation φ equals:

$$u_{4;w} = L_{yw}\left(\cos\varphi_w - \cos(\varphi_w + \varphi)\right) \tag{3.25}$$

Using 3.20 and 3.21 into equation 3.25:

$$u_{4;w} = L_{yw}\left(\cos\varphi_w - \cos(\varphi_w + \varphi)\right) = L_{yw}\cos\varphi_w \text{-} L_{yw}\left(\cos\varphi_w\cos\varphi - \sin\varphi_w\sin\varphi\right) \Leftrightarrow$$

$$u_{4;w} = L_{yw}\frac{L_{bf}}{L_{yw}} \text{-} L_{yw}\left(\frac{L_{bf}}{L_{yw}}\cos\varphi - \frac{h_w}{L_{yw}}\sin\varphi\right) = L_{bf} \text{-} L_{bf}\cos\varphi + h_w\sin\varphi \tag{3.26}$$

Compatibility requires that $u_{4;tf}$ should be equal to $u_{4;w}$. Setting equal equation 3.24 and 3.26 yields w_{tf}:

$$L_{bf} - \sqrt{L_{bf}^2 - w_{tf}^2} = L_{bf} \text{-} L_{bf}\cos\varphi + h_w\sin\varphi \Leftrightarrow$$

$$\sqrt{L_{bf}^2 - w_{tf}^2} = L_{bf}\cos\varphi - h_w\sin\varphi \Leftrightarrow$$

$$w_{tf} = \sqrt{L_{bf}^2 - \left(L_{bf}\cos\varphi - h_w\sin\varphi\right)^2} \tag{3.27}$$

Inserting equation 3.27 into equation 3.23 describes the relationship between the web crippling deformation Δh_w and the rotation φ:

$$\Delta h_w = -\left(h_w \cos\varphi + L_{bf} \sin\varphi\right) + \sqrt{L_{bf}{}^2 - \left(L_{bf} \cos\varphi - h_w \sin\varphi\right)^2} + h_w \tag{3.28}$$

This equation can be differentiated with respect to φ as follows:

$$\frac{\delta \Delta h_w}{\delta \varphi} = \left(h_w \sin\varphi - L_{bf} \cos\varphi\right) + \frac{\left(L_{bf} \cos\varphi - h_w \sin\varphi\right)\left(L_{bf} \sin\varphi + h_w \cos\varphi\right)}{\sqrt{L_{bf}{}^2 - \left(L_{bf} \cos\varphi - h_w \sin\varphi\right)^2}} \tag{3.29}$$

Rewriting equations 3.23 and 3.27, it can be concluded that:

$$\Delta h_w = -\left(h_w \cos\varphi + L_{bf} \sin\varphi\right) + w_{tf} + h_w \Leftrightarrow \left(h_w \cos\varphi + L_{bf} \sin\varphi\right) = h_w + w_{tf} - \Delta h_w \tag{3.30}$$

$$w_{tf} = \sqrt{L_{bf}{}^2 - \left(L_{bf} \cos\varphi - h_w \sin\varphi\right)^2} \Leftrightarrow \left(L_{bf} \cos\varphi - h_w \sin\varphi\right) = \sqrt{L_{bf}{}^2 - w_{tf}{}^2} \tag{3.31}$$

Substituting 3.30 and 3.31 into 3.29 yields:

$$\frac{\delta \Delta h_w}{\delta \varphi} = -\sqrt{L_{bf}{}^2 - w_{tf}{}^2} + \frac{\sqrt{L_{bf}{}^2 - w_{tf}{}^2}\left(h_w + w_{tf} - \Delta h_w\right)}{w_{tf}} = \frac{\sqrt{L_{bf}{}^2 - w_{tf}{}^2}\left(h_w - \Delta h_w\right)}{w_{tf}} \tag{3.32}$$

Now, the incremental change of φ for an incremental change of Δh_w can be determined as follows:

$$\frac{\delta \varphi}{\delta \Delta h_w} = \frac{w_{tf}}{\sqrt{L_{bf}{}^2 - w_{tf}{}^2}\left(h_w - \Delta h_w\right)} \tag{3.33}$$

The variable w_{tf} can be predicted using 3.27. The variable φ in 3.27 can be determined by iterative solving 3.28. Figure 3-2 shows:

$$\varphi_e = \arcsin \frac{w_{tf}}{L_{bf}} \tag{3.34}$$

This equation 3.34 can be differentiated with respect to Δh_w, yielding:

$$\frac{\delta \varphi_e}{\delta \Delta h_w} = \frac{1}{L_{bf} \cos\varphi_e} \frac{\delta w_{tf}}{\delta \Delta h_w} \tag{3.35}$$

Figure 3-2 shows:

$$\cos\varphi_e = \frac{\sqrt{L_{bf}{}^2 - w_{tf}{}^2}}{L_{bf}} \tag{3.36}$$

Furthermore:

$$\frac{\delta w_{tf}}{\delta\Delta h_w} = \frac{\delta w_{tf}}{\delta\varphi}\frac{\delta\varphi}{\delta\Delta h_w} = \frac{(L_{bf}\cos\varphi - h_w\sin\varphi)(L_{bf}\sin\varphi + h_w\cos\varphi)}{w_{tf}}\frac{w_{tf}}{\sqrt{L_{bf}{}^2 - w_{tf}{}^2}\,(h_w - \Delta h_w)} \tag{3.37}$$

Using 3.30 and 3.31, equation 3.37 can be rewritten as:

$$\frac{\delta w_{tf}}{\delta\Delta h_w} = \frac{\delta w_{tf}}{\delta\varphi}\frac{\delta\varphi}{\delta\Delta h_w} = \frac{\sqrt{L_{bf}\,2 - w_{tf}\,2}\,(h_w + w_{tf} - \Delta h_w)}{w_{tf}}\frac{w_{tf}}{\sqrt{L_{bf}{}^2 - w_{tf}{}^2}\,(h_w - \Delta h_w)} \Leftrightarrow$$

$$\frac{\delta w_{tf}}{\delta\Delta h_w} = \frac{(h_w + w_{tf} - \Delta h_w)}{(h_w - \Delta h_w)} \tag{3.38}$$

Now, using equation 3.36 and 3.37, formula 3.35 yields:

$$\frac{\delta\varphi_e}{\delta\Delta h_w} = \frac{(h_w + w_{tf} - \Delta h_w)}{(h_w - \Delta h_w)\sqrt{L_{bf}{}^2 - w_{tf}{}^2}} \tag{3.39}$$

From figure 3-2 it can also be seen that:

$$\varphi_d = \varphi_e - \varphi \Leftrightarrow \frac{\delta\varphi_d}{\delta\Delta h_w} = \frac{\delta\varphi_e}{\delta\Delta h_w} - \frac{\delta\varphi}{\delta\Delta h_w} \tag{3.40}$$

In this appendix, formulae 2.26, 2.27, 2.28, and 2.29 have been derived as equation 3.18, 3.39, 3.27 and 3.40.

3.4 Derivation of formulae 2.69, 2.70, 2.71, 2.72, and 2.73

These formulae predict the plastic behaviour of the rolling post-failure mode, for the modelled cross-section (figure 2-17). Figure 2-19 in appendix 2 shows the rolling post-failure mode, however, in this appendix 3 more detailed drawings will be used. Figure 3-4 shows the rolling post-failure mode for the modelled cross-section.

Although the derivations of these formulae can be red in the Bakker's thesis [Bakk92a], they will be copied here for convenience.

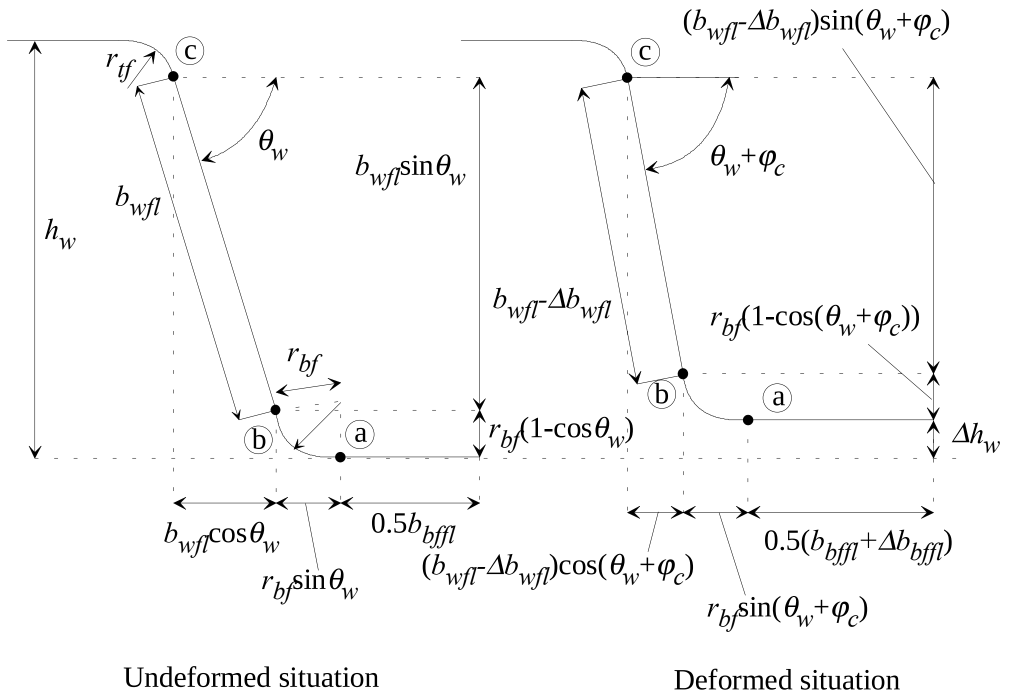

Figure 3-4. Geometry of rolling post-failure mode for modelled cross-section.

Bakker stated [Bakk92a] that the incremental amount of energy dissipated by a moving yield line (no strains in length direction) could be predicted using the following formula:

$$\delta E_\mathrm{i} = \frac{\delta u_i}{r_{bf}} \frac{2}{\sqrt{3}} \frac{f_y t^2}{4} L_i \tag{3.41}$$

δE_i	= incremental internal dissipated energy.
δu_i	= incremental movement of yield line i.
f_y	= yield stress.
L_i	= length of yield line i.
r_{bf}	= radius of circle along which yield line moves.
t	= steel plate thickness.

The external energy due to an incremental change of the web crippling deformation Δh_w equals:

$$\delta E_\mathrm{e} = F \delta \Delta h_w \tag{3.42}$$

δE_e	= incremental external energy.
F	= force of support.
$\delta\Delta h_w$	= incremental change of web crippling deformation.

Because incremental energy should be equal internal and external, formula 3.41 and 3.42 can be used to predict the plastic load needed to deform the modelled cross-section. For yield line "c" in figure 3-4, which is a normal fixed yield line (this yield line rotates only), formula 3.3 is used.

$$F\delta\Delta h_w = \frac{\delta u_i}{r_{bf}} \frac{2}{\sqrt{3}} \frac{f_y t^2}{4} L_i \Leftrightarrow$$

$$F = 2\frac{\delta u_a}{\delta\Delta h_w} \frac{1}{r_{bf}} \frac{2}{\sqrt{3}} \frac{f_y t^2}{4} L_{lb} + 2\frac{\delta u_b}{\delta\Delta h_w} \frac{1}{r_{bf}} \frac{2}{\sqrt{3}} \frac{f_y t^2}{4} L_{lb} + 2\frac{\delta\varphi_c}{\delta\Delta h_w} \frac{2}{\sqrt{3}} \frac{f_y t^2}{4} L_{lb} \tag{3.43}$$

Formula 3.43 equals formula 2.69. Now, the incremental movements of yield lines "a" and "b" should be determined as a result of an incremental change of the web crippling deformation Δh_w. First, the flat widths of several cross-section variables are determined, see figure 3-4 for their definition. The variables b_{bf} and b_w are the widths of the bottom flange and the web measured between the points of intersection of the web and flange midlines.

$$b_{bffl} = b_{bf} - 2r_{bf} \tan\left(\frac{\theta_w}{2}\right) \tag{3.44}$$

$$b_{wfl} = b_w - \left(r_{tf} + r_{bf}\right)\tan\left(\frac{\theta_w}{2}\right) \tag{3.45}$$

Due to the rolling post-failure mode, the flat width of the bottom flange increases from b_{bffl} to (b_{bffl}+Δb_{bffl}), the flat width of the web decreases from b_{wfl} to (b_{wfl}-Δb_{wfl}). The yield line displacements u_1 and u_2 can then be determined as:

$$u_a = \frac{1}{2}\Delta b_{bffl} \tag{3.46}$$

$$u_b = \Delta b_{wfl} \tag{3.47}$$

The formulae describing the incremental yield line deformations due to an incremental web crippling deformation $\delta\Delta h_w$ can best be derived as follows. First by determining the incremental yield line deformations due to the incremental rotation $\delta\varphi_c$ in yield line "c" at the top of the web. Therefore the changes in the flat widths of the elements must be expressed as a function of the rotation φ_c. Since the total length of flange and web elements does not change, it can be derived from figure 3-4 that:

$$b_{wfl} + r_{bf}\theta_w + \frac{1}{2}b_{bffl} = b_{wfl} - \Delta b_{wfl} + r_{bf}\left(\theta_w + \varphi_c\right) + \frac{1}{2}\left(b_{bffl} - \Delta b_{bffl}\right) \Leftrightarrow$$

$$\Delta b_{bffl} = 2\left(\Delta b_{wfl} - r_{bf}\varphi_c\right) \tag{3.48}$$

The distance between the tops of the webs does not change either, and therefore:

$$b_{wfl}\cos\theta_w + r_{bf}\sin\theta_w + \frac{1}{2}b_{bffl} = \left(b_{wfl} - \Delta b_{wfl}\right)\cos(\theta_w + \varphi_c) + \\ r_{bf}\sin(\theta_w + \varphi_3) + \frac{1}{2}\left(b_{bffl} + \Delta b_{bffl}\right) \tag{3.49}$$

Combining formulae 3.48 and 3.49 results in:

$$\Delta b_{wfl} = \frac{b_{wfl}\left(\cos\theta_w - \cos(\theta_w + \varphi_c)\right) + r_{bf}\left(\sin\theta_w + \varphi_c - \sin(\theta_w + \varphi_c)\right)}{1 - \cos(\theta_w + \varphi_c)} \tag{3.50}$$

The incremental changes in the flat widths of the bottom flange and the web due to the incremental rotation $\delta\varphi_c$ can be determined by deriving these widths with respect to φ_c:

$$\frac{\delta\Delta b_{bffl}}{\delta\varphi_c} = \frac{\partial\Delta b_{bffl}}{\partial\varphi_c} = \left(\frac{\partial\Delta b_{wfl}}{\partial\varphi_c} - r_{bf}\right) \tag{3.51}$$

$$\frac{\delta\Delta b_{wfl}}{\delta\varphi_c} = \frac{\partial\Delta b_{wfl}}{\partial\varphi_c} = \frac{\left(b_{wfl} - \Delta b_{wfl}\right)\sin(\theta_w + \varphi_c)}{1 - \cos(\theta_w + \varphi_c)} + r_{bf} \tag{3.52}$$

To determine the incremental yield line displacements δu_a and δu_b due to an incremental web crippling deformation $\delta\Delta h_w$, this deformation must be determined as a function of the incremental rotation $\delta\varphi_c$. Therefore the web crippling deformation Δh_w must be expressed as a function of the rotation φ_c.

From figure 3-4 it can be seen that:

$$\Delta h_w = b_{wfl}\sin\theta_w - \left(b_{wfl} - \Delta b_{wfl}\right)\sin(\theta_w + \varphi_c) + r_{bf}\left(\cos(\theta_w + \varphi_c) - \cos\theta_w\right) \tag{3.53}$$

Hence:

$$\frac{\delta\Delta h_w}{\delta\varphi_c} = \frac{\delta\Delta b_{wfl}}{\delta\varphi_c}\sin(\theta_w + \varphi_c) - \left(b_{wfl} - \Delta b_{wfl}\right)\cos(\theta_w + \varphi_c) - r_{bf}\sin(\theta_w + \varphi_c) \tag{3.54}$$

Inserting formula 3.52 into 3.54 results in:

$$\frac{\delta\Delta h_w}{\delta\varphi_c} = b_{wfl} - \Delta b_{wfl} \tag{3.55}$$

From formulae 3.46, 3.47, 3.51, 3.52, and 3.55 it can then be derived that:

$$\frac{\delta u_a}{\delta \Delta h_w} = \frac{\delta u_a}{\delta \varphi_c}\frac{\delta \varphi_c}{\delta \Delta h_w} = \frac{1}{2}\frac{\delta \Delta b_{tffl}}{\delta \varphi_c}\frac{\delta \varphi_c}{\delta \Delta h_w} = \frac{\sin(\theta_w + \varphi_c)}{1-\cos(\theta_w + \varphi_c)} \tag{3.56}$$

$$\frac{\delta u_b}{\delta \Delta h_w} = \frac{\delta u_b}{\delta \varphi_c}\frac{\delta \varphi_c}{\delta \Delta h_w} = \frac{1}{2}\frac{\delta \Delta b_{wfl}}{\delta \varphi_c}\frac{\delta \varphi_c}{\delta \Delta h_w} = \frac{\sin(\theta_w + \varphi_c)}{1-\cos(\theta_w + \varphi_c)} + \frac{r_{bf}}{b_{wfl}\text{-}\Delta b_{wfl}} \tag{3.57}$$

where Δb_{wfl} is given by formula 3.50. Note that (figure 3-4):

$$u_b = u_a + r_{bf}\,\varphi_c \tag{3.58}$$

and hence:

$$\delta u_b = \delta u_a + r_{bf}\,\delta\varphi_c \tag{3.59}$$

The incremental yield line displacements depend on the yield line rotation φ_c. For finding the relationship between the web crippling deformation Δh_w and the rotation φ_c some simplifications in the geometry of the sheet section cross-section have been made. This is shown in figure 3-5. The corners are flattened and three new distances are defined: distance b_1, b_2, and b_3. The dotted line shows the deformed cross-section. It should be noted that the webs reduce in length and the (bottom) flange increases in length. This is not due to axial deformations of the webs or flange, but due to the movement of the two yield lines in the corner. Normally, these yield lines are located at different positions (see figure 3-4). Nevertheless, here, for finding the relationship between Δh_w and φ_c it is assumed that both yield lines are at the same location. In figure 3-5, the yield lines are not exactly at the same location. They are drawn in this way to show them both.

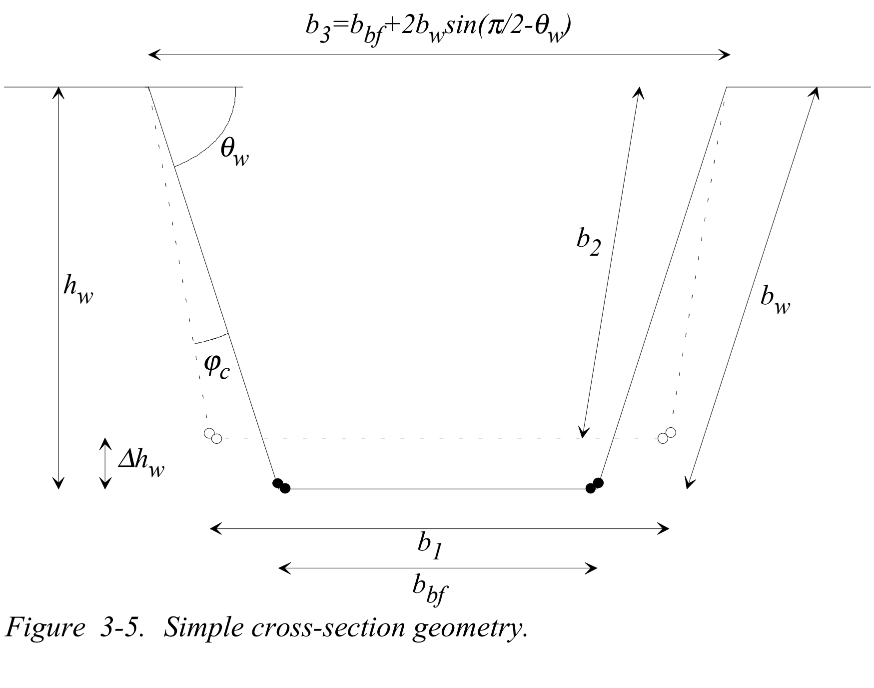

Figure 3-5. Simple cross-section geometry.

Using figure 3-5 it can be shown that:

$$\Delta h_w = h_w - b_2 \cos\left(\frac{\pi}{2} - \theta_w - \varphi_c\right) \tag{3.60}$$

The distance between the tops of the webs b_3 is assumed to remain equal. For sheet sections and sheeting, this is true. If the distance remains equal then:

$$\sin\left(\frac{\pi}{2} - \theta_w - \varphi_c\right) = \frac{0.5(b_3 - b_1)}{b_2} \tag{3.61}$$

The total length of the two webs and bottom flange cannot change:

$$b_{bf} + 2b_w = b_1 + 2b_2 \tag{3.62}$$

Formula 3.62 can be solved for b_1 that can be substituted in formula 3.61. Note that c_1 is a new substitution variable used.

$$\sin\left(\frac{\pi}{2} - \theta_w - \varphi_c\right) = \frac{0.5b_3 - 0.5b_{bf} - b_w + b_2}{b_2} = \frac{c_1 + b_2}{b_2} = 1 + \frac{c_1}{b_2} \tag{3.63}$$

Formula 3.63 can be used to solve b_2 that can be inserted into formula 3.60:

$$\Delta h_w = h_w - \frac{c_1 \cos\left(\frac{\pi}{2} - \theta_w - \varphi_c\right)}{\sin\left(\frac{\pi}{2} - \theta_w - \varphi_c\right) - 1} \tag{3.64}$$

With c_1 and b_3 defined in formula 3.63 and figure 3-5 respectively. If it is assumed that angle φ_c is small, the following parts of formula 3.64 can be rewritten as follows:

$$\begin{aligned} &\cos\left(\frac{\pi}{2} - \theta_w - \varphi_c\right) = \\ &\cos\left(\frac{\pi}{2} - \theta_w\right)\cos\varphi_c + \sin\left(\frac{\pi}{2} - \theta_w\right)\sin\varphi_c \end{aligned} \tag{3.65}$$

$$\begin{aligned} &\sin\left(\frac{\pi}{2} - \theta_w - \varphi_c\right) = \\ &\sin\left(\frac{\pi}{2} - \theta_w\right)\cos\varphi_c - \cos\left(\frac{\pi}{2} - \theta_w\right)\sin\varphi_c = \sin\left(\frac{\pi}{2} - \theta_w\right) - \varphi_c \cos\left(\frac{\pi}{2} - \theta_w\right) \end{aligned} \tag{3.66}$$

Using formulae 3.65 and 3.66 for formula 3.64:

$$\Delta h_w = h_w - \frac{c_1 \cos\left(\frac{\pi}{2} - \theta_w\right) + c_1 \varphi_c \sin\left(\frac{\pi}{2} - \theta_w\right)}{\sin\left(\frac{\pi}{2} - \theta_w\right) - \varphi_c \cos\left(\frac{\pi}{2} - \theta_w\right) - 1} \tag{3.67}$$

Solving formula 3.67 for angle φ_c results in:

$$\varphi_c = -\frac{\Delta h_w \sin\left(\frac{\theta_w}{2}\right)}{\Delta h_w \cos\left(\frac{\theta_w}{2}\right) - b_w \sin\left(\frac{\theta_w}{2}\right)} \tag{3.68}$$

Formulae 3.56, 3.57, 3.50, and 3.68 equal formulae 2.70, 2.71, 2.72, and 2.73 in the thesis [Hofm00a].

3.5 Derivation of formula 2.35

This formula has been derived using mathematical technique M1 (paragraph 2.1.5 in the thesis [Hofm00a]) for formulae 2.18, 2.19, and 2.21.

Formulae 2.18 and 2.19 have been rewritten as follows:

$$F_e = \frac{\Delta h_w}{A + B + C} \tag{3.69}$$

$$A = \frac{b_w \sin^2(\theta_w)}{EA} \tag{3.70}$$

$$B = \frac{\cos(\theta_w)}{EA} \frac{b_w \cos(\theta_w)\left(\frac{2}{3} b_w + b_{bf}\right) + r_{ibf} b_{bf} \sin(\theta_w) - r_{ibf}{}^2 \sin^2(\theta_w)}{b_{bf} + \frac{2}{3} b_w} \tag{3.71}$$

$$C = r_{ibf}{}^2 \sin^2(\theta_w) \frac{b_w\left(b_{bf} - \frac{4}{3} r_{ibf} \sin(\theta_w)\right) + r_{ibf} \sin(\theta_w)\left(b_{bf} - \frac{3}{2} r_{ibf} \sin(\theta_w)\right)}{EI\left(3b_{bf} + 2b_w\right)} \tag{3.72}$$

Formulae 2.18 and 2.19 have been written as Δh_w divided by a summation of three terms A, B, and C. Because the formulae 3.69 to 3.72 describe sheet sections in practice, all variables in the formulae will have practical values. For all variables in formulae 3.69 to 3.72, these practical values are:

$$50 < b_w < 150 \text{ [mm]} \tag{2.36}$$

$$50 < \theta_w < 90 \text{ [degrees]} \tag{2.37}$$

$$50 < L_{lb} < 150 \text{ [mm]} \tag{2.38}$$

$$0.5 < t < 1.5 \text{ [mm]} \tag{2.39}$$

$$40 < b_{bf} < 150 \text{ [mm]} \tag{2.40}$$

$$1 < r_{bf} < 12 \text{ [mm]} \tag{2.41}$$

$$0.1 < \Delta h_w < 10 \text{ [mm]} \tag{2.42}$$

These values are part of defined variable space A (paragraph 2.2.3). Now, every variable except the web width b_w is kept on its average value. The parameter b_w is varied between 50 and 150 mm. For these values, term A, B, and C are calculated. Figure 3-6 on the left shows the results. It can be seen that only factor C plays an important role. Factor A and B can be neglected compared to factor C.

The angle between web and flange θ_w has been varied, keeping all other variables on their average value. The factor values are shown in figure 3-6 on the right. Only factor C plays an important role.

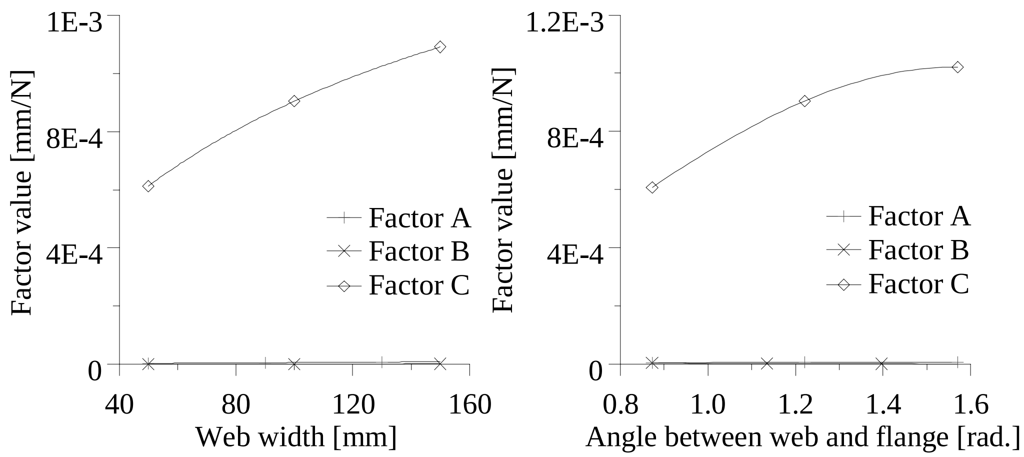

Figure 3-6. Factor A, B, and C values for web width b_w and for angle between web and flange θ_w.

Likewise, for the next four variables, the same strategy is followed. The results are shown in figure 3-7 and 3-8. For all variables, only factor C plays an important role. Without exception, factors A and B can be neglected. The last variable, Δh_w, needs not to be varied, because this variable is not a part of the factors A, B, and C.

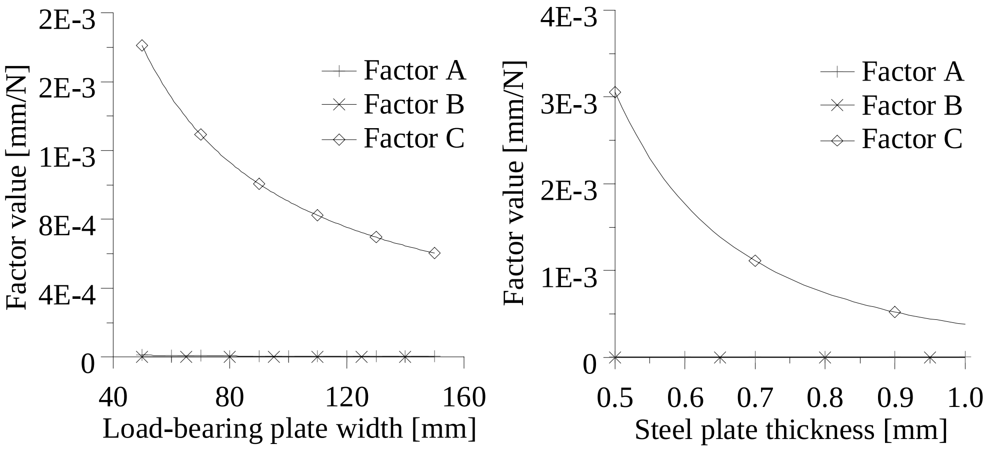

Figure 3-7. Factor A, B, and C values for load-bearing plate width L_{lb} and steel plate thickness t.

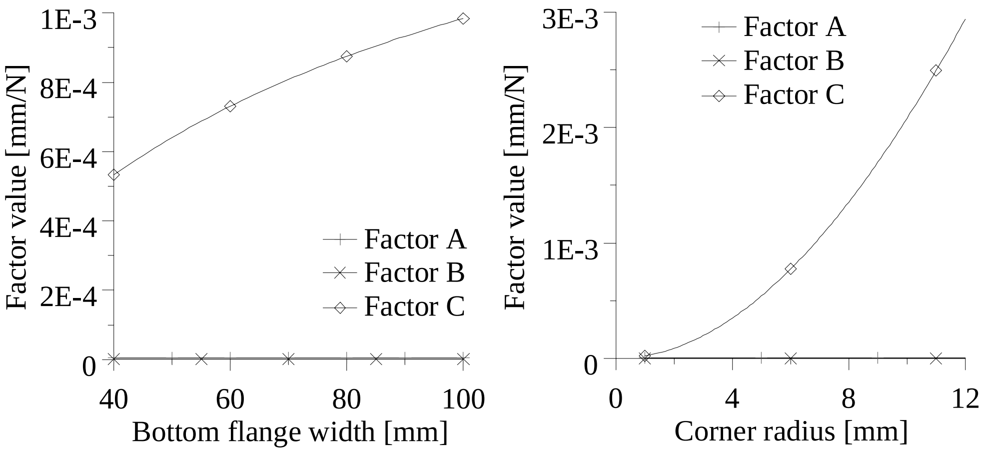

Figure 3-8. Factor A, B, and C values for bottom flange width b_{bf} and for corner radius r_{bf}.

Neglecting the factors A and B in formula 3.69 and using formula 3.72, the following formula remains:

$$F_e = \frac{\Delta h_w}{\left[r_{ibf}{}^2 \sin^2(\theta_w) \dfrac{b_w\left(b_{bf} - \frac{4}{3} r_{ibf} \sin(\theta_w)\right) + r_{ibf} \sin(\theta_w)\left(b_{bf} - \frac{3}{2} r_{ibf} \sin(\theta_w)\right)}{EI\left(3b_{bf} + 2b_w\right)} \right]^C} \tag{3.73}$$

This formula can be split up again and yields in rewritten form to:

$$F_e = \frac{\Delta h_w}{D + E} \tag{3.74}$$

$$D = \frac{r_{ibf}{}^2 \sin^2(\theta_w) * b_w \left(b_{bf} - \frac{4}{3} r_{ibf} \sin(\theta_w) \right)}{EI(3b_{bf} + 2b_w)} \tag{3.75}$$

$$E = \frac{r_{ibf}{}^2 \sin^2(\theta_w) * r_{ibf} \sin(\theta_w) \left(b_{bf} - \frac{3}{2} r_{ibf} \sin(\theta_w) \right)}{EI(3b_{bf} + 2b_w)} \tag{3.76}$$

As the method followed for factors A, B, and C, now the factors D and E are evaluated for one variable each time. All other variables keep their average value. Figure 3-9 to 3-11 present the results.

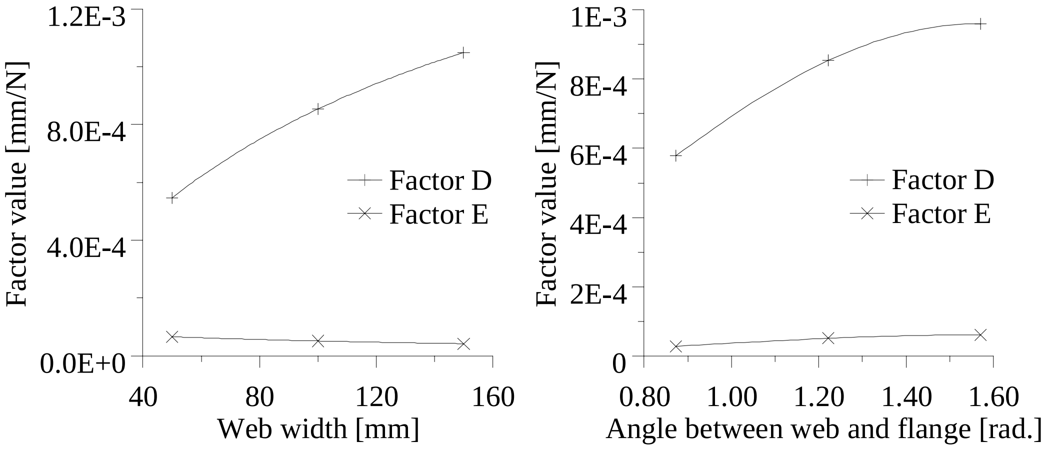

Figure 3-9. Factor D and E values for web width b_w and angle between web and flange θ_w.

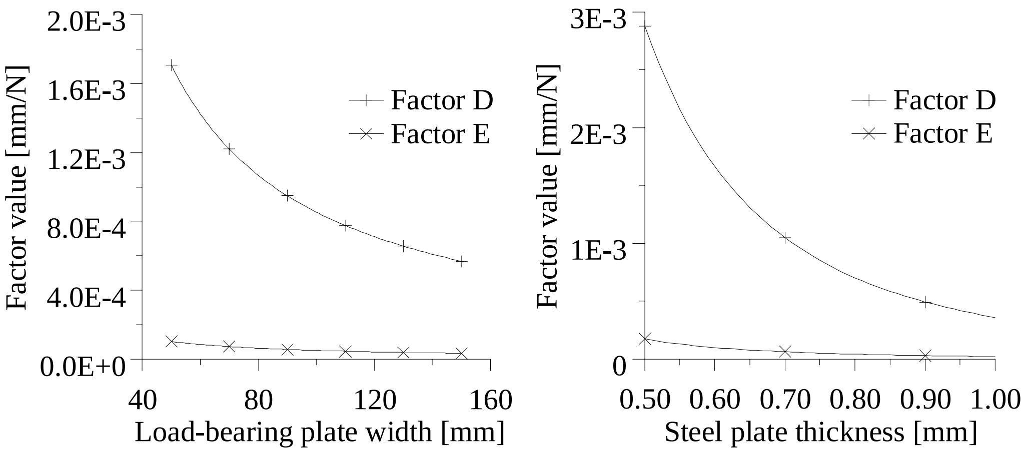

Figure 3-10. Factor D and E values for load-bearing plate width L_{lb} and steel plate thickness t.

For all variables, only factor D is an important factor. The value of factor E can be neglected for all variables.

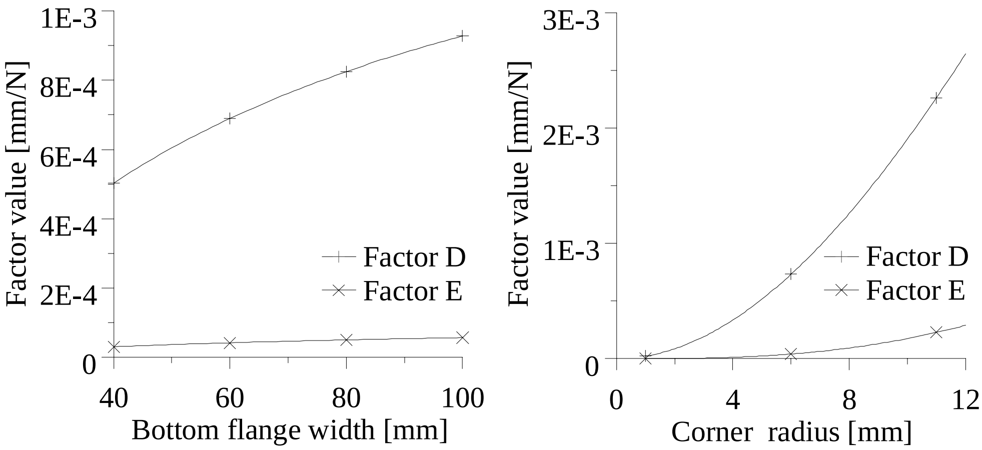

Figure 3-11. Factor D and E values for bottom flange width b_{bf} and corner radius r_{bf}.

Therefore, formulae 3.74 and 3.75 yield to:

$$F_e = \frac{EI\left(3b_{bf} + 2b_w\right)\Delta h_w}{r_{ibf}{}^2 \sin^2(\theta_w) * b_w\left(b_{bf} - \frac{4}{3} r_{ibf} \sin(\theta_w)\right)} \tag{3.77}$$

This is equal to formula 2.35 in chapter 2.

3.6 Derivation of formulae 2.43 to 2.49

Formula 3.5 together with formulae 3.14 to 3.17 predict the plastic load needed to deform the modelled cross-section for a certain web crippling deformation Δh_w. First, mathematical technique M1 (section 2.1.5) will be used. For this reason formula 3.5 is rewritten as:

$$F_p = 2\frac{2}{\sqrt{3}}\frac{f_y t^2}{4} L_{lb}(F + G + H) \tag{3.78}$$

$$F = \frac{\delta\varphi_a}{\delta\Delta h_w} \tag{3.79}$$

$$G = \frac{\delta\varphi_b}{\delta\Delta h_w} \tag{3.80}$$

$$H = \frac{\delta\varphi_c}{\delta\Delta h_w} \tag{3.81}$$

The following variables are part of formula 3.78 to 3.81. Together, they form variable space B:

$$50 < b_w < 150 \text{ [mm]} \tag{2.36}$$

$$50 < \theta_w < 90 \text{ [deg.]} \tag{2.37}$$

$$0.1 < \Delta h_w < 10 \text{ [mm]} \tag{2.42}$$

$$5 < L_w < 35 \text{ [mm]} \tag{3.82}$$

Now, every variable except the yield line distance L_w is kept on its average value. The variable L_w is varied between 5 and 35 mm. For these factors F, G, and H are calculated. Figure 3-12 on the left shows the results.

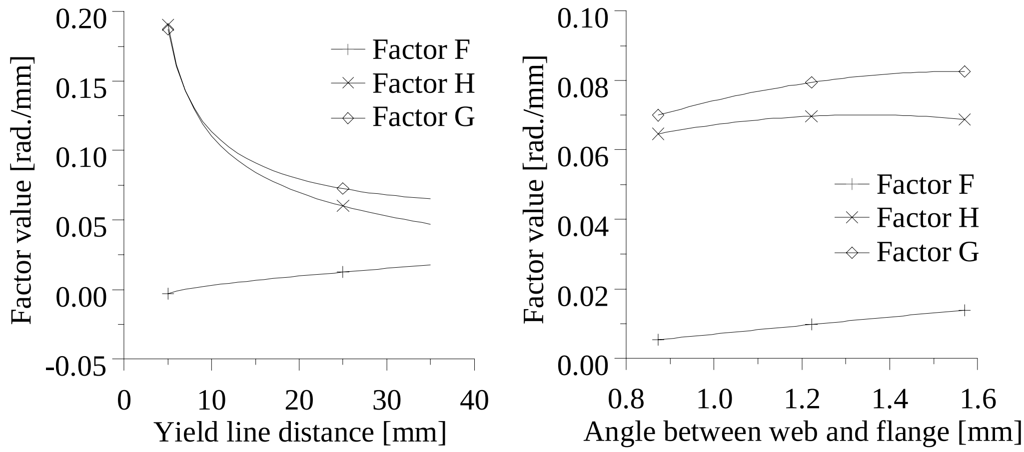

Figure 3-12. Factor F, G, and H values for yield line distance L_w and angle between web and flange θ_w.

The angle between web and flange θ_w has been varied, keeping all other variables on their average value. The factor values are shown in figure 3-12 on the right.

Likewise, for the next two variables, the same strategy is followed. The results are shown in figure 3-13.

Figure 3-12 and 3-13 show that the behaviour of factor G and H can be compared very well. Factor H values are a bit lower than factor G values. Compared to the values of factors G and H, factor F values can be neglected.

Therefore, formula 3.78 is simplified to:

$$F_p = 4 \frac{2}{\sqrt{3}} \frac{f_y t^2}{4} L_{lb} \frac{\delta \varphi_b}{\delta \Delta h_w} \tag{3.83}$$

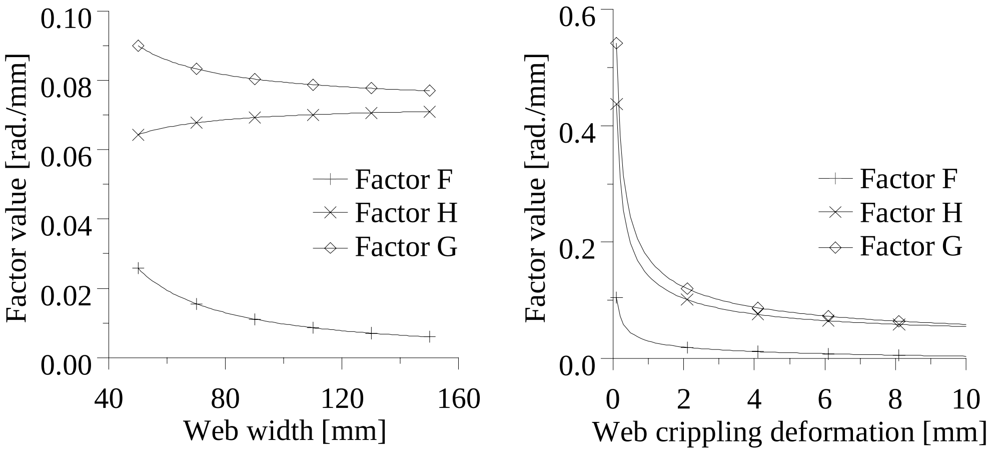

Figure 3-13. Factor F, G, and H values for web width b_W and web crippling deformation Δh_W.

Using formula 3.7, 3.15, and 3.17, this formula can be written as:

$$F_p = \frac{2}{\sqrt{3}} f_y t^2 L_{lb} * \frac{(h_W - \Delta h_W)}{(b_W - L_W) L_W \sqrt{1 - \frac{\left(-L_W{}^2 - (b_W - L_W)^2 + (h_W - \Delta h_W)^2 + b_W{}^2 \cos^2\theta_W\right)^2}{4(b_W - L_W)^2 L_W{}^2}}} \quad (3.84)$$

If the ultimate load of the modelled cross-section should be predicted, the elastic and the plastic load of the cross-section should be set equal. Therefore, formulae 3.77 and 3.84 should be set equal. Hereafter, Δh_W should be solved. However, due to the complexity of formulae 3.84, this is an almost impossible job. Therefore, formula 3.84 should be simplified, more specific the part below the square root sign. For this, mathematical technique M3 will be used (section 2.1.5).

First, the sensitivity of the part below the square root sign will be tested for every variable. The variables in this part and their practical values are equal to variable space B:

$$50 < b_W < 150 \text{ [mm]} \quad (2.36)$$

$$50 < \theta_W < 90 \text{ [degrees]} \quad (2.37)$$

$$0.1 < \Delta h_W < 10 \text{ [mm]} \quad (2.42)$$

$$5 < L_W < 35 \text{ [mm]} \quad (3.82)$$

Note that the variable h_W need not to be investigated because the web width b_W and the angle between web and flange θ_W determine the section height h_W. Each variable has been varied, keeping the other variables constant on their average value. Figure 3-14 shows the factor values compared with the varying variables.

In this figure 3-14, the horizontal axis scale is different for every variable. For example, the scale for the angle between web and flange θ_W equals the range of 50 to 90 degrees.

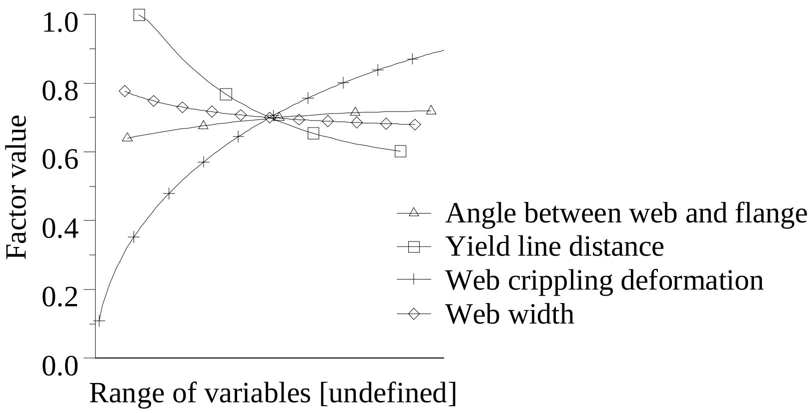

Figure 3-14. Behaviour of term for several variables. The x-axis scale is different for every variable.

Figure 3-14 shows clearly the factor below the square root sign is sensitive for the web crippling deformation Δh_W and the yield line distance L_W. For the other two variables, the factor is less sensitive. It is assumed that the factor can be simplified by writing it as a linear function of Δh_W and L_W as follows:

$$\sqrt{1-\frac{\left(-L_W{}^2-(b_W-L_W)^2+(h_W-\Delta h_W)^2+b_W{}^2\cos^2\theta_W\right)^2}{4(b_W-L_W)^2L_W{}^2}} \approx A\Delta h_W + BL_W + C \qquad (3.85)$$

Linear regression can solve the parameters A, B, and C as follows. The web crippling deformation Δh_W is varied in discrete steps of 0.1 mm (100 steps). For every possible value of the web crippling deformation, distance L_W is varied in discrete steps of 1 mm (30 steps). The two other variables are kept on their average value. In total, 30000 combinations of Δh_W and L_W occur, for which the value of the square root is determined. Using these data, the factors A, B, and C can be determined by linear regression. In this case, the regression was carried out by means of the computer program SPSS. This results in:

$$\sqrt{1-\frac{\left(-L_W{}^2-(b_W-L_W)^2+(h_W-\Delta h_W)^2+b_W{}^2\cos^2\theta_W\right)^2}{4(b_W-L_W)^2L_W{}^2}} \approx \qquad (3.86)$$
$$0.0624*\Delta h_W - 0.0101*L_W + 0.5633$$

Formula 3.86 can be substituted into formula 3.84 that results in:

$$F_p = f_y t^2 L_{lb} \frac{(h_w - \Delta h_w)}{(b_w - L_w)L_w((0.0624)\Delta h_w + (-0.0101)L_w + (0.5633))} \tag{3.87}$$

Setting equal formulae 3.77 and 3.87 (and thus equal elastic and plastic behaviour of the cross-section) makes it possible to solve Δh_w. For this purpose, some parts of the formulae are renamed.

$$f_y t^2 L_{lb} \frac{h_w - \Delta h_w}{(b_w - L_w)L_w((0.0624)\Delta h_w + (0.0101)L_w + (0.5633))} =$$

$$\frac{EI(3b_{bf} + 2b_w)\Delta h_w}{r_{ibf}{}^2 \sin^2(\theta_w) * b_w\left(b_{bf} - \frac{4}{3} r_{ibf} \sin(\theta_w)\right)} \Leftrightarrow$$

$$f_y t^2 L_{lb} \frac{h_w - \Delta h_w}{(b_w - L_w)L_w(A\Delta h_w + BL_w + C)} = k\Delta h_w \Leftrightarrow$$

$$\Delta h_w = \frac{-\phi - \sqrt{4Af_y h_w k L_{lb}(b_w - L_w)L_w t^2 + (\phi)^2}}{2Ak(b_w - L_w)L_w} \tag{3.88}$$

$$\phi = b_w CkL_w + Bb_w kL_w{}^2 - CkL_w{}^2 - BkL_w{}^3 + f_y L_{lb} t^2 \tag{3.89}$$

In the last derivation, k is defined as the elastic web crippling stiffness. Therefore, formula 2.44 has been derived. Now, the ultimate load of the modelled cross-section F_{csu} can easily be determined by calculating F_p or F_e for solved Δh_w. Furthermore, the factor ϕ can be rewritten as follows:

$$\phi = b_w CkL_w + Bb_w kL_w{}^2 - CkL_w{}^2 - BkL_w{}^3 + f_y L_{lb} t^2 =$$

$$= kL_w\left(b_w C + Bb_w L_w - CL_w - BL_w{}^2\right) + f_y L_{lb} t^2 =$$

$$= kL_w(C(b_w - L_w) + BL_w(b_w - L_w)) + f_y L_{lb} t^2 =$$

$$= kL_w(C + BL_w)(b_w - L_w) + f_y L_{lb} t^2 =$$

$$= \beta + \alpha \tag{3.90}$$

$$\alpha = f_y L_{lb} t^2 \tag{3.91}$$

$$\beta = k L_w (C + B L_w)(b_w - L_w) \tag{3.92}$$

Thus, load F_{csu} can be described as follows:

$$F_{csu} = k\Delta h_w = \frac{-\alpha - \beta + \sqrt{4A\alpha h_w (b_w - L_w) L_w k + (\beta + \alpha)^2}}{2A(b_w - L_w)L_w} \tag{3.93}$$

Formulae 3.91, 3.92, and 3.93 are equal to formulae 2.45, 2.46, and 2.43 in appendix 2. Formulae 2.47, 2.48, and 2.49 can be derived from formulae 3.85 and 3.86.

3.7 Derivation of formula 2.53

Formula 3.28 describes the web crippling deformation Δh_w as a function of the rotation φ. If it assumed that the rotation φ is small (out of the experimental data it can be shown that φ will not exceed 5 degrees at failure), the following can be stated.

$$\sin\varphi \approx \varphi \tag{3.94}$$

$$\cos\varphi \approx 1 \tag{3.95}$$

Using the two formulae presented above, formula 3.28 can be rewritten.

$$\Delta h_w = -(h_w + L_{bf}\varphi) + \sqrt{L_{bf}^2 - (L_{bf} - h_w\varphi)^2} + h_w = \sqrt{L_{bf}^2 - (L_{bf} - h_w\varphi)^2} - L_{bf}\varphi \tag{3.96}$$

Now, the rotation φ can be solved straightforward:

$$\Delta h_w = -L_{bf}\varphi + \sqrt{L_{bf}^2 - (L_{bf} - h_w\varphi)^2} \Leftrightarrow (\Delta h_w + L_{bf}\varphi)^2 = L_{bf}^2 - (L_{bf} - h_w\varphi)^2 \Leftrightarrow$$

$$\Delta h_w^2 + 2\Delta h_w L_{bf}\varphi + L_{bf}^2\varphi^2 = L_{bf}^2 - L_{bf}^2 + 2L_{bf} h_w\varphi - h_w^2\varphi^2 \Leftrightarrow$$

$$\Delta h_w^2 + 2\Delta h_w L_{bf}\varphi + L_{bf}^2\varphi^2 - 2h_w L_{bf}\varphi + h_w^2\varphi^2 = 0 \Leftrightarrow$$

$$\left(L_{bf}^2 + h_w^2\right)\varphi^2 + \left(2L_{bf}(\Delta h_w - h_w)\right)\varphi + \left(\Delta h_w^2\right) = 0 \Leftrightarrow$$

$$\varphi = \frac{-\left(2L_{bf}(\Delta h_w - h_w)\right) \pm \sqrt{\left(2L_{bf}(\Delta h_w - h_w)\right)^2 - 4\left(L_{bf}^2 + h_w^2\right)\left(\Delta h_w^2\right)}}{2\left(L_{bf}^2 + h_w^2\right)} \tag{3.97}$$

This simple prediction of rotation φ can be derived to Δh_W, however, this leads to a complicated formula. Instead, formula 3.27 and 3.33 are used, assuming a small rotation φ:

$$\left.\begin{aligned} \frac{\delta\varphi}{\delta\Delta h_W} &= \frac{w_{tf}}{\sqrt{L_{bf}{}^2 - w_{tf}{}^2}\,(h_W - \Delta h_W)} \\ w_{tf} &= \sqrt{L_{bf}{}^2 - (L_{bf}\cos\varphi - h_W\sin\varphi)^2} \end{aligned}\right\} \Rightarrow$$

$$\frac{\delta\varphi}{\delta\Delta h_W} = \frac{\sqrt{L_{bf}{}^2 - (L_{bf}\cos\varphi - h_W\sin\varphi)^2}}{(L_{bf}\cos\varphi - h_W\sin\varphi)(h_W - \Delta h_W)} \approx \frac{\sqrt{L_{bf}{}^2 - (L_{bf} - h_W\varphi)^2}}{(L_{bf} - h_W\varphi)(h_W - \Delta h_W)} \tag{3.98}$$

Using formula 2.32 the first length factor f_{l1} can now be written as:

$$f_{l1} = \frac{1}{1 + \left(\dfrac{L_{span} - L_{lb}}{2}\right)\dfrac{\sqrt{L_{bf}{}^2 - (L_{bf} - h_W\varphi)^2}}{(L_{bf} - h_W\varphi)(h_W - \Delta h_W)}} \tag{3.99}$$

This formula equals formula 2.53 in appendix 2.

3.8 Derivation of formula 2.57

Appendix 2 shows that the sheet section ultimate load F_u can be calculated using more or less refinement (model MA1 to MA12, MR1 to MR12, and ME1). The distance between yield lines L_{bf} can be found by minimising F_u to L_{bf}, in other words to find a distance L_{bf} for which F_u will be as small as possible. Although the ultimate load F_u can be predicted by formula 2.54, a very complex one, it is nearly impossible to minimise L_{bf} using this formula. Deriving the length factor f_{l1} to L_{bf} is an almost impossible job. Therefore, the following strategy is followed. Why not chose a simple formula predicting F_u to determine L_{bf}, even if a complex formula is used to predicting F_u itself? The only thing that should be considered is to choose such a simple formula predicting F_u that it makes sense to minimise L_{bf}. This situation can be found for formula 2.65. Common sense dictates that F_{2p} and F_{ylbf} should be considered during a L_{bf} determination. These loads predict the extra forces that are needed to deform the sections adjacent to the modelled cross-section. The length factor is not included for formula 2.65. Although this is theoretically not correct, it's derivation will result into lengthy formulae. Besides this aspect, common sense again dictates that the length factor will be less influenced by L_{bf} than the parts that directly relate their widths to L_{bf}. If L_{bf} determination will be successful using formula 2.65, the length factor relationship to L_{bf} will indeed be considered unimportant. If not, reconsideration of the above mentioned strategy surely will be needed. Looking at formula 2.65, the derivative to L_{bf} equals:

$$\frac{\delta F_u}{\delta L_{bf}} = \frac{\delta F_{csu}}{\delta L_{bf}} + \frac{\delta F_{2p}}{\delta L_{bf}} + \frac{\delta F_{ylbf}}{\delta L_{bf}} \tag{3.100}$$

This derivative should be zero to find the minimal F_u. Furthermore, formula 3.93 shows F_{csu} is not a function of L_{bf}. Therefore:

$$0 = \frac{\delta F_{2p}}{\delta L_{bf}} + \frac{\delta F_{ylbf}}{\delta L_{bf}} \tag{3.101}$$

For convenience, the function predicting F_{2p} and F_{ylbf} will be presented here again. For F_{ylbf}, formula 2.26 is used.

$$F_{2p} = F_{csu} \frac{L_{bf}}{L_{lb}} \tag{2.50}$$

$$F_{ylbf} = 2 \frac{2}{\sqrt{3}} \frac{f_y t^2}{4} b_{bf} \left(\frac{\delta \varphi_d}{\delta \Delta h_w} + \frac{\delta \varphi_e}{\delta \Delta h_w} \right) \tag{2.26}$$

The derivative of formula 2.50 can be presented straightforward:

$$\frac{\delta F_{2p}}{\delta L_{bf}} = \frac{F_{csu}}{L_{lb}} \tag{3.102}$$

Although the derivative of formula 2.26 can be derived, this leads to complex formulae. Therefore, a linear approximation of F_{ylbf} will be used. Formula 2.26 will first be simplified using mathematical technique M3: make complex functions linear. L_{bf} and Δh_w will differ as follows:

$$10 < L_{bf} < 95 \text{ [mm]} \tag{3.103}$$

$$0.1 < \Delta h_w < 8 \text{ [mm]} \tag{3.104}$$

Now, F_{ylbf} is written as:

$$F_{ylbf} \approx 2 \frac{2}{\sqrt{3}} \frac{f_y t^2}{4} b_{bf} \left(\frac{A}{L_{bf}} + B \Delta h_w^2 + C \right) \tag{3.105}$$

Linear regression can solve the parameters A, B, and C as follows. The web crippling deformation Δh_w is varied in discrete steps of 0.8 mm (10 steps). For every possible value of the web crippling deformation, distance L_{bf} is varied in discrete steps of 8.5 mm (10 steps). In total, 100 combinations of Δh_w and L_{bf} occur, for which the value of F_{ylbf} is determined. Using these data, the factors A, B, and C can be determined by linear regression.

This results in:

$$F_{ylbf} \approx 2\frac{2}{\sqrt{3}}\frac{f_y t^2}{4} b_{bf}\left(\frac{2.601}{L_{bf}} + 0.000393\Delta h_w^2 - 0.019\right) \tag{3.106}$$

The above-presented formula has a correlation of 0.951 to the standard formula for the data used. To try the suggestion that F_{ylbf} is not seriously influenced by Δh_w, a new simplified formula is proposed:

$$F_{ylbf} \approx 2\frac{2}{\sqrt{3}}\frac{f_y t^2}{4} b_{bf}\left(\frac{A}{L_{bf}} + B\right) \tag{3.107}$$

Using the computer program and the data, factors A and B are:

$$F_{ylbf} \approx 2\frac{2}{\sqrt{3}}\frac{f_y t^2}{4} b_{bf}\left(\frac{2.601}{L_{bf}} - 0.001\right) \tag{3.108}$$

The above-presented formula has a correlation of 0.944 to the standard formula. The derivative of this formula to L_{bf} equals:

$$\frac{\delta F_{ylbf}}{\delta L_{bf}} \approx -2\frac{2}{\sqrt{3}}\frac{f_y t^2}{4} b_{bf}\,\frac{2.601}{L_{bf}^2} \tag{3.109}$$

Substituting formula 3.102 and 3.109 into 3.101 leads to:

$$0 = \frac{F_{csu}}{L_{lb}} - 2\frac{2}{\sqrt{3}}\frac{f_y t^2}{4} b_{bf}\,\frac{(2.601)}{L_{bf}^2} \Leftrightarrow$$

$$L_{bf} = \sqrt{\frac{2 f_y t^2 L_{lb} b_{bf}\, 2.601}{4 F_{csu}}} \tag{3.110}$$

The last formula equals formula 2.57 in appendix 2.

3.9 Derivation of formulae 2.74 and 2.75

Formula 3.43 showed how the plastic load for the rolling post-failure mode can be calculated. Now this formula will be rewritten as built up out of components:

$$F_p = I + J + K \tag{3.111}$$

With:

$$I = 2\frac{\delta u_a}{\delta \Delta h_w}\frac{1}{r_{bf}}\frac{2}{\sqrt{3}}\frac{f_y t^2}{4}L_{lb} \tag{3.112}$$

$$J = 2\frac{\delta u_b}{\delta \Delta h_w}\frac{1}{r_{bf}}\frac{2}{\sqrt{3}}\frac{f_y t^2}{4}L_{lb} \tag{3.113}$$

$$K = 2\frac{\delta \varphi_c}{\delta \Delta h_w}\frac{2}{\sqrt{3}}\frac{f_y t^2}{4}L_{lb} \tag{3.114}$$

Component K can be calculated using formula 3.50, 3.55, and 3.68. For the derivation of formula 3.68, it was assumed that angle φ_c is small and corner radius r_{bf} equals zero. This also applies for formula 3.50:

$$\Delta b_{wfl} \approx \frac{b_{wfl}\varphi_c \sin(\theta_w)}{1-\cos(\theta_w)+\varphi_c \sin(\theta_w)} \tag{3.115}$$

Component I and J can be calculated using formulae 3.56 and 3.57. These formulae can be rewritten in the same way as for formula 3.50:

$$\frac{\delta u_a}{\delta \Delta h_w} = \frac{\sin(\theta_w+\varphi_c)}{1-\cos(\theta_w+\varphi_c)} \approx \frac{\sin(\theta_w)+\varphi_c\cos(\theta_w)}{1-\cos(\theta_w)+\varphi_c\sin(\theta_w)} \tag{3.116}$$

$$\frac{\delta u_b}{\delta \Delta h_w} = \frac{\sin(\theta_w+\varphi_c)}{1-\cos(\theta_w+\varphi_c)} + \frac{r_{bf}}{b_{wfl}\text{-}\Delta b_{wfl}} \approx \frac{\sin(\theta_w)+\varphi_c\cos(\theta_w)}{1-\cos(\theta_w)+\varphi_c\sin(\theta_w)} \tag{3.117}$$

For all variables, defined variable space A is used (section 2.2.3):

$50 < b_w < 150$ [mm]. (2.36)

$50 < \theta_w < 90$ [degrees]. (2.37)

$50 < L_{lb} < 150$ [mm]. (2.38)

$0.5 < t < 1.5$ [mm]. (2.39)

$40 < b_{bf} < 150$ [mm]. (2.40)

$1 < r_{bf} < 12$ [mm]. (2.41)

$$0.1 < \Delta h_w < 10 \ \text{[mm]}. \tag{2.42}$$

Now, every variable except the web width b_w is kept on its average value. The variable b_w is varied between 50 and 150 mm. For these values, terms I and K are calculated (term J equals term I). Figure 3-15 on the left shows the results. It can be seen that only factor I plays an important role. Factor K can be neglected compared to factor I.

The angle between web and flange θ_w has been varied, keeping all other variables on their average value. The factor values are shown in 3-15 on the right. Only factor I plays an important role.

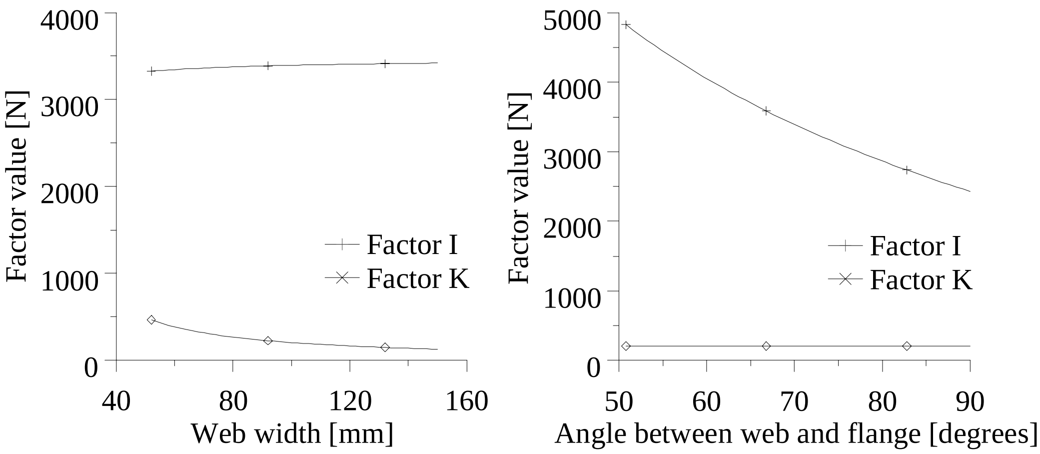

Figure 3-15. Factor I and K values for web width b_w and angle between web and flange θ_w.

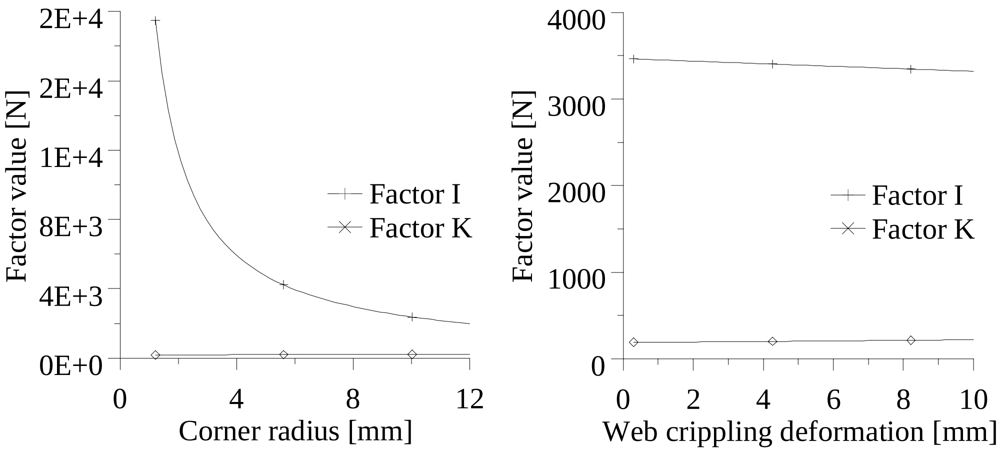

Figure 3-16. Factor I and K values for corner radius r_{bf} and web crippling deformation Δh_w.

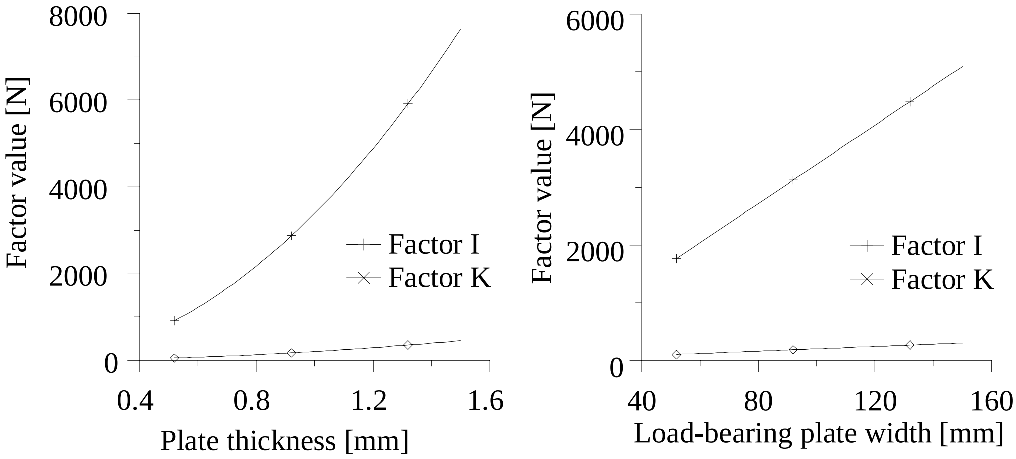

Figure 3-17. Factor I and K values for plate thickness t and load-bearing plate width L_{lb}.

Likewise, for the next four variables, the same strategy is followed. The results are shown in figure 3-16 and 3-17. For all variables, only factor I plays an important role. Without exception, factor K can be neglected. Factor J equals factor I. Therefore, formula 3.111 can be written as:

$$F_p = 2*2\frac{\sin(\theta_w)+\varphi_c\cos(\theta_w)}{1-\cos(\theta_w)+\varphi_c\sin(\theta_w)}\frac{1}{r_{bf}}\frac{2}{\sqrt{3}}\frac{f_y t^2}{4}L_{lb} \tag{3.118}$$

The plastic load for the modelled cross-section can be set equal to the elastic load, like for the yield-arc post-failure mode:

$$\left.\begin{array}{l} F_p = \dfrac{\sin\theta_w+\varphi_c\cos\theta_w}{1-\cos\theta_w+\varphi_c\sin\theta_w}\dfrac{2}{\sqrt{3}}\dfrac{f_y t^2 L_{lb}}{r_{bf}} \\ F_e = k\Delta h_w \\ F_e = F_p \end{array}\right\}\Rightarrow \tag{3.119}$$

$$k\Delta h_w = \frac{\sin\theta_w+\varphi_c\cos\theta_w}{1-\cos\theta_w+\varphi_c\sin\theta_w}\frac{2}{\sqrt{3}}\frac{f_y t^2 L_{lb}}{r_{bf}}$$

Substituting 3.68 into the last presented formula and solving for Δh_w leads to:

$$\Delta h_w = -\frac{2b_w\left(\frac{L_{lb}2f_y t^2}{\sqrt{3}r_{bf}}\right)\cos\left(\frac{\theta_w}{2}\right)\sin\left(\frac{\theta_w}{2}\right)}{-b_w k - \left(\frac{L_{lb}2f_y t^2}{\sqrt{3}r_{bf}}\right) + b_w k\cos(\theta_w)} \tag{3.120}$$

Then the load at which the cross-section fails F_{csu} can be calculated as:

$$F_{csu} = k * \Delta h_w \tag{3.121}$$

Formulae 3.120 and 3.121 together form formula 2.75 in appendix 2. Formula 3.118 equals formula 2.74.

4 Appendix cross-section behaviour

Introduction
The experiments in chapter 3 of thesis [Hofm00a] indicated that for a large concentrated load and a small bending moment (short span lengths), two post-failure modes could occur: the rolling and the yield arc post-failure modes, see also table 3-7, thesis [Hofm00a]. Research in the past indicated that the corner radius has a strong influence on which of these two post-failure modes occurs [Bakk92a], [Hofm96a].

In this appendix, it has been investigated whether small strips of the sheet section's cross-section can be used to gather insight into the differences of the two post-failure modes. For small corner radii, it will be shown that strip behaviour and section behaviour is comparable. For large corner radii, this is not the case.

Finite element models have been used to describe the cross-sectional behaviour of sheet sections for varying corner radii. Relatively simple mechanical models have been derived that determine the location of first yield in the cross-section's web and the cross-section's plastic behaviour. Except for the largest corner radius, mechanical models and finite element models give comparable results.

4.1 Introduction

Chapter 3 of the thesis [Hofm00a] presented three-point bending tests on sheet sections. Figure 4-1 shows these experiments schematically.

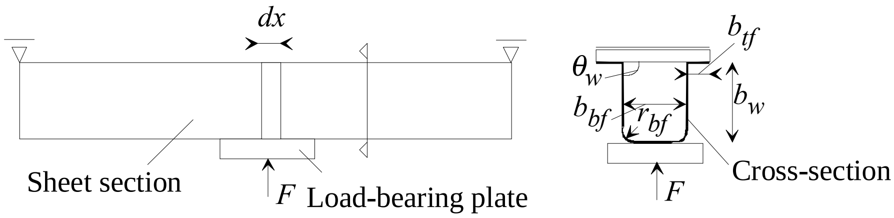

Figure 4-1. Three point bending test and cross-section variables.

These three-point bending tests indicate that sheet sections subjected to a large concentrated load and a small bending moment (short span lengths) can fail by two post-failure modes: the rolling and the yield arc post-failure modes, figure 4-3. Bakker [Bakk92a] studied the rolling and yield arc post-failure modes (called "mechanisms" in her thesis) and some of her observations of this research are presented in the next paragraphs.

Rolling and yield-arc post-failure modes
Bakker [Bakk92a] found that one very important sheet section variable that determines whether the yield arc or rolling post-failure mode occurs is the corner radius (r_{bf} in figure 4-1).

Although web crippling deformation was already defined in the previous appendices (1, 2 and 3), it is shown in figure 4-2 on the left again. The rolling and yield arc post-failure modes each have a characteristic load versus web crippling deformation curve as shown in figure 4-2 on the right.

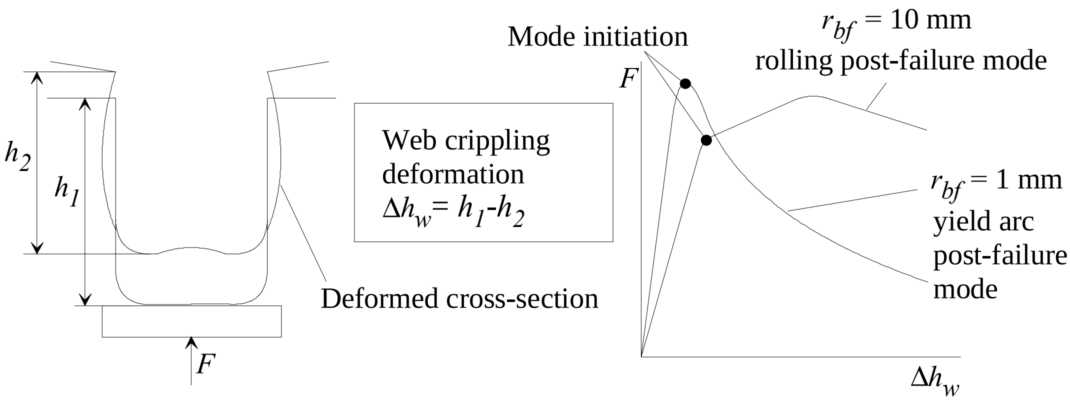

Figure 4-2. Qualitative load versus web crippling deformation curves for rolling and yield arc post-failure modes.

Before both post-failure modes initiate, the sheet sections first behave elastically: the straight lines in the load versus web crippling deformation curves. Thereafter, the post-failure mode initiates and plasticity occurs. The initiation of the post-failure mode is marked with a bold dot for both modes (the mode initiation points). After mode initiation, the rolling post-failure mode increases in strength. After some deformation, the ultimate load is reached and the load decreases again. For the yield arc post-failure mode, the load decreases immediately after mode initiation. Mode initiation occurs at ultimate load.

Figure 4-3 shows the yield line patterns of the two post-failure modes. A rolling post-failure mode (figure 4-3 at the bottom) starts with the moving yield lines 7 and 8 near the bottom corner. For an increase of the load, yield line 8 in the web moves upward in the web. Yield line 7 in the bottom flange moves through the corner. After further increase of the load, other yield lines (1 to 6) occur in the flange and web for reasons of compatibility. A yield arc post-failure mode (figure 4-3 at the top) starts with the curved yield line 8 in the web. For an increase of the load, the movement of this yield line is negligible small. As for the rolling post-failure mode, other yield lines (1 to 7) will occur for reasons of compatibility after some loading.

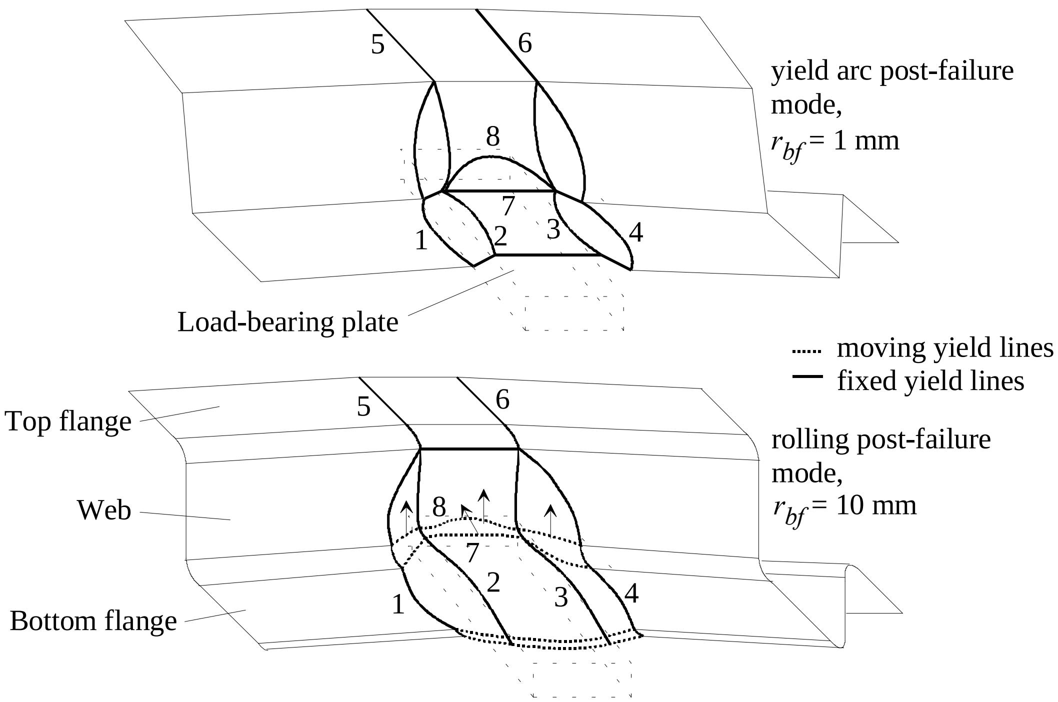

Figure 4-3. Rolling and yield arc post-failure modes.

Cross-sectional behaviour
Bakker introduced the rolling and yield arc post-failure modes by simple mechanical models as shown in figure 4-4. Yield line numbers are according to figure 4-3.

For the longitudinal section, the rolling and yield arc post-failure modes are quite similar: yield lines 1 to 6 are all fixed and have more or less the same positions for the rolling and yield-arc post-failure modes in figure 4-3. Thus, only one simple mechanical model for the longitudinal section is used in figure 4-4. For the cross-section, the rolling and yield-arc post-failure modes are different: yield lines 7 and 8 are moving for the rolling post-failure mode, but fixed for the yield arc post-failure mode. Thus, two simple mechanical models are used for the cross-sectional behaviour in figure 4-4.

The simple mechanical models in figure 4-4 suggest that the differences between the two post-failure modes may be explained by investigating the differences of the modes for the cross-section only.

For this reason, only the cross-sectional behaviour of sheet sections is investigated in this appendix. With a finite element method, a small strip *dx* of the sheet section as shown in figure 4-1 is modelled. The simulations are presented in section 4.2. For the same strip *dx*, a mechanical model has been derived. This model makes it possible to predict the behaviour of the two post-failure modes for the strip *dx*. The mechanical model is presented in section 4.3. Section 4.4 presents a comparison between finite element models for a strip *dx* and whole sheet sections.

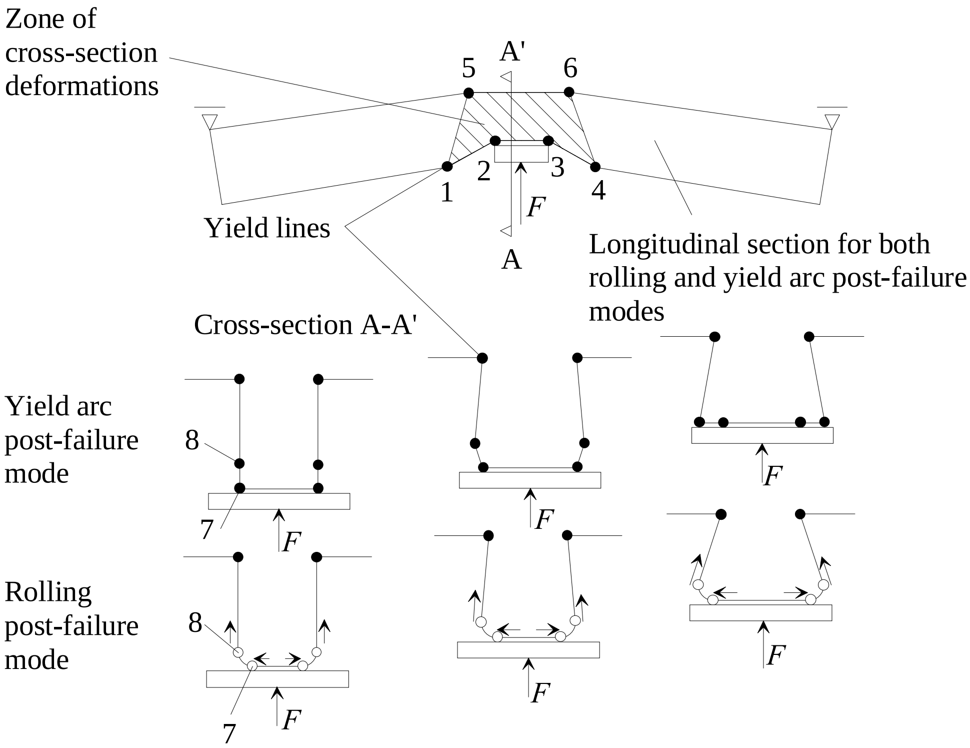

Figure 4-4. Rolling and yield-arc post-failure modes presented by mechanical models, [Bakk92a].

4.2 Finite element models

Support conditions

In the previous section, it was explained that the cross-sectional behaviour of sheet sections is studied by the behaviour of a strip *dx* of the sheet section. Normally, this strip *dx* is kept in place by the flanges and web adjacent to the strip. Without these adjacent parts, the strip *dx* has to be fixed to make loading possible. It can only be fixed at the top because otherwise, cross-sectional deformations will not be possible. Figure 4-4 shows that for the cross-section, the top flange and top corner do not play a significant role in the cross-sectional behaviour. Therefore, the top flange and top corners are not modelled in the finite element model. Regarding the possible rotation of the top of the web, two extreme situations are modelled: hinged and clamped, figure 4-5.

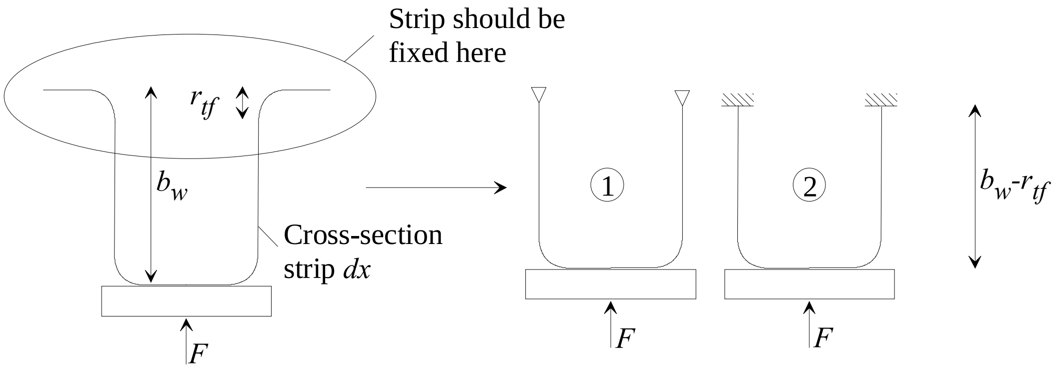

Figure 4-5. Two possibilities to fix the strip dx: hinged (1) and clamped (2).

Finite element model

Figure 4-6 presents a finite element model for the strip *dx*. At the bottom of the figure, the load-bearing plate is shown. This plate is modelled as a solid piece of steel. Load is applied by a forced displacement of the load-bearing plate along the negative *y*-axis. Contact elements are modelled between the load-bearing plate and the bottom flange to prevent penetration of the load-bearing plate into the strip. Contact elements were presented in the thesis [Hofm00aa] chapter 4, section 4.1.3. A geometrically non-linear analysis has been carried out, accounting for large displacements, large rotations, and small strains.

Elements sizes are 3*3 mm for web and bottom flange. The corner is modelled by 10 elements. Shell elements are used, having four nodes with six degrees of freedom each and five integration points in thickness direction. The material behaviour is given by points of the stress-strain curve of the steel used (see thesis [Hofm00a], chapter 4, section 4.1.2). Plasticity and hardening is thus taken into account. Some variables of the steel used are: yield strength 335 [N/mm^2], modulus of elasticity 210.000 [N/mm^2], strain at yielding 0.003.

Boundary conditions are shown in figure 4-6. The two sides of the strip (for which z = 0 and z = 3 mm) are part of a symmetry surface. This is also true for the nodes at the bottom flange edge.

Because of these symmetry conditions, the strip width is not of importance. The strip width of the model is chosen arbitrarily to be dx = 3 mm. Nodes at the top of the web are fixed for movement along the x- and y-axis. The rotation around the z-axis is free or fixed for a hinged or clamped condition.

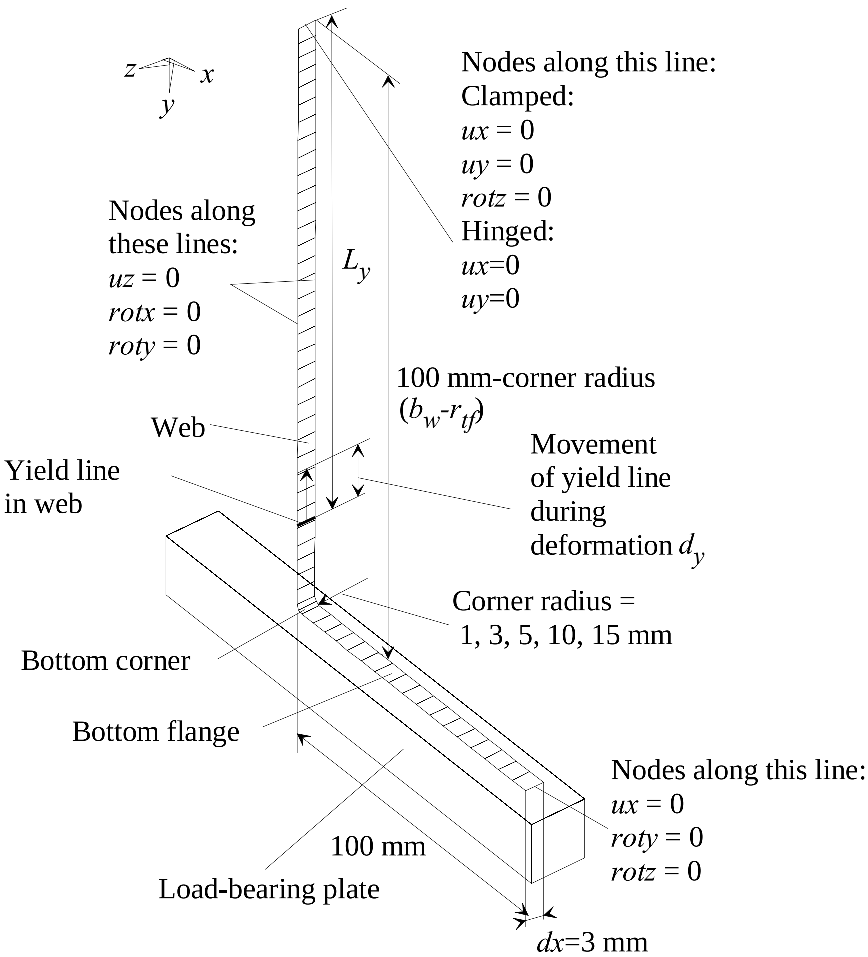

Figure 4-6. Finite element model for strip dx.

Results of the simulations are interesting for two aspects. Load-deformation behaviour, and location and movement of the first yield line. Both aspects are presented in a separate paragraph.

Load-deformation behaviour

Figure 4-2 presented qualitatively load versus web-crippling deformation curves for the rolling and yield arc post-failure modes for sheet sections.

Figure 4-7 presents the load versus deformation curves for the strips of the finite element models. From r_{bf} = 1 mm to r_{bf} = 10 mm, the qualitative behaviour of the strip dx is the same for the hinged and clamped situation. However, the ultimate loads are greater for the clamped situation. For r_{bf} = 15 mm, the clamped situation leads to an ascending curve after elastic behaviour. In the next paragraph, it is shown that an additional yield line occurs for r_{bf} = 15 mm. This difference is a possible cause for the ascending curve for r_{bf} = 15 mm.

If the curves on the right in figure 4-2 and figure 4-7 are compared, it can be seen that for r_{bf} = 1 mm the load versus deformation curves are qualitatively similar for both figures. For r_{bf} = 10 mm, the curves are qualitatively different. Figure 4-2 shows an ascending curve after mode initiation and hereafter a descending curve. Figure 4-7, however, shows a descending curve directly after elastic behaviour. This means that for r_{bf} = 10 mm, the cross-sectional behaviour according the finite element model, cannot be used to explain the ascending curve in the three-point bending tests.

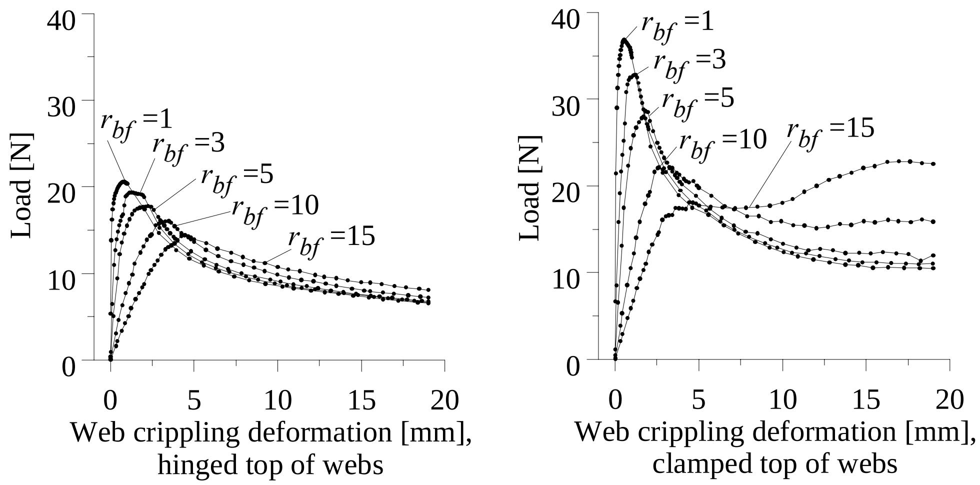

Figure 4-7. Load versus deformation curves for finite element models for different corner radii, hinged top of webs on the left, clamped top of webs on the right.

Looking at all curves for all corner radii in figure 4-7, it seems that there is not really a typical curve for small corner radii (r_{bf} = 1 mm) or large corner radii (r_{bf} = 10 mm), but a smooth transition between the curves. In the next paragraph, it will be shown that for the location and movement of yield lines, an equivalent transitional behaviour occurs.

Location and movement of the first yield line

In the finite element model, the location of a yield line is determined as follows. A plot is made of plastic Von Mises strains at the top and bottom surface of the shell elements. If plastic strains occur, for certain deformation, it is assumed a yield line has formed. The location of the yield line is determined by taking the location of highest plastic strains plotted.

A yield line will occur in the web as shown in figure 4-8 with a continuous bold line. During further loading this yield line will move upward in the web. Figure 4-8 defines the initial position (L_y), the movement direction (arrow), and distance moved (d_y) of the yield line. After the forming of a yield line in the web, yield lines will occur in the bottom flange (dotted in figure 4-8) and at the top of the web for clamped tops of the web. For r_{bf} = 15 mm, for clamped tops of the web, an additional yield line occurred in the bottom, also dotted in figure 4-8. This yield line in the bottom corner may cause the different load-deformation behaviour for r_{bf} = 15 mm. All yield lines contain significantly smaller plastic strains than the first yield line in the web and therefore they will not be subject to further investigation in this appendix.

Table 4-1 presents the distance L_y for r_{bf} = 1 mm to r_{bf} = 15 mm for hinged and clamped tops of the web. For clamped tops of the web, for r_{bf} = 10 mm, the yield line in the web is located almost at the bottom corner. For r_{bf} = 1 mm, the yield line is located beneath the middle in the web. This is also true for three-point bending tests (see figure 4-3). For hinged tops of the web, the yield line in the web is located approximately in the middle for all corner radii r_{bf}. From now on, only the model with clamped tops of the web will be used, because this model has more similarities with full three-point bending tests.

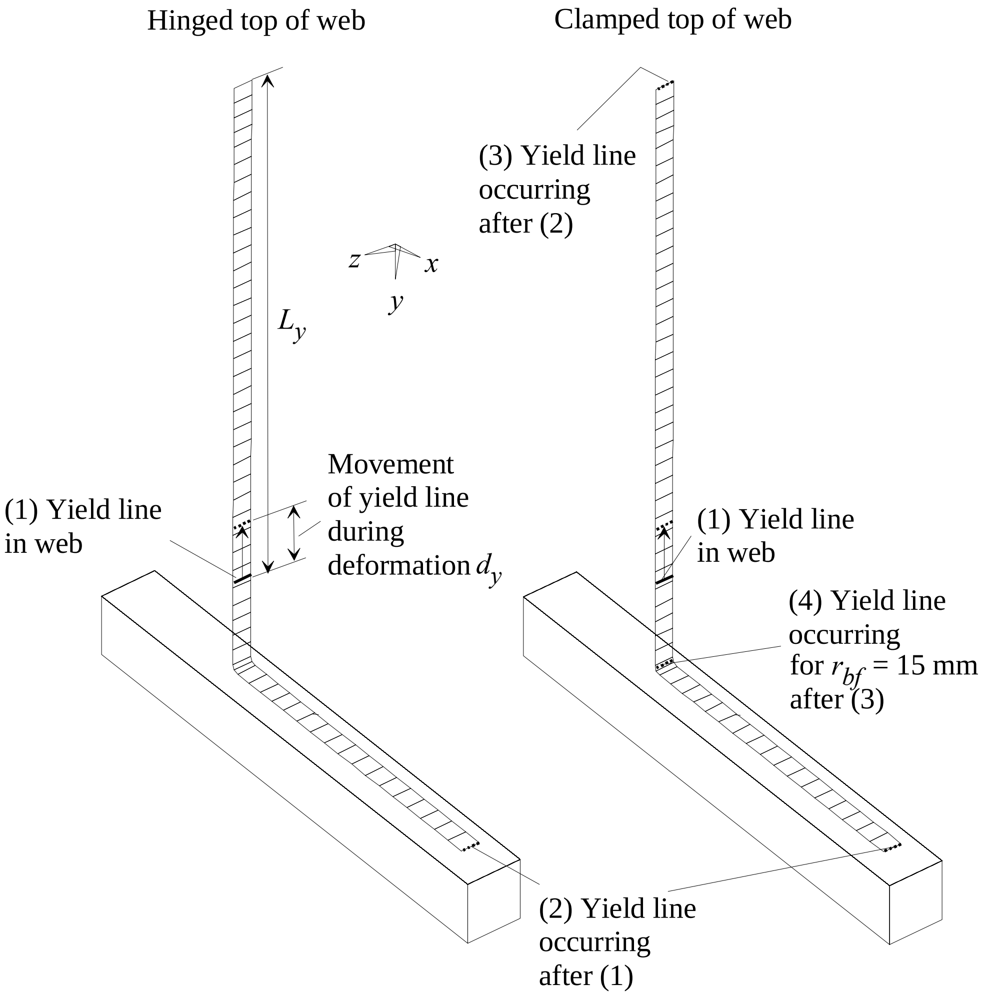

Figure 4-8. Location of yield lines.

Figure 4-9 presents yield line position L_y and yield line movement d_y for r_{bf} = 1 mm to r_{bf} = 15 mm for clamped tops of the web.

Table 4-1. Distance L_y for all simulations at mode initiation.

r_{bf} [mm]	L_y [mm], hinged bottoms of the web	L_y [mm], clamped bottoms of the web
1	46.0	64.3
3	47.0	66.2
5	49.4	69.8
10	56.5	80.0
15	61.3	72.5

As figure 4-9 shows in the left graph, the yield line is located higher if the corner radius is smaller. Because the graph presents the yield line position as function of the web crippling deformation, it can be seen that for increasing deformation, the yield lines move. This is true for all corner radii. The graph on the right presents the movement of the yield lines d_y. In general, yield line movement increases for larger corner radii. As an exception, for a corner radius equal to 15 mm, the yield lines move comparable to r_{bf} = 1 mm and r_{bf} = 3 mm. This may be an indication that for r_{bf} = 15 mm another failure mode occurs. This indication is strengthened by the occurrence of an extra yield line in the bottom corner for r_{bf} = 15 mm (see also figure 4-8 on the right).

In section 4.1, it was mentioned that for whole sheet sections, there are moving yield lines for the rolling post-failure mode (r_{bf} = 10 mm) and there are fixed yield lines for the yield arc post-failure mode (r_{bf} = 1 mm). Figure 4-9 points out that for r_{bf} = 1 mm the yield line in the web indeed is almost fixed in position and that for r_{bf} = 10 mm the yield line is moving strongly.

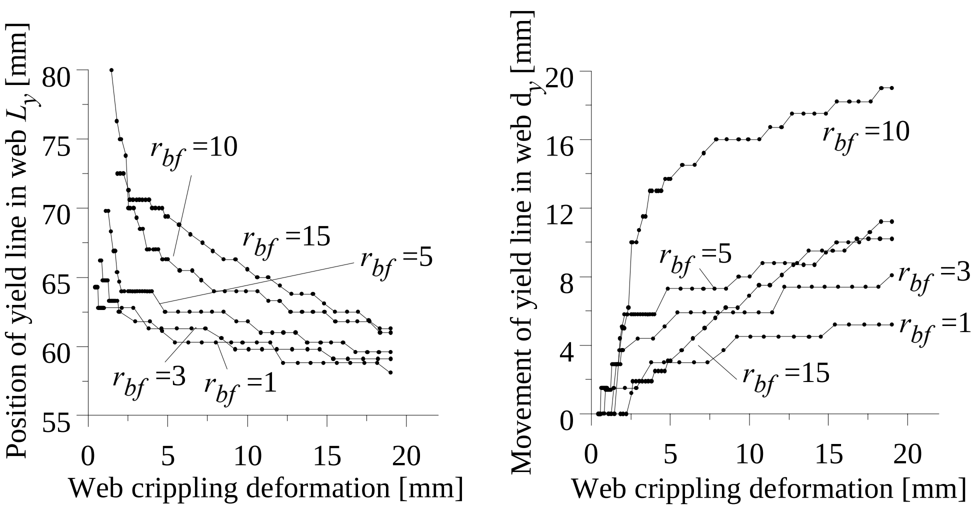

Figure 4-9. Location and movement of yield lines. On the left yield line position L_y and on the right yield line movement d_y.

4.3 Mechanical models

For describing the behaviour of a small strip *dx* of the sheet section, a mechanical model has been developed. First, the location of the first yield line in the web is determined by calculating the maximum bending moment in the web. Then, a mechanical model is presented, which predicts the plastic behaviour of the strip. Both models are based on a geometrically non-linear analysis, accounting for large displacements, small rotations, and small strains.

4.3.1 Location of first yield line

The geometry for the calculation of the maximum bending moment in the web is shown in figure 4-10. Positive direction of forces and bending moments is as drawn in the figure. On the left of figure 4-10, the cross-section of the strip *dx* is shown. The load-bearing plate and the load *F* acting on this plate have been replaced by two forces *F*/2 at the intersection of the bottom corners and the bottom flange. This is acceptable because if the cross-section is loaded, it will deform as shown in figure 4-2 on the left. Then, the load-bearing plate only makes contact at the intersections of bottom corners and bottom flange. The cross-section on the left is simplified on the right side of the figure. The top flange has been removed, as for the finite element models in section 4.2. The corner radius has been flattened. Instead of the force *F/2* having a distance *e* to the web in horizontal direction, the load is applied directly on the web plus an additional bending moment (*F/2*)**e*. Because the strip *dx* is symmetrical, the right web needs not to be modelled.

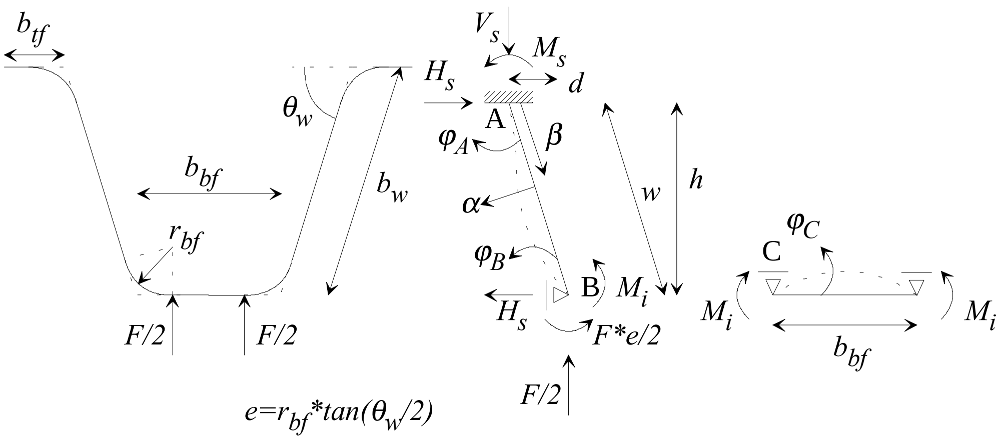

Figure 4-10. Cross-section and simplified cross-section of strip dx.

Now, the second-order bending moment in the web as a function of the distance β will be derived. The rotation at location C can be calculated by:

$$\varphi_C = -\frac{M_i b_{bf}}{2EI} \tag{4.1}$$

Horizontal forces in the bottom flange are neglected because they will make the calculation very complex and the finite element models showed these forces to be very small compared to the Euler load of the bottom flange.

The second-order rotation at location B can be calculated by using equations for bending of prismatic bars presented by Timoshenko [Timo36a]:

$$\varphi_B = \frac{(Fe/2 + M_i)w}{3EI}\psi(\eta) - \frac{M_s w}{6EI}\phi(\eta) \tag{4.2}$$

$$\phi(\eta) = \frac{3}{\eta}\left(\frac{1}{\sin(2\eta)} - \frac{1}{2\eta}\right) \tag{4.3}$$

$$\psi(\eta) = \frac{3}{2\eta}\left(\frac{1}{2\eta} - \frac{1}{\tan(2\eta)}\right) \tag{4.4}$$

$$\eta = \frac{\pi}{2}\sqrt{\frac{P}{P_{cr}}} \tag{4.5}$$

With P the axial load in the web:

$$P = \frac{F}{2}\cos\left(\frac{\pi}{2} - \theta_w\right) + H_s\cos(\theta_w) \tag{4.6}$$

And P_{cr} the buckling load of the web:

$$P_{cr} = \frac{\pi^2 EI}{\left(\frac{w}{\sqrt{2}}\right)^2} \tag{4.7}$$

The rotation at location A can be calculated by using the same equations for bars by Timoshenko [Timo36a]:

$$\varphi_A = \frac{(Fe/2 + M_i)w}{6EI}\phi(\eta) - \frac{M_s w}{3EI}\psi(\eta) \tag{4.8}$$

The rotation at location B and C should be equal. Furthermore, the rotation at location A should be zero. Using formulae 4.1, 4.2, and 4.8 with these constrains, the internal bending moment M_i and the reaction bending moment M_s can be calculated as:

$$M_i = \frac{w(F/2)e\left(\phi^2 - 4\psi^2\right)}{-w\phi^2 + 6b_{bf}\psi + 4w\psi^2} \tag{4.9}$$

$$M_s = \frac{3b_{bf}(F/2)e\phi}{-w\phi^2 + 6b_{bf}\psi + 4w\psi^2} \tag{4.10}$$

If the two above presented moments are known, the displacement $\alpha(\beta)$ of the web can be calculated, using equations presented by Timoshenko [Timo36a]:

$$\alpha(\beta) = -\frac{M_s}{P}\left(\frac{\sin(k(w-\beta))}{\sin(kw)} - \frac{w-\beta}{w}\right) + \frac{(F/2)e + M_i}{P}\left(\frac{\sin(k\beta)}{\sin(kw)} - \frac{\beta}{w}\right) \tag{4.11}$$

The horizontal reaction H_s can be calculated by moment equilibrium at the rigid support:

$$H_s = \frac{M_s + \frac{F}{2} * d + \frac{F}{2} e + M_i}{h} \tag{4.12}$$

The bending moment in the web as a function of β can now be written as:

$$M(\beta) = M_s - \beta H_s \sin(\theta_w) + \beta \frac{F}{2}\sin\left(\frac{\pi}{2} - \theta_w\right) - \alpha(\beta)\left(\frac{F}{2}\cos\left(\frac{\pi}{2} - \theta_w\right) + H_s \cos(\theta_w)\right) \tag{4.13}$$

Using the yield strength f_y and steel plate thickness t, the plastic moment of the strip dx can be calculated by:

$$M_{pl} = \frac{2}{\sqrt{3}} * \frac{1}{4} * t^2 * f_y * dx \tag{4.14}$$

Formula 4.14 has been derived by Hill [Hill50a] for a yield line for which the strains in longitudinal direction equal zero. This is the case because there is symmetry for the model (see figure 4-6). Formula 4.13 is used to find the location of the yield line in the web. Therefore, the next sequential steps will be followed:

1. A load (*F/2*) is assumed. Formula 4.3 to 4.7 and 4.9 to 4.13 can be used to calculate the bending moment $M(\beta)$ for a set of positions β. The maximum bending moment is the maximum value found for the set of positions.

2. Because the horizontal reaction H_s is predicted first in equation 4.12 but is already needed in formula 4.6 a prediction for this load is made now. Then equation 4.6, 4.7, and 4.9 to 4.12 are used to estimate a new load H_s. This is repeated as long as useful (successive substitution).

3. The calculated maximum bending moment $M(\beta)$ is compared to the plastic bending moment of the strip M_{pl} (formula 4.14). If $M(\beta)$ is lower than M_{pl}, the assumed load (*F/2*) should be greater. If $M(\beta)$ is greater than M_{pl}, the assumed load (*F/2*) should be lower.

4. If the calculated value of the bending moment $M(\beta)$ equals the yielding moment M_{pl}, the load ($F/2$) to initiate a yield line in the web has been found.

The above-presented sequence is carried out for a strip dx for five different corner radii: 1, 3, 5, 10, and 15 mm. All other variable values are equal to those used in the finite element model. Thus, a comparison is possible between the mechanical model and the finite element models. Table 4-2 presents the results.

Table 4-2. Initial position of the yield line in the web for strips dx, width 3 mm, having different corner radii.

	Location L_y [mm] for plastic bending moment $M(\beta)=M_{pl}$		($F/2$) [N] for plastic bending moment $M(\beta)=M_{pl}$		$M(\beta)=M_{pl}$ [Nmm]
r_{bf} [mm]	Mechanical model	Finite element models	Mechanical Model	Finite element models	Both
1	64	64	67	37	138
3	70	66	50	32	138
5	76	70	38	26	138
10	80	80	22	16	138
15	70	73	16	11	138

There are some differences between the results obtained with the mechanical model and the finite element model, but table 4-2 shows the mechanical model gives a fairly good indication of the location of the first yield line and a rough indication of the load ($F/2$) at which the first yield line occurs. Differences can be caused by:

1. The modelling of the corner radius in the mechanical model is different (more simple) than for the finite element model.

2. The mechanical model predicts the location of the yield line by using the full plastic moment that occurs in the web, whereas the finite element model indicates first yield by (some) plastic strains on the outer fibres of the web.

3. In the mechanical model, first order rotations are calculated for the bottom flange because the influence of the horizontal load in the bottom flange is not taken into account.

4. The mechanical model is based on a large displacement, small rotation, and small strain analysis while the finite element model is based on a large displacement, large rotation, and small strain analysis.

Table 4-3 presents mechanical model results for the same five strips as in table 4-2, but now all are loaded by the same load (F/2) equal to 70 N. Distance L_y and the value of the bending moment $M(\beta)$ are listed.

Table 4-3. Results for constant load.

r_{bf} [mm]	L_y for maximum $M(\beta)$ [mm]	$M(\beta)$ [Nmm]	$F/2$ [N]
1	64	53	70
3	64	149	70
5	63	235	70
10	62	417	70
15	61	578	70

Table 4-3 shows that distance L_y is almost constant for an increasing corner radius r_{bf} and fixed load $F/2$ (conclusion 1). The maximum bending moment value increases for an increasing corner radius (conclusion 2).

Table 4-4 presents mechanical model results for a strip having a corner radius r_{bf} equal to 1 mm. The load is varied between 10 and 30 N. Table 4-4 shows that for increasing load, distance L_y decreases (conclusion 3) and the maximum bending moment value increases (conclusion 4). Conclusion 3 can be explained as follows. If the force $F/2$ increases, the normal force in the web increases, making second-order effects larger. If second-order effects are larger, the highest bending moment will be more in the middle of the web, thus distance L_y will decrease.

Using the four conclusions presented above, it can be explained why the yield line is located near the bottom corner for large corner radii and in the middle of the web for small corner radii.

Table 4-4. Results for constant corner radius.

r_{bf} [mm]	L_y for maximum $M(\beta)$ [mm]	$M(\beta)$ [Nmm]	$F/2$ [N]
1	98	4.2	10
1	98	6.1	15
1	97	7.8	20
1	90	9.6	25
1	84	11.6	30

If the corner radius r_{bf} is small, a load results in a small moment $M(\beta)$ (conclusion 2). Therefore, the load $F/2$ has to be high to reach the yielding bending moment (conclusion 4). If the load is high, distance L_y is lower (conclusion 3). If distance L_y is low, the yield line is more near the middle of the web. For a large corner radius, the same reasoning can be used to show that the yield line occurs near the bottom corner.

A second-order calculation is needed to predict the position of the first yield line, as shown in figure 4-10. If only a first-order approach is used, the components of H_s and V_s in web direction are not used. Then the maximum bending moment is always located at the bottom or at the top of the web depending on the magnitude of V_s and H_s compared to M_s. If a second-order approach is used an additional bending moment in the web occurs equal to the components of V_S and H_S in α-direction times β. For this case, the position of the maximum bending moment depends on the reactions and the deflection of the web.

4.3.2 Plastic behaviour

In the previous section, a mechanical model was presented to find the first yield line of a sheet section strip dx, for different corner radii. If this location is known, a mechanical model can be developed which makes it possible to predict plastic strip behaviour. Figure 4-11 presents the geometry of the model.

On the left of figure 4-11, the normal geometry is shown. Yield lines are shown by a bold dot. The yield line in the web has a distance L_y from the top of the web. This distance L_y depends on the corner radius and was predicted in the previous section. Yield lines are modelled at the top of the web and at the right in the bottom flange. The locations of these yield lines are according to the observations of the finite element models in section 4.2.

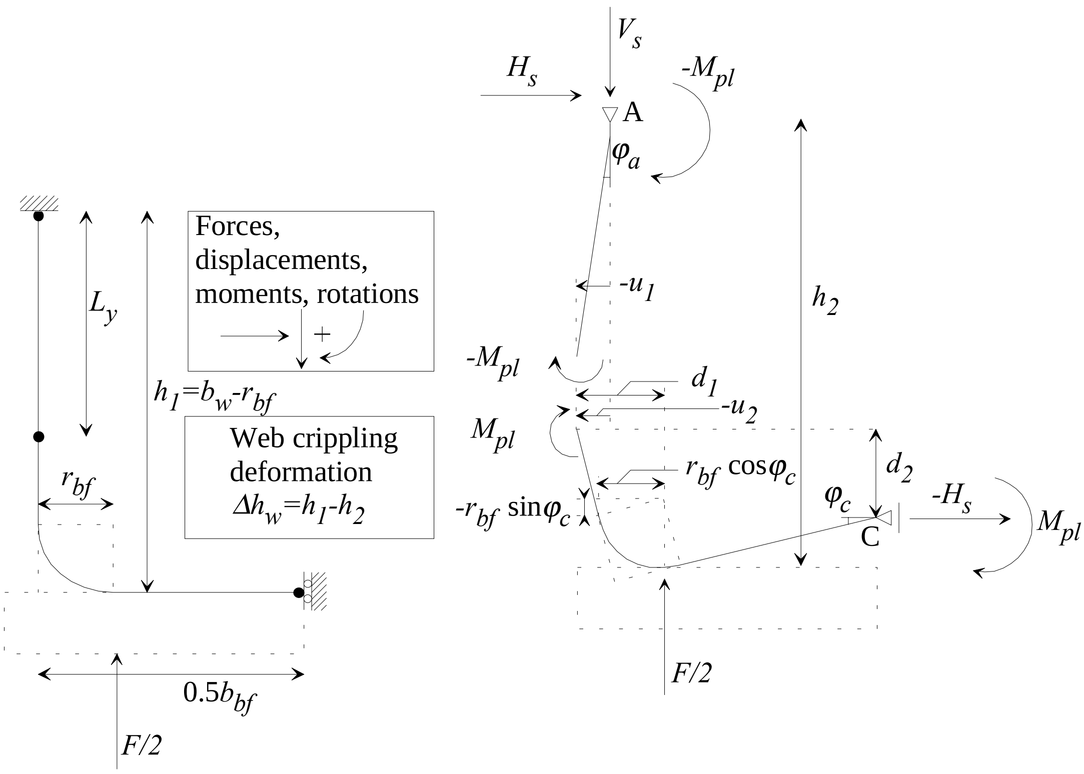

Figure 4-11. Detailed geometry to determine plastic behaviour.

The displacement of the web u_1 and the lower part u_2 should be equal, therefore:

$$u_1 = u_2 \Leftrightarrow -L_y \sin\varphi_a = \frac{b_{bf}}{2}(1-\cos\varphi_c) + (b_w - r_{bf} - L_y)\sin\varphi_c \Leftrightarrow$$

$$\varphi_a = \arcsin\left(\frac{\frac{b_{bf}}{2}(1-\cos\varphi_c)+\left(b_w - r_{bf} - L_y\right)\sin\varphi_c}{-L_y}\right) \tag{4.15}$$

The web crippling deformation Δh_w equals to the reduction of height of the two parts of the web and the bottom corner:

$$\Delta h_w = L_y(1-\cos\varphi_a) + (b_w - 2r_{bf} - L_y)(1-\cos\varphi_c) - r_{bf}\sin\varphi_c \tag{4.16}$$

The vertical reaction V_s at the top of the web equals the load *F/2*. At the yield line in the web, there is moment equilibrium for the upper part of the web:

$$-M_{pl} - M_{pl} + H_s * L_y\cos\varphi_a + \frac{F}{2} * L_y\sin\varphi_a = 0 \tag{4.17}$$

At the yield line in the web, there is moment equilibrium for the lower part of the web, the bottom corner and bottom flange:

$$M_{pl} + M_{pl} - \frac{F}{2} * d_1 + H_s * d_2 = 0 \tag{4.18}$$

And:

$$d_1 = -\left(b_w - 2r_{bf} - L_y\right)\sin\varphi_c + r_{bf}\cos\varphi_c \tag{4.19}$$

$$d_2 = \left(b_w - r_{bf} - L_y\right)\cos\varphi_c + \frac{b_{bf}}{2}\sin\varphi_c \tag{4.20}$$

The load *F/2* can be solved from equations 4.17 and 4.18:

$$\frac{F}{2} = \frac{2\left(L_y M_{pl} + d_2 M_{pl}\sec\varphi_a\right)}{L_y(d_1 + d_2\tan\varphi_a)} \tag{4.21}$$

A plastic curve of a strip *dx* can be calculated as follows. A rotation φ_c is taken. Then rotation φ_a can be calculated by formula 4.15 and the web crippling deformation Δh_w by formula 4.16. A fixed value for the distance L_y can be taken from the mechanical model of the previous section. Nevertheless, it is also possible, for the web crippling deformation Δh_w, to find the distance L_y in the curves of figure 4-9. Note however that the model does not describe the energy dissipated by the movement of the yield line. Both results are presented in figure 4-12. Because formulae 4.15 and 4.16 are dependent on the value of distance L_y, these formulae should be solved iterative using the curves of figure 4-9. Formula 4.21 calculates the load (*F*/2). Figure 4-12 presents plastic curves (bold lines) including the results of the finite element models (normal lines) for r_{bf} = 1, 10, and 15 mm. The results for r_{bf} = 3 mm and r_{bf} = 5 mm are almost equal to the results for r_{bf} = 1 mm and not presented here. The dotted lines represent the same calculation as the normal plastic line, only the distance L_y has been fixed on its initial value.

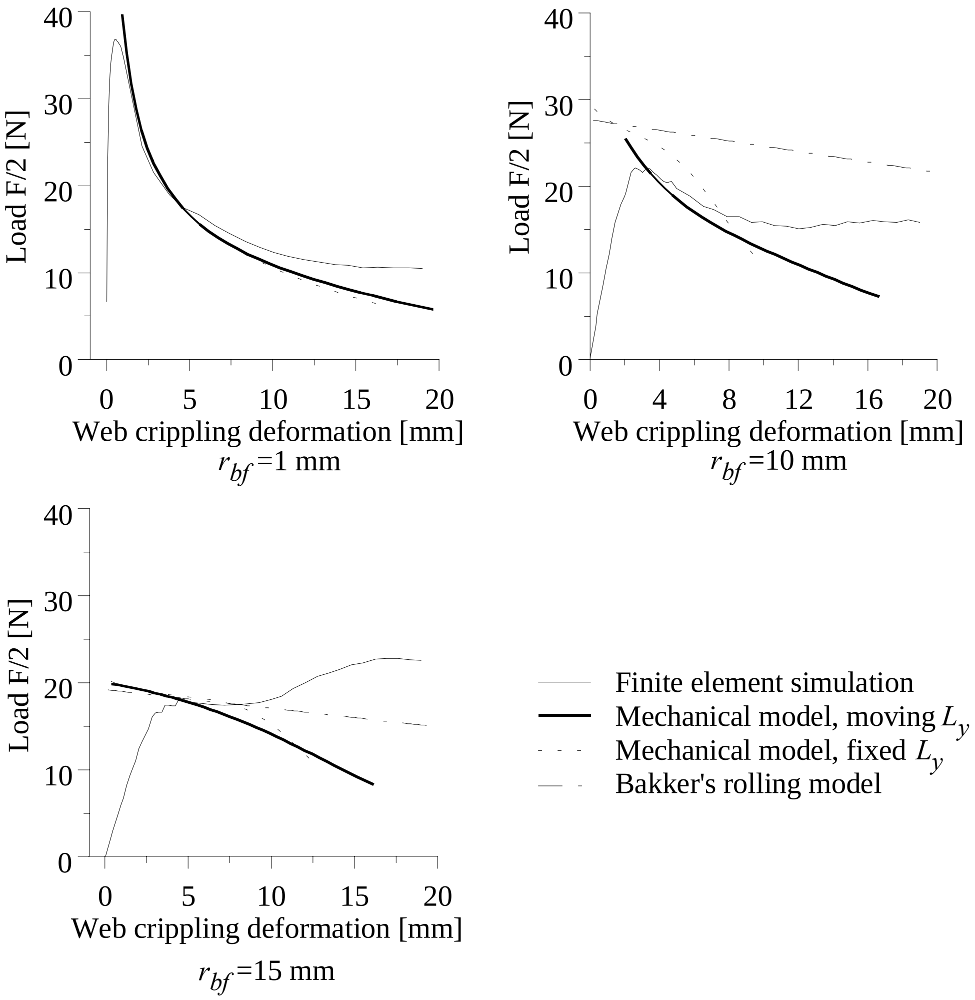

Figure 4-12. Several curves for strips for different corner radii.

Existing model for rolling post-failure mode

Bakker developed a mechanical model for the rolling post-failure mode in 1992 [Bakk92a]. A part of this model is shown in figure 4-13. This part of the model predicts the ultimate load for a small strip having three yield lines: two moving yield lines near the corner and one fixed yield line at the top of the web. The energy dissipated by the movement of the yield lines is taken into account.

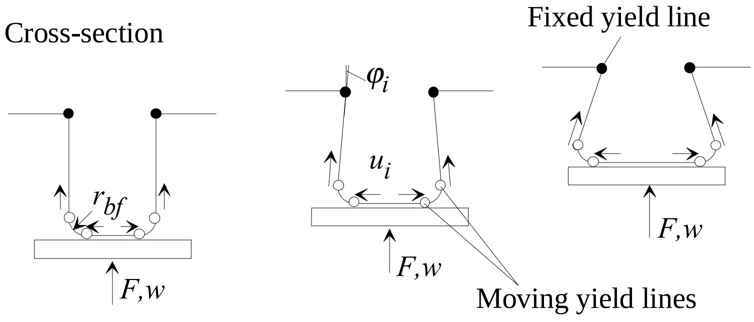

$$F\delta w = \underbrace{\Sigma M_{pl}\delta\varphi_i}_{\text{Fixed yield lines}} + \underbrace{\Sigma M_{pl}\delta u_i / r_{bf}}_{\text{Moving yield lines}}$$

Figure 4-13. A part of Bakker's mechanical model for the rolling post-failure mode.

4.4 Discussion

4.4.1 Difference for small and large corner radii

Looking at figure 4-12, especially the strips with small corner radii show an extremely close correlation between the mechanical model and the finite element model. For large corner radii, r_{bf} = 15 mm, the plastic curve only joins the finite element model around the mode initiation load. This means the plastic behaviour of the strip dx for a corner radius r_{bf} = 15 mm is not correctly described by the mechanical model, despite the fact that the mechanical model has no geometrical simplifications. This can be due to:

1. Possible strong deformations of the relatively weak corner radius lead to a different geometry, which seriously influences the load deformation behaviour. Indeed, the finite element models show that the corner radius deforms during the load deformation path.

2. It was already shown that an extra yield occurs in the bottom flange for r_{bf} = 15 mm. This means a different post-failure mode can occur, which makes it logical that the curves of the developed model and the finite element model do not agree.

3. The movement of the yield line in the web dissipates energy, which is not taken into account in the mechanical model. This should lead to an increasing underestimation of the plastic load for larger deformations, if yield line movement is strong (this is the case for large corner radii).

However, for r_{bf} = 15 mm, Bakker's already existing mechanical model for the rolling post-failure mode was tried. Note that this model considers the dissipated energy due to yield line movement. Figure 4-13 shows that for a strip with r_{bf} = 15 mm, the existing model only predicts a part of the curve of the finite element model well. This means that the lack of modelling the energy dissipation for moving yield lines of the new model is not likely the cause for differences between the new model and the finite element simulations.

4.4.2 Comparison of strips and whole sheet sections using finite element models

A finite element model for a real sheet section with r_{bf} = 3 mm (thesis [Hofm00a], experiment 30, table 4-6, chapter 4) was studied. This is shown in figure 4-14. Concerning the yield lines, only the yielding at and near the symmetry line has been studied (the bold part of the yield lines), in order to study as much as possible cross-sectional behaviour only. Away from the symmetry line, yield lines are affected by the end of the load-bearing plate, as is clearly visible. After elastic behaviour, yield lines occur in the bottom flange (C) near the corner and in the web between the middle of the web and the bottom corner (B). After some web crippling deformation, the yield line in the bottom flange (C) stops rotating and the yield line in the web (B) rotates further and moves slowly up in the web. Finally, a yield line occurs at the top of the web (A).

A strip with r_{bf} = 3 mm behaves almost in the same manner as the real sheet section. After elastic behaviour, it shows a yield line in the web (B), but not in the bottom flange. The line in the web is located a little bit higher than for the real sheet section. After some web crippling deformation, the yield line in the web moves slowly up in the web. Finally, yield lines occur at the top of the web (A) and in the middle of the bottom flange (C).

Also a finite element model for a real sheet section with r_{bf} = 10 mm (Bakker's experiment 54, thesis [Hofm00a], table 4-8, chapter 4) was studied. This is shown in figure 4-14 on the right. Concerning the yield lines, only the yielding at and near the symmetry line has been studied (the bold part of the yield lines), in order to study as much as possible cross-sectional behaviour only. Away from the symmetry line, yield lines are affected by the end of the load-bearing plate, as is clearly visible. After elastic behaviour, two yield lines occur near the bottom corner: one in the web (B) and one in the bottom flange (D). For more web crippling deformation, the yield line in the web (B) moves strongly up through the web and the yield line in the bottom flange (D) moves through the corner. Finally, a yield line occurs at the top of the web (A) and in the middle of the bottom flange (C).

A strip with r_{bf} = 10 mm behaves equal to a strip with r_{bf} = 3 mm (see previous paragraph).

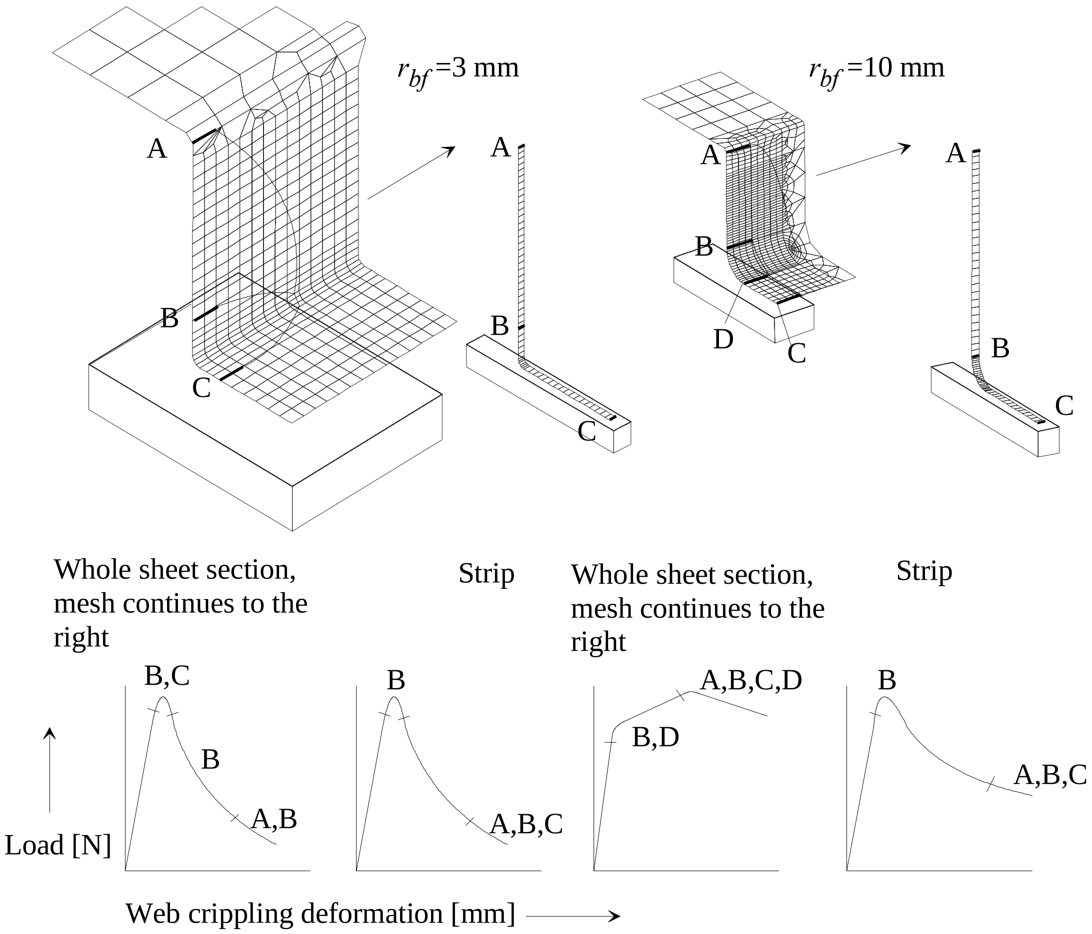

Figure 4-14. Behaviour of whole sheet sections and strips for r_{bf} = 3 mm and r_{bf} = 10 mm.

4.5 Conclusions

For three-point bending tests of sheet sections, the location of the first yield line in the web depends on the post-failure mode. For a rolling post-failure mode, the first yield line occurs in the web near the bottom corner and for a yield arc post-failure mode, the first yield line occurs in the lower middle of the web. The mechanical model for a strip *dx* of the sheet section, explains these different yield line locations. Only one mechanical model was used to show this for both post-failure modes. A second-order calculation is necessary to predict the location of the first yield line in the web. The mechanical model can be used to predict the position of the yield line in the web, for both strips and whole sheet sections.

For the finite element models of the strips *dx*, for intermediate corner radii, behaviour occurs that is a transition between the behaviour for large corner radii and small corner radii. This is not only seen for the load deformation behaviour, but also for the location and movement of the first yield line. As a conclusion, the strips *dx* do not fail by two completely different post-failure modes. This was also observed for three-point bending tests [Bakk92a], where sometimes a failure occurred which was a mixture of the yield arc and rolling post-failure modes.

A mechanical model has been developed to find the plastic curves for comparison with the finite element models of the strips *dx*. Only one model was used. The model predicts the plastic curve of the strips well for r_{bf} =1, 3, 5, and 10 mm. For the large corner radius r_{bf} = 15 mm only a small part of the curve is covered.

For small corner radii, the behaviour of a strip of a sheet section's cross-section is qualitatively similar to the behaviour of a real sheet section in a three-point bending test. For r_{bf} = 10 mm, this is not the case (comparisons made based on finite element analysis). Thus, strip behaviour cannot be used to explain whole sheet section behaviour.

For a large corner radius, r_{bf} = 15 mm, an already existing mechanical model for the rolling post-failure mode predicts the first part of the plastic curve well. The finite element model shows that for a strip with r_{bf} = 15 mm, two yield lines occur near the bottom corner. This makes it possible that for a strip with r_{bf} = 15 mm, indeed a rolling post-failure mode occurs. This needs further investigation.

Further research can be focussed on two items. First, boundary conditions of the strips can be studied for large corner radii. In this way, an explanation can be found for the different behaviour between strips and three-point bending tests. Secondly, for small corner radii, it can be investigated how the strip behaviour can be translated into behaviour of three-point bending tests.

5 Appendix Turbo Pascal programs

5.1 Program for Eurocode3 predictions

```
VAR

{Input/output}
bbffl,b1,b2:Real;
htest,out:Text;
counter:Integer;
testno:Real;
btf2:Real;

{UFF Format}
typee,ref,btf,rtf,bw,bbf,rbf,tw,Lspan,Llb,t,fy,Ftest,Fimec:Real;

{Section}
E:Real;

{Sheeting/three point bending tests}
sh,ctp:Real;

{5.4.3 Effects of shear lag}
sla,slb,slc,sld,beta2,delta,neta:Real;

{5.4.1 Calculating Mu, top flange yields first}
error2:Real;

{5.4.1 Calculation Mu, bottom flange yields first}
Cy,sc,la1,la2:Real;

{5.9.3 Web crippling strength}
error1,lafu,alfa,Rw:Real;

{5.11 Combined bending and web crippling}
fac1,fac2,eta,F:Real;

rholx,bfyields,ftf,fbf,yc,Mu,Mn,Cy2:Real;

FUNCTION tan(x:Real):Real;
BEGIN
tan:=sin(x)/cos(x);
END;

FUNCTION power(x,y:Real):Real;
{calculates x to the power y}
BEGIN
Power:=EXP(y*LN(x));
END;
```

```
PROCEDURE EFFECTIVE_WIDTH;

  {Calculates ultimate bending moment Mn if only outer fibre}
  {tension or compression flange yields}

  VAR

  sest,s,ebf,etf,bbfp,ksig,lap,be3,rho:Real;
  e1,e2,f1,f2,psi,bwp,be1,be2,sest2,s22,sub1,sub2,sub3,sub4:Real;
  a1,s1,a2,s2,a34,s34,a6,s6,a7,s7,a8,s8,I,w:Real;

  BEGIN

  sest:=0.5*bw*sin(tw);
  s:=10000;

  WHILE abs(s-sest)>0.001 DO

     BEGIN

     s:=sest;

     IF (bfyields=1) THEN
     BEGIN
     ebf:=fy/E;
     etf:=ebf*(bw*sin(tw)-(s-0.5*t))/(s-0.5*t);
     END;

     IF (bfyields=0) THEN
     BEGIN
     etf:=fy/E;
     ebf:=etf*(s-0.5*t)/(bw*sin(tw)-(s-0.5*t));
     END;

     fbf:=ebf*E;
     ftf:=etf*E;

     {4.2 Plane elements without stiffeners}

     bbfp:=bbf-2*rbf*(tan(tw/2)-sin(tw/2));
     ksig:=4;
     lap:=1.052*(bbfp/t)*sqrt(fy/(E*ksig));
     lap:=lap*sqrt(fbf/fy);
     IF (lap<=0.673) THEN BEGIN rho:=rholx*1; END;
     IF (lap>0.673) THEN BEGIN rho:=rholx*(1-0.22/lap)/lap; END;
     be3:=0.5*rho*bbfp;

     e1:=ebf*(s-0.5*t-rbf*tan(0.5*tw)*sin(tw))/(s-0.5*t);
     e2:=etf*((bw*sin(tw)-(s-0.5*t))-rtf*tan(0.5*tw)*sin(tw));
     e2:=e2/(bw*sin(tw)-(s-0.5*t));
     f1:=e1*E;
```

```
f2:=-e2*E;
psi:=f2/f1;
bwp:=bw-(rbf+rtf)*(tan(tw/2)-sin(tw/2));
ksig:=7.81-6.29*psi+9.78*sqr(psi);
IF (psi<-1) AND (psi>-3) THEN BEGIN ksig:=5.98*sqr(1-psi); END;
lap:=1.052*(bwp/t)*sqrt(fy/(E*ksig));
lap:=lap*sqrt(f1/fy);
IF (lap<=0.673) THEN BEGIN rho:=1; END;
IF (lap>0.673) THEN BEGIN rho:=(1-0.22/lap)/lap; END;
be1:=0.4*rho*bwp;
be2:=0.6*rho*bwp;

sest2:=s;
s22:=10000;

WHILE abs(sest2-s22)>0.001 DO

    BEGIN

    s22:=sest2;

    sub1:=rtf*tan(0.5*tw);
    sub2:=rtf*tan(0.5*tw)*sin(tw);
    sub3:=rbf*tan(0.5*tw);
    sub4:=rbf*tan(0.5*tw)*sin(tw);

    a1:=0.5*btf-sub1;
    a1:=a1*t;
    s1:=bw*sin(tw)+0.5*t;

    a2:=t*rtf*tw;
    s2:=bw*sin(tw)+0.5*t-rtf+(rtf*sin(tw)/tw);

    a34:=bw-(s22-0.5*t)/sin(tw)-sub1+be2;
    a34:=a34*t;
    s34:=bw*sin(tw)+0.5*t-(sub1+(a34/t)*0.5)*sin(tw);

    a6:=be1-rbf*(sin(tw/2));
    a6:=a6*t;
    s6:=(0.5*be1+rbf*(tan(tw/2)-sin(tw/2)))*sin(tw)+0.5*t;

    a7:=t*rbf*tw;
    s7:=rbf+0.5*t-(rbf*sin(tw)/tw);

    a8:=be3-rbf*(sin(tw/2));
    a8:=a8*t;
    s8:=0.5*t;

    sest2:=(a1*s1+a2*s2+a34*s34+a6*s6+a7*s7+a8*s8);
    sest2:=sest2/(a1+a2+a34+a6+a7+a8);
    END;
```

```
    sest:=s22;

    {--------------------------------------------------------------}

    END;

  {MOMENT OF INERTIA--------------------------------------------------}

  I:=a1*sqr(s1)+a2*sqr(s2)+a34*sqr(s34)+a6*sqr(s6)+a7*sqr(s7)+a8*sqr(s8);
  I:=I-(a1+a2+a34+a6+a7+a8)*sqr(s);
  I:=I*2;

  {--------------------------------------------------------------------}

  W:=I/s;
  IF bfyields=0 THEN BEGIN W:=I/(bw*sin(tw)-s); END;
  Mn:=W*fy;
  END;

PROCEDURE INELASTIC_CAP;

  {Calculates ultimate bending moment for plastic compression and, if}
  {applicable, tension zone}

  {Reck, Pekoz, and Winter do not take into account corner geometry}
  {and only use fully effective webs}
  {Fully effective webs can be used because: }

  {Situation 1, bottom flange (tension) yields}
  {bwp/t<2.22*sqrt(E/fy) (is requested by code), than psi=-1, ksig=23.9}
  {lap=0.48, rho=1, be1=0.4bwp, be2=0.6bwp, be1 and be2 together}
  {more than 0.5bwp, thus web fully effective}

  {Situation 2, bottom flange (tension) does not yield}
  {most extreme situation: no tension at all in web: psi=0, k=7.81}
  {bwp/t<1.11*sqrt(E/fy), lap=0.42, rho=1, be1=(2/5)bwp, be2=bwp-be1}
  {be1 and be2 equal to bwp thus web fully effective}

  VAR
  {Procedure inelastic_cap}
  bbfp,ksig,lap,rho,be3,bc,bt,d,la1,la2,ycest,sc,Cy:Real;
  yp,yt,ycp,ytp,eqa,eqb,eqc,yc1,yc2,ft:Real;

  BEGIN

  bbfp:=bbf-2*rbf*(tan(tw/2)-sin(tw/2));
  ksig:=4;
  lap:=1.052*(bbfp/t)*sqrt(fy/(E*ksig));
  IF (lap<=0.673) THEN BEGIN rho:=rholx*1; END;
  IF (lap>0.673) THEN BEGIN rho:=rholx*(1-0.22/lap)/lap; END;
  be3:=0.5*rho*bbfp;
```

```
bc:=2*be3+2*rbf*(tan(tw/2)-sin(tw/2));
bt:=btf;
d:=bw*sin(tw);

{5.4.2 Partially plastic resistance}

la1:=1.11*sqrt(E/fy);
la2:=1.29*sqrt(E/fy);

    Cy:=3-((bc/t)*sqrt(fy/E)-1.11)/0.09;
    IF (bc/t) <= la1 THEN BEGIN Cy:=3; END;
    IF (bc/t) >= la2 THEN BEGIN Cy:=1; END;

    {Paper Reck, Pekoz, Winter. J. of the Struc. Div. Nov, 1975}
    {with an self-made extension for inclined webs}

    yc:=0.25*(bt*sin(tw)-bc*sin(tw)+2*d);
    yp:=yc/Cy;
    yt:=d-yc;
    ycp:=yc-yp;
    ytp:=yt-yp;

    Mu:=fy*t*bc*yc;
    Mu:=Mu+2*fy*t*(ycp/sin(tw))*(yc-0.5*ycp);
    Mu:=Mu+2*0.5*fy*t*(yp/sin(tw))*((2/3)*yp);

    Mu:=Mu+2*0.5*fy*t*(yp/sin(tw))*((2/3)*yp);
    Mu:=Mu+2*fy*t*(ytp/sin(tw))*(yt-0.5*ytp);
    Mu:=Mu+fy*t*bt*yt;

    IF (yp>yt) AND (Cy>1) THEN

        BEGIN
        eqa:=(2/sin(tw))-(1/(Cy*sin(tw)))-(Cy/sin(tw));
        eqb:=bc+(2*Cy*d/sin(tw))+Cy*bt;
        eqc:=-Cy*sqr(d)/sin(tw)-Cy*bt*d;
        yc1:=(-eqb+sqrt(sqr(eqb)-4*eqa*eqc))/(2*eqa);
        yc2:=(-eqb-sqrt(sqr(eqb)-4*eqa*eqc))/(2*eqa);

        {yc1 gives normal values, yc2 > 100 * h}

        yc:=yc1;
        yp:=yc/Cy;
        yt:=d-yc;
        ycp:=yc-yp;
        ft:=fy*Cy*yt/yc;

        Mu:=fy*t*bc*yc;
        Mu:=Mu+2*fy*t*(ycp/sin(tw))*(yc-0.5*ycp);
        Mu:=Mu+2*0.5*fy*t*(yp/sin(tw))*((2/3)*yp);
```

```
          Mu:=Mu+2*0.5*ft*t*(yt/sin(tw))*((2/3)*yt);
          Mu:=Mu+ft*t*bt*yt;
          END;

    END;

BEGIN {Program}

ASSIGN(htest,'tswt3.prn');
ASSIGN(out,'tswteta.dat');
REWRITE(out);

FOR counter:=1 to 196 DO

   BEGIN

   writeln('Counter: ',counter);

   {Input--------------------------------------------------------------}

   RESET(htest);
   READ(htest,testno);

   WHILE testno<>counter DO
      BEGIN
      READLN(htest);
      READ(htest,testno);
      END;

   READ(htest,ref,typee,btf,rtf,bw,bbf,rbf,tw,Lspan,Llb,t,fy,Ftest,Fimec);

   sh:=1;  {1:sheeting, 2:hat sections}
   ctp:=2; {1:continuous, 2:three point bending test}

   tw:=tw/57.29577951;
   E:=210000;
   CLOSE(htest);

   {3.1.2 Average yield strength (strength increase cold work)-----------}

   {Not used: 3.1.2(5):no fully effective flanges------------------------}

   {---------------------------------------------------------------------}

   {Flange curling------------------------------------------------------}

   {No clauses in Eurocode about flange curling--------------------------}

   {---------------------------------------------------------------------}
```

```
{5.4.3 Effects of shear lag------------------------------------------}

IF ctp=1 THEN
BEGIN
sla:=6;
slb:=1.6;
slc:=1.155;
sld:=7.76;
END;

IF ctp=2 THEN
BEGIN
sla:=4;
slb:=3.2;
slc:=1.115;
sld:=5.74;
END;

{top flange under tension}

IF ((0.5*btf)/Lspan) > (1/20) THEN
BEGIN
beta2:=1+sla*(0.5*btf/Lspan)+slb*sqr(0.5*btf/Lspan);
beta2:=1/beta2;
END;

IF ((0.5*btf)/Lspan) < (1/50) THEN
BEGIN
beta2:=1.0;
END;

IF (((0.5*btf)/Lspan) <= (1/20)) AND (((0.5*btf)/Lspan) >= (1/50)) THEN
BEGIN
beta2:=slc-sld*(0.5*btf/Lspan);
END;

btf:=beta2*btf;

{bottom flange under compression}

IF ((0.5*bbf)/Lspan) > (1/20) THEN
BEGIN
beta2:=1+sla*(0.5*bbf/Lspan)+slb*sqr(0.5*bbf/Lspan);
beta2:=1/beta2;
END;

IF ((0.5*bbf)/Lspan < (1/50)) THEN
BEGIN
beta2:=1.0;
END;
```

```
IF (((0.5*bbf)/Lspan) <= (1/20)) AND (((0.5*bbf)/Lspan) >= (1/50)) THEN
BEGIN
beta2:=slc-sld*(0.5*bbf/Lspan);
END;

delta:=(bbf/t)*sqrt(fy/E);
IF delta <= 1 THEN
BEGIN
delta:=1;
END;
neta:=(0.5*bbf/Lspan)/delta;
rholx:=power(beta2,neta);

{-----------------------------------------------------------------}

{5.4.1 Calculating Mu--------------------------------------------}

bfyields:=1;
EFFECTIVE_WIDTH;

IF ftf >= fy THEN
BEGIN
bfyields:=0;
EFFECTIVE_WIDTH;
END;

INELASTIC_CAP;

    error2:=0;
    IF (tw<(60/57.29577951)) THEN BEGIN error2:=1; END;
    IF ((((yc/sin(tw))-rtf*tan(0.5*tw))/t)>(1.11*sqrt(E/fy))) THEN
    BEGIN
    error2:=1;
    END;

    IF error2=0 THEN

        BEGIN
        Mn:=Mu;
        END;

{5.9.3 Web crippling strength---------------------------------------}

error1:=0;
IF ((rbf-0.5*t)/t) > 10 THEN BEGIN error1:=1; END;
IF (bw*sin(tw)/t) > 200*sin(tw) THEN BEGIN error1:=1; END;
IF tw < (45/57.29577951) THEN BEGIN error1:=1; END;
IF tw > (90/57.29577951) THEN BEGIN error1:=1; END;
IF error1=1 THEN
    BEGIN
    writeln('WARNING:');
```

```
        writeln('SECTION PROPERTIES ARE NOT IN VALID RANGE');
        writeln('AS SPECIFIED BY THE EUROCODE FOR Rw CALCULATION');
        END;

    IF (Lspan-Llb)/2 <= 1.5*bw*sin(tw) THEN
    BEGIN
    lafu:=10;
    IF sh=1 THEN BEGIN alfa:=0.075; END;
    IF sh=2 THEN BEGIN alfa:=0.057; END;
    END;

    IF (Lspan-Llb)/2 > 1.5*bw*sin(tw) THEN
    BEGIN
    lafu:=Llb;
    IF sh=1 THEN BEGIN alfa:=0.15; END;
    IF sh=2 THEN BEGIN alfa:=0.115; END;
    END;

    Rw:=alfa*sqr(t)*sqrt(fy*E)*(1-0.1*sqrt((rbf-0.5*t)/t));
    Rw:=2*Rw*(0.5+sqrt(0.02*lafu/t))*(2.4+sqr(tw*57.29577951/90));

    {-----------------------------------------------------------------}

    {5.11 Combined bending and web crippling strength--------------------}

    fac1:=-1;
    fac2:=+1.25;
    eta:=0.25*(Rw/Mn)*(Lspan-Llb);

    F:=(fac2*Rw/(eta-fac1));
    IF (eta<((fac1+fac2)/1)) THEN BEGIN F:=Rw; END;
    IF (eta>(fac1/(1-fac2))) THEN BEGIN F:=Rw/eta; END;

    {-----------------------------------------------------------------}

        IF error1=0 THEN
        BEGIN
        writeln(out,counter,chr(9),eta,chr(9),F);
        END;
        IF error1=1 THEN
        BEGIN
        writeln(out,counter,chr(9),'0',chr(9),'0');
        END;

END;

CLOSE(out);

END.
```

5.2 Program for ultimate failure mechanical model

```
var

out:Text;
teller:Integer;
testno:Real;

{UFF-format}
ref,typee,btf,rtf,bw,bbf,rbf,tw,Lspan,Llb,t,fy,Ftest,Fimec:Real;

F,Fmin,Fmax:Real;
KK1,KK2,alfa,I,I2,k,k2,e,beta,dhw,dhw2:Real;
{2}
Rh,dhcs,dhcs2:Real;
{3}
Fbf:Real;
{4}
w0max,w0min,pa:Real;
marker:Real;

M,ee,mu,pi,b,L,w0,y0,x,z:Real;
be,la,w,y,D,c1,c2:Real;
p,p2,sx,sz,txz,sxm,sx2,szm,svm,svm2:Real;

harpje,Fcr:Real;

hn,zpnov,Inov,Wnov,Snov:Real;

function power(x,y:Real):Real;
{calculates x to the power y}
begin
  power:=exp(y*ln(x));
end;

function cosh(x:Real):Real;
{calculates the hyperbolic cosine for x}
begin
  cosh:=0.5*(exp(x)+exp(-x));
end;

function sinh(x:Real):Real;
{calculates the hyperbolic sine for x}
begin
  sinh:=0.5*(-exp(-x)+exp(x));
end;

function TAN(x:Real):Real;
begin
  TAN:=SIN(x)/COS(x);
end;
```

```
function coth(x:Real):Real;
{calculates the hyperbolic cot for x}
begin
  coth:=cosh(x)/sinh(x);
end;

begin

assign(out,'tswt3a.dat');
REWRITE(out);

ASSIGN(input,'tswt3.prn');

FOR teller:= 1 TO 196 DO
  BEGIN {FOR for all tested sections}
  RESET(input);
  READ(input,testno);
  while teller<>testno DO
  begin
  READLN(input);
  READ(input,testno);
  end;
  READ(input,ref,typee,btf,rtf,bw,bbf,rbf,tw,Lspan,Llb,t,fy,Ftest,Fimec);
  CLOSE(input);
  tw:=tw/57.29577951;

{initialisation}
writeln(teller);
writeln('rbf ',rbf);
writeln('bw ',bw);
writeln('btf ',btf);
writeln('tw ',tw*57.29577951);
writeln('Lspan ',Lspan);
writeln('Llb ',Llb);
writeln('fy ',fy);

e:=210000;

{0) assuming load}

Fmin:=0;
Fmax:=4*Ftest;
svm:=0;

WHILE abs(svm-fy) > 0.1 DO

        begin

        F:=(Fmin+Fmax)/2;

        {1) calculating dhw}
```

```
{using beam on elastic foundation model}

alfa:=0.118*power(rbf,0.89);

I:=((t*alfa*bw)/2)*sqr((bbf*alfa*bw*sin(tw)+t*bbf)/(bbf+2*alfa*bw));
I:=I+bbf*t*sqr((alfa*alfa*bw*bw*sin(tw)+alfa*bw*t)/(bbf+2*alfa*bw));
I2:=(alfa*alfa+bw*bw+t*t)/12;
I2:=I2-(cos(2*tw)*(alfa*alfa*bw*bw-t*t))/12;
I2:=I2+(t*alfa*bw*sin(2*tw))/2;
I2:=I2*t*alfa*bw;
I:=((bbf*t*t*t)/12)+I2+I;

k:=bw*(bbf-(4/3)*rbf*sin(tw))+rbf*sin(tw)*(bbf-(3/2)*rbf*sin(tw));
k:=(k/(e*(3*bbf+2*bw)))*rbf*rbf*sin(tw)*sin(tw)*(12/(t*t*t));
k2:=bw*cos(tw)*((2/3)*bw+bbf)+rbf*bbf*sin(tw)-rbf*rbf*sin(tw)*sin(tw);
k2:=(k2/(bbf+(2/3)*bw))*((cos(tw))/(e*t));
k:=k+k2+((bw*sin(tw)*sin(tw))/(e*t));
k:=1/k;

beta:=k/(4*e*I);
beta:=power(beta,0.25);

dhw:=exp(-beta*0.5*(Lspan-Llb))*(cos(beta*0.5*(Lspan-Llb))-sin(beta*0.5*(Lspan-Llb)));
dhw:=dhw+exp(-beta*0.5*(Lspan+Llb))*(cos(beta*0.5*(Lspan+Llb))-
sin(beta*0.5*(Lspan+Llb)));
dhw2:=exp(-beta*(Lspan-Llb))*sin(beta*(Lspan-Llb));
dhw2:=dhw2+exp(-beta*(Lspan+Llb))*sin(beta*(Lspan+Llb));
dhw:=dhw*dhw2;
dhw:=1+exp(-beta*Llb)*(cos(beta*Llb)+sin(beta*Llb))-dhw;
dhw:=dhw*((F*beta)/(4*k));

{2) calculating cross-section deformation dhcs}

rh:=(2/3)*bw*bw*cos(tw)+rbf*sin(tw)*bbf+bbf*bw*cos(tw)-rbf*rbf+sin(tw)*sin(tw);
rh:=rh/((1/2)*bbf+(1/3)*bw);
rh:=(rh*k*dhw)/(4*bw*sin(tw));

dhcs:=((k*dhw)/(2))*(bw*cos(tw)+rbf*sin(tw));
dhcs:=dhcs-rh*(bw*sin(tw)-dhw);
dhcs:=dhcs/(2*((1/12)*1*t*t*t)*e);
dhcs:=dhw+abs(dhcs*sqr((bbf/2)-rbf*sin(tw)));

hn:=bw*sin(tw);
zpnov:=(2*hn*t*0.5*hn)+(bbf*t*hn);
zpnov:=zpnov/(t*(btf+hn+hn+bbf));
Inov:=(1/12)*power(t,3)*btf+zpnov*zpnov*t*btf;
Inov:=Inov+2*(power(hn,3)*t*(1/12)+sqr((hn/2)-zpnov)*hn*t);
Inov:=Inov+power(t,3)*bbf*(1/12)+sqr(hn-zpnov)*bbf*t;
Wnov:=Inov/(hn-zpnov);
Snov:=(F*(Lspan-Llb)/4)/Wnov;
Fbf:=Snov*bbf*t;
```

```
{4) find wo for this situation}

   y0:=sqrt(2)*(dhcs-dhw);
   w0min:=0;
   w0max:=bbf/10;

   {Marquerre equations ......................................................}

   e:=210000;                  {N/mm2, Youngs modulus}
   mu:=0.3;                    {1, Poissons ratio}
   pi:=3.14159265;             {1}

   b:=bbf-2*rbf*tan(0.5*tw);   {mm, steel plate width}
   L:=b;                       {mm, steel plate length}

   x:=b/2;                     {mm, position in x-direction}
   z:=0*b;                     {mm, position in z-direction}

   {calculating  w, y, be, la, and D, some variables needed}

   be:=pi/b;
   la:=pi/L;
   pa:=1;

   WHILE abs(Fbf-pa*e*t*b)>0.01 DO

           begin

   w0:=(w0min+w0max)/2;
   w:=w0*cos(be*x)*cos(la*z);
           y:=y0*cos(be*x)*cos(la*z);
           D:=(e*t*t*t)/(12*(1-mu*mu));
     KK1:=0;
     KK2:=1;

           {calculating c1 and c2, constants needed to predict stresses}

           c1:=b*sinh(la*b);
           c1:=c1-b*cosh(la*b)*coth(la*b);
           c1:=c1-(1/la)*cosh(la*b);
           c1:=c1*32*la*la;
           c1:=(-be*be*(b*coth(la*b)+(1/la)))/c1;
           c1:=c1*w0*(w0+2*y0);

           c2:=b*sinh(la*b);
           c2:=c2-b*cosh(la*b)*coth(la*b);
           c2:=c2-(1/la)*cosh(la*b);
           c2:=c2*16*la*la;
           c2:=(be*be)/c2;
           c2:=c2*w0*(w0+2*y0);
```

```
            {Finding p, average axial compressive stress in z direction}

            p:=(1/2)*(((sqr(la)-sqr(be))/(sqr(sqr(la)+sqr(be))))-(1/(sqr(la))))*sinh(la*b);
            p:=p+((la*b)/2)*((1/(sqr(la)))-((1)/(sqr(la)+sqr(be))))*cosh(la*b);
            p:=p*(1/8)*L*sqr(la)*c2*KK2*(w0+y0)*(sqr(be)-sqr(la));
            p:=p+(1/8)*L*sqr(be)*c1*KK2*la*(w0+y0)*sinh(la*b);

            p2:=((be*b)/2)*cosh(la*b);
            p2:=p2-((be*la)/(sqr(la)+sqr(be)))*sinh(la*b);
            p2:=p2*(w0+y0);
            p2:=p2*((L*c2*KK2*la*la*la*be)/(4*(sqr(la)+sqr(be))));

            p:=p+p2;
            p:=p/((b*L)/(32));
            p:=p-(1/8)*w0*(w0+y0)*(w0+2*y0)*(la*la*la*la+be*be*be*be*(2*KK1+1));
            p:=p-2*((d*w0)/(e*t))*sqr(sqr(la)+sqr(be));
            p:=p/(2*(w0+y0)*(sqr(la)+mu*be*be*KK1));
   pa:=abs(p);

   if (pa*e*t*b)<Fbf then w0min:=w0;
   if (pa*e*t*b)>Fbf then w0max:=w0;
   if (pa*e*t*b)=Fbf then w0:=w0;

            end;

   {Calculating the membrane stresses sz, sx, and txz}

   sz:=4*sqr(la)*x*sinh(2*la*x)+4*la*cosh(2*la*x);
   sz:=sz*c2;
   sz:=sz+4*c1*sqr(la)*cosh(2*la*x);
   sz:=sz*cos(2*la*z)*KK2;
   sz:=sz+w0*(w0+2*y0)*((sqr(la))/(8))*cos(2*be*x);
   sz:=sz+p;
   sz:=sz*e;

sx:=c1*cosh(2*la*x);
   sx:=sx2+c2*x*sinh(2*la*x);
   sx:=sx2*-4*sqr(la)*cos(2*la*z)*KK2;
sx:=sx2+w0*(w0+2*y0)*((sqr(be))/(8))*(KK1+cos(2*la*z));
sx:=sx2+mu*KK1*p;
   sx:=sx2*e;

txz:=2*la*x*cosh(2*la*x)+sinh(2*la*x);
   txz:=txz*c2;
   txz:=txz+2*la*c1*sinh(2*la*x);
   txz:=txz*2*la*sin(2*la*z)*KK2;
   txz:=txz*e;

   {Calculating the bending moment stresses szm and sxm}

   szm:=E*w0*t*(la*la+mu*be*be);
```

```
        szm:=szm/(2*(1-mu*mu));
        szm:=szm*cos(la*z)*cos(be*x);

        sxm:=E*w0*t*(be*be+mu*la*la);
        sxm:=sxm/(2*(1-mu*mu));
        sxm:=sxm*cos(la*z)*cos(be*x);

        {Calculating the Von Mises stress at (x,z)}

        svm:=sqrt((sx+sxm)*(sx+sxm)+(sz+szm)*(sz+szm)-(sx+sxm)*(sz+szm)+3*txz*txz);
        svm2:=sqrt((sx-sxm)*(sx-sxm)+(sz-szm)*(sz-szm)-(sx-sxm)*(sz-szm)+3*txz*txz);

        if svm >= svm2 then
        begin
        svm:=svm;
        end;

        if svm < svm2 then
        begin
        svm:=svm2;
        end;

        {Marquerre equations.......................................................}

    if svm >= fy then
    begin
    Fmax:=F;
    end;

    if svm < fy then
    begin
    Fmin:=F;
    end;

    end;

Fcr:=12*(1-sqr(0.3))*sqr(b);
Fcr:=b*t*4*210000*sqr(pi)*sqr(t)/Fcr;
IF Fcr<Fbf THEN
BEGIN
harpje:=1;
END;
writeln(out,teller,chr(9),F);

end;

close(out);

end.
```

5.3 Program for post-failure mechanical model MA1

```
var

{Input and output variables}
out:Text;
teller:Integer;
yax6tab:Text;
testno,destestno:String[4];
woord1,woord2:String;

{Section variables}
hw,btf,bw,bbf,th,rbf,rtf:Real;
k,E,Llb,L,Lw,Lbf,t,fy:Real;
typee,Ltf,A,I,ref,Ftest,Fimec:Real;

{Calculation variables}
dhw,Fp,AA,BB,CC,s,c,pi,alfa,beta:Real;
Lwtry,aaaa,bbbb,cccc,fi2,wtf,ddhw_dfi,dfi_ddhw,lfb:Real;

{Finding Lw}
mpl,d,w,h,sigma1,sigma2,sigma,upsilon,xmax,Mmax,M,F,Mi,Mr,Hr:Real;
Fmin,Fmax,Pcr,P,u,kk,fi,psi,Hrest:Real;
tau:Integer;

function Sec(x:Real):Real;
begin
  Sec:=1/Cos(x);
end;

function Tan(x:Real):Real;
begin
  Tan:=Sin(x)/Cos(x);
end;

function Cot(x:Real):Real;
begin
  Cot:=Cos(x)/Sin(x);
end;

function ArcSin(x:Real):Real;
{-90<ArcSin(x)<90}
var sinx,cosx:Real;
begin
  sinx:=x;
  cosx:=SQRT(1-SQR(sinx));
  ArcSin:=ArcTan(sinx/cosx);
end;

function ArcCos(x:Real):Real;
{0<ArcCos(x)<180}
```

```
var sinx,cosx:Real;
begin
  cosx:=x;
  sinx:=SQRT(1-SQR(cosx));
  if x=0 then ArcCos:=pi/2;
  if x>0 then ArcCos:=ArcTan(sinx/cosx);
  if x<0 then ArcCos:=ArcTan(sinx/cosx)+pi;
end;

function Power(x,y:Real):Real;
{calculates x to the power y}
begin
  Power:=EXP(y*LN(x));
end;
BEGIN

ASSIGN(out,'uff234b.dat');
REWRITE(out);

FOR teller:= 1 TO 58 DO
BEGIN {FOR for all tested sections}
str(teller,woord1);
woord2:='   ';
destestno:=woord1+woord2;
ASSIGN(yax6tab,'uff234.uff');
RESET(yax6tab);
READ(yax6tab,testno);
while testno<>destestno do
begin
READLN(yax6tab);
READ(yax6tab,testno);
end;
READ(yax6tab,ref,typee,btf,rtf,bw,bbf,rbf,th,L,Llb,t,fy,Ftest,Fimec);
th:=th/57.29577951;
CLOSE(yax6tab);
pi:=3.141592654;
E:=210000;
s:=Sin(th);
c:=Cos(th);
hw:=bw*s;

{FINDING LW ------------------------------------------------------------------}

I:=(1/12)*3*power(t,3);
w:=bw-rbf*tan(th/2);

Pcr:=sqr(pi)*E*I/sqr(0.7*w);
mpl:=(2/sqrt(3))*3*0.25*1.155*fy*sqr(t);
Mmax:=0;
Fmin:=0.1;
Fmax:=2.2*Pcr;
```

```
IF (ref=1) OR (ref=22) OR (ref=26) THEN
BEGIN
Fmax:=3*Pcr;
END;

IF (ref=27) OR (ref=28) OR (ref=29) THEN
BEGIN
Fmax:=2.5*Pcr;
END;

WHILE abs(abs(Mmax)-mpl) > 1 DO

BEGIN

F:=(Fmin+Fmax)/2;
Mmax:=0;

   FOR tau:= 1 TO round(w-rbf*tan(th/2)) DO

   BEGIN

   d:=w*cos(th);
   h:=w*sin(th);

   Hr:=1;
   Hrest:=0;

      WHILE abs(Hrest-Hr)>0.1 DO

      BEGIN

      Hrest:=Hr;

      Pcr:=sqr(pi)*E*I/sqr(0.7*w);
      P:=F*cos((pi/2)-th)+Hrest*cos(th);
      u:=(pi/2)*sqrt(P/Pcr);
      fi:=(3/u)*(1/sin(2*u)-1/(2*u));
      psi:=(3/(2*u))*(1/(2*u)-1/tan(2*u));
      kk:=u*2/w;

      Mi:=w*F*rbf*tan(th/2)*(sqr(fi)-4*sqr(psi))/(-sqr(fi)*w+6*bbf*psi+4*w*sqr(psi));
      Mr:=3*bbf*F*rbf*tan(th/2)*fi/(-sqr(fi)*w+6*bbf*psi+4*w*sqr(psi));
      Hr:=(Mr+F*d+F*rbf*tan(th/2)+Mi)/h;

      END;

   upsilon:=w-tau;
   sigma1:=(Mr/P)*((sin(kk*upsilon)/sin(kk*w))-(upsilon/w));
   sigma2:=((F*rbf*tan(th/2)+Mi)/P)*((sin(kk*tau)/sin(kk*w))-(tau/w));
   sigma:=-sigma1+sigma2;
   M:=Mr-tau*Hr*sin(th)+tau*F*sin((pi/2)-th)-sigma*(F*cos((pi/2)-th)+Hr*cos(th));
```

```
      IF abs(M)>abs(Mmax) THEN
      BEGIN
      Mmax:=M;
      xmax:=tau;
      END;

   END;

IF abs(Mmax)>=mpl THEN
BEGIN
Fmax:=F;
END;

IF abs(Mmax)<mpl THEN
BEGIN
Fmin:=F;
END;

END;

Lw:=w-xmax;
writeln(round(teller),chr(9),round(Lw));

{END FINDING LW --------------------------------------------------------------}

alfa:=1.155*fy*SQR(t)*Llb;
AA:=0.0624;
BB:=-0.0101;
CC:=0.5633;
I:=(1/12)*Llb*power(t,3);
rbf:=rbf-0.5*t;
k:=(E*I*(3*bbf+2*bw))/(SQR(rbf)*SQR(sin(th))*bw*(bbf-(4/3)*rbf*sin(th)));
beta:=k*(CC+BB*Lw)*(bw-Lw)*Lw;

Fp:=(-alfa-beta+SQRT(4*AA*alfa*hw*(bw-Lw)*Lw*k+SQR(alfa+beta)))/(2*AA*(bw-Lw)*Lw);
dhw:=Fp/k;
rbf:=rbf+0.5*t;
Lbf:=Sqrt((2.601*0.5*bbf*Llb*1.155*fy*sqr(t))/(Fp));

{Parts adjacent to load bearing plate}

{Fp:=Fp*(1+2*(Lbf/Llb));}

{Fp:=Fp+1.155*fy*Sqr(t)*bbf/(Sqrt(Sqr(Lbf)-Sqr(dhw)));}

{Complex length factor}

aaaa:=Sqr(hw)+Sqr(Lbf);
bbbb:=2*Lbf*(dhw-hw);
cccc:=Sqr(dhw);
fi2:=(-bbbb-Sqrt(Sqr(bbbb)-4*aaaa*cccc))/(2*aaaa);
```

```
wtf:=Sqrt(Sqr(Lbf)-Sqr(Lbf-hw*fi2));
ddhw_dfi:=Sqrt(Sqr(Lbf)-Sqr(wtf))*(hw-dhw)/wtf;
dfi_ddhw:=1/ddhw_dfi;
lfb:=1+((L-Llb)/2)*dfi_ddhw;
lfb:=1/lfb;
{Fp:=Fp*lfb;
}
{Simple length factor}

lfb:=1/(1+(L*dhw)/(4*hw*Sqrt(Sqr(Lbf)-Sqr(dhw))));

{Fp:=Fp*lfb;
}
IF (typee=3) THEN
BEGIN
writeln(out,ref,chr(9),Fp,chr(9),Ftest,chr(9),Fp/Ftest);
END;
END;

CLOSE(out);

END.
```

5.4 Program for post-failure mechanical model MR1

```
var

{Input and output variables}

out:Text;
teller:Integer;
testno,destestno:String[4];
woord1,woord2:String;
typee:Real;

{Section variables}

th,bw,btf,bbf,rbf,rtf,t,L,Llb,fy,Ftest,Lbf:Real;
Fimec,ref,A,I,k,hw:Real;

{Calculation variables}

E,dhw,Fp,fi2,lfb:Real;
aaaa,bbbb,cccc,wtf,ddhw_dfi,dfi_ddhw:Real;

function ArcSin(x:Real):Real;
{-90<ArcSin(x)<90}
var sinx,cosx:Real;
begin
  sinx:=x;
  cosx:=SQRT(1-SQR(sinx));
  ArcSin:=ArcTan(sinx/cosx);
end;

function ArcCos(x:Real):Real;
{0<ArcCos(x)<180}
var sinx,cosx:Real;
begin
  cosx:=x;
  sinx:=SQRT(1-SQR(cosx));
  if x=0 then ArcCos:=pi/2;
  if x>0 then ArcCos:=ArcTan(sinx/cosx);
  if x<0 then ArcCos:=ArcTan(sinx/cosx)+pi;
end;

function Power(x,y:Real):Real;
{calculates x to the power y}
begin
  Power:=EXP(y*LN(x));
end;

{FUNCTION DECLARATION}

BEGIN {PROGRAM}
```

```
ASSIGN(out,'uff16e.dat');
REWRITE(out);

FOR teller:= 1 TO 34 DO

BEGIN {FOR for all tested sections}
writeln(teller);
str(teller,woord1);
woord2:='   ';
destestno:=woord1+woord2;
ASSIGN(input,'uff16.prn');
RESET(input);
READ(input,testno);
while testno<>destestno do
begin
READLN(input);
READ(input,testno);
end;
READ(input,ref,typee,btf,rtf,bw,bbf,rbf,th,L,Llb,t,fy,Ftest,Fimec);
CLOSE(input);

th:=th/57.29577951;
E:=210000;
hw:=bw*sin(th);

I:=(1/12)*(Llb)*t*t*t;
k:=(E*I*(3*bbf+2*bw))/(SQR(rbf)*SQR(sin(th))*bw*(bbf-(4/3)*rbf*sin(th)));
dhw:=2*bw*((1.155*fy*sqr(t)*Llb)/rbf)*Cos(th/2)*Sin(th/2);
dhw:=-dhw/(-bw*k-((1.155*fy*sqr(t)*Llb)/rbf)+bw*k*Cos(th));
Fp:=k*dhw;

{EXTRA FORCES FOR ADJACENT PARTS}

Lbf:=Sqrt((2.601*0.5*bbf*Llb*1.155*fy*sqr(t))/(Fp));
{Fp:=Fp*(1+2*(Lbf/Llb));}
{Fp:=Fp+1.155*fy*sqr(t)*bbf/(sqrt(sqr(Lbf)-Sqr(dhw)));}

{SIMPLE LENGTH FACTOR}

{Fp:=Fp/(1+(L*dhw)/(4*hw*Sqrt(Sqr(Lbf)-Sqr(dhw))));}

{COMPLEX LENGTH FACTOR}

aaaa:=Sqr(hw)+Sqr(Lbf);
bbbb:=2*Lbf*(dhw-hw);
cccc:=Sqr(dhw);
fi2:=(-bbbb-Sqrt(Sqr(bbbb)-4*aaaa*cccc))/(2*aaaa);
wtf:=Sqrt(Sqr(Lbf)-Sqr(Lbf-hw*fi2));
ddhw_dfi:=Sqrt(Sqr(Lbf)-Sqr(wtf))*(hw-dhw)/wtf;
dfi_ddhw:=1/ddhw_dfi;
lfb:=1+((L-Llb)/2)*dfi_ddhw;
```

```
lfb:=1/lfb;

{Fp:=Fp*lfb;}

writeln(out,Fp,chr(9),Fimec,chr(9),Fp/Fimec);

END; {Cycle for all tested sections}

CLOSE(out);

END. {PROGRAM}
```

5.5 Program for post-failure mechanical model ME1

```
var

{input/output}
out:Text;
teller:Integer;
testno:Real;

{section}
ref,typee,btf,rtf,bw,bbf,rbf,theta,L,Llb,t,fy,Ftest,Fimec:Real;
E,I,k,d,a,b,dhw:Real;

{finding d}
dmin,dmax,Fp,Fe:Real;

{finding point of inertia}
hn,zpnov,Inov:Real;

function power(x,y:Real):Real;
{calculates x to the power y}
begin
  power:=exp(y*ln(x));
end;

function TAN(x:Real):Real;
begin
  TAN:=SIN(x)/COS(x);
end;

BEGIN {PROGRAM}

ASSIGN(out,'uff5.dat');
REWRITE(out);

FOR teller:= 1 TO 7 DO
  BEGIN {FOR for all tested sections}
  writeln(teller);
  {str(teller,woord1);
  woord2:='   ';
  destestno:=woord1+woord2;}
  ASSIGN(input,'uff5.prn');
  RESET(input);
  READ(input,testno);
  while testno<>teller do
  begin
  READLN(input);
  READ(input,testno);
  end;
  READ(input,ref,typee,btf,rtf,bw,bbf,rbf,theta,L,Llb,t,fy,Ftest,Fimec);
  writeln(btf,rtf,bw,bbf,rbf,theta,L,Llb,t,fy,Ftest);
```

```
  theta:=theta/57.29577951;
  CLOSE(input);

  E:=210000;
  I:=(1/12)*Llb*t*t*t;
  k:=(E*I*(3*bbf+2*bw));
  k:=k/(SQR(rbf)*SQR(sin(theta))*bw*(bbf-(4/3)*(rbf)*sin(theta)));

  dmin:=0;
  dmax:=10;
  Fp:=0;
  Fe:=2;

  WHILE abs(Fp-Fe) > 1 DO {Minimalisatie ...}
  BEGIN
  d:=(dmin+dmax)/2;

  a:=bbf/5;
  b:=bbf;
  dhw:=2*d;

  Fe:=k*dhw;

  Fp:=1-(2*d)/t+Sqrt(Sqr(2*d/t)+1)-6*d/(t*(1+4*Sqr(a)/Sqr(b)));
  Fp:=Fp+4*Sqrt(Sqr(3*d/(2*t*(1+4*Sqr(a)/Sqr(b))))+1);
  Fp:=Fp*fy*t*bbf/6;

      hn:=bw*sin(theta);
      zpnov:=(2*hn*t*0.5*hn)+(bbf*t*hn);
      zpnov:=zpnov/(t*(btf+hn+hn+btf));
      Inov:=(1/12)*power(t,3)*btf+zpnov*zpnov*t*btf;
      Inov:=Inov+2*(power(hn,3)*t*(1/12)+sqr((hn/2)-zpnov)*hn*t);
      Inov:=Inov+power(t,3)*bbf*(1/12)+sqr(hn-zpnov)*bbf*t;
      Fp:=Fp*4*Inov/((L-Llb)*(hn-zpnov)*bbf*t);

  IF Fp>=Fe THEN
  BEGIN
  dmin:=d;
  END;

  IF Fp < Fe THEN
  BEGIN
  dmax:=d;
  END;

  END; {WHILE}

  writeln(out,Fp,chr(9),Ftest);
 END; {FOR-loop}
 CLOSE(out);
 END. {PROGRAM}
```

6 Input files for Ansys 5.4

6.1 Input file for yield arc finite element model (experiment 36)

```
/FILENAM,h36

/PREP7

! 75 MM FINE MESH AT THE LEFT OF LOAD BEARING PLATE (700-75-75=550)
! 20 MM TRANSISTION ZONE IN THIS FINE MESH

L1=550
L2=570
L3=700

! MODELLING SECTION AROUND LOAD BEARING PLATE

! KEYNODES SECTION

! THIS DATA HAS BEEN GENERATED BY TURBO-PASCAL PROGRAM ANSYS2.PAS

K,11, 0.0000000000E+00, 0.0000000000E+00,L1
K,12, 5.3832450986E+01, 0.0000000000E+00,L1
K,13, 6.3832450986E+01, 0.0000000000E+00,L1
K,14, 7.0363070639E+01, 2.0559640973E+00,L1
K,15, 7.4538125460E+01, 7.4822794824E+00,L1
K,16, 7.7974722406E+01, 1.6873222004E+01,L1
K,17, 1.0188137537E+02, 8.2201221595E+01,L1
K,18, 1.0531797231E+02, 9.1592164116E+01,L1
K,19, 1.0949302713E+02, 9.7018479501E+01,L1
K,110, 1.1602364679E+02, 9.9074443598E+01,L1
K,111, 1.2602364679E+02, 9.9074443598E+01,L1
K,112, 1.6060609777E+02, 9.9074443598E+01,L1

K,21, 0.0000000000E+00, 0.0000000000E+00,L2
K,22, 5.3832450986E+01, 0.0000000000E+00,L2
K,23, 6.3832450986E+01, 0.0000000000E+00,L2
K,24, 7.0363070639E+01, 2.0559640973E+00,L2
K,25, 7.4538125460E+01, 7.4822794824E+00,L2
K,26, 7.7974722406E+01, 1.6873222004E+01,L2
K,27, 1.0188137537E+02, 8.2201221595E+01,L2
K,28, 1.0531797231E+02, 9.1592164116E+01,L2
K,29, 1.0949302713E+02, 9.7018479501E+01,L2
K,210, 1.1602364679E+02, 9.9074443598E+01,L2
K,211, 1.2602364679E+02, 9.9074443598E+01,L2
K,212, 1.6060609777E+02, 9.9074443598E+01,L2

K,31, 0.0000000000E+00, 0.0000000000E+00,L3
K,32, 5.3832450986E+01, 0.0000000000E+00,L3
K,33, 6.3832450986E+01, 0.0000000000E+00,L3
```

```
K,34, 7.0363070639E+01, 2.0559640973E+00,L3
K,35, 7.4538125460E+01, 7.4822794824E+00,L3
K,36, 7.7974722406E+01, 1.6873222004E+01,L3
K,37, 1.0188137537E+02, 8.2201221595E+01,L3
K,38, 1.0531797231E+02, 9.1592164116E+01,L3
K,39, 1.0949302713E+02, 9.7018479501E+01,L3
K,310, 1.1602364679E+02, 9.9074443598E+01,L3
K,311, 1.2602364679E+02, 9.9074443598E+01,L3
K,312, 1.6060609777E+02, 9.9074443598E+01,L3

! LINES

LSTR,11,12          ! 1
LSTR,12,13          ! 2
LARC,13,15,14       ! 3
LSTR,15,16          ! 4
LSTR,16,17          ! 5
LSTR,17,18          ! 6
LARC,18,110,19      ! 7
LSTR,110,111        ! 8
LSTR,111,112        ! 9

LSTR,21,22          ! 10
LSTR,22,23          ! 11
LARC,23,25,24       ! 12
LSTR,25,26          ! 13
LSTR,26,27          ! 14
LSTR,27,28          ! 15
LARC,28,210,29      ! 16
LSTR,210,211        ! 17
LSTR,211,212        ! 18

LSTR,31,32          ! 19
LSTR,32,33          ! 20
LARC,33,35,34       ! 21
LSTR,35,36          ! 22
LSTR,36,37          ! 23
LSTR,37,38          ! 24
LARC,38,310,39      ! 25
LSTR,310,311        ! 26
LSTR,311,312        ! 27

LSTR,11,21          ! 28
LSTR,12,22          ! 29
LSTR,13,23          ! 30
LSTR,15,25          ! 31
LSTR,16,26          ! 32
LSTR,17,27          ! 33
LSTR,18,28          ! 34
LSTR,110,210        ! 35
LSTR,111,211        ! 36
```

```
LSTR,112,212            ! 37

LSTR,21,31              ! 38
LSTR,22,32              ! 39
LSTR,23,33              ! 40
LSTR,25,35              ! 41
LSTR,26,36              ! 42
LSTR,27,37              ! 43
LSTR,28,38              ! 44
LSTR,210,310            ! 45
LSTR,211,311            ! 46
LSTR,212,312            ! 47

! AREAS

AL,1,29,10,28           ! 1
AL,2,30,11,29           ! 2
AL,3,31,12,30           ! 3
AL,4,32,13,31           ! 4
AL,5,33,14,32           ! 5
AL,6,34,15,33           ! 6
AL,7,35,16,34           ! 7
AL,8,36,17,35           ! 8
AL,9,37,18,36           ! 9

AL,10,39,19,38          ! 10
AL,11,40,20,39          ! 11
AL,12,41,21,40          ! 12
AL,13,42,22,41          ! 13
AL,14,43,23,42          ! 14
AL,15,44,24,43          ! 15
AL,16,45,25,44          ! 16
AL,17,46,26,45          ! 17
AL,18,47,27,46          ! 18

! ELEMENT DISTRIBUTION ALONG LINES

! LENGTH CORNER RADIUS = 69.9/360 * 2 * PI * 11.4 = 13.9

! CROSS-SECTION LINES

! ROUGH MESHED PART
! CORNER RADIUS IS MODELLED BY 1 ELEMENT, LENGTH 13.9
! THUS WIDTH 13.9*4 = 55.6 (MAX 24)

! LINE 1 TO 9
LESIZE,1,24     ! MAIN MESH
LESIZE,2,19     ! AVERAGE
LESIZE,3,,,1    ! ONE ELEMENT FOR RADIUS
LESIZE,4,19     ! AVERAGAE
LESIZE,5,24     ! MAIN MESH
```

```
LESIZE,6,19     ! AVERAGE
LESIZE,7,,,1    ! ONE ELEMENT FOR RADIUS
LESIZE,8,19     ! MAIN MESH
LESIZE,9,24     ! AVERAGE

! FINE MESHED PART

! LINE 10 TO 18
LESIZE,10,24   ! MAIN MESH
LESIZE,11,19   ! AVERAGE
LESIZE,12,,,1  ! ONE ELEMENT FOR RADIUS
LESIZE,13,6    ! AVERAGE
LESIZE,14,4    ! MAIN MESH
LESIZE,15,1.4  ! EXTRA SMALL TO DESCRIBE ROLLING CORRECTLY
LESIZE,16,,,10 ! TEN (DANGER FOR ROLLING) ELEMENTS FOR RADIUS
LESIZE,17,4    ! AVERAGE
LESIZE,18,6    ! MAIN MESH

! LINE 19 TO 27
LESIZE,19,24   ! ALL THE SAME AS ABOVE PRESENTED
LESIZE,20,19
LESIZE,21,,,1
LESIZE,22,6
LESIZE,23,4
LESIZE,24,1.4
LESIZE,25,,,10
LESIZE,26,4
LESIZE,27,6

! LONGITUDINAL LINES

! LINE 28 TO 37
LESIZE,28,22   ! ALL VALUES ARE AVERAGE OF FINE AND ROUGH MESHED PART
LESIZE,29,22
LESIZE,30,22
LESIZE,31,22
LESIZE,32,15
LESIZE,33,15
LESIZE,34,15
LESIZE,35,15
LESIZE,36,15
LESIZE,37,15

! FINE MESHED PART

! LINE 38 TO 47
LESIZE,38,20          ! REDUCED TO AVOID BAD ELEMENTS
LESIZE,39,20          ! REDUCED TO AVOID BAD ELEMENTS
LESIZE,40,20          ! 4 TIMES ELEMENT LENGTH = 4 * 13.9 = MAX 24
LESIZE,41,20
LESIZE,42,5           ! SAME AS MAIN MESH
```

```
LESIZE,43,5
LESIZE,44,5    ! 4 TIME ELEMENT LENGTH = 4 * 1.39 = 5
LESIZE,45,5    ! MAKE 6 TO MESH AREA 15 EQUALLY NORMAL = 9
LESIZE,46,6    ! SAME AS MAIN MESH
LESIZE,47,6

! ELEMENT DATA

ET,1,SHELL43
KEYOPT,1,3,0 !(INCLUDE IN-PLANE EXTRA DISPLACEMENT SHAPES)
KEYOPT,1,4,0 !(NO USER SUBROUTINE TO DEFINE ELEMENT COORDINATE SYSTEM)
KEYOPT,1,5,1
KEYOPT,1,6,0 !(BASIC ELEMENT SOLUTION)

ET,2,CONTAC49
KEYOPT,2,1,0 !(NORMAL DOF)
KEYOPT,2,2,1 !(PENALTY FUNCTION + LAGRANGE MULTIPLIER)
KEYOPT,2,3,0 !(NO FRICTION)
KEYOPT,2,7,1 !(RECOMMENDED TIME STEP PREDICTION METHOD)

ET,3,SOLID45

! REAL CONSTANT SETS

! STEEL PLATE THICKNESS = 0.67

R,1,0.67
R,2,3000,,0.01

! MATERIALS, TEST PIECE 2-DW-B/C

MP,EX,1,210000
TB,MISO,1, ,8
TBPT,DEFI,0.001685,353.8947
TBPT,DEFI,0.031064,362.3426
TBPT,DEFI,0.050218,404.1098
TBPT,DEFI,0.075107,441.8740
TBPT,DEFI,0.101202,467.9757
TBPT,DEFI,0.150143,504.1821
TBPT,DEFI,0.200080,532.8928
TBPT,DEFI,0.250370,554.6708

UIMP,2,EX, , ,210000,
UIMP,2,NUXY, , ,0.3,


! MESHING COMPRESSED ELEMENT

TYPE,1
MAT,1
REAL,1
```

```
ESYS,0

! MAPPED MESHING

ESHAPE,2

ASEL,S,AREA,,10
ASEL,A,AREA,,12
ASEL,A,AREA,,14
ASEL,A,AREA,,16
ASEL,A,AREA,,18
ASEL,A,AREA,,15

AMESH,ALL
ASEL,ALL

! FREE MESHING

ESHAPE,0

ASEL,S,AREA,,11
ASEL,A,AREA,,13
!ASEL,A,AREA,,15
ASEL,A,AREA,,17

ASEL,A,AREA,,1,9

AMESH,ALL
ASEL,ALL

! ONE SECTION PART TO MULTIPLY

L7=0
L8=50

! THIS DATA HAS BEEN PRODUCED BY TURBO-PASCAL PROGRAM ANSYS2.PAS

K,71, 0.0000000000E+00, 0.0000000000E+00,L7
K,72, 5.3832450986E+01, 0.0000000000E+00,L7
K,73, 6.3832450986E+01, 0.0000000000E+00,L7
K,74, 7.0363070639E+01, 2.0559640973E+00,L7
K,75, 7.4538125460E+01, 7.4822794824E+00,L7
K,76, 7.7974722406E+01, 1.6873222004E+01,L7
K,77, 1.0188137537E+02, 8.2201221595E+01,L7
K,78, 1.0531797231E+02, 9.1592164116E+01,L7
K,79, 1.0949302713E+02, 9.7018479501E+01,L7
K,710, 1.1602364679E+02, 9.9074443598E+01,L7
K,711, 1.2602364679E+02, 9.9074443598E+01,L7
K,712, 1.6060609777E+02, 9.9074443598E+01,L7

K,81, 0.0000000000E+00, 0.0000000000E+00,L8
```

```
K,82, 5.3832450986E+01, 0.0000000000E+00,L8
K,83, 6.3832450986E+01, 0.0000000000E+00,L8
K,84, 7.0363070639E+01, 2.0559640973E+00,L8
K,85, 7.4538125460E+01, 7.4822794824E+00,L8
K,86, 7.7974722406E+01, 1.6873222004E+01,L8
K,87, 1.0188137537E+02, 8.2201221595E+01,L8
K,88, 1.0531797231E+02, 9.1592164116E+01,L8
K,89, 1.0949302713E+02, 9.7018479501E+01,L8
K,810, 1.1602364679E+02, 9.9074443598E+01,L8
K,811, 1.2602364679E+02, 9.9074443598E+01,L8
K,812, 1.6060609777E+02, 9.9074443598E+01,L8

! LINE 48 TO 56
LSTR,71,72            ! 48
LSTR,72,73            ! 49
LARC,73,75,74         ! 50
LSTR,75,76            ! 51
LSTR,76,77            ! 52
LSTR,77,78            ! 53
LARC,78,710,79        ! 54
LSTR,710,711          ! 55
LSTR,711,712          ! 56

! LINE 57 TO 65
LSTR,81,82            ! 57
LSTR,82,83            ! 58
LARC,83,85,84         ! 59
LSTR,85,86            ! 60
LSTR,86,87            ! 61
LSTR,87,88            ! 62
LARC,88,810,89        ! 63
LSTR,810,811          ! 64
LSTR,811,812          ! 65

! LINE 66 TO 75
LSTR,71,81            ! 66
LSTR,72,82            ! 67
LSTR,73,83            ! 68
LSTR,75,85            ! 69
LSTR,76,86            ! 70
LSTR,77,87            ! 71
LSTR,78,88            ! 72
LSTR,710,810          ! 73
LSTR,711,811          ! 74
LSTR,712,812          ! 75

AL,48,67,57,66        ! 19
AL,49,68,58,67        ! 20
AL,50,69,59,68        ! 21
AL,51,70,60,69        ! 22
AL,52,71,61,70        ! 23
```

```
AL,53,72,62,71          ! 24
AL,54,73,63,72          ! 25
AL,55,74,64,73          ! 26
AL,56,75,65,74          ! 27

! ELEMENT DISTRIBUTION ALONG LINES

! CROSS-SECTION LINES

! LINE 48 TO 56
LESIZE,48,24   ! MAIN MESH
LESIZE,49,19   ! AVERAGE
LESIZE,50,,,1  ! ONE ELEMENT FOR CORNER RADIUS, LENGTH 13.9 MM
LESIZE,51,19   ! AVERAGE
LESIZE,52,24   ! MAIN MESH
LESIZE,53,19   ! AVERAGE
LESIZE,54,,,1  ! ONE ELEMENT FOR CORNER RADIUS, LENGTH 13.9 MM
LESIZE,55,19   ! AVERAGE
LESIZE,56,24   ! MAIN MESH

! LINE 57 TO 65
LESIZE,57,24   ! ALL THE SAME AS ABOVE PRESENTED DATA
LESIZE,58,19
LESIZE,59,,,1
LESIZE,60,19
LESIZE,61,24
LESIZE,62,19
LESIZE,63,,,1
LESIZE,64,19
LESIZE,65,24

! LONGITUDINAL LINES

! LINE 66 TO 75
LESIZE,66,24   ! MAIN MESH
LESIZE,67,24
LESIZE,68,24   ! FOUR TIMES CORNER RADIUS LENGTH
LESIZE,69,24
LESIZE,70,24   ! MAIN MESH
LESIZE,71,24
LESIZE,72,24   ! FOUR TIMES CORNER RADIUS LENGTH
LESIZE,73,24
LESIZE,74,24   ! MAIN MESH
LESIZE,75,24


! MESHING COMPRESSED ELEMENT

TYPE,1
MAT,1
REAL,1
```

```
ESYS,0

! MAPPED MESHING

ESHAPE,2

ASEL,S,AREA,,19
ASEL,A,AREA,,21
ASEL,A,AREA,,23
ASEL,A,AREA,,25
ASEL,A,AREA,,27

AMESH,ALL
ASEL,ALL

! FREE MESHING

ESHAPE,0

ASEL,S,AREA,,20
ASEL,A,AREA,,22
ASEL,A,AREA,,24
ASEL,A,AREA,,26

AMESH,ALL
ASEL,ALL

! GENERATING ADDITIONAL PARTS

AGEN,2,19,27,1,,,50,,0,0
AGEN,2,19,27,1,,,100,,0,0
AGEN,2,19,27,1,,,150,,0,0
AGEN,2,19,27,1,,,200,,0,0
AGEN,2,19,27,1,,,250,,0,0
AGEN,2,19,27,1,,,300,,0,0
AGEN,2,19,27,1,,,350,,0,0
AGEN,2,19,27,1,,,400,,0,0
AGEN,2,19,27,1,,,450,,0,0
AGEN,2,19,27,1,,,500,,0,0

! YIELD ALL NODES TOGETHER

NUMMRG,ALL

! EXCENTRICITY LOAD BEARING PLATE

EXC=0

! KEYNODES LOAD BEARING PLATE

H=99.07		! HEIGHT OF SECTION
```

```
B=160.61          ! WIDTH OF SECTION
C=116.02          ! START OF TOP FLANGE FROM 0
D=63.83           ! END OF BOTTOM FLANGE FROM 0

K,40001,C-30,H+1,625 ! LOAD BEARING PLATE STARTS IN Z-DIRECTION ON 625
K,40002,C-30,H+1,725
K,40003,C-30,H+1+20,725
K,40004,C-30,H+1+20,625

K,40005,B+25,H+1,625
K,40006,B+25,H+1,725
K,40007,B+25,H+1+20,725
K,40008,B+25,H+1+20,625

! VOLUME (LOAD BEARING PLATE)

V,40001,40002,40003,40004,40005,40006,40007,40008

! LOAD BEARING PLATE ELEMENT DISTRIBUTION

LSEL,S,LOC,Y,H+0.5,200
LESIZE,ALL,,,1
ALLSEL,ALL

! MESHING SOLID ELEMENT

TYPE,3
MAT,2
VMESH,1

! SYMMETRIC BOUNDARY CONDITIONS

! LONGITUDINAL DIRECTION
NSEL,ALL
NSEL,S,LOC,X,B-0.1,B+0.1
NSEL,R,LOC,Y,H-0.5,H+0.5
D,ALL,UX,0,,,,ROTY,ROTZ
NSEL,ALL

! CROSS DIRECTION
NSEL,S,LOC,Y,-10,H+0.5
NSEL,R,LOC,Z,699.9,700.1
D,ALL,UZ,O,,,,ROTX,ROTY
NSEL,ALL

! SUPPORTS

NSEL,S,LOC,Z,99.9,100.1
NSEL,R,LOC,X,-0.2,D+0.1
D,ALL,UX,0,,,,UY,ROTY,ROTZ
NSEL,ALL
```

```
! NODES TARGET

NSEL,S,LOC,Y,H+1-0.1,H+1+0.1
CM,target,NODE
NSEL,ALL

! NODES CONTACT

NSEL,S,LOC,Z,650,710
NSEL,R,LOC,Y,H-25,H+0.1
CM,contact,NODE
NSEL,ALL

! BOUNDARY CONDITIONS LOAD BEARING PLATE

NSEL,S,LOC,Y,H+1+20-0.1,H+1+20+0.1
D,ALL,UX,0,,,,UZ,ROTX,ROTY,ROTZ
NSEL,ALL

! GENERATE CONTACTELEMENTS BETWEEN LOAD BEARING PLATE AND
COMPRESSED ELEMENT

TYPE,2,
REAL,2,
ESYS,0,
GCGEN,contact,target, , ,TOP,

! STRIPS PREVENTING SPREADING OF THE WEBS

! FIX STRIPS EVERY 250 MM BETWEEN WCMS AND SUPPORT

NSEL,S,LOC,Y,-0.1,0.01
NSEL,R,LOC,Z,500-1,500+20
D,ALL,UX,0
NSEL,ALL

NSEL,S,LOC,Y,-0.1,0.01
NSEL,R,LOC,Z,300-1,300+20
D,ALL,UX,0
NSEL,ALL

! WEB CRIPPLING MEASUREMENT STRIP (WCMS)

NSEL,S,LOC,Y,-0.1,0.1
NSEL,R,LOC,Z,700-10-0.1,700+0.1
D,ALL,UX,0,,,,ROTZ
NSEL,ALL

MODMSH,DETACH
```

```
! START SUBSTRUCTURE 50 MM FROM TRANSISTION ZONE (FINE-ROUGH MESH)

NSEL,S,LOC,Z,0,500
ESLN,S,1
EDELE,ALL
NDELE,ALL
ALLSEL,ALL

ET,4,MATRIX50
TYPE,4
SE,h31-2gen

! PARAMETERS CALCULATION

/SOLU
ANTYPE,0
NLGEOM,1
SSTIF,ON
NROPT,FULL, ,ON
EQSLV,FRONT
OUTRES,ALL,-1
TIME,1.1
AUTOTS,1
DELTIM,1.1,1.1,1.1,0
KBC,0
NCNV,0,0,0,0,0,
PRED,ON,,ON
NEQIT,20,
LNSRCH,ON

! LOAD

NSEL,S,LOC,Y,H+1+20-0.1,H+1+20+0.1
D,ALL,UY,-1.1
NSEL,ALL

! SAVE & SOLVE

SAVE
SOLVE

! NEXT LOAD STEP

NSEL,S,LOC,Y,H+1+20-0.1,H+1+20+0.1
D,ALL,UY,-8
NSEL,ALL

TIME,8
OUTRES,ALL,-8
OUTRES,NSOL,-40
OUTRES,RSOL,-40
```

```
DELTIM,0.01,0.005,0.05

SAVE
SOLVE
```

6.2 Input file for rolling finite element model (experiment 54 Bakker)

```
/FILENAM,m54

/PREP7

! KEYNODES SECTION

K,1,0,0,0
K,2,49,0,0
K,3,49.7071,0.2929,0
K,4,50,1,0
K,5,50,40,0
K,6,52.9289,47.0711,0
K,7,60,50,0
K,8,80,50,0
K,9,40,0,0
K,10,50,10,0

K,11,0,0,100
K,12,49,0,100
K,13,49.7071,0.2929,100
K,14,50,1,100
K,15,50,40,100
K,16,52.9289,47.0711,100
K,17,60,50,100
K,18,80,50,100
K,19,40,0,100
K,20,50,10,100

K,21,0,0,197.5
K,22,49,0,197.5
K,23,49.7071,0.2929,197.5
K,24,50,1,197.5
K,25,50,40,197.5
K,26,52.9289,47.0711,197.5
K,27,60,50,197.5
K,28,80,50,197.5
K,29,40,0,197.5
K,30,50,10,197.5

K,31,0,0,207.5
K,32,49,0,207.5
K,33,49.7071,0.2929,207.5
K,34,50,1,207.5
K,35,50,40,207.5
K,36,52.9289,47.0711,207.5
K,37,60,50,207.5
K,38,80,50,207.5
K,39,40,0,207.5
K,40,50,10,207.5
```

```
K,41,0,0,232.5
K,42,49,0,232.5
K,43,49.7071,0.2929,232.5
K,44,50,1,232.5
K,45,50,40,232.5
K,46,52.9289,47.0711,232.5
K,47,60,50,232.5
K,48,80,50,232.5
K,49,40,0,232.5
K,50,50,10,232.5

! KEYNODES LOAD BEARING PLATE

K,61,25,52,220
K,62,25,52,237.5
K,63,25,62,237.5
K,64,25,62,220

K,65,85,52,220
K,66,85,52,237.5
K,67,85,62,237.5
K,68,85,62,220

! LINES AND ARCS

LSTR,1,9
LSTR,9,2
LARC,2,4,3
LSTR,4,10
LSTR,10,5
LARC,5,7,6
LSTR,7,8

LSTR,11,19
LSTR,19,12
LARC,12,14,13
LSTR,14,20
LSTR,20,15
LARC,15,17,16
LSTR,17,18

LSTR,21,29
LSTR,29,22
LARC,22,24,23
LSTR,24,30
LSTR,30,25
LARC,25,27,26
LSTR,27,28

LSTR,31,39
LSTR,39,32
```

LARC,32,34,33
LSTR,34,40
LSTR,40,35
LARC,35,37,36
LSTR,37,38

LSTR,41,49
LSTR,49,42
LARC,42,44,43
LSTR,44,50
LSTR,50,45
LARC,45,47,46
LSTR,47,48

LSTR,1,11
LSTR,2,12
LSTR,4,14
LSTR,5,15
LSTR,7,17
LSTR,8,18
LSTR,9,19
LSTR,10,20

LSTR,11,21
LSTR,12,22
LSTR,14,24
LSTR,15,25
LSTR,17,27
LSTR,18,28
LSTR,19,29
LSTR,20,30

LSTR,21,31
LSTR,22,32
LSTR,24,34
LSTR,25,35
LSTR,27,37
LSTR,28,38
LSTR,29,39
LSTR,30,40

LSTR,31,41
LSTR,32,42
LSTR,34,44
LSTR,35,45
LSTR,37,47
LSTR,38,48
LSTR,39,49
LSTR,40,50

```
! AREAS (SECTION)

AL,1,36,8,42
AL,42,9,37,2
AL,3,37,10,38
AL,4,38,11,43
AL,5,43,12,39
AL,6,39,13,40
AL,7,40,14,41

AL,8,44,15,50
AL,9,50,16,45
AL,10,45,17,46
AL,11,46,18,51
AL,12,51,19,47
AL,13,47,20,48
AL,14,48,21,49

AL,15,52,22,58
AL,16,58,23,53
AL,17,53,24,54
AL,18,54,25,59
AL,19,59,26,55
AL,20,55,27,56
AL,21,56,28,57

AL,22,60,29,66
AL,23,66,30,61
AL,24,61,31,62
AL,25,62,32,67
AL,26,67,33,63
AL,27,63,34,64
AL,28,64,35,65

! DISTRIBUTION ELEMENTS ALONG LINES
! FIRST PART

LESIZE,1,10
LESIZE,36,10
LESIZE,8,10
LESIZE,42,10
LESIZE,5,10
LESIZE,43,10
LESIZE,12,10
LESIZE,39,10
LESIZE,7,10
LESIZE,40,10
LESIZE,14,10
LESIZE,41,10
LESIZE,6,10
LESIZE,13,10
```

```
LESIZE,3,,,1
LESIZE,10,,,1

LESIZE,37,4
LESIZE,38,4
LESIZE,2,4
LESIZE,4,4
LESIZE,9,4
LESIZE,11,4

! SECOND PART

LESIZE,44,10
LESIZE,15,10
LESIZE,50,10
LESIZE,51,10
LESIZE,19,10
LESIZE,47,10
LESIZE,20,10
LESIZE,48,10
LESIZE,21,10
LESIZE,49,10

LESIZE,17,,,1

LESIZE,16,4
LESIZE,18,4
LESIZE,45,4
LESIZE,46,4

! THIRD PART

LESIZE,22,10
LESIZE,60,10
LESIZE,29,10
LESIZE,66,10

LESIZE,26,1
LESIZE,67,3
LESIZE,33,1
LESIZE,63,3
LESIZE,27,1
LESIZE,34,1
LESIZE,28,3
LESIZE,64,3
LESIZE,35,3
LESIZE,65,3

LESIZE,31,,,1
LESIZE,24,,,1
```

```
LESIZE,61,4
LESIZE,62,4

! FOURTH PART

LESIZE,52,10
LESIZE,58,10
LESIZE,53,4
LESIZE,54,4

LESIZE,55,6
LESIZE,56,6
LESIZE,57,6
LESIZE,59,6

LESIZE,25,2
LESIZE,32,2
LESIZE,23,5
LESIZE,30,5

! VOLUME (LOAD BEARING PLATE)

V,61,62,63,64,65,66,67,68

! LOAD BEARING PLATE ELEMENT DISTRIBUTION

LSEL,S,LINE,,68,79
LESIZE,ALL,,,1
LSEL,ALL

! ELEMENT DATA

ET,1,SHELL43
KEYOPT,1,3,0
KEYOPT,1,4,0
KEYOPT,1,5,0
KEYOPT,1,6,0

ET,2,CONTAC49
KEYOPT,2,1,0
KEYOPT,2,2,1
KEYOPT,2,3,0
KEYOPT,2,7,1

ET,3,SOLID45

! REAL CONSTANT SETS

R,1,0.62
R,2,3000,,0.05
```

```
! MATERIALS

MP,EX,1,210000
TB,MISO,1, ,7
TBPT,DEFI,0.0018,378
TBPT,DEFI,0.041,393
TBPT,DEFI,0.049,431
TBPT,DEFI,0.072,473
TBPT,DEFI,0.095,495
TBPT,DEFI,0.336,630
TBPT,DEFI,0.588,810

UIMP,2,EX, , ,210000,
UIMP,2,NUXY, , ,0.3,

! MESHING COMPRESSED ELEMENT

TYPE,1
MAT,1
REAL,1
ESYS,0

ESHAPE,2
ASEL,S,AREA,,1
ASEL,A,AREA,,3
ASEL,A,AREA,,5,7
ASEL,A,AREA,,8
ASEL,A,AREA,,10
ASEL,A,AREA,,12,14
ASEL,A,AREA,,22
ASEL,A,AREA,,24
ASEL,A,AREA,,26,28
AMESH,ALL
ASEL,ALL

ESHAPE,0
ASEL,S,AREA,,2
ASEL,A,AREA,,4
ASEL,A,AREA,,9
ASEL,A,AREA,,11
ASEL,A,AREA,,15,21
ASEL,A,AREA,,23
ASEL,A,AREA,,25
AMESH,ALL,
ASEL,ALL

! MESHING SOLID ELEMENT

TYPE,3
MAT,2
VMESH,1
```

```
! SYMMETRIC BOUNDARY CONDITIONS

NSEL,ALL
NSEL,S,LOC,X,79,81
NSEL,R,LOC,Y,0,51
D,ALL,UX,0,,,,ROTY,ROTZ
NSEL,ALL

NSEL,S,LOC,Z,232.4,233
NSEL,R,LOC,Y,0,51
D,ALL,UZ,0,,,,ROTX,ROTY
NSEL,ALL

! SUPPORTS

NSEL,S,LOC,Z,99.9,100.1
NSEL,R,LOC,X,-0.1,49.1
D,ALL,UX,0,,,,UY,ROTY,ROTZ
NSEL,ALL

! NODES TARGET

NSEL,S,LOC,Y,51,53
CM,target,NODE
NSEL,ALL

! NODES CONTACT

NSEL,S,LOC,Z,208.5,233
NSEL,R,LOC,Y,30,51
CM,contact,NODE
NSEL,ALL

! BOUNDARY CONDITIONS LOAD BEARING PLATE

NSEL,S,LOC,Y,55,100
D,ALL,UX,0,,,,UZ,ROTX,ROTY,ROTZ
NSEL,ALL

! GENERATE CONTACTELEMENTS BETWEEN LOAD BEARING PLATE AND
COMPRESSED ELEMENT

TYPE,2,
REAL,2,
ESYS,0,
GCGEN,contact,target, , ,TOP,

! BREAKING LINK BETWEEN AREAS AND ELEMENTS

!MODMSH,DETACH
```

```
! SELECTING NODES AND ELEMENTS TO DELETE, DELETING

!NSEL,S,LOC,Z,-10,190
!ESLN,S,1
!EDELE,ALL
!NDELE,ALL
!ALLSEL,ALL

! ATTACHING SUPERELEMENT

!ET,4,MATRIX50
!TYPE,4
!SE,m54sub

! PARAMETERS CALCULATION

/SOLU
ANTYPE,0
NLGEOM,1
NROPT,AUTO
EQSLV,FRONT
OUTRES,ALL,-1
TIME,2
AUTOTS,1
DELTIM,2,2,2,0
KBC,0
NCNV,0,0,0,0,0
PRED,OFF
NEQIT,5
LNSRCH,OFF

! LOAD

NSEL,S,LOC,Y,55,100
D,ALL,UY,-2
NSEL,ALL

! CALCULATE FIRST LOAD STEP (12 MM) AND SAVE

SAVE
SOLVE

! LOAD 2

NSEL,S,LOC,Y,55,100
D,ALL,UY,-22
NSEL,ALL

TIME,22
OUTRES,ALL,-44
OUTRES,NSOL,-88
```

```
OUTRES,RSOL,-88
DELTIM,0.1,0.01,1
NEQIT,20

SAVE
SOLVE
```

6.3 Input file for yield eye finite element model (experiment 40)

```
/FILENAM,t40

/PREP7

L1=-150
L2=-120
L3=120
L4=150

K,11, 0.0000000000E+00, 0.0000000000E+00,L1
K,12, 5.8423378809E+01, 0.0000000000E+00,L1
K,13, 6.8423378809E+01, 0.0000000000E+00,L1
K,14, 6.9475675948E+01, 4.3104222166E-01,L1
K,15, 6.9923193757E+01, 1.4764390242E+00,L1
K,16, 7.0080266930E+01, 1.1475205349E+01,L1
K,17, 7.1296747720E+01, 8.8912408552E+01,L1
K,18, 7.1453820892E+01, 9.8911174877E+01,L1
K,19, 7.1901338702E+01, 9.9956571679E+01,L1
K,110, 7.2953635841E+01, 1.0038761390E+02,L1
K,111, 8.2953635841E+01, 1.0038761390E+02,L1
K,112, 1.2077701465E+02, 1.0038761390E+02,L1

K,21, 0.0000000000E+00, 0.0000000000E+00,L2
K,22, 5.8423378809E+01, 0.0000000000E+00,L2
K,23, 6.8423378809E+01, 0.0000000000E+00,L2
K,24, 6.9475675948E+01, 4.3104222166E-01,L2
K,25, 6.9923193757E+01, 1.4764390242E+00,L2
K,26, 7.0080266930E+01, 1.1475205349E+01,L2
K,27, 7.1296747720E+01, 8.8912408552E+01,L2
K,28, 7.1453820892E+01, 9.8911174877E+01,L2
K,29, 7.1901338702E+01, 9.9956571679E+01,L2
K,210, 7.2953635841E+01, 1.0038761390E+02,L2
K,211, 8.2953635841E+01, 1.0038761390E+02,L2
K,212, 1.2077701465E+02, 1.0038761390E+02,L2

K,31, 0.0000000000E+00, 0.0000000000E+00,L3
K,32, 5.8423378809E+01, 0.0000000000E+00,L3
K,33, 6.8423378809E+01, 0.0000000000E+00,L3
K,34, 6.9475675948E+01, 4.3104222166E-01,L3
K,35, 6.9923193757E+01, 1.4764390242E+00,L3
K,36, 7.0080266930E+01, 1.1475205349E+01,L3
K,37, 7.1296747720E+01, 8.8912408552E+01,L3
K,38, 7.1453820892E+01, 9.8911174877E+01,L3
K,39, 7.1901338702E+01, 9.9956571679E+01,L3
K,310, 7.2953635841E+01, 1.0038761390E+02,L3
K,311, 8.2953635841E+01, 1.0038761390E+02,L3
K,312, 1.2077701465E+02, 1.0038761390E+02,L3

K,41, 0.0000000000E+00, 0.0000000000E+00,L4
```

```
K,42, 5.8423378809E+01, 0.0000000000E+00,L4
K,43, 6.8423378809E+01, 0.0000000000E+00,L4
K,44, 6.9475675948E+01, 4.3104222166E-01,L4
K,45, 6.9923193757E+01, 1.4764390242E+00,L4
K,46, 7.0080266930E+01, 1.1475205349E+01,L4
K,47, 7.1296747720E+01, 8.8912408552E+01,L4
K,48, 7.1453820892E+01, 9.8911174877E+01,L4
K,49, 7.1901338702E+01, 9.9956571679E+01,L4
K,410, 7.2953635841E+01, 1.0038761390E+02,L4
K,411, 8.2953635841E+01, 1.0038761390E+02,L4
K,412, 1.2077701465E+02, 1.0038761390E+02,L4

! LINES

LSTR,11,12          ! 1
LSTR,12,13          ! 2
LARC,13,15,14       ! 3
LSTR,15,16          ! 4
LSTR,16,17          ! 5
LSTR,17,18          ! 6
LARC,18,110,19      ! 7
LSTR,110,111        ! 8
LSTR,111,112        ! 9

LSTR,21,22          ! 10
LSTR,22,23          ! 11
LARC,23,25,24       ! 12
LSTR,25,26          ! 13
LSTR,26,27          ! 14
LSTR,27,28          ! 15
LARC,28,210,29      ! 16
LSTR,210,211        ! 17
LSTR,211,212        ! 18

LSTR,31,32          ! 19
LSTR,32,33          ! 20
LARC,33,35,34       ! 21
LSTR,35,36          ! 22
LSTR,36,37          ! 23
LSTR,37,38          ! 24
LARC,38,310,39      ! 25
LSTR,310,311        ! 26
LSTR,311,312        ! 27

LSTR,41,42          ! 28
LSTR,42,43          ! 29
LARC,43,45,44       ! 30
LSTR,45,46          ! 31
LSTR,46,47          ! 32
LSTR,47,48          ! 33
LARC,48,410,49      ! 34
```

```
LSTR,410,411            ! 35
LSTR,411,412            ! 36

LSTR,11,21              ! 37
LSTR,12,22              ! 38
LSTR,13,23              ! 39
LSTR,15,25              ! 40
LSTR,16,26              ! 41
LSTR,17,27              ! 42
LSTR,18,28              ! 43
LSTR,110,210            ! 44
LSTR,111,211            ! 45
LSTR,112,212            ! 46

LSTR,21,31              ! 47
LSTR,22,32              ! 48
LSTR,23,33              ! 49
LSTR,25,35              ! 50
LSTR,26,36              ! 51
LSTR,27,37              ! 52
LSTR,28,38              ! 53
LSTR,210,310            ! 54
LSTR,211,311            ! 55
LSTR,212,312            ! 56

LSTR,31,41              ! 57
LSTR,32,42              ! 58
LSTR,33,43              ! 59
LSTR,35,45              ! 60
LSTR,36,46              ! 61
LSTR,37,47              ! 62
LSTR,38,48              ! 63
LSTR,310,410            ! 64
LSTR,311,411            ! 65
LSTR,312,412            ! 66

! AREAS

AL,1,38,10,37           ! 1
AL,2,39,11,38           ! 2
AL,3,40,12,39           ! 3
AL,4,41,13,40           ! 4
AL,5,42,14,41           ! 5
AL,6,43,15,42           ! 6
AL,7,44,16,43           ! 7
AL,8,45,17,44           ! 8
AL,9,46,18,45           ! 9

AL,10,48,19,47          ! 10
AL,11,49,20,48          ! 11
AL,12,50,21,49          ! 12
```

```
AL,13,51,22,50          ! 13
AL,14,52,23,51          ! 14
AL,15,53,24,52          ! 15
AL,16,54,25,53          ! 16
AL,17,55,26,54          ! 17
AL,18,56,27,55          ! 18

AL,19,58,28,57          ! 19
AL,20,59,29,58          ! 20
AL,21,60,30,59          ! 21
AL,22,61,31,60          ! 22
AL,23,62,32,61          ! 23
AL,24,63,33,62          ! 24
AL,25,64,34,63          ! 25
AL,26,65,35,64          ! 26
AL,27,66,36,65          ! 27

! ELEMENT DISTRIBUTION
! LENGTH CORNER RADIUS = 89.1/360 * 2 * PI * 1.5 = 2.33
! CORNER RADIUS IS MODELLED BY 3 ELEMENTS, WIDTH 0.78
! THUS LENGTH 0.78 * 4 = 3

! FINE MESHED MIDDLE PART, CROSS-SECTION LINES, BENEATH LOAD BEARING
PLATE

! LINE 10 TO 18
LESIZE,10,10
LESIZE,11,5
LESIZE,12,,,3
LESIZE,13,5
LESIZE,14,10
LESIZE,15,5
LESIZE,16,,,3
LESIZE,17,2
LESIZE,18,4

! LINE 19 TO 27
LESIZE,19,10
LESIZE,20,5
LESIZE,21,,,3
LESIZE,22,5
LESIZE,23,10
LESIZE,24,5
LESIZE,25,,,3
LESIZE,26,2
LESIZE,27,4

!LONGITUDINAL LINES

! LINE 47 TO 56
LESIZE,47,10
```

```
LESIZE,48,10
LESIZE,49,3
LESIZE,50,3
LESIZE,51,10
LESIZE,52,10
LESIZE,53,3
LESIZE,54,3
LESIZE,55,4
LESIZE,56,4

! ROUGH MESHED PARTS
! CROSS-SECTION, SAME AS OUTER PARTS

! LINE 1 TO 9
LESIZE,1,24
LESIZE,2,15
LESIZE,3,,,1
LESIZE,4,15
LESIZE,5,24
LESIZE,6,15
LESIZE,7,,,1
LESIZE,8,15
LESIZE,9,24

! LINE 28 TO 36
LESIZE,28,24
LESIZE,29,15
LESIZE,30,,,1
LESIZE,31,15
LESIZE,32,24
LESIZE,33,15
LESIZE,34,,,1
LESIZE,35,15
LESIZE,36,24

!LONGITUDINAL LINES

! LINE 37 TO 46
LESIZE,37,17
LESIZE,38,17
LESIZE,39,7
LESIZE,40,7
LESIZE,41,17
LESIZE,42,17
LESIZE,43,7
LESIZE,44,7
LESIZE,45,14
LESIZE,46,14

! LINE 57 TO 66
LESIZE,57,17
```

```
LESIZE,58,17
LESIZE,59,7
LESIZE,60,7
LESIZE,61,17
LESIZE,62,17
LESIZE,63,7
LESIZE,64,7
LESIZE,65,14
LESIZE,66,14

! ELEMENT DATA

ET,1,SHELL43
KEYOPT,1,3,0 !(INCLUDE IN-PLANE EXTRA DISPLACEMENT SHAPES)
KEYOPT,1,4,0 !(NO USER SUBROUTINE TO DEFINE ELEMENT COORDINATE SYSTEM)
KEYOPT,1,5,1
KEYOPT,1,6,0 !(BASIC ELEMENT SOLUTION)

! STEEL PLATE THICKNESS = 0.68 (T-SERIES)

R,1,0.68

! MATERIALS, TEST PIECE 2-DW-B/C

MP,EX,1,210000
TB,MISO,1, ,8
TBPT,DEFI,0.001685,353.8947
TBPT,DEFI,0.031064,362.3426
TBPT,DEFI,0.050218,404.1098
TBPT,DEFI,0.075107,441.8740
TBPT,DEFI,0.101202,467.9757
TBPT,DEFI,0.150143,504.1821
TBPT,DEFI,0.200080,532.8928
TBPT,DEFI,0.250370,554.6708

! MESHING COMPRESSED ELEMENT

TYPE,1
MAT,1
REAL,1
ESYS,0

! MAPPED MESHING

ESHAPE,2

ASEL,S,AREA,,10
ASEL,A,AREA,,12
ASEL,A,AREA,,14
ASEL,A,AREA,,16
ASEL,A,AREA,,18
```

```
AMESH,ALL
ASEL,ALL

! FREE MESHING

ESHAPE,0

ASEL,S,AREA,,11
ASEL,A,AREA,,13
ASEL,A,AREA,,15
ASEL,A,AREA,,17

ASEL,A,AREA,,1
ASEL,A,AREA,,2
ASEL,A,AREA,,3
ASEL,A,AREA,,4
ASEL,A,AREA,,5
ASEL,A,AREA,,6
ASEL,A,AREA,,7
ASEL,A,AREA,,8
ASEL,A,AREA,,9

ASEL,A,AREA,,19
ASEL,A,AREA,,20
ASEL,A,AREA,,21
ASEL,A,AREA,,22
ASEL,A,AREA,,23
ASEL,A,AREA,,24
ASEL,A,AREA,,25
ASEL,A,AREA,,26
ASEL,A,AREA,,27

AMESH,ALL
ASEL,ALL

! ONE SECTION PART TO MULTIPLY

L7=-1000
L8=-950

! THIS DATA HAS BEEN PRODUCED BY TURBO-PASCAL PROGRAM ANSYS2.PAS

K,71, 0.0000000000E+00, 0.0000000000E+00,L7
K,72, 5.8423378809E+01, 0.0000000000E+00,L7
K,73, 6.8423378809E+01, 0.0000000000E+00,L7
K,74, 6.9475675948E+01, 4.3104222166E-01,L7
K,75, 6.9923193757E+01, 1.4764390242E+00,L7
K,76, 7.0080266930E+01, 1.1475205349E+01,L7
K,77, 7.1296747720E+01, 8.8912408552E+01,L7
K,78, 7.1453820892E+01, 9.8911174877E+01,L7
K,79, 7.1901338702E+01, 9.9956571679E+01,L7
```

```
K,710, 7.2953635841E+01, 1.0038761390E+02,L7
K,711, 8.2953635841E+01, 1.0038761390E+02,L7
K,712, 1.2077701465E+02, 1.0038761390E+02,L7

K,81, 0.0000000000E+00, 0.0000000000E+00,L8
K,82, 5.8423378809E+01, 0.0000000000E+00,L8
K,83, 6.8423378809E+01, 0.0000000000E+00,L8
K,84, 6.9475675948E+01, 4.3104222166E-01,L8
K,85, 6.9923193757E+01, 1.4764390242E+00,L8
K,86, 7.0080266930E+01, 1.1475205349E+01,L8
K,87, 7.1296747720E+01, 8.8912408552E+01,L8
K,88, 7.1453820892E+01, 9.8911174877E+01,L8
K,89, 7.1901338702E+01, 9.9956571679E+01,L8
K,810, 7.2953635841E+01, 1.0038761390E+02,L8
K,811, 8.2953635841E+01, 1.0038761390E+02,L8
K,812, 1.2077701465E+02, 1.0038761390E+02,L8

! LINE 67 TO 75

LSTR,71,72          ! 67
LSTR,72,73          ! 68
LARC,73,75,74       ! 69
LSTR,75,76          ! 70
LSTR,76,77          ! 71
LSTR,77,78          ! 72
LARC,78,710,79      ! 73
LSTR,710,711        ! 74
LSTR,711,712        ! 75

! LINE 76 TO 84
LSTR,81,82          ! 76
LSTR,82,83          ! 77
LARC,83,85,84       ! 78
LSTR,85,86          ! 79
LSTR,86,87          ! 80
LSTR,87,88          ! 81
LARC,88,810,89      ! 82
LSTR,810,811        ! 83
LSTR,811,812        ! 84

! LINE 85 TO 94
LSTR,71,81          ! 85
LSTR,72,82          ! 86
LSTR,73,83          ! 87
LSTR,75,85          ! 88
LSTR,76,86          ! 89
LSTR,77,87          ! 90
LSTR,78,88          ! 91
LSTR,710,810        ! 92
LSTR,711,811        ! 93
LSTR,712,812        ! 94
```

```
AL,67,86,76,85          ! 28
AL,68,87,77,86          ! 29
AL,69,88,78,87          ! 30
AL,70,89,79,88          ! 31
AL,71,90,80,89          ! 32
AL,72,91,81,90          ! 33
AL,73,92,82,91          ! 34
AL,74,93,83,92          ! 35
AL,75,94,84,93          ! 36

! ELEMENT DISTRIBUTION ALONG LINES

! CROSS-SECTION LINES

! LINE 67 TO 75
LESIZE,67,24   ! MAIN MESH
LESIZE,68,15   ! AVERAGE
LESIZE,69,,,1  ! ONE ELEMENT FOR CORNER RADIUS, LENGTH 3 MM
LESIZE,70,15   ! AVERAGE
LESIZE,71,24   ! MAIN MESH
LESIZE,72,15   ! AVERAGE
LESIZE,73,,,1  ! ONE ELEMENT FOR CORNER RADIUS, LENGTH 3 MM
LESIZE,74,15   ! AVERAGE
LESIZE,75,24   ! MAIN MESH

! LINE 76 TO 84
LESIZE,76,24   ! ALL THE SAME AS ABOVE PRESENTED DATA
LESIZE,77,15
LESIZE,78,,,1
LESIZE,79,15
LESIZE,80,24
LESIZE,81,15
LESIZE,82,,,1
LESIZE,83,15
LESIZE,84,24

! LONGITUDINAL LINES

! LINE 85 TO 94
LESIZE,85,24   ! MAIN MESH
LESIZE,86,24
LESIZE,87,12   ! FOUR TIMES CORNER RADIUS LENGTH
LESIZE,88,12
LESIZE,89,24   ! MAIN MESH
LESIZE,90,24
LESIZE,91,12   ! FOUR TIMES CORNER RADIUS LENGTH
LESIZE,92,12
LESIZE,93,24   ! MAIN MESH
LESIZE,94,24
```

```
! MESHING COMPRESSED ELEMENT

TYPE,1
MAT,1
REAL,1
ESYS,0

! MAPPED MESHING

ESHAPE,2

ASEL,S,AREA,,28
ASEL,A,AREA,,30
ASEL,A,AREA,,32
ASEL,A,AREA,,34
ASEL,A,AREA,,36

AMESH,ALL
ASEL,ALL

! FREE MESHING

ESHAPE,0

ASEL,S,AREA,,29
ASEL,A,AREA,,31
ASEL,A,AREA,,33
ASEL,A,AREA,,35

AMESH,ALL
ASEL,ALL

! GENERATING ADDITIONAL PARTS

AGEN,2,28,36,1,,,50,,0,0
AGEN,2,28,36,1,,,100,,0,0
AGEN,2,28,36,1,,,150,,0,0
AGEN,2,28,36,1,,,200,,0,0
AGEN,2,28,36,1,,,250,,0,0
AGEN,2,28,36,1,,,300,,0,0
AGEN,2,28,36,1,,,350,,0,0
AGEN,2,28,36,1,,,400,,0,0
AGEN,2,28,36,1,,,450,,0,0
AGEN,2,28,36,1,,,500,,0,0
AGEN,2,28,36,1,,,550,,0,0
AGEN,2,28,36,1,,,600,,0,0
AGEN,2,28,36,1,,,650,,0,0
AGEN,2,28,36,1,,,700,,0,0
AGEN,2,28,36,1,,,750,,0,0
AGEN,2,28,36,1,,,800,,0,0
```

```
AGEN,2,28,36,1,,,1150,,0,0
AGEN,2,28,36,1,,,1200,,0,0
AGEN,2,28,36,1,,,1250,,0,0
AGEN,2,28,36,1,,,1300,,0,0
AGEN,2,28,36,1,,,1350,,0,0
AGEN,2,28,36,1,,,1400,,0,0
AGEN,2,28,36,1,,,1450,,0,0
AGEN,2,28,36,1,,,1500,,0,0
AGEN,2,28,36,1,,,1550,,0,0
AGEN,2,28,36,1,,,1600,,0,0
AGEN,2,28,36,1,,,1650,,0,0
AGEN,2,28,36,1,,,1700,,0,0
AGEN,2,28,36,1,,,1750,,0,0
AGEN,2,28,36,1,,,1800,,0,0
AGEN,2,28,36,1,,,1850,,0,0
AGEN,2,28,36,1,,,1900,,0,0
AGEN,2,28,36,1,,,1950,,0,0

! YIELD ALL NODES TOGETHER

NUMMRG,ALL

! BOUNDARY CONDITIONS

D,302,UZ,0

! SUPPORTS

C=68.42338

NSEL,S,LOC,Z,-900-0.1,-900+0.1
NSEL,R,LOC,X,-0.1,C+0.1
D,ALL,UY,0,,,,UX,ROTY,ROTZ
NSEL,ALL

NSEL,S,LOC,Z,900-0.1,900+0.1
NSEL,R,LOC,X,-0.1,C+0.1
D,ALL,UY,0,,,,UX,ROTY,ROTZ
NSEL,ALL

! SYMMETRY CONDITIONS

BB=1.2077701465E+02

NSEL,S,LOC,X,BB-0.1,BB+0.1
D,ALL,UX,0,,,,ROTZ,ROTY
NSEL,ALL
```

```
! STRIPS PREVENTING SPREADING OF THE WEBS

M=10

NSEL,S,LOC,X,-0.1,C+0.1
NSEL,R,LOC,Z,-675-M,-675+M
D,ALL,UX,0
NSEL,ALL

NSEL,S,LOC,X,-0.1,C+0.1
NSEL,R,LOC,Z,-450-M,-450+M
D,ALL,UX,0
NSEL,ALL

NSEL,S,LOC,X,-0.1,C+0.1
NSEL,R,LOC,Z,-225-M,-225+M
D,ALL,UX,0
NSEL,ALL

NSEL,S,LOC,X,-0.1,C+0.1
NSEL,R,LOC,Z,225-M,225+M
D,ALL,UX,0
NSEL,ALL

NSEL,S,LOC,X,-0.1,C+0.1
NSEL,R,LOC,Z,450-M,450+M
D,ALL,UX,0
NSEL,ALL

NSEL,S,LOC,X,-0.1,C+0.1
NSEL,R,LOC,Z,675-M,675+M
D,ALL,UX,0
NSEL,ALL

! WEB CRIPPLING MEASUREMENT STRIP (WCMS)

NSEL,S,LOC,Z,-0.1,0.1
NSEL,R,LOC,X,0-0.1,C+0.1
D,ALL,UX,0,,,,ROTZ
NSEL,ALL

MODMSH,DETACH

! SUBSTRUCTURES

NSEL,S,LOC,Z,-1500,-200
ESLN,S,1
EDELE,ALL
NDELE,ALL
ALLSEL,ALL
```

```
NSEL,S,LOC,Z,200,1500
ESLN,S,1
EDELE,ALL
NDELE,ALL
ALLSEL,ALL

ET,4,MATRIX50
TYPE,4
SE,t40genl

ET,4,MATRIX50
TYPE,4
SE,t40genr

! ELASTIC CALCULATION

!NSEL,S,LOC,Z,-50,50
!NSEL,R,LOC,X,72.95-0.1,72.95+0.1
!D,ALL,UY,-1
!NSEL,ALL

!ANTYPE,0
!NLGEOM,OFF
!SSTIF,OFF
!OUTRES,ALL,ALL
!TIME,1

! PARAMETERS CALCULATION

/SOLU

ANTYPE,0
NLGEOM,ON
SSTIF,ON

ARCLEN,ON,10,0.001
NSUBST,1000
ARCTRM,U,10,UY

NROPT,AUTO,,OFF

EQSLV,FRONT
OUTRES,ALL,3

! FORCES

V=12.899

! SUM = -249.469 FTEST = 3218

F,     753,FY,  -58.928*V
```

```
F,     754,FY,  -6.8001*V
F,     755,FY,  -14.582*V
F,     756,FY,  -6.2869*V
F,     757,FY,  -8.7935*V
F,     758,FY,  -4.1374*V
F,     759,FY,  -4.9191*V
F,     760,FY,  -3.7102*V
F,     761,FY,  -3.1654*V
F,     762,FY,  -2.4758*V
F,     763,FY,  -2.2145*V
F,     764,FY,  -1.9513*V
F,     765,FY,  -1.7788*V
F,     766,FY,  -1.4736*V
F,     767,FY,  -1.4589*V
F,     768,FY,  -1.3364*V
F,     769,FY,  -1.1519*V
F,     770,FY,  -1.1799*V
F,     771,FY,  -1.4158*V
F,     772,FY,  -1.6199*V
F,     773,FY,  -1.8150*V
F,     774,FY,  -1.9024*V
F,     775,FY,  -2.3027*V
F,     776,FY,  -2.2289*V
F,     777,FY,  -3.0797*V
F,     778,FY,  -3.6234*V
F,     779,FY,  -4.9989*V
F,     780,FY,  -3.9068*V
F,     781,FY,  -9.2043*V
F,     782,FY,  -6.3672*V
F,     783,FY,  -14.752*V
F,     784,FY,  -7.1844*V
F,     785,FY,  -58.724*V

! SAVE & SOLVE

SAVE
SOLVE
```

Literature

[Bakk92a] Bakker, Monique, C.M.: Web Crippling of Cold-Formed Steel Members, Dissertation Eindhoven University of Technology, The Netherlands, ISBN 90-386-0122-0, 1992.

[Bakk99a] Bakker, M.C.M., Snijder, H.H., Kerstens, J.G.M. Elastic Web Crippling of Thin-Walled Cold Formed Steel Members. Proceedings Light-Weight Steel and Aluminium Structures, Fourth International Conference on Steel and Aluminium Structures, Mäkeläinen, P; Hassinen, P., June 1999, Espoo, Finland.

[Hill50a] Hill, R., The Mathematical Theory of Plasticity, London, Oxford University Press, 1950.

[Hofm00a] Hofmeyer, H.: Combined Web Crippling and Bending Moment Failure of First-Generation Trapezoidal Steel Sheeting, Ph.D.-thesis, Eindhoven University of Technology, Faculty of Architecture, Department of Structural Design, ISBN 90-6814-114-7, The Netherlands, 2000.

[Hofm96a] Hofmeyer, H.; Kerstens, J.G.M.; Snijder, H.H.; Bakker, M.C.M.: Research on the Behaviour of Combined Web Crippling and Bending of Steel Deck Sections, published at the 13th International Speciality Conference on Cold-Formed Steel Structures, St. Louis, Missouri, U.S.A., October 18-19, 1996.

[Marg38a] Marguerre, K.: Zur Theorie der gekrümmter Platte grosser Formänderung, Proc. Fifth. Int. Congress Appl. Mech., page 93, 1938.

[Merc56a] Merchant, W.: Frame Instability in the Plastic Range, British Welding Journal, 1956, page 366, 1956.

[Murr81a] Murray, N.W.; Khoo, P.S.: Some Basic Plastic Mechanisms in the Local Buckling of Thin-Walled Steel Structures, International Journal of Mechanical Science, Vol. 23, No. 12, page 703-713, 1981.

[Murr85a] Murray, Noel W.: Introduction to the Theory of Thin-Walled Structures, Oxford Engineering Science Series 13, Clarendon Press Oxford, ISBN 0-19-856186-5, 1985.

[Robe28a] Robertson, A.: The strength of tubular struts, Proc. Roy. Soc. London, A121, (A788), page 558-585, 1928.

[Timo36a] Timoshenko, S.: Theory of Elastic Stability, Engineering Societies Monographs, McGraw-Hill Book Company, New York and London, First edition, 1936.

[Vaes95a] Vaessen, M.: On the elastic web crippling stiffness of thin-walled cold-formed steel sections, Graduate Thesis TUE-BKO-95-17, Eindhoven University of Technology, The Netherlands, 1995.